DETERMINAÇÃO DE PARÂMETROS DE FONTE DE EVENTOS SÍSMICOS NO BRASIL CENTRAL

Juraci Mário de Carvalho

TESE DE DOUTORADO n° 49

Orientador: Lucas Vieira Barros (Universidade de Brasília)
Coorientador: Jiri Zahradnik (Charles University in Prague)

Brasília-DF, 07 de junho de 2019

Universidade de Brasília

Instituto de Geociências

DETERMINAÇÃO DE PARÂMETROS DE FONTE DE EVENTOS
SÍSMICOS NO BRASIL CENTRAL

Juraci Mário de Carvalho

Tese apresentada ao Programa de Pós-Graduação em Geociências Aplicadas e Geodinâmica do Instituto de Geociências da Universidade de Brasília como parte dos requisitos para obtenção do título de Doutor em Geociências. Área de concentração: Geofísica Aplicada e Geodinâmica. Linha de pesquisa: Sismologia.

Orientador: Prof. Dr. Lucas Vieira Barros

Coorientador: Prof. Dr. Jiri Zahradnik

Brasília-DF, 07 de junho de 2019

Universidade de Brasília

Instituto de Geociências

FOLHA DE JULGAMENTO

DETERMINAÇÃO DE PARÂMETROS DE FONTE DE EVENTOS SÍSMICOS NO BRASIL CENTRAL

Candidato: Juraci Mário de Carvalho

Programa de Pós-Graduação em Geociências Aplicadas e Geodinâmica do Instituto de Geociências da Universidade de Brasília como parte dos requisitos para obtenção do título de Doutor em Geociências. Área de concentração: Geofísica Aplicada e Geodinâmica. Linha de pesquisa: Sismologia.

Data de defesa: 07 de junho de 2019

Banca examinadora:

Prof. Dr. Lucas Vieira Barros – Orientador (UnB)
Prof. Dr. George Sand Leão Araújo de França (UnB)
Prof. Dr. Marcelo Sousa de Assumpção (USP)
Prof. Dr. Aderson Farias Do Nascimento (UFRN)

There are three principal means of acquiring knowledge. observation of nature, reflection, and experimentation. Observation collects facts; reflection combines them; experimentation verifies the result of that combination.

Denis Diderot

Agradecimentos

Agradeço à minha mulher e aos meus filhos Rodrigo Fontenele Carvalho, Victor Fontenele Carvalho e Bruno Fontenele Carvalho, pelo apoio e pela compreensão do tempo de convívio muitas vezes sacrificado para realização deste trabalho. Agradeço especialmente a minha esposa Jackeline Portela Fontenele Carvalho pelo apoio, carinho, compreensão e incentivo. Agradeço aos meus pais Armínio Eustáquio de Carvalho e Maria de Jesus Carvalho por serem fontes de inspiração.

Ao Prof. Dr. Lucas Barros, meu orientador e amigo, pela confiança. Agradeço por ter acreditado no meu potencial e por ter me acompanhado durante toda essa caminhada.

Ao Prof. Dr. Jiří Zahradník, meu coorientador, por sua valiosa ajuda e paciência durante o processo de desenvolvimento dessa dissertação. Um amigo que ganhei durante essa jornada.

Ao Prof. Dr. Marcelo Assumpção pela ajuda e suporte, informações durante o processo de elaboração dos artigos publicados.

Ao Prof. Dr. Jose E. P. Soares pela disponibilização dos dados das estações sismográficas RETs adquiridos no âmbito do projeto: Estudos sobre o Lineamento Transbrasiliano (Rede de Estudos Tectônicos Petrobras).

Agradeço aos meus colegas de trabalho, Darlan Portela Fontenele, Vinicius Martins, Diogo Farrapo e outros que me ajudaram no decorrer do doutorado com dados, instrumentação, scripts de mapas, correção de textos e apoio pessoal.

Agradeço aos meus professores do Instituto de Geociências da UnB com quem muito aprendi durante essa jornada.

Agradeço ao Observatório Sismológico da Universidade de Brasília pela disponibilização de recursos, dados da rede sismográfica brasileira e de outras estações sismográficas.

Abstract

The knowledge on the distribution of tectonic stress in Brazil is limited due to the low magnitude of events associated to the low density of the seismographic network. This scenario was improved after the installation of the Brazilian Seismographic Network (RSBR). In this work we investigate the seismicity in the central region of Brazil comprised mainly by the Tocantins Province and parts of the Amazonian Craton, Parnaíba Basin, São Francisco Craton and Paraná Basin. The area is crossed by the Transbrasiliano Lineament (LTB). In the Brazilian seismic catalog it is possible to distinguish a seismic zone following the LTB and some events scattered to the north, south, west and east. The study area is characterized mainly by low magnitude with only one event of magnitude 5. Station phase polarities are used in the inversion either as a constraint or as a result quality indicator. To avoid the misinterpretation of results, we study the uncertainties related to the resolution of the velocity model that affects the projection of the station (polarity) in the focal sphere. The goal of the uncertainty study is to show that the focal mechanism can be influenced by the variations of the takeoff angle caused by the inaccuracy of the velocity model. These uncertainties are more significant for smaller epicentral distances (<200 km). The takeoff angle uncertainty study was extended to the CSPS method as an indicator of stability. In this thesis we relocated a set of 118 events using the iLoc code and the RSTT (Regional Seismic Travel Time) velocity model, inverted the waveform of ten low magnitude events ($2.0 \leq M \leq 4.0$), nine with the new envelope inversion technique and one with the CSPS code and we inverted these focal mechanisms for the stress field. The relocation shows that the seismicity of the area is mainly concentrated in two relatively narrow seismic bands. The inversion of stress of twelve focal mechanisms, 10 obtained in this work and two from other studies, presented a stable result of the main stress axis ($\sigma 1$) azimuth ~133° and plunge ~12°. We conclude that the inversion of waveform envelopes is a promising technique that can be useful in determining the focal mechanisms of weak events detected by sparse networks where the waveform inversion for such weak events is not efficient.

Resumo

O conhecimento sobre a distribuição do esforço tectônico no Brasil é limitado devido à baixa magnitude dos eventos sísmicos associado à baixa densidade da rede sismográfica. Este cenário melhorou após a instalação da Rede Sismográfica Brasileira (RSBR). Neste trabalho investigamos a sismicidade na região central do Brasil compreendida principalmente pela Província Tocantins e partes do Cráton Amazônico, Bacia do Parnaíba, Cráton do São Francisco e Bacia do Paraná. A área é cruzada pelo lineamento Transbrasiliano (LTB). No catálogo sísmico brasileiro é possível distinguir uma zona sísmica paralela ao LTB e grupos de eventos espalhados ao norte, sul, oeste e leste. A área de estudo é caracterizada principalmente por eventos de baixas magnitudes com apenas um evento de magnitude 5. As polaridades das fases P são usadas na inversão como restrição ou como indicador de qualidade, e para evitar a interpretação errônea dos resultados, estudamos as incertezas relacionadas à imprecisão do modelo de velocidade que afeta a projeção da estação (polaridade) na esfera focal. Essas incertezas são mais significativas para distâncias epicentrais menores que 200 km. O estudo da incerteza foi estendido ao método CSPS como um indicador de estabilidade. Nesta tese realocalizamos um conjunto de 118 eventos usando o código iLoc e o modelo de velocidade RSTT (Regional Seismic Travel Time), invertemos formas de ondas de dez eventos de baixa magnitude (2,0 ≤ M ≤ 4,0), nove usando a nova técnica de inversão de envelopes de formas de ondas e um com o código CSPS e invertemos esses mecanismos focais para o campo de esforço. A realocalização dos eventos mostra que a sismicidade da área está concentrada principalmente em duas faixas sísmicas relativamente estreitas. A inversão de esforço de doze mecanismos focais, 10 obtidos neste trabalho e dois de outros estudos, apresentou um resultado estável do principal eixo de esforço (σ1) azimute ~133° e mergulho ~12°. Concluímos que a inversão de envelopes de forma de onda é uma técnica promissora que pode ser útil na determinação de mecanismos focais de eventos fracos detectados por redes esparsas, onde a inversão da formas de ondas para tais eventos não é eficiente.

Sumário

Lista de Figuras

Lista de Tabelas

CAPÍTULO 1 - INTRODUÇÃO

1.1 A importância do tema da tese

Esta tese é apresentada na forma de artigos e tem como objetivo principal o estudo de fontes sísmicas de eventos de baixas magnitudes (M ≤ 3.5) com epicentros na região central do Brasil envolvendo o estudo de sismicidade, mecanismo focal e inversão para o campo de esforços. A sismicidade do Brasil é menor que em outras Regiões Continentais Estáveis (SCI) semelhantes, como o leste dos Estados Unidos, Índia e Austrália, onde magnitudes superiores a 7.0 já foram observadas. No Brasil apenas duas magnitudes superiores a 6.0 foram detectadas: 6,2 em janeiro de 1955, na litosfera continental (Porto dos Gaúchos/MT) e 6,1 em fevereiro de 1955, na margem passiva no litoral do Espirito Santo (Barros et al. 2011).

A sismicidade brasileira (Figura 1-1) é não uniforme, típica de regiões intraplacas. Existem zonas de alta concentração e outras completamente assísmicas. A ausência de sismos em algumas áreas, como nas regiões norte e centro-oeste pode não estar necessariamente relacionada com assismicidade, pois o processo de ocupação territorial e a tardia instalação de estações sismográficas afetaram os registros históricos e instrumentais nessas duas regiões (Berrocal et al. 1984). As concentrações sísmicas em outras partes, particularmente na região nordeste (estados do Rio Grande do Norte e Ceará), com epicentros distribuídos ao redor da bacia marginal potiguar, refletem, de fato, a presença de uma área sísmica expressiva. Ferreira et al. (1998) mostraram que a atividade sísmica nesta área está confinada nos primeiros 10 km da crosta superior e que um campo de esforços de cisalhamento atua nessa região com compressão paralela e extensão perpendicular à costa. Três terremotos importantes ocorreram nesta área, todos produzindo severos danos em suas respectivas áreas epicentrais intensidades VII na Escala de Mercalli Modificada (MM): terremoto de Pacajus, de 20/11/1980, 5.2 m_b, terremotos de João Câmara, de 30/11/1986 (5,1 m_b) e de São Paulo do Potêngi 10/03/1989 (5,0 m_b) (Assumpção, 1998a, 1998b; Takeya et al., 1989).
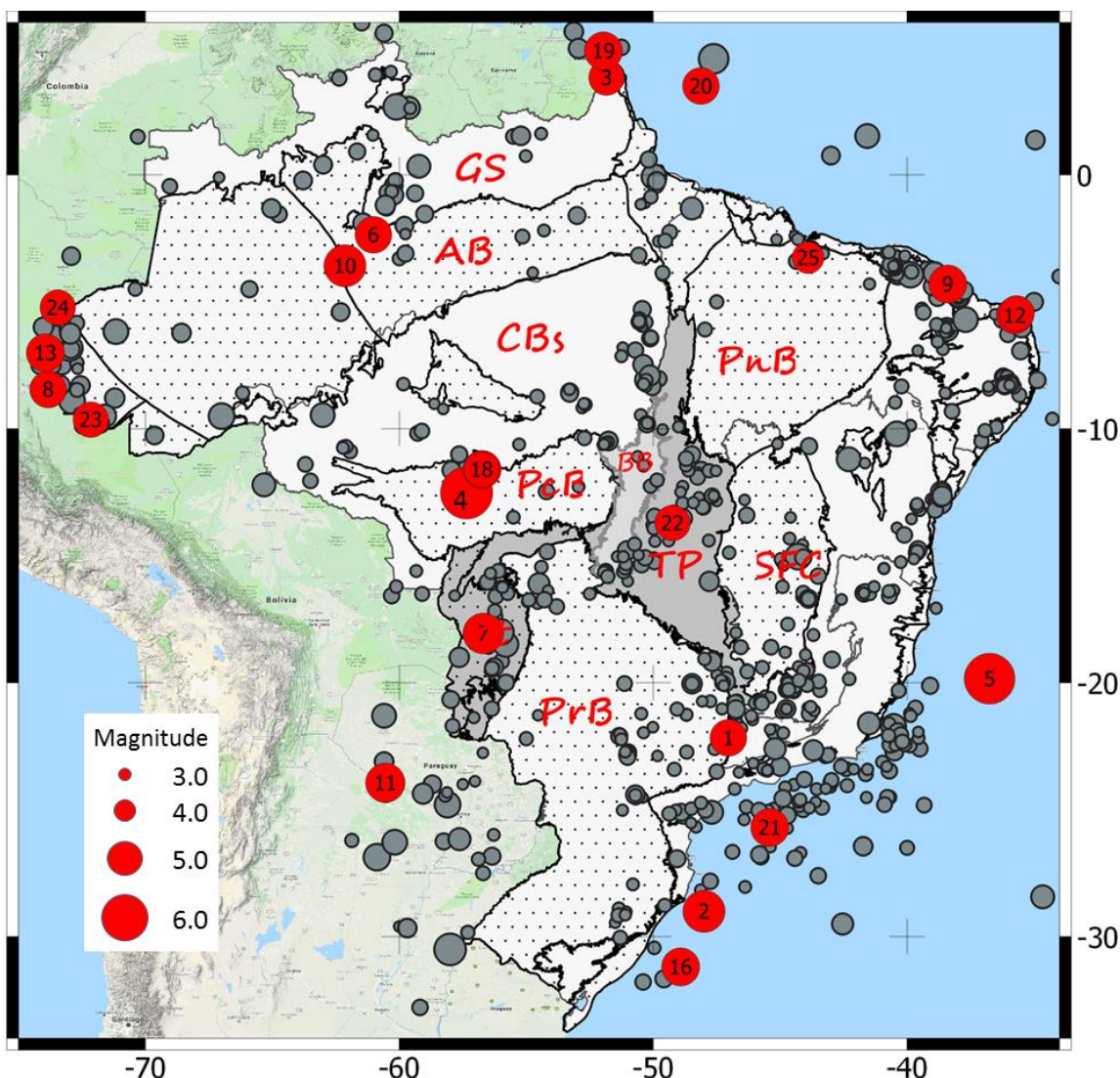
*Figura 1-1 – Catalogo sísmico brasileiro com magnitudes ≥ 3.0 m_b, desde 1720. A área de estudo está destacada pelo retângulo preto. Os círculos vermelhos indicam as magnitudes iguais ou superiores a 5.0 e os círculos azuis indicam os eventos de magnitudes menores que 5.0 e maiores ou iguais a 3.0. As linhas separam as principais províncias geológicas brasileiras (Almeida et al. 2000). GS e CBS denotam os escudos das Guianas e Brasil Central, respectivamente (os quais compõem o Craton Amazonas, formado do Arqueano ao Mesoproterozóico); Bacias Fanerozóicas são: AmB Bacia do Amazonas; PnB Bacia do Parnaíba; PcB Bacia dos Parecis; PrB Bacia do Paraná; Pt Bacia do Pantanal; SFC é o Craton Arqueano a Mesoproterozóico do São Francisco. As faixas de dobramento Neoproterozóicas/Paleozóicas são: TP Província Tocantins, e Província Mantiqueira. Os epicentros são do catálogo de Berrocal et al. (1984) + Boletins Sísmicos Brasileiros (*http://moho.iag.usp.br/eq/bulletin*).*

Uma zona sismica linear SW-NE, que abrange terrenos dos estados de Goiás e Tocantins, é claramente observada no mapa da Figura 1-1 e considerada em outros estudos como paralela, mas não coincidente com o Lineamento Transbrasiliano (LTB). O lineamento é formado por uma série de falhas do

Proterozóico superior e Paleozóico inferior, de direção SW-NE. Essa zona sísmica é correlacionada com altos gravimétricos de direção SW-NE (Fernandes et al. 1991; Assumpção & Sacek 2013; Rocha et al. 2011). Como é uma zona de baixas magnitudes ($m_b \leq 3,5$), somente veio a ser melhor definida recentemente, com a instalação de estações na área (Veloso et al. 1997). O maior sismo associado a essa feição ocorreu em Mara Rosa/GO, magnitude 5,0 m_b, em 8/10/2010 (VI MM) (Barros et al. 2015). Até então o maior evento detectado tinha ocorrido em Aruanã/GO, em 12/07/1993, com magnitude 4,1 m_R e intensidade $I_{máx} = V(MM)$ (Veloso et al. 1997).

A distribuição dos esforços crustais, fundamental para o entendimento da sismicidade intraplaca é, principalmente, determinada com a utilização de mecanismos focais de terremotos. No Brasil, apenas algumas poucas dezenas de mecanismos focais são conhecidas, e isso se deve a dois fatores importantes, baixa sismicidade e escassez de estações sismográficas. Em algumas regiões, como no Centro Oeste e Norte, o estudo de mecanismos focais é ainda mais escasso. Porém, essa realidade vem melhorando com à implantação da Rede Sismográfica Brasileira (RSBR) a partir de 2013.

O estado dos esforços na região da intraplaca brasileira resulta da combinação de forças de origem regional e local. As forças locais são causadas por heterogeneidades estruturais resultantes de carregamento da crosta, como forças de flexuras e anomalias térmicas na astenosfera (Assumpção 1992). As de origem regional estão relacionadas com forças tectônicas originadas nas bordas e contato de placas, tais como: empurrão da dorsal Mesoatlântica, produzindo esforço de compressão no interior da placa Sul Americana e forças de oposição produzidas no contato da placa Sul Americana (SA) com as placas de Nazca, do Caribe à norte e da Escócia ao sul. As duas últimas (Caribe e Escócia) devido ao movimento transcorrente e a primeira (Nazca) devido à subducção sob a placa Sul Americana. Por último, o empuxo negativo da placa de Nazca sob a Sul Americana (Assumpção 1992), que faz a placa de Nazca, mais densa e fria, afundar por debaixo da SA exercendo sobre esta um esforço de compressão e freando o seu movimento para oeste.

A determinação de mecanismos focais é muito importante, não só para melhorar o conhecimento da distribuição dos esforços na litosfera, mas também para inferir sobre os processos físicos que ocorrem durante um terremoto, ou seja, durante o rompimento da falha.

O método mais comum adotado na solução dos planos nodais de terremotos usa a direção de movimento da primeira chegada da onda P (polaridade do primeiro movimento, que pode ser (*UP/DOWN*) e/ou a razão de amplitudes da onda S com a onda P: S vertical e a P (SV/P), S horizontal e a P (SH/P) e S vertical com S horizontal (SV/SH). A grande desvantagem dessa técnica é o fato de requerer o registro claro do evento em muitas estações, com distribuição mais ou menos uniforme em torno da área epicentral, condição difícil de ser atingida em regiões de baixa sismicidade e rede sismográfica esparsa, como é o caso do Brasil.

Para superar essas dificuldades, nesta tese são utilizadas três técnicas independentes que envolvem a extração de informações de todo o sismograma, e não só das primeiras chegadas da onda P. quais sejam: inversão de formas de ondas; inversão de envelopes de formas de ondas e; uma combinação de inversão de formas de ondas e polaridades. Nos três casos, o número de estações requeridas diminui enormemente, ou seja, com apenas poucas estações é possível determinar a solução dos planos nodais, daí a relevância do tema desta tese.

Para aumentar a confiabilidade dos resultados e também diminuir o esforço computacional, foi incluído no pré-processamento a utilização das poucas polaridades disponíveis, implicando na diminuição do conjunto total de soluções possíveis a serem invertidas. Com esse procedimento, somente são processadas as soluções que atendem ao critério de polaridades.

O método de inversão de formas de ondas já foi empregado com sucesso na área de estudo por Carvalho et al. (2016), na determinação de parâmetros de fonte de réplicas do evento principal de Mara Rosa, de 08/10/2010, magnitude 5.0 m_R e intensidade VI MM (Barros et al. 2015; Dias et al. 2016).

Portanto, esta tese envolve a determinação dos paramentos de fonte de sismos de baixas magnitudes, com epicentros na região central do Brasil, Figura 1-2, usando as três técnicas mencionadas com restrições feitas pela distribuição apropriada das poucas polaridades disponíveis.

A inversão de formas de ondas foi realizada com o código ISOLA (veja capitulo 2), desenvolvido por Sokos & Zahradnik (2008); Sokos & Zahradnik (2013). Este código determina o Momento Tensor (MT) pelo método dos mínimos quadrados, identificando a melhor fonte, sua localização e tempo do centroide. As funções de Green são calculadas seguindo o método do número de ondas discreto, desenvolvido por Bouchon (1981) com a utilização do modelo de velocidade (1D) NewBR (Assumpção et al. 2010). Uma análise de incerteza nos resultados inerentes a falta de resolução nos modelos de velocidade usados nessa tese é assunto é tratado no artigo 1 (capítulo 3).

Esta tese está dividida em seis capítulos: Capítulo 1, introdução, apresenta o problema, justificativa, área de estudo, dados, e objetivos gerais e específicos; Capítulo 2 apresenta a metodologia adotada na obtenção de mecanismos focais por polaridades e inversão de formas de ondas, bem como por inversão de envelope (ENV) de formas de ondas. Por último, nesse capítulo é apresentado o método de inversão de mecanismos focais para a obtenção do esforço resultante ou estado dos esforços na área de estudo; no capítulo 3 é apresentado o primeiro artigo da tese *Compromising polarity and waveform constraints in focal-mechanism solutions; the Mara Rosa 2010 M_w 4 central Brazil earthquake revisited,* publicado no *Journal of South American Earth Science*; no capítulo 4 é apresentado o segundo artigo *Inversion for focal mechanism using waveforms envelope and inacurate velocity models, examples for Brazil,* publicado no *Buletin of Seismological Society of America*; no Capítulo 5, artigo 3 *Earthquake relocation, focal mechanism and stress field determination in central Brazil,* submetido ao *Journal South American Earth Science* e, finalmente, no capitulo 6 são apresentadas as discursões e conclusões.

1.2 Área de estudo e Dados

O retângulo preto, destacado nos mapas das 1-1 e Figura 1-3, mostra a área de estudo, região central do Brasil com 910.000 km^2, que compreende várias províncias geológicas: o Craton da Amazônia Oriental; sudoeste da Bacia do Parnaíba; porção ocidental do Cráton São Francisco; norte da Bacia do Paraná, e inclui quase toda a província do Tocantins. A estrutura principal da área consiste de um conjunto de estruturas geológicas formadas no Neoproterozóico, pela convergência do Craton São Francisco e do Craton Amazônico, durante a formação da parte oriental do supercontinente Gondwana (Fuck 1994; Fuck et al. 1994). Essas estruturas são denominadas de lineamento Transbrasiliano (LTB) com orientação SW-NE.

A área de estudo é caracterizada principalmente por eventos de baixas magnitudes (M <4); apenas 11 eventos relatados no catálogo sísmico Brasileiro (CSB) com M>=4 ocorreram, e apenas um com magnitude 5. Nos últimos cinco anos foram registrados apenas 2 eventos com magnitudes acima de quatro. No CSB (1724-2019), Figura 1.2, é possível distinguir uma faixa sísmica seguindo o lineamento LTB e alguns eventos dispersos nas áreas ao norte, a oeste e a leste. A Faixa Sísmica Goiás Tocantins (GTSZ) se estende desde o noroeste da Bacia do Paraná até o sudoeste da Bacia do Parnaíba e cuja expressão geofísica é caracterizada pelas altas anomalias gravimétricas junto à faixa de dobramento Tocantins Araguaia (Assumpção et al. 1986; Fernandes et al. 1991).
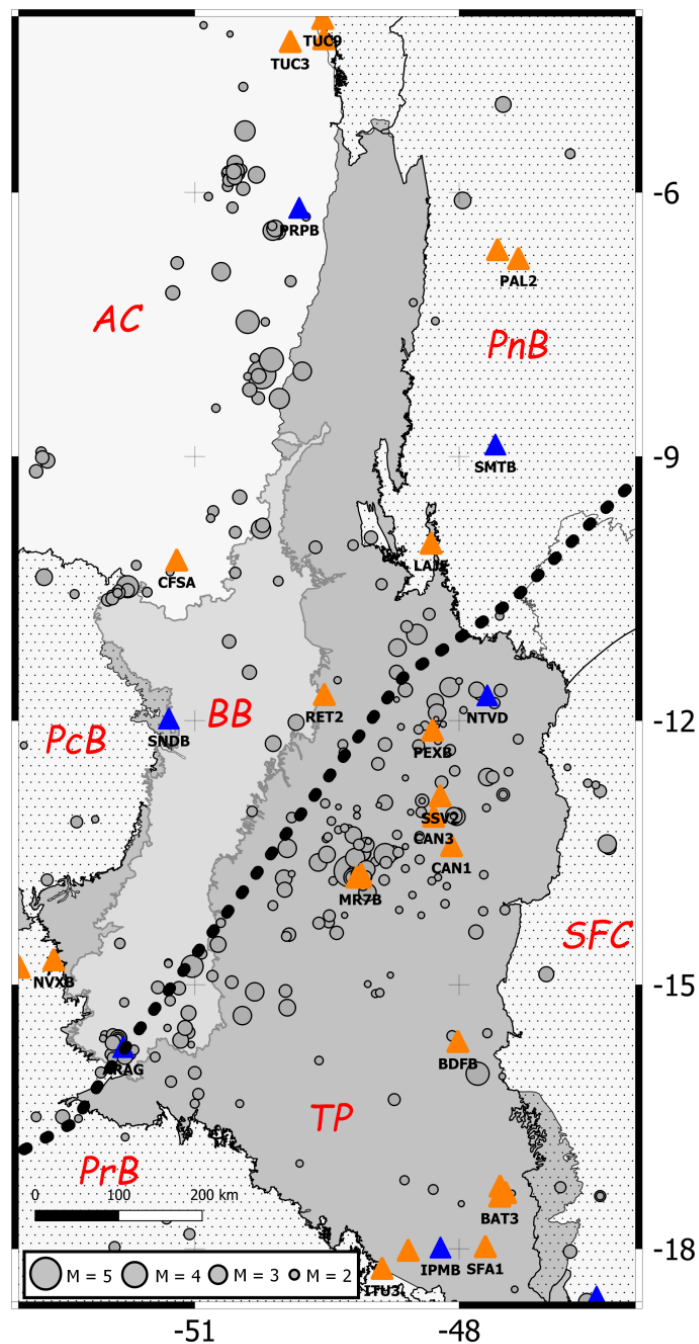
Figura 1-2 – Sismicidade da área de estudo - Zona Sísmica Brasil Central. A linha pontilhada indica o Lineamento Transbrasiliano. As principais províncias geológicas são indicadas: Cráton São Francisco (SFC), Cráton Amazônico (AC), Bacia Parnaíba (PnB), Bacia Parecis (PcB), Bacia Paraná (PrB), Bacia Bananal (BB) e Província Tocantins (TP). Os círculos cinzas denotam eventos do catalogo sísmico Brasileiro, classificados por magnitude. Os triângulos indicam as localizações das estações sismográficas: Estações da RSBR (azul), e Rede do SIS-UnB incluindo a estação da rede Global BDFB (laranja).

Os dados utilizados nesta tese foram detectados pelas estações da Rede Sismográfica Brasileira (RSBR), (triângulos azuis); estações da rede mundial

(GT – triângulo verde) e pelas estações da rede do Observatório Sismológico da Universidade de Brasília SIS-UnB (triângulos laranja), Figura 1-3. As estações da RSBR são todas de banda larga, na faixa de 120 s a 100 Hz, as estações do SIS – UnB são de banda larga e de período curto (1Hz a 100 Hz). O sensor da estação da Rede Mundial (BDFB) é de banda larga e instalada em poço profundo, portanto, é uma estação de baixo ruído.
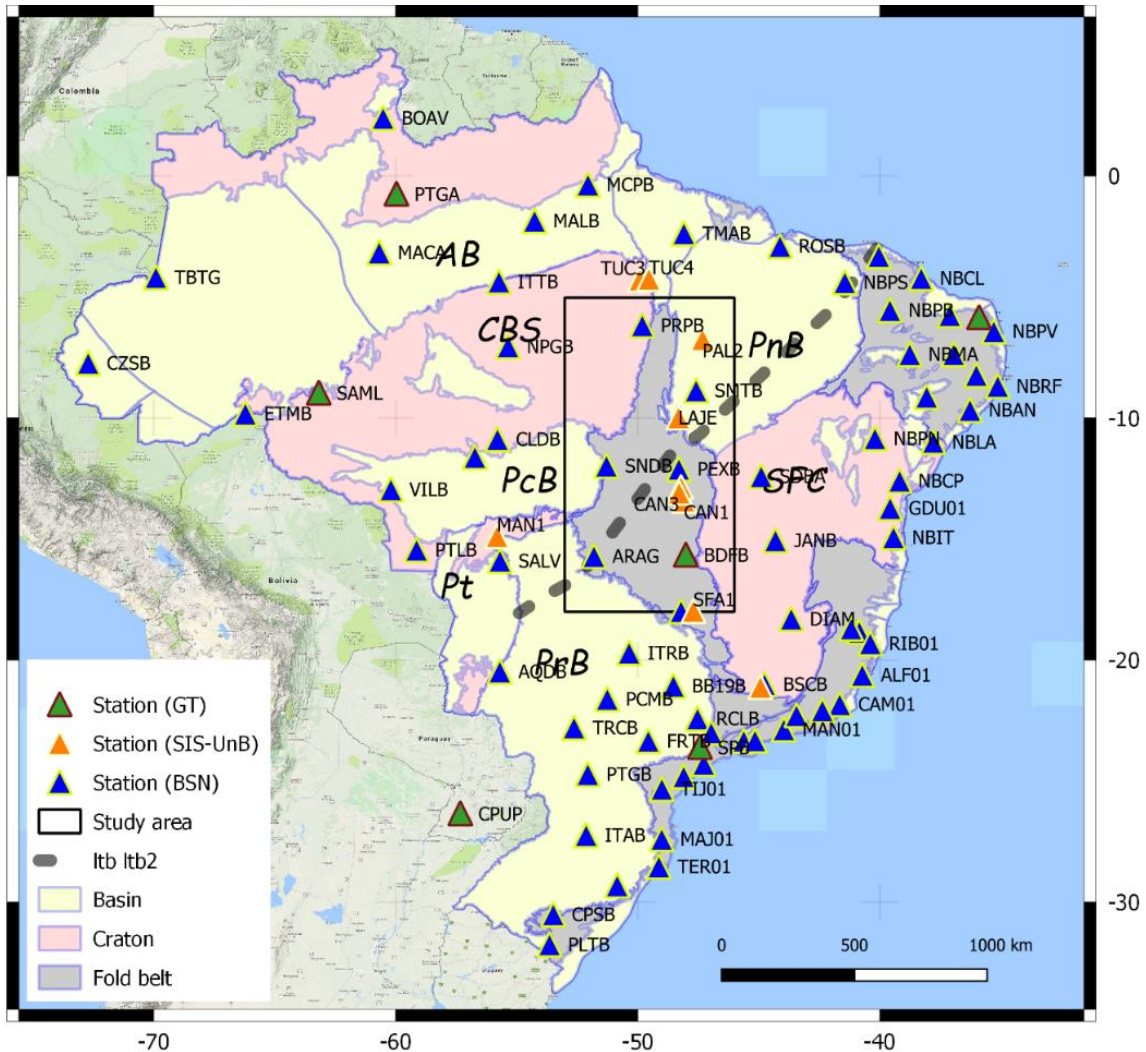
Figura 1-3 – Mapa com as estações da Rede Sismográfica Brasileira (RSBR) (triângulos azuis), estações da rede do Observatório Sismológico (triângulos laranja) e estações da rede mundial (triângulos verdes). A área de estudo está indicada pelo retângulo preto. São mostradas também as províncias geológicas descritas na Figura 1.1.

Os eventos ocorridos na área são, em sua maioria, de baixas magnitudes e para possibilitar um trabalho de qualidade, adotou-se dois critérios de seleção de eventos do catalogo ocorridos na área de estudo (337), com potencial de

serem relocalizados com baixos erros e para serem invertidos para o momento tensor. No primeiro caso foram selecionados 118 eventos (Tabela 1-1) e no seguinte critério: registrados por no mínimo quatro estações, cobertura azimutal mínima de 180° e ocorrência após 2010 e no segundo critério foram selecionados 10 eventos seguindo o seguinte critério: registrado por no mínimo 4 estações a distancias menores que 300 km, boa relação sinal-ruído na faixa de frequência 0.8 Hz a 1.2 Hz e ocorrência após 2010,Tabela 1-2.

Tabela 1-1 – Eventos do Catalogo Sísmico Brasileira usados na relocalização. Os eventos destacados em negrito foram selecionados para inversão de formas de ondas para mecanismo focal.

Nu.	Data	Hora	Lat (°)	Lon (°)	Mag (m_R*)
1	08/10/2010	20:16:52	-13.710	-49.240	5.0
2	08/10/2010	20:25:20	-13.770	-49.160	2.2
3	**08/01/2011**	**11:49:23**	**-13.580**	**-48.890**	**4.1**
4	26/02/2011	22:51:31	-13.780	-49.210	3.2
5	**02/03/2011**	**19:16:56**	**-11.450**	**-48.710**	**2.2**
6	04/03/2011	06:59:41	-13.780	-49.210	3.3
7	30/04/2011	08:16:21	-11.170	-48.700	2.2
8	24/04/2012	01:34:13	-13.770	-49.110	2.2
9	19/07/2012	14:59:06	-15.630	-51.160	3.4
10	28/07/2012	12:49:26	-15.490	-51.110	3.3
11	08/12/2012	18:52:34	-13.560	-49.180	3.7
12	22/06/2013	06:04:50	-13.950	-49.040	3.5
13	30/07/2013	04:22:02	-13.770	-49.060	3.0
14	15/05/2014	15:03:30	-10.450	-48.880	2.8
15	19/06/2014	04:39:30	-16.240	-50.960	2.8
16	19/07/2014	12:37:06	-13.680	-48.610	2.3
17	07/08/2014	20:13:41	-14.290	-49.480	2.3
18	06/09/2014	23:11:17	-12.940	-49.520	2.5
19	09/09/2014	16:02:19	-14.210	-49.300	2.0
20	30/09/2014	05:02:26	-11.880	-47.950	2.1
21	28/10/2014	01:40:29	-12.980	-49.370	2.3
22	23/11/2014	00:46:09	-15.321	-51.071	3.1
23	25/12/2014	16:41:50	-10.234	-51.664	2.4
24	31/12/2014	03:09:34	-7.880	-50.320	2.6
25	18/01/2015	00:33:13	-8.090	-50.400	2.4
26	19/01/2015	03:54:16	-7.470	-50.200	2.3
27	23/01/2015	05:06:29	-13.220	-49.300	2.4
28	29/01/2015	05:22:04	-15.490	-51.310	2.2
29	**11/02/2015**	**09:46:33**	**-10.478**	**-51.762**	**4.0**

Nu.	Data	Hora	Lat (°)	Lon (°)	Mag (m$_R$*)
30	12/02/2015	04:44:39	-12.530	-46.770	2.0
31	12/02/2015	13:07:35	-10.518	-51.761	2.7
32	15/02/2015	12:25:25	-10.543	-51.867	2.9
33	19/02/2015	01:25:07	-12.650	-48.610	2.3
34	05/03/2015	20:05:42	-15.100	-48.950	2.3
35	11/03/2015	03:57:51	-10.564	-51.950	2.3
36	11/03/2015	11:24:01	-14.100	-50.114	2.4
37	16/03/2015	19:44:54	-9.620	-50.790	2.7
38	30/03/2015	03:32:37	-10.627	-51.986	2.6
39	01/04/2015	08:09:08	-10.612	-51.936	2.8
40	07/04/2015	11:50:18	-9.167	-52.800	3.0
41	08/04/2015	20:25:21	-15.090	-48.900	3.0
42	**09/04/2015**	**16:09:26**	**-16.304**	**-48.736**	**2.4**
43	18/04/2015	13:19:29	-10.310	-51.280	2.7
44	19/05/2015	20:24:18	-13.800	-49.130	2.3
45	16/06/2015	08:20:19	-9.700	-50.820	2.4
46	19/06/2015	01:13:01	-14.750	-51.300	2.4
47	19/06/2015	03:01:40	-11.760	-48.710	2.1
48	22/06/2015	14:00:27	-9.010	-52.730	2.0
49	24/06/2015	13:00:45	-13.040	-48.550	3.1
50	**07/07/2015**	**21:17:32**	**-12.057**	**-48.388**	**2.0**
51	29/07/2015	06:55:04	-8.450	-50.760	2.4
52	16/08/2015	19:47:10	-13.120	-52.130	2.4
53	15/09/2015	21:27:05	-14.542	-50.735	2.3
54	17/09/2015	10:24:47	-14.760	-51.300	3.2
55	21/09/2015	22:13:54	-10.500	-51.870	2.2
56	27/09/2015	07:15:10	-5.560	-46.740	2.3
57	27/09/2015	17:41:58	-13.808	-52.675	2.6
58	08/10/2015	18:25:41	-15.860	-49.590	2.7
59	12/10/2015	03:21:25	-12.730	-46.450	2.4
60	24/10/2015	20:02:28	-12.070	-48.660	2.3
61	**15/11/2015**	**10:55:11**	**-12.284**	**-48.460**	**2.0**
62	25/11/2015	20:19:07	-13.340	-49.510	2.6
63	13/12/2015	17:46:21	-8.085	-50.275	2.3
64	16/12/2015	03:12:42	-13.000	-49.160	3.1
65	16/12/2015	18:59:33	-14.648	-50.921	2.3
66	25/12/2015	18:10:14	-12.580	-47.440	2.4
67	18/01/2016	18:29:12	-14.297	-50.704	2.2
68	**30/01/2016**	**07:40:30**	**-13.871**	**-49.091**	**2.3**
69	13/02/2016	09:02:48	-10.414	-50.052	2.4
70	28/03/2016	02:41:42	-17.832	-51.060	2.5
71	29/03/2016	03:35:21	-13.697	-49.069	2.6

Nu.	Data	Hora	Lat (°)	Lon (°)	Mag (m_R*)
72	06/04/2016	07:40:49	-7.460	-48.270	2.0
73	01/05/2016	02:33:30	-9.780	-50.230	2.3
74	08/06/2016	12:28:43	-11.550	-48.000	3.2
75	11/06/2016	21:51:17	-12.210	-47.330	2.2
76	08/07/2016	23:07:11	-12.040	-48.180	2.6
77	03/08/2016	21:41:29	-10.540	-51.540	2.0
78	08/08/2016	02:02:18	-13.407	-49.136	2.6
79	12/08/2016	17:14:47	-7.250	-48.520	2.4
80	04/10/2016	01:18:01	-8.335	-50.280	2.3
81	07/10/2016	19:59:57	-13.688	-49.053	3.6
82	29/10/2016	03:47:32	-8.240	-50.377	3.6
83	07/12/2016	03:30:18	-12.990	-47.690	3.6
84	25/12/2016	13:59:35	-6.434	-50.116	2.3
85	11/01/2017	10:05:12	-13.610	-48.830	3.8
86	28/01/2017	00:36:39	-13.320	-49.490	2.9
87	12/03/2017	02:27:41	-13.769	-49.057	2.4
88	14/04/2017	16:01:02	-15.996	-52.065	2.8
89	18/05/2017	16:55:57	-12.333	-48.104	2.3
90	26/05/2017	17:58:20	-12.130	-48.290	2.4
91	07/06/2017	08:41:15	-12.710	-46.540	2.0
92	12/06/2017	01:23:43	-17.658	-51.320	2.5
93	22/06/2017	02:25:29	-16.040	-47.510	2.4
94	31/08/2017	06:41:00	-6.408	-50.089	2.0
95	09/09/2017	04:13:42	-15.814	-51.793	3.4
96	21/09/2017	08:33:58	-13.750	-49.142	3.2
97	01/10/2017	01:46:22	-5.832	-50.563	3.2
98	**04/10/2017**	**16:46:57**	**-5.779**	**-50.547**	**3.2**
99	12/10/2017	22:40:22	-12.960	-48.910	3.4
100	09/11/2017	06:18:24	-13.750	-49.160	2.2
101	23/11/2017	02:52:25	-5.750	-50.570	2.2
102	03/12/2017	07:03:28	-10.810	-47.540	2.6
103	**25/12/2017**	**13:59:35**	**-50.090**	**-6.420**	**3.8**
104	03/01/2018	05:55:23	-12.060	-48.250	2.2
105	18/01/2018	11:39:51	-13.740	-49.900	2.2
106	20/01/2018	12:09:24	-13.920	-49.980	2.1
107	24/01/2018	22:53:23	-5.860	-50.610	3.2
108	13/02/2018	04:51:05	-12.230	-48.240	3.0
109	02/03/2018	04:17:51	-6.380	-50.120	2.2
110	15/03/2018	20:48:58	-10.931	-48.594	2.4
111	**12/04/2018**	**03:56:34**	**-17.370**	**-47.400**	**2.8**
112	12/05/2018	02:36:22	-10.320	-50.540	2.1
113	26/05/2018	13:45:40	-13.830	-49.100	2.6

Nu.	Data	Hora	Lat (°)	Lon (°)	Mag (m_R*)
114	03/07/2018	01:25:12	-15.680	-51.040	2.5
115	04/08/2018	13:42:32	-11.540	-49.380	2.1
116	21/08/2018	00:19:27	-13.800	-49.110	2.0
117	11/09/2018	05:57:19	-10.562	-52.365	2.6
118	14/09/2018	06:08:26	-12.490	-48.921	2.2

Tabela 1-2 – Eventos usados na inversão de envelopes de formas de onda e CSPS.

Nu*.	Data	Hora	Lat (°)	Lon (°)	Mag (m_R*)
3	08/01/2011	11:49:23	-13.580	-48.890	4.1
5	02/03/2011	19:16:56	-11.450	-48.710	2.2
29	11/02/2015	09:46:33	-10.478	-51.762	4.0
42	09/04/2015	16:09:26	-16.304	-48.736	2.4
50	07/07/2015	21:17:32	-12.057	-48.388	2.0
61	15/11/2015	10:55:11	-12.284	-48.460	2.0
68	30/01/2016	07:40:30	-13.871	-49.091	2.3
98	04/10/2017	16:46:57	-5.779	-50.547	3.2
103	25/12/2017	13:59:35	-50.090	-6.420	3.8
111	12/04/2018	03:56:34	-17.370	-47.400	2.8

Nu* = numeração de eventos equivalente a Tabela 1-1

1.4. Modelos de velocidades

A crosta terrestre é formada por varias camadas com espessura variando conforme a geologia local. As velocidades nas camadas são definidas pelas propriedades elásticas do meio. A fronteira entre a crosta e o manto, definida por um contraste acentuado na velocidade sísmica é denominada de descontinuidade de Mohorovičić (Moho). Na localização de um evento sísmico se utilizam os tempos de chegadas das diversas fases sísmicas nas estações de uma rede sismográfica e um modelo teórico de velocidades em relação ao qual as localização são feitas. Portanto, da precisão do modelo utilizado depende a qualidade das localizações. Neste trabalho, utilizou-se os seguintes modelos de velocidades:

O modelo 1D NewBR (Assumpção et al., 2010) foi utilizado na inversão de formas de ondas e de envelope de formas de ondas. Os modelos 1D Barros (Barros et al. 2015), Soares/Soares_gradient (J. Soares et al. 2006) e Dias

(Dias et al. 2016) foram realizados em testes variados e relatados nos artigos da tese Tabela 1-3 e Figura 1-4. O modelo 3D RSTT – *Regional Seismic Travel Time* (Myers et al. 2010) foi utilizado na relocalização dos eventos selecionados da Tabela 1-1. Este assunto será novamente abordado nos capítulos referentes aos artigos.

Tabela 1-3 – Modelos de velocidades usados na inversão e testes nos artigos dessa tese. A razão VP/VS dos modelos são: Dias = 1.74, Barros = 1.70; NewBR = 1.72 e Soares = 1.70.

Depth	Dias (P)	Depth	Barros (P)	Depth	NewBR (P)	Depth	Soares (P)
0.0	5.55	0.0	6.00	0.0	5.80	0.0	5.810
2.0	5.78	12.0	6.60	20.0	6.40	2.0	6.150
3.0	5.94	25.0	6.80	42.0	8.10	12.0	6.520
4.0	6.02	38.0	8.30				
12.0	6.09						
13.7	6.12						
15.6	6.15						
17.3	6.20						
20.0	6.23						
22.0	6.27						
22.5	6.29						
38.0	6.31						
42.0	7.31						
54.3	7.35						
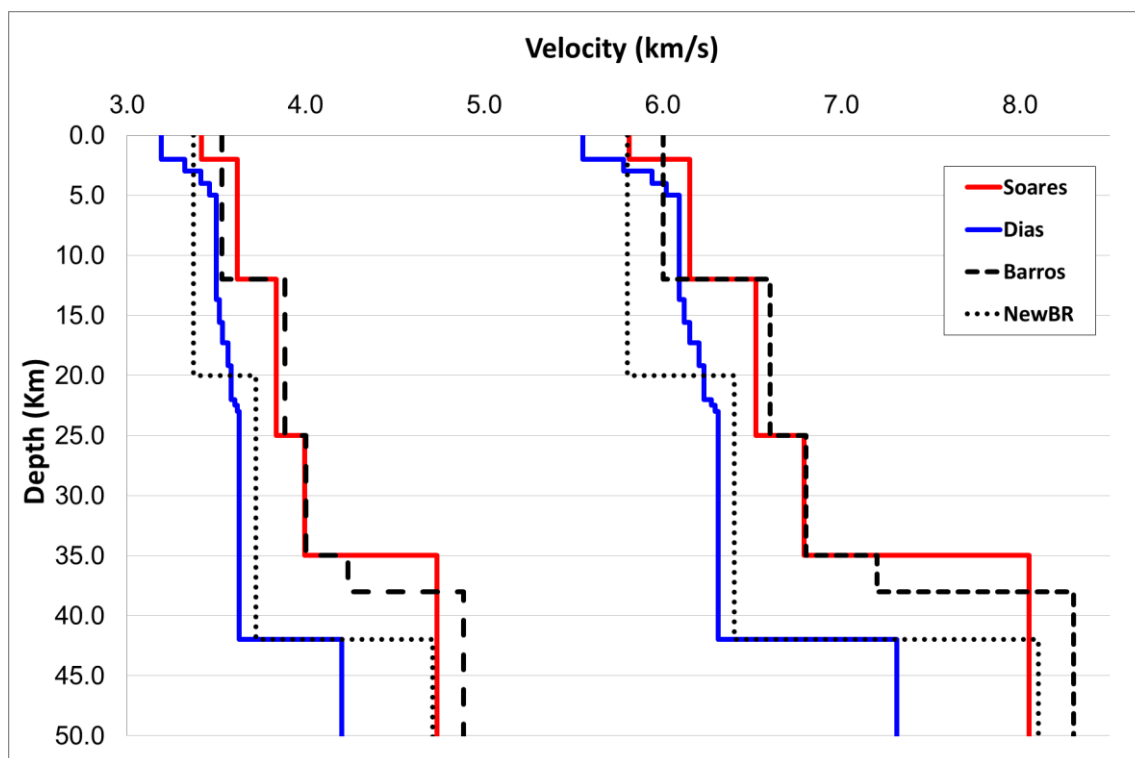
Figura 1-4 – Modelos de velocidades usados nessa tese Soares (vermelho), Dias (azul), Barros (pontilhado) e NewBR (tracejado). Dias = 1.74, Barros = 1.70, NewBR = 1.72 e Soares = 1.70. A descontinuidade da Moho nos modelos usados são: Soares = 35 km; Barros = 38 km e Dias, NewBR = 42 km.

1.3   Objetivos

São objetivos gerais desta tese, o estudo de fontes sísmicas de eventos de baixas magnitudes (2.0 ≤ M ≤ 4.0) com epicentros na região central do Brasil, compreendendo da relocalização hipocentral com o modelo RSTT, determinação de momento tensor e inversão dos mecanismos focais para obtenção do estado dos esforços.

1.3.1   Objetivos específicos:

1. Estudar as incertezas envolvidas no processo de obtenção de mecanismos focais por polaridades (artigo 1, capítulo 3);

2. Elaborar ferramenta (metodologia) que possibilite a inversão de formas de ondas de eventos de baixas magnitudes (artigo 2, capítulo 4);

3. Relocalizar os eventos da Tabela 1.1 com o código iLoc (Bondar, 2011) e modelo RSTT (Myers et al. 2010);

4. Correlacionar os eventos relocalizados com as estruturas geológicas existentes;

5. Determinar mecanismos focais para os eventos da Tabela 1.2;

6. Inverter os mecanismos focais para obtenção do estado dos esforços na área de estudo.

Os itens 3-6 são abordados e discutidos no artigo 3, capítulo 5.

1.4 Resumo dos artigos

Nesta seção são apresentados os resumos em português dos dois trabalhos já publicados e do terceiro submetido.

1.4.1 Artigo 1 – Capítulo 3

Compromising polarity and waveform constraints in focal-mechanism solutions; the Mara Rosa 2010 M_w 4 central Brazil earthquake revisited.

A determinação do mecanismo focal de eventos fracos registrados em redes esparsas é um desafio. Frequentemente usamos o primeiro movimento das fases P de estações relativamente distantes, mas a modelagem das formas de ondas é viável apenas em algumas estações próximas. Uma abordagem em duas etapas de como combinar esses dados foi sugerida recentemente por Fojtikova & Zahradnik (2014) (método CSPS - *Cyclic Scanning of the Polarity Solutions*). O processamento começa com a determinação de um conjunto de soluções a partir das polaridades disponíveis que muitas vezes é disperso e não possibilita a obtenção de uma fonte exclusiva, mas sim um grupo disperso de fontes (~100 - 500 fontes). O próximo passo consiste em repetir a inversão completa da forma de onda apenas para as soluções obtidas com polaridades. Mesmo utilizando poucas estações (6-10) pode se eficientemente reduzir a não-exclusividade das soluções de polaridade. Também é possível obter uma

estimativa das soluções de *double-couple* bem ajustadas. Nesse artigo propomos um novo recurso ao método CSPS, ou seja, inversões repetidas usando múltiplos conjuntos de polaridade. Os conjuntos de polaridades são criados projetando as estações na esfera focal correspondendo aos vários modelos de velocidade conhecidos, contabilizando assim a incerteza do ângulo de saída da onda (*takeoff angle*). Os conjuntos de polaridades múltiplas permite uma avaliação da estabilidade da solução CSPS. Essa ideia é demonstrada na análise de um evento no Brasil central com magnitude Mw ~4,3 e ocorrido em Mara Rosa 2010. Foi utilizado 11 polaridades provenientes de estações regionais a distâncias variando de 81 km até 730 km. Foi utilizado o método de inversão de formas de onda completas em duas estações apenas (CAN3 e BDFB) com distancias epicentrais de 120 km e 240 km respectivamente, e para bandas de frequências independentes 0.1-0.2 Hz (CAN3) e 0.05-0.125 Hz (BDFB). Para os testes os conjuntos de polaridades foram classificados em seis categorias conforme os ângulos de saída demonstrando que para essa simulação uma mesma estação pode ocupar até seis posições na esfera focal traduzindo em incertezas nos parâmetros de inversão. Os resultados obtidos mostraram estabilidade, mas, pode se verificar uma dispersão nos planos nodais em consequência das incertezas ângulos de saída. O mecanismo focal de Mara Rosa teve um desvio na solução de até 38° *K-Angle* (Kagan 1992). O estudo também inclui um teste simulando situações em que apenas uma única forma de onda é usada e o resultado mostrou que a estabilidade da solução foi afetada negativamente.

1.4.2   Artigo 2 – Capítulo 4

Inversion for focal mechanisms using waveform envelopes and inaccurate velocity models, examples from Brazil

Um dos maiores desafios para a determinação do momento tensor está associados a eventos de magnitude relativamente baixas (M_w ~4) registrados por poucas estações e, às distâncias das estações mais próximas que são relativamente grandes (300 km a 600 km). As dificuldades surgem durante a inversão devido às formas de ondas sintéticas produzidas com modelos genéricos usados para localização de eventos não serem comparáveis com as formas de onda reais; propiciando desvios no tempo e discrepâncias nas amplitudes, por exemplo, os modelos de velocidade são compilados para minimizar os resíduos de localização, e essas técnicas não são sensíveis a camadas superficiais mais rasas que não tem raios se propagando ate as estações. A situação é ainda pior quando, em alguns casos, as formas de ondas sintéticas tem boa correlação com as observadas, mas o mecanismo focal obtido é incorreto. Este artigo investiga uma metodologia alternativa, mais robusta em relação aos modelos de velocidade genéricos: que é a inversão dos envelopes das formas de ondas. O método foi desenvolvido de forma empírica e estuda os efeitos de modelos de velocidade em formas de onda sintéticas e propõe que a informação da fonte, mecanismo focal, está codificada na variação das formas dos envelopes e na variação das amplitudes entre as componentes dos sismogramas. O método foi testado em dados sintéticos e em dados reais de dois terremotos ocorridos no Brasil: a Mara Rosa (M_w 4,3, 2010) e Maranhão (M_w 4,3, 2017). Quando comparado com soluções de estudos anteriores, baseadas em muitas polaridades e modelos específicos, fonte estação, obtidos através da analise da dispersão de ondas de superfície, obtivemos em ambos os casos o mesmo mecanismo com um único modelo 1D genérico, e usando apenas uma de polaridade. A inversão de envelopes de formas de ondas é uma técnica promissora que pode ser aplicada em regiões como no Brasil que tem atividade sísmica de baixas magnitudes e associado ao fato de o monitoramento ser feito com uma rede sismográfica esparsa.

1.4.3 Artigo 3 – Capítulo 5

Earthquake relocation, focal mechanism and stress field determination in central Brazil

Artigo submetido para a revista *Journal South American Earth Science* (JSAMES)

Submetido em 22 de maio de 2019

Neste trabalho, realizamos uma investigação da sismicidade na região central do Brasil (área de estudo). Esta grande área (910.000 km^2) é cercada por várias províncias geológicas: o Cráton da Amazônia; Bacia do Parnaíba; Cráton do São Francisco; Bacia do Paraná, e a área inclui quase toda a província do Tocantins e é integralmente cruzada, na direção SW-NE, pela descontinuidade de escala continental - lineamento Transbrasiliano (LTB). No catálogo sísmico brasileiro (1724-2019), é possível distinguir uma faixa sísmica seguindo o lineamento LTB e muitos eventos dispersos nas áreas norte, oeste e leste. A área de estudo é caracterizada principalmente por eventos de baixas magnitudes (M<4); apenas 11 eventos relatados no catálogo com M>4 ocorreram, e entre eles apenas um com magnitude 5. Com base em um critério de qualidade, um conjunto de 118 eventos de 337 presentes no catálogo, foi selecionado para uma análise completa neste artigo. Este trabalho foi dividido em três partes: (i) Relocalização de eventos com o código iLoc e o modelo de velocidade RSTT (Regional Seismic Travel Time); (ii) determinação de mecanismos focais de 10 eventos, nove usando envelopes de forma de onda e polaridades e um com o código CSPS, e; (iii) Inversão de mecanismos focais para o campo de esforço. O resultado do estudo mostra que a sismicidade da área está concentrada principalmente em duas faixas relativamente estreitas e o principal eixo de esforço da área é bem resolvido, apresentando azimute ~133° e mergulho ~12°. Para estudar eventos de pequenas magnitudes em uma área tão grande, a instalação de estações sísmicas adicionais é necessária, assim como mais estudos de replicas por redes locais temporárias.

1.5   Referências (Introdução)

Almeida, F.F.M. de, Brito Neves, B.B. de, Dal Ré Carneiro, C., 2000. The origin and evolution of the South American Platform. Earth-Science Rev. 50, 77–111. https://doi.org/10.1016/S0012-8252(99)00072-0

Assumpção, M., 1998a. Seismicity and stresses in the Brazilian passive margin. Bull. Seismol. Soc. Am. 88, 160–169.

Assumpção, M., 1998b. Focal mechanisms of small earthquakes in the southeastern Brazilian shield: a test of stress models of the South American plate. Geophys. J. Int. 133, 490–498. https://doi.org/10.1046/j.1365-246X.1998.00532.x

Assumpção, M., 1992. The regional intraplate stress field in South America. J. Geophys. Res. 97, 11889. https://doi.org/10.1029/91JB01590

Assumpção, M., Ardito, J.E., Barbosa, J.R., 2010. An improved velocity model for regional epicentre determination in Brazi. IV Simpóosio Bras. Geofísica. Brasília 13 e 16 de novembro de 2010.

Assumpção, M., Barbosa, J.R., Berrocal, J., Bassini, A.M., Veloso, J.A. V., Marza, V.I., Huelsen, M.G., Ribotta, L.C., 1997. Seismicity patterns and focal mechanisms in southeastern Brazil. Bras. Geofísica 15, 119–132.

Assumpção, M., Lima, T.M., Tomás, L.A., 1986. O sismo de Araguapaz de 14.01.1986 e o Lineamento Transbrasiliano, in: 34o Congresso Brasileiro de Geologia, GoiâNia. p. 5p.

Assumpção, M., Sacek, V., 2013. Intra-plate seismicity and flexural stresses in central Brazil. Geophys. Res. Lett. 40, 487–491. https://doi.org/10.1002/grl.50142

Barros, L.V., Assumpção, M., Quintero, R., Caixeta, D., 2009. The intraplate Porto dos Gaúchos seismic zone in the Amazon craton — Brazil. Tectonophysics 469, 37–47. https://doi.org/10.1016/j.tecto.2009.01.006

Barros, L.V., Assumpção, M., Quintero, R., Ferreira, V.M., 2011. Coda wave attenuation in the Parecis Basin, Amazon Craton, Brazil: sensitivity to basement depth. J. Seismol. 15, 391–409. https://doi.org/10.1007/s10950-011-9231-1

Barros, L. V., Assumpção, M., Chimpliganond, C., Carvalho, J.M., Von Huelsen, M.G., Caixeta, D., França, G.S., de Albuquerque, D.F., Ferreira, V.M., Fontenele, D.P., 2015. The Mara Rosa 2010 GT-5 earthquake and its possible relationship with the continental-scale transbrasiliano lineament. J. South Am. Earth Sci. 60, 1–9. https://doi.org/10.1016/j.jsames.2015.02.002

Berrocal, J., Assumpção, M., ARTEZANA, R.DIAS NETO, C.M., Ortega, R., FRANÇA, H., VELOSO, J.A.V., Antezana, R., Neto, C.M.D., Franca, H., 1984. Sismicidade do Brasil. Instituto Astronômico e Geofísico, Sao Paulo.

Bouchon, M., 1981. A simple method to calculate Green's functions for elastic layered media. Bull. Seismol. Soc. Am. 71, 959–971.

Carvalho, J., Barros, L.V., Zahradník, J., 2016. Focal mechanisms and moment magnitudes of micro-earthquakes in central Brazil by waveform inversion with quality assessment and inference of the local stress field. J. South Am. Earth Sci. 71, 333–343. https://doi.org/10.1016/j.jsames.2015.07.020

Dias, F., Zahradník, J., Assumpção, M., 2016. Path-specific, dispersion-based velocity models and moment tensors of moderate events recorded at few distant stations: Examples from Brazil and Greece. J. South Am. Earth Sci. 71, 344–358. https://doi.org/10.1016/j.jsames.2016.07.004

Fernandes, E.P., Blum, M.L.A., Ribeiro, R., 1991. The Goiás seismic zone, a new approach, in: Extended Abstract. 35° Congress Braz. Geol. Soc., Salvador/BA. pp. 553–558.

Ferreira, J., Oliveira, T., Takeya, M.K., Assumpção, M., 1998. Superposition of local and regional stresses in northeast Brazil: evidence from focal mechanisms around the Potiguar marginal basin. Geophys. J. Int. 134, 341–355. https://doi.org/doi.org/10.1046/j.1365-246x.1998.00563.x

Fojtikova, L., Zahradnik, J., 2014. A New Strategy for Weak Events in Sparse Networks: The First-Motion Polarity Solutions Constrained by Single-Station Waveform Inversion. Seismol. Res. Lett. 85, 1265–1274. https://doi.org/10.1785/0220140072

Fuck, R.A., 1994. A Faixa Brasília e a Compartimentação Tectônica na Província Tocantins, IV Simpósio de Geologia do Centro-Oeste. SBG, Brasília 184–187.

Fuck, R.A., Pimentel, M., Silva, L., 1994. Compartimentação Tectônica na Porção Oriental da Província Tocantins, IV Simpósio de Geologia do Centro-Oeste,. SBG , Brasília, 215–216.

Kagan, Y.Y., 1992. Correlations of earthquake focal mechanisms. Geophys. J. Int. 110, 305–320. https://doi.org/10.1046/j.1365-246X.2000.00281.x

Myers, S.C., Begnaud, M.L., Ballard, S., Pasyanos, M.E., Phillips, W.S., Ramirez, A.L., Antolik, M.S., Hutchenson, K.D., Dwyer, J.J., Rowe, C.A., Wagner, G.S., 2010. A Crust and Upper-Mantle Model of Eurasia and North Africa for Pn Travel-Time Calculation. Bull. Seismol. Soc. Am. 100, 640–656. https://doi.org/10.1785/0120090198

Rocha, M.P., Schimmel, M., Assumpção, M., 2011. Upper-mantle seismic structure beneath SE and Central Brazil from P- and S-wave regional traveltime tomography. Geophys. J. Int. 184, 268–286. https://doi.org/10.1111/j.1365-246X.2010.04831.x

Soares, J., Berrocal, J., Fuck, R.A., Mooney, W., Ventura, D.B.R., 2006. Seismic characteristics of central Brazil crust and upper mantle: A deep seismic refraction study. J. Geophys. Res. 111, B12302. https://doi.org/10.1029/2005JB003769

Sokos, E., Zahradnik, J., 2013. Evaluating Centroid-Moment-Tensor Uncertainty in the New Version of ISOLA Software. Seismol. Res. Lett. 84, 656–665. https://doi.org/10.1785/0220130002

Sokos, E.N., Zahradnik, J., 2008. ISOLA a Fortran code and a Matlab GUI to perform multiple-point source inversion of seismic data. Comput. Geosci. 34, 967–977. https://doi.org/10.1016/j.cageo.2007.07.005

Takeya, M., Ferreira, J.M., Pearce, R.G., Assumpçao, M., Costa, J.M., Sophia, C.M., 1989. The 1986–1988 intraplate earthquake sequence near João Câmara, northeast Brazil—evolution of seismicity. Tectonophysics 167, 117–131. https://doi.org/10.1016/0040-1951(89)90062-0

Veloso, J.A.V., Marza, V.I., Carvalho, J.M., Barros, L.V., 1997. Recent seismic activity in the S-W edge of the Mato Grosso-Goiás-Tocantins (MGT) Belt (Central Brazil)., in: 5th International Congress of the Brazilian Geophysical Society. Sao Paulo, pp. V2-964–967.

CAPÍTULO 2 - METODOLOGIA

2.1 Fontes sísmica

O primeiro modelo matemático usado para representar uma fonte sísmica foi desenvolvido por Nakano (1923), que representou a ruptura de uma falha por um modelo de esforço do tipo par-de-forças simples (*single-couple*). Posteriormente, Maruyama (1963); Burridge and Knopoff (1964, 2003) propuseram que a movimentação de uma falha cisalhante em meio elástico e isotrópico é equivalente a uma fonte do tipo duplo-par-de-forças (*double-couple*).

No Brasil foram realizados estudos de mecanismos focais, os primeiros trabalhos foram realizados por Mendiguren and Richter (1978) e Assumpção and Suarez (1988). Mais recentemente destacamos os trabalhos de Ferreira (1997); Chimpliganond *et al.* (2010); Assumpção *et al.* (2014); Carvalho *et al.* (2014); Barros *et al.* (2015) e mostram que a região intraplaca brasileira está submetida a um esforço compressional de orientação preferencial E-W, com exceção na parte norte, onde os esforços estão rotacionados para Norte (Zoback and Richardson, 1996).

O mecanismo focal define a falha, sua movimentação e os parâmetros que a definem são: *strike* (orientação da falha em relação ao norte geográfico, variando de 0º a 360º); *dip* ou mergulho (ângulo do plano da falha a partir da superfície, varia de 0º a 90º); *rake* ou ângulo do vetor deslocamento/slip (ângulo entre a direção da falha e a direção do escorregamento do bloco superior, denominado de teto (hang-wall), varia de -180º a 180º) (Aki & Richards 2002). Além dos parâmetros acima, o estudo de mecanismo focal fornece ainda a orientação dos esforços de compressão (P) e tensão(T). responsáveis pela ruptura da falha, bem como seus respectivos ângulos de strike e dip (plunge).

A assinatura sísmica de um sismograma é definida na fonte sísmica pela orientação da falha, ângulo de mergulho e pela direção de movimentação dos blocos falhados durante o processo de ruptura do terremoto (Lay & Wallace,

1995). Os métodos mais utilizados na determinação de mecanismos focais, simples e compostos, são baseados nas polaridades da fase P e na razão entre as amplitudes da fase P com as fases SV e SH (Stauder & Bollinger 1964; Hirasawa 1970; Herrmann 1979; Kisslinger 1980; Wang & Herrmann 1980; Snoke et al. 1984; Nakamura 2002; Snoke 2003). A obtenção de mecanismos focais pela modelagem de formas de ondas de terremotos médios e grandes, já se tornou uma rotina em Observatórios Sismológicos (Jiménez et al. 1989; Lay & Wallace T. C. 1995). Vários softwares são usados na inversão de formas de ondas para o momento tensor de eventos registrados a distâncias telessísmicas estão disponíveis (Dreger & Helmberger 1993; Kikuchi & Kanamori 1991; McCaffrey, R., Abers, G., Zwick 1991). Entretanto, o momento tensor de eventos menores, com distancias locais e regionais é mais difícil de obter, mas alguns programas também já estão disponíveis para esse propósito. E.g.: TDMT_INV desenvolvido por D. Dreger (2003); ISOLA por Sokos and Zahradnik (2008); FMNEAREG por Delouis, Charlety and Vallée (2008); Maercklin et al. (2011); KIWI por Cesca et al. (2010) e o código F-NET MT por Yagi Y. and Nishimura N. (2011). No entanto, a aplicação desses programas para eventos de baixas magnitudes (M < 3.5) ainda é um desafio. Como regra geral, eventos fracos e registrados por estações locais tem boa relação sinal ruído geralmente para frequências acima de 1 Hz, sendo possível a inversão somente se registrados por estações sismográficas em distâncias locais (Benetatos et al. 2012; Fojtikova & Zahradnik 2014; Fojtíková et al. 2010).

2.1.1 Representação de uma fonte sísmica

Uma fonte sísmica pode ser representada pelo momento tensor, e esse por sua vez pode ser descrito por uma combinação linear dos seis tipos básicos de falhas. A teoria fundamental de fonte sísmica estabelece que uma falha cisalhante em meio elástico e isotrópico é equivalente a uma fonte do tipo duplo-par-de-forças, Figura 2.1.
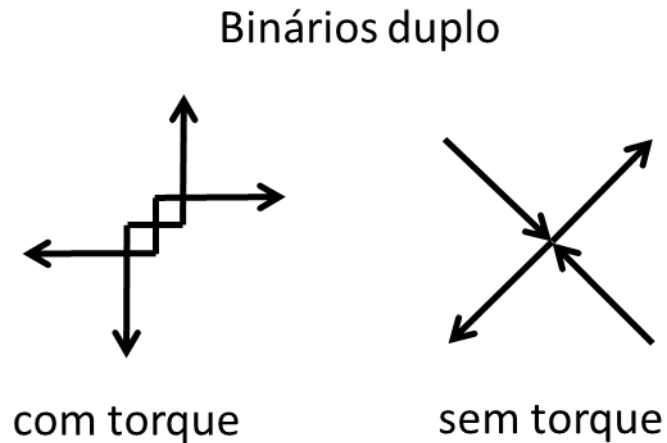
Figura 2-1 – Tipos de forças que podem gerar deslocamento observados a longas distâncias (far-field) provenientes da ruptura de uma falha (Havskov & Ottemöller 2010).

O modelo adotado na solução do plano de falha é equivalente a um duplo par-de-forças do tipo binário duplo com e sem torque que podem ser descrito matematicamente como a soma de dois pares-de-forças simples. No entanto, em condições reais, uma fonte sísmica pode ser mais complexa do que apenas um binário duplo. A maioria das fontes sísmicas podem ser descritas como a combinação de nove binários duplos, três deles são dipolos ao longo dos eixos das ortogonais e 6 são do tipo binários simples, que reagrupadas formam três binários duplos, um em cada plano, Figura 2.2.
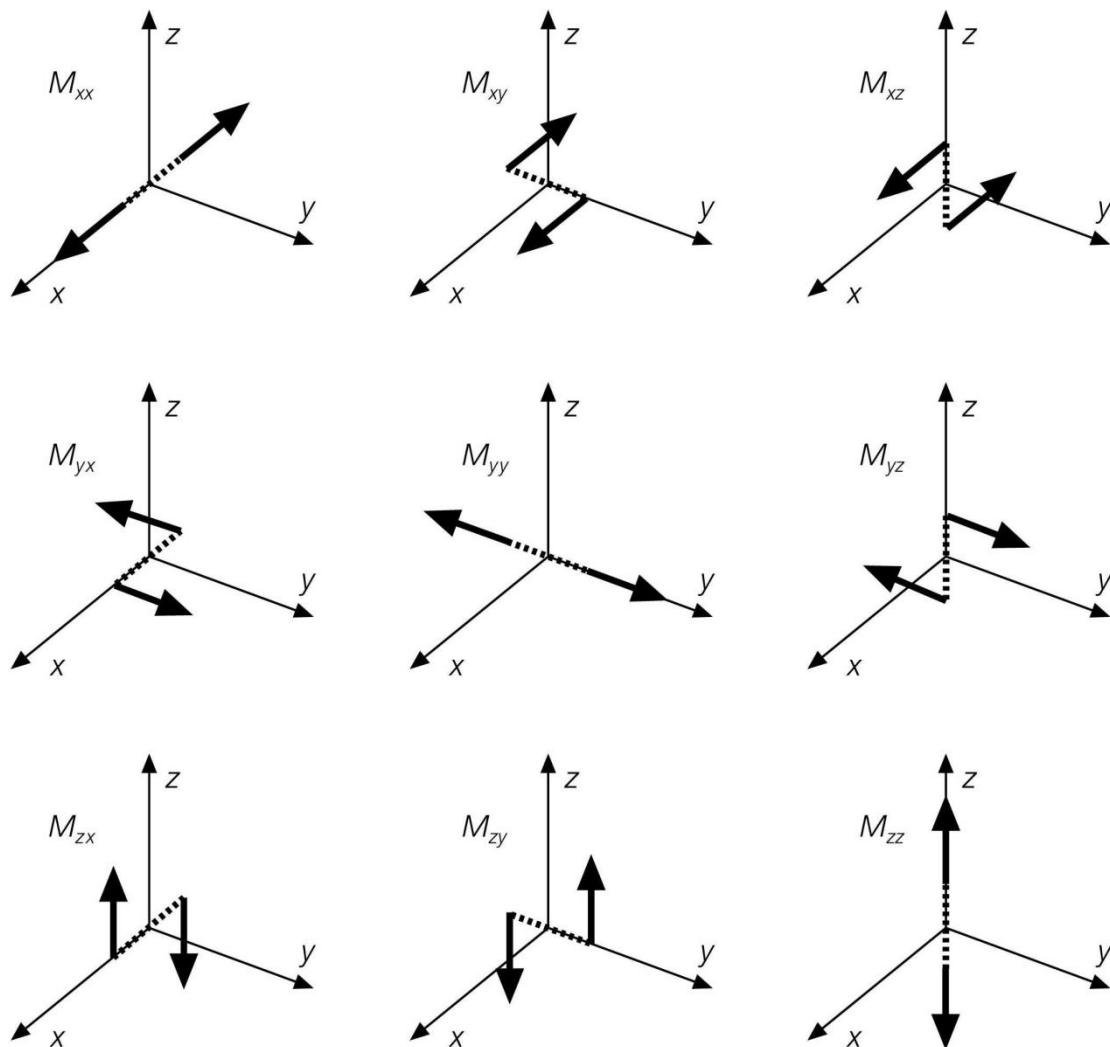
Figura 2-2 – Os nove pares de forças que compõem o momento tensor, cada um consistindo de duas forças iguais e opostas separadas por uma distância d (linha pontilhada). Por exemplo, Mxy é o par de forças no plano xy atuando na direção do eixo x (Stein & Wysession 2003).

O momento sísmico escalar (Mo) e o mecanismo focal descrevem, respectivamente, a deformação inelástica permanente (devido a um terremoto) e a geometria da falha (Figura 2.3). O mecanismo focal define uma falha geológica (*strike/dip/rake*) e pode ser derivado da solução do momento tensor através da análise das formas de ondas observadas nas diversas estações sismográficas.
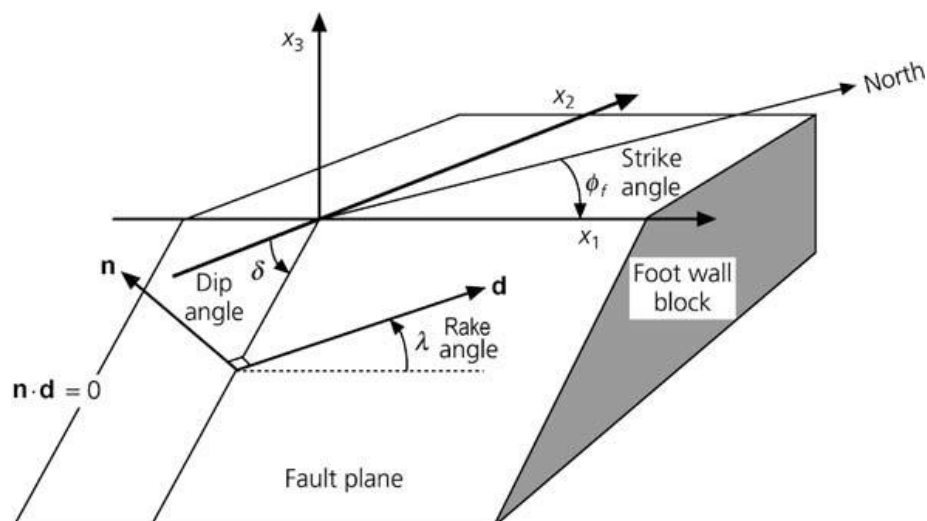
Figura 2-3 – Parâmetros que definem uma falha. A orientação do plano da falha é definida pelos ângulos dip e strike, e o movimento relativo dos blocos é definido pelo ângulo do vetor slip ou rake, (Stein & Wysession 2003).

A direção do deslizamento da falha em um terremoto e respectiva orientação é mostrada pelo mecanismo focal exibido em uma bola de praia (*beachballs*). A bola de praia é a projeção em um plano horizontal da metade inferior de uma concha esférica e imaginária, denominada de esfera focal envolvendo a fonte do terremoto, Figura 2.4A. Uma linha interceptando a esfera focal mostra o plano de falha. A direção do deslizamento da falha é governada pelo campo de esforço existente no local no momento da ruptura, também e representada no beachball. Os quadrantes cinza contêm o eixo de tensão (T) e os quadrantes brancos contêm o eixo de pressão (P). A Figura 2.4B mostra os tipos básicos de falhas e suas respectivas bolas de praias.
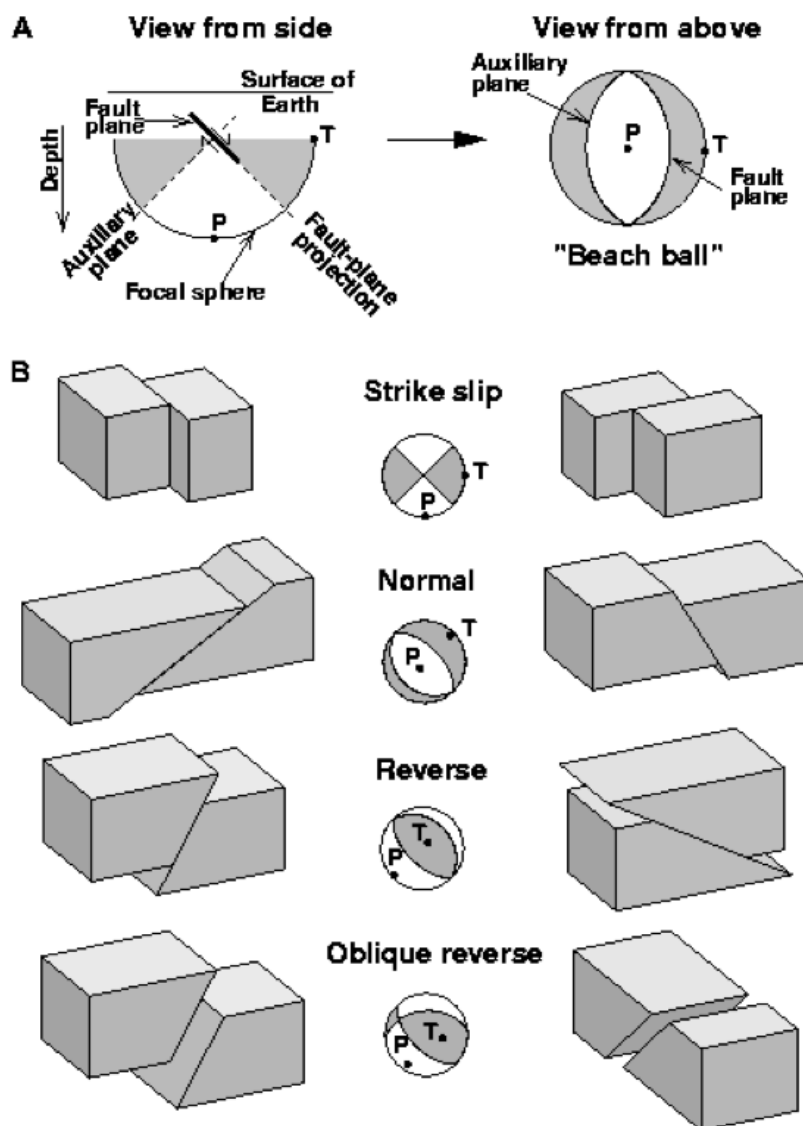
Figura 2-4 – A esfera focal é a projeção da falha na metade inferior de uma concha esférica denominado mecanismo focal ou beachballs (A). O mecanismo focal descreve graficamente uma falha e sua direção de moviemento. O painel (B) mostra os tipos de falhas e os respectivos beachballs, que também descreve os esforços (P e T) necessários para a ruptura da falha. Figura do site do USGS (1996), (http://earthquake.usgs.gov/learn/topics/beachball.php).

A bola de praia mostra a projeção na esfera focal, hemisfério inferior, dos raios irradiados, a partir do foco de um evento como mostrado na (Figura 2.5b). O plano nodal principal é posicionado conforme a orientação da falha perpendicularmente ao plano auxiliar que conjuntamente indicam as orientações dos eixos (P) e (T). As partes em preto na Figura 2.5a representam as áreas de tensão. O deslocamento do chão, registrado em uma estação

sismográfica correspondente a essa área, tem a primeira fase (P) para cima, e as partes em branco são áreas de compressão e o respectivo deslocamento tem a primeira fase (P) para baixo.
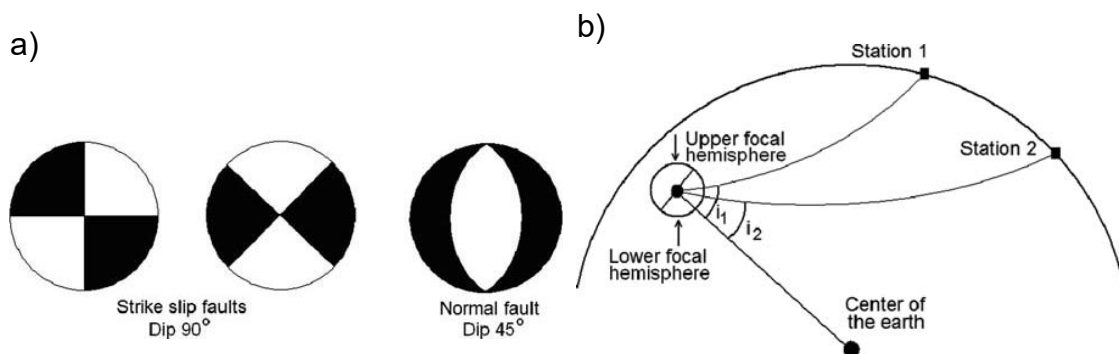
Figura 2-5 – O painel (a), mostra diagramas de mecanismos focais (beachballs) correspondentes a falhas do tipo strike slip e normal, os quadrantes hachurados em preto e branco correspondem as áreas de tensão e compressão, respectivamente. O painel (b) mostra a esfera focal, centralizada no foco de um evento sísmico, e a projeção dos raios em direção às estações sismográficas (Havskov & Ottemöller 2010).

As amplitudes das ondas P e S dependem da magnitude e da direção de radiação dos raios sísmicos a partir da fonte (Figura 2.6). Portanto, em cada ponto em torno da fonte temos diferentes padrões de sismogramas a depender da posição da estação. Os métodos mais utilizados na determinação de mecanismos focais, simples e compostos, são baseados nas polaridades da fase P e na razão entre as amplitudes da fase P com as fases SV e SH. Este assunto é abordado em várias literaturas de sismologia, veja por exemplo: Lay and Wallace (1995); Snoke (2003); Stein and Wysession (2003). Entretanto, as formas de ondas contém muito mais informação a cerca da fonte que apenas as polaridades das primeiras chegadas da P e razão P/SV e P/SH, como será visto na próxima seção.
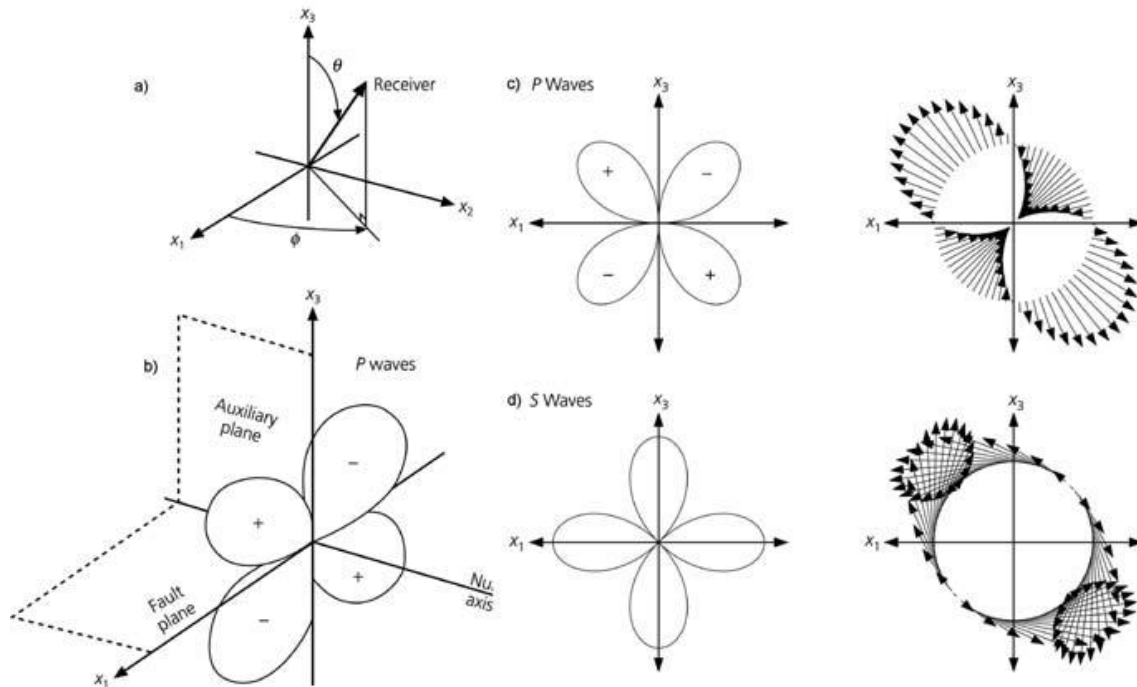
Figura 2-6 – Padrão de radiação de uma fonte sísmica do tipo duplo-par-de-força no plano x1-x2. (a) sistema de coordenadas esféricas, (b) e (c): Padrão de radiação da onda P, (d) padrão de radiação da onda S. O painel (b) e os dois painéis no centro mostram as amplitudes das P (c) e S (d) e os painéis à direita mostram a direção do movimento. Para as ondas P (c), a amplitude é zero no plano de falha e no plano auxiliar (planos nodais). As ondas S não possuem um plano nodal, mas a amplitude é zero ao longo do eixo x2 (eixo nulo) (Stein and Wysession, 2003).

2.2 Inversão de formas de ondas

O deslocamento *u(t)* de uma fonte pontual com localização e tempo de origem conhecidos pode ser representado pela convolução do momento tensor *M* com o tensor de Green *G* (Aki & Richards 2002):

$$u_i(t) = \sum_{p=1}^{3} \sum_{q=1}^{3} M_{pq} * G_{ip,q} \qquad (2.1)$$

O momento tensor *M* pode ser expresso pela combinação linear dos seis tensores elementares adimensionais *M^i* (Figura 2.7).

$$M_{pq} = \sum_{i=1}^{6} a_i M_{pq}^i \tag{2.2}$$

A fonte é caracterizada pela composição dos seis coeficientes escalares a_i.
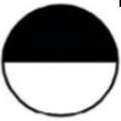
Figura 2-7 – Momentos tensores elementares e mecanismos focais associados. Os mecanismos focais M1-M5 correspondem a diferentes fontes de pares duplos, que representam os modos de fratura da falha. O mecanismo focal M6 indica uma fonte isotrópica (fonte explosiva). (modificado de Stein and Wysession (2003).

São usados os tensores elementares e as funções de Green são calculadas pelo método do número de onda discreto (Bouchon 1981). Os tensores $\textbf{\textit{M}}^1$ a $\textbf{\textit{M}}^5$ representam as cinco variações básicas dos mecanismos focais do tipo *double-couple* (DC), enquanto $\textbf{\textit{M}}^6$ representa uma fonte puramente isotrópica. Combinando (2.2) com os tensores elementares; tem se:

$$\textbf{\textit{M}} = \begin{bmatrix} -a_4 + a_6 & a_1 & a_2 \\ a_1 & -a_5 + a_6 & -a_3 \\ a_2 & -a_3 & a_4 + a_5 + a_6 \end{bmatrix} \tag{2.3}$$

Onde os a_i (dimensão de momento) são coeficientes da combinação linear da equação (2.2). Podemos deduzir que o traço do momento tensor, $tr(\boldsymbol{M}) = 3a_6$ (somatório dos elementos da diagonal principal da matriz).

$$M_o = \sqrt{\left(\sum_{p=1}^{3}\sum_{q=1}^{3}\left(M_{pq}\right)^2\right)/2} \qquad (2.4)$$

Combinando as equações temos:

$$u_i(t) = \sum_{j-1}^{6} a_j E_i^j(t) \qquad (2.5)$$

Onde E^j denota o *j-enésimo* sismograma elementar correspondendo ao momento tensor elementar *j-enésimo*. Aqui é assumido que a função momento é conhecida.

No caso de a posição e do tempo de origem não serem conhecidos, esses parâmetros adicionais (posição e tempo do centroide) seriam buscados com o auxílio de uma grade de busca.

A grade de busca tem como objetivo encontrar a máxima correlação ($Corr$) entre os sismogramas observados *(u)* e o sintético *(s)*.

$$Corr = \frac{\int u\,s}{\sqrt{\int u^2\,s^2}} \qquad (2.6)$$

Onde $\int us$ (Eq. 2.7) é a somatória de todas as estações e componentes.

$$\int us = \sum_i \int us(t)S_i(t)dt \qquad (2.7)$$

A medida do desajuste (misfit) entre o sismograma real e o sismograma de melhor ajuste (sintético) é obtida pela norma-L2

$$misfit = \int (u - s)^2 \qquad (2.8)$$

e/ou pela média global da redução de variância (VR).

$$VR = 1 - \frac{misfit}{\int u^2} \qquad (2.9)$$

Se o sismograma sintético for encontrado pela minimização do desajuste (*misfit)* usando o método dos mínimos quadrados a relação entre a correlação e a redução de variância (VR) é dada por:

$$Corr^2 = \text{VR} \qquad (2.10)$$

2.2.1 Programa ISOLA

O código ISOLA (Sokos & Zahradnik, 2008; Sokos & Zahradnik, 2013) usado nesta tese foi programado em Fortran e a interface gráfica roda em ambiente MATLAB. A resposta do meio ou funções de Green são calculadas tanto para um modelo de velocidade 1-D quanto para vários modelos específicos, ou seja, da fonte para cada estação específica.

O programa de inversão usa informação da velocidade do chão registrada por instrumentos de banda larga de três componentes. Um filtro passa banda é aplicado para selecionar a faixa de frequência de interesse. Os sismogramas de velocidade (observados) são transformados em deslocamento. Paralelamente, a inversão é feita gerando sismogramas sintéticos *s(t) (*em deslocamento) a partir de uma combinação de sismogramas elementares, correspondentes aos seis mecanismos focais básicos.

O software ISOLA usado na inversão para momento tensor, modela uma fonte sísmica pontual única ou uma série de fontes pontuais. As fontes pontuais são chamadas de subeventos. Os momentos tensores (MT) são calculados pelo

método dos mínimos quadrados, usando o modo completo (deviatoric) ou limitando para modo DC=100% (double-couple puro). No modo DC puro os mecanismos focais dos subevents são mantidos fixos (DC=100%) e a inversão é realizada apenas para definir posição, tempo de origem do centroide e momento sísmico.

A posição e o tempo de origem dos subeventos são calculados através de busca em uma grade espaço/tempo. A configuração das redes espaciais da grade de busca pode ser linear, ou seja varia apenas na profundidade ou planar variando ao longo de planos horizontais ou ainda variando sobre um plano coincidente com o plano da falha. Para a função de tempo do subevento, também chamado de função de tempo elementar, é adotado uma função delta ou triangular com duração fixa. Neste trabalho usamos uma função delta. Alternativamente, a função de tempo pode ser calculada com os dados de formas de ondas assumindo que o mecanismo focal é conhecido. Se um subevento dominante e único for obtido no processamento, é assumido como sendo a posição do centroide, ou seja correspondente aos parâmetros de fonte do evento (centroide momento tensor). O centroide corresponde ao centro de gravidade da falha. Para pequenos terremotos é assumido que a posição do centróide e do hipocentro são idênticas.

O programa tem como resultado final um boletim com os parâmetros de fonte do evento processado Figura 2.8.
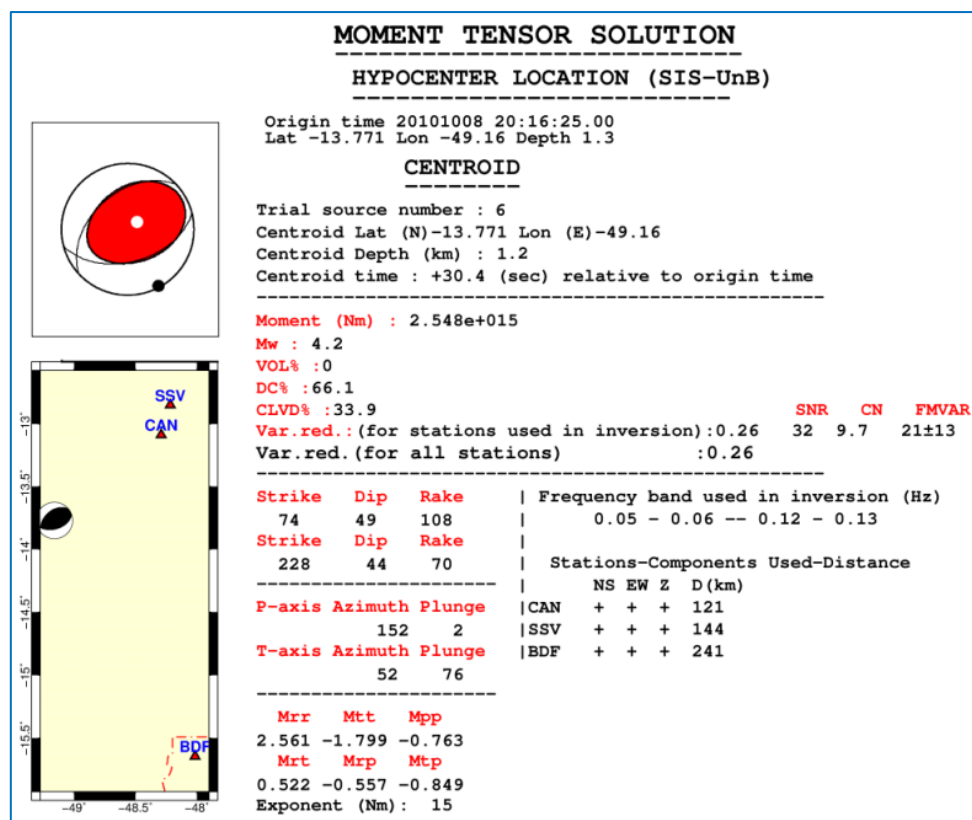
Figura 2-8 – Resultados da inversão de formas de ondas do sismo principal de Mara Rosa, 8 Outubro 2010, magnitude 5.0 m_b e intensidade VI (MM). As estações utilizadas na inversão foram CAN3 (CAN), SSV2 (SSV) e BDFB (BDF).

2.2.2 Técnica CSPS-W

A técnica CSPS-W (*Cyclic Scanning of the Polarity Solutions - waveform*) desenvolvida por Fojtikova & Zahradnik (2014), foi optimizada para inversão de eventos com magnitudes M<4, que são difíceis de serem processados com o programa ISOLA padrão. A técnica CSPS-W combina o método tradicional de polaridades FOCMEC (Snoke 2003) com a inversão de formas de ondas. Neste caso, devido ao reduzido número de polaridades, se obtém um número grande de soluções possíveis, por exemplo, até 100 ou mais soluções. Entretanto, menor que o número de soluções testadas no processo de busca iterativa de inversão de formas de ondas. Com a técnica CSPS-W, as inversões são feitas apenas das soluções obtidas pelo método de polaridades, ou seja, a inversão é realizada apenas para um número fixo de soluções, aquelas obtidas com um número reduzido de polaridades. Esta técnica produz soluções confiáveis e com melhor ajuste (Figura 2.9).
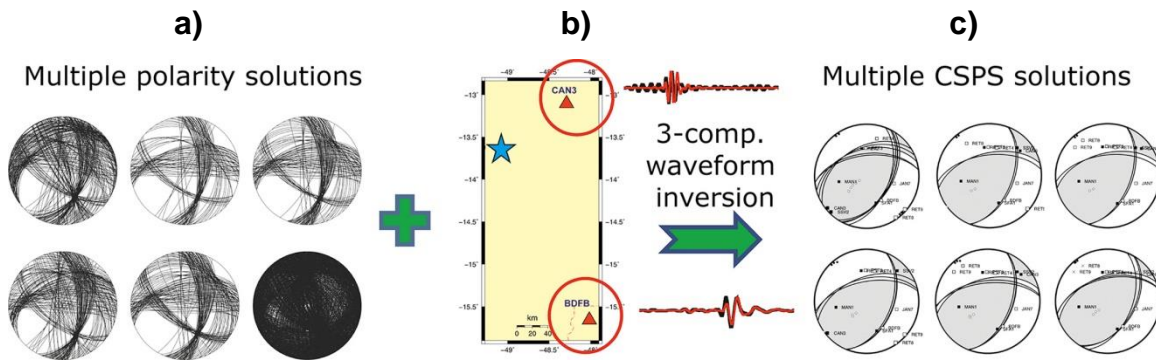
Figura 2-9 – (a) Resultados dos Sets, polaridades e modelos de velocidades, obtidas com o programa FOCMEC. (b) Estações CAN3 e BDFB e respectivas formas de ondas (sintético=vermelho, observado=cinza), e o resultado da combinação das duas técnicas (FOCMEC+ISOLA) mostrando a solução dos mecanismos focais para os diversos modelos crustais testados (c).

O método CSPS-W foi ajustado para possibilitar a inclusão de incertezas causadas por variações nos ângulos de partida introduzidas com utilização de diferentes modelos crustais (Figura 2.10a). Para cada modelo é avaliado a posição da projeção das polaridades na esfera focal (Figura 2.10b).
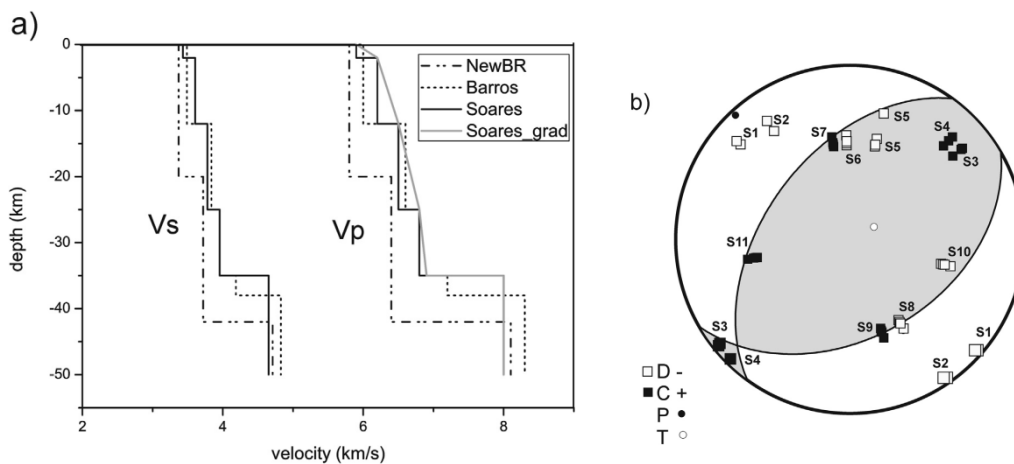
Figura 2-10 – a) Modelos crustais e efeitos de suas diferentes camadas na projeção das polaridades na esfera focal (b). Os Modelos de velocidades são denominados de NewBR, Barros, Soares (J. Soares et al. 2006) e Soares_grad. (b) Esfera focal com as polaridades nas estações. Cada estação aparece quatro vezes, uma para cada modelo crustal usado.

As incertezas serão analisadas no capitulo 3 (artigo 1) desta tese.

2.2.3 Inversão de envelopes de formas de ondas (ENV)

A técnica ENV, também implementada no código ISOLA, inverte os envelopes das formas de ondas. Esta técnica foi aplicada neste trabalho para eventos com magnitudes $2.0 \leq M \leq 4.0$.

Um conjunto de estações/componentes é selecionado e um filtro causal, passa-banda, de quarta ordem do tipo *butterworth* é aplicado para restringir a banda de frequência apropriada. Os envelopes das formas de ondas são extraídos pela aplicação da transformada de Hilbert e não é aplicado nenhum tipo de suavização no processo.

Enquanto o deslocamento é linearmente relacionado com o momento tensor os envelopes (ENV) não são. É por isso que ENV é invertido para MT por busca em uma grade variando os ângulos strike, dip e rake (s/d/r). O código permite duas variações: com e sem restrição no modo de busca. No método sem restrição simplesmente prescrevemos os limites dos ângulos (s/d/r) e seus incrementos e o código faz uma busca livre por todas as fontes possíveis. No método com restrição o código inverte apenas as soluções s/d/r previamente obtidas com o código FOCMEC, ou seja, as soluções que compõem a grade de busca para o processamento, são apenas aquelas que satisfazem ao critério de polaridades que é a estratégia do método CSPS. Como regra geral, o método restrito é mais eficiente e o número de soluções testadas é menor. O método não restrito, além de requerer maior esforço computacional, os mecanismos focais resultantes devem passar posteriormente por uma verificação de polaridade devido ao fato de que o método ENV não resolve a ambiguidade de 180° do rake.

A posição da fonte no espaço é também pesquisada na grade de busca, utilizando um conjunto predefinido de fontes com posições abaixo do epicentro (= profundidades testadas), mas podem ter também uma distribuição mais geral, por exemplo, ao longo de um plano ou linha. O tempo do centroide, calculado apenas na inversão ENV, é pesquisado em uma janela de tempo ajustável a partir da origem.

A pesquisa de grade para envelope serve para buscar as soluções que oferecem um melhor ajuste entre dados reais e sintéticos, utilizando a norma L2 e pesos (*W*). O desajuste (*misfit*) entre os dados observados (*O*) e sintéticos (*S*) é definido como:

$$misfit = \sum W_i(O_i - S_i)^2 \qquad (2.\underline{11})$$

Onde o somatório é feito sobre todas as estações, componentes e amostras de dados. Os pesos são individuais e especifico para cada componente. Pesos zero são usados para remover da inversão uma componente deteriorada, enquanto pesos não nulos podem ser entendidos como uma medida da incerteza (variância) dos dados, isto é.

$$\frac{1}{W_i} = \sum O_i^2 \qquad (2.\underline{12})$$

O código não inclui qualquer análise estatística de erro, bem como sua propagação devido ao modelo. Essa tarefa, complicada pela não linearidade do problema, precisa ser resolvida em futuras versões do código ISOLA.

Além do desajuste (misfit), a redução de variância, Variance Reduction (VR), também é calculada:

$$VR = 1 - \left(\frac{misfit}{Onorm}\right) \qquad (2.\underline{13})$$

Onde os dados observados e normalizados (Onorm) é:

$$Onorm = \sum (WiOi^2) \qquad (2.\underline{14})$$

A inversão consiste em dois círculos (*loops*) principais de busca na grade de soluções, - o círculos externo sobre a posição da fonte e o círculos interno sobre os ângulos dos planos nodais (s/d/r). Ao terminar o círculos interno, os

desajustes (*misfit*) para todos os ângulos s/d/r vão para o arquivo de saída. A solução s/d/r de melhor ajuste em uma determinada posição e tempo de origem é identificada, gravada no arquivo de saída. Os dados sintéticos não são salvos. Depois de terminar a busca no loop externo, o usuário inspeciona os resultados e escolhe a posição de fonte preferida. A interação é necessária, evitando a solução automática com menor desvio em relação às posições de fonte, porque a resolução da posição pode ser baixa. Nesse caso é mais razoável escolher, por exemplo, uma posição próxima do hipocentro já conhecido. Selecionando a profundidade da fonte e confirmando o mecanismo focal mais adequado, os dados sintéticos são recalculados para o mecanismo focal escolhido. Em seguida, o momento sísmico é determinado e os dados sintéticos vão para os arquivos de saída para serem plotados juntamente com os dados observados.

Além da solução de melhor ajuste, estamos interessados também em sua incerteza e não apenas numa solução singular. Isto pode ser conseguido identificando-se o conjunto das soluções com ajustes próximos. Portanto, usando um limite especificado pelo usuário, um arquivo de saída é criado contendo as soluções no intervalo especificado; Por exemplo, um limiar de 10% significa a saída de s/d/r para um conjunto de soluções variando entre soluções com o melhor ajuste e as soluções de melhor ajuste -10%. Todas as informações dos planos nodais dentro desse limiar são plotadas juntamente com as polaridades. Se uma verificação de polaridade posterior é realizada, um arquivo de saída similar é criado, desta vez limitando apenas às soluções que concordam com todas as polaridades.

Características do código:

    (i)   Normalização;
    (ii)   Deslocamentos no tempo (time shift);
    (iii)   Determinação de momentos.

(i)   Normalização

A normalização dos gráficos ENV observados foi introduzida devido aos dados reais e sintéticos muitas vezes sofrerem diferente decaimento de amplitude com a distância epicentral. É por isso que todos os dados observados (*O)*, são normalizados, individualmente em cada estação, de tal forma que as três componentes são divididas pelo módulo do valor máximo de uma delas:

$$O_i = O_{ij}/MO_i$$

(2.15)

Onde MOi = Máximo valor da componente na estação (i). Aqui os sub índices i e j denotam a estação e a componente (j = 1,2,3), respectivamente. As constantes de normalização, dependentes da estação MOi, são guardadas para a sua utilização posterior. A normalização dos dados observados ocorre antes dos dois círculos de inversão e antes da avalição do desajuste. Os dados sintéticos *S* são normalizados igualmente. No entanto, a sua normalização (e as constantes gravadas MOi) ocorre repetidamente para cada passagem através do círculos de inversão interno, isto é, em cada posição de fonte testada s/d/r. Opcionalmente, através da mudança de parâmetro (normalizado/não-normalizado), o código permite a supressão de todas as normalizações.

(ii) Deslocamentos no tempo (time shift)

A inversão ENV é sensível ao deslocamento das ondas no tempo entre os dados reais e observados. Os deslocamentos no tempo são necessários por duas razões: determinar o tempo de centroide e compensar os deslocamentos das ondas no tempo devido à imprecisão nos modelos de velocidades. Por conseguinte, para cada passagem no círculo interno, isto é, para cada combinação s/d/r em cada posição de teste, o código inclui um alinhamento artificial dos envelopes observados e sintéticos (normalizados). Para este objetivo, o atraso temporal ótimo é calculado (individualmente para cada componente) de modo a maximizar a correlação cruzada através da busca na grade dentro do intervalo e dentro de um limite pré-estabelecido. Este limite é controlado pelo usuário para refletir as variações temporais esperadas devido a

modelos de velocidade inapropriados e devido à incerteza do tempo do centroide. Os deslocamentos no tempo são aplicados antes da computação do desajuste. Existem algumas operações especiais necessárias no caso do ENV não estar normalizado. Nesse caso todas as inversões serão normalizadas.

Observe que o código alinha envelopes completos. Este procedimento pode ser problemático se os envelopes apresentarem vários grupos de ondas distintos, tais como ondas P e S de amplitude comparável. A aplicação com melhores chances de sucesso é para o caso de os envelopes serem dominados por um único grupo de ondas de superfície. Isto pode talvez indicar uma necessidade de rotacional as componentes para Radiais (R) e Transversais (T).

(iii)   Determinação do momento

A determinação de momento para a solução de melhor ajustamento é realizada com os dados observados e sintéticos re-normalizados, isto é, multiplicando-os pelos valores de MOi e MSi. Desta forma, devolvemos aos dados suas "verdadeiras amplitudes"; Portanto, comparando o *O* e *S* re-normalizados, calcular-se o momento escalar com a utilização da equação 9 de Zahradník and Gallovič (2010):

$$Mo = \frac{\sum(Wi^2 OiSi)}{\sum(Wi^2 Si^2)}$$

(2.16)

Finalmente, Mo é convertido em momento-magnitude Mw (Hanks & Kanamori 1979).

2.2.4 Parâmetros de entrada

A entrada do código inclui formas de ondas reais, arquivo de resposta dos instrumentos (pólos e zeros), parâmetros de fonte (informações de epicentro), coordenadas das estações e modelo(s) de velocidades.

2.3   Inversão de mecanismos focais para esforço

Vários métodos estão atualmente disponíveis para obtenção de esforço a partir de mecanismos focais (Angelier, 2002; Gephart e Forsyth, 1984; Hardebeck e

Michael, 2006; Michael, 1984; Vavryčuk, 2014; Michael (1987). Estes métodos geralmente assumem que: i) o esforço tectônico é uniforme (homogêneo) na região; ii) os terremotos ocorrem em falhas pré-existentes e com orientações variadas, e iii) o vetor de deslizamento aponta na direção da tensão de cisalhamento na falha (Wallace 1951; Bott 1959). Com as suposições acima satisfeitas, os métodos de inversão de esforços podem determinar quatro parâmetros do tensor de esforço: três ângulos que definem as direções das tensões principais, σ1, σ2 e σ3, e o fator de forma R (Gephart & Forsyth 1984).

$$R = \frac{\sigma_1 - \sigma_2}{\sigma_{1-}\sigma_3}$$ (2.17)

Neste trabalho usamos o código STRESSINVERSE de Vavryčuk (2014), que é uma modificação do método de Michael (1984), adicionando o cálculo da instabilidade para identificar o plano de falha de cada solução do mecanismo focal, possivelmente aumentando a robustez do parâmetro fator de forma (R).

Uma rocha é fraturada ao ser submetida a um esforço critico, esse processo é associado a um terremoto. O regime de falha depende do tipo de esforço (tração, compressão ou cisalhamento) e pode ocorrer em uma fratura nova ou pré-existente, Figura 2.11. A condição sob a qual a fratura ou falha ocorre é descrita pelos chamados critérios de falha. Os critérios mais simples e conhecidos são: falha de Griffith, critério derivado das condições energéticas impostas à propagação de fissuras em uma rocha; e Critério de falha de Coulomb, que é baseado no conceito de fricção entre dois blocos deslizantes. Ambos os critérios preveem valores de esforço critico de cisalhamento como uma função do esforço normal que leva à falha à ruptura. A Figura 2.11 apresenta os três tipos básicos de falhas e o correspondente beachballs.
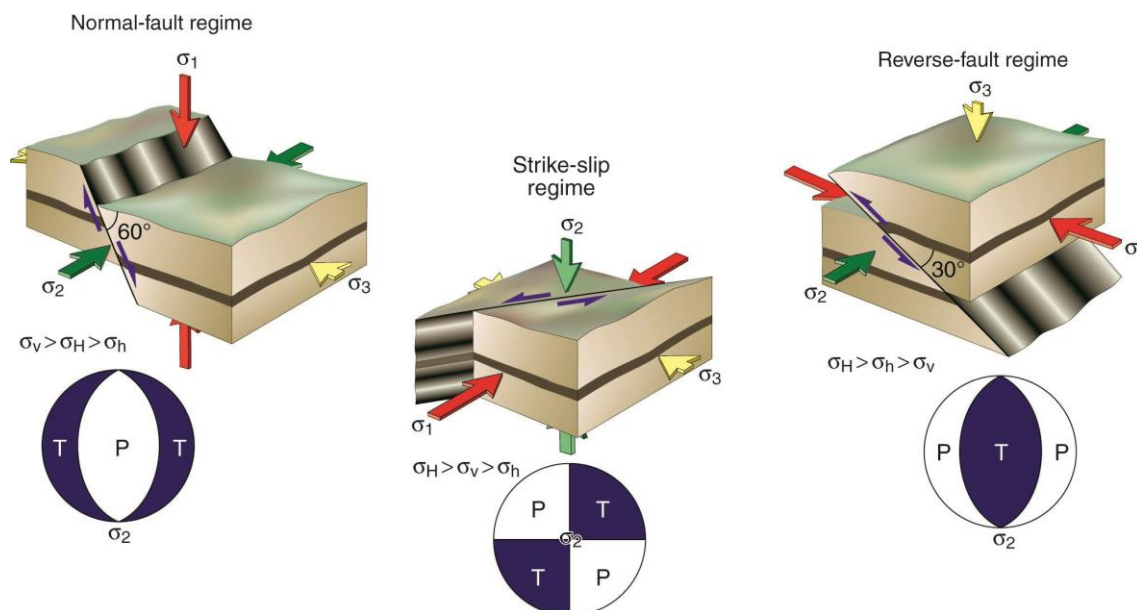
Figura 2-11 – Classificação de Anderson de esforço tectônico e respectivo regime de falhamento. Beachballs correspondentes regimes as falhas normal, strike slip e reversa. (Figura do site http://geologylearn.blogspot.com/2015/06/tectonic-regimes-and-stress.html)

2.3.1 O código STRESSINVERSE – inversão iterativa

No código STRESINVERSE Vavryčuk (2014) propõe a aplicação de restrição de instabilidade de falha de Gephart & Forsyth (1984) no método de Michael (1984). Como o algoritmo de Gephart & Forsyth é não-linear, a restrição de instabilidade da falha pode facilmente ser encontrada através da avaliação do ajuste (busca em grade). Ao contrário do método de Gephart & Forsyth, o método de Michael é linear e pode resolver a inversão dos esforços nas iterações com a implementação de restrição de instabilidade de falha. Primeiro, o método de Michael é aplicado em sua forma padrão, sem considerar qualquer restrição e sem o conhecimento da orientação dos planos de falha. Depois de encontrar as principais direções dos esforços e o fator de forma (R), esses valores são usados para avaliar a instabilidade dos planos nodais para todos os mecanismos focais, equação 16 de Vavryčuk (2014). O plano de falha é o plano nodal que é mais instável. As orientações dos planos de falha encontrados na primeira iteração são usadas na segunda iteração, novamente

usando o método de Michael. O procedimento é repetido até que o esforço converge para valores ótimos.

Ao avaliar a instabilidade de falha usando equação 16 de Vavryčuk (2014), um valor de fricção μ é necessário. Conforme Vavryčuk (2014) a fricção nas falhas geralmente varia entre 0.2 e 0.8, mas seu valor é geralmente desconhecido. Testes numéricos revelaram, no entanto, que a inversão é insensível a μ, por isso, é recomendável atribuir algum valor médio a fricção durante a inversão, por exemplo, μ = 0,6. Outra abordagem é executar a inversão para vários valores de fricção e adotar o valor que produz a maior instabilidade global de falhas. Esta abordagem é usada no processo de testes com sintéticos e também nas aplicações para dados reais.

Em complemento aos resultados do código STRESSINVERSE, para testar a instabilidade nos resultados, adicionamos o teste jackknifing, isto é, a inversão de esforços é repetida sempre com um mecanismo focal a menos e variando com todas as possibilidades.

2.4   Referências (Metodologia)

Aki, K., Richards, P.G., 2002. Quantitative seismology, 2nd ed., University Science Books, Sausalito, CA.

Assumpção, M., Ferreira, J., Barros, L. V., Bezerra, H., Franca, G.S., Barbosa, J.R., Menezes, E., Ribotta, L.C., Pirchiner, M., Nascimento, A., Dourado, J.C., 2014. Intraplate Seismicity in Brazil. In Intraplate Earthquakes, in: Cambridge U.P (Ed.), Talwani, P.

Barros, L. V., Assumpção, M., Chimpliganond, C., Carvalho, J.M., Von Huelsen, M.G., Caixeta, D., França, G.S., de Albuquerque, D.F., Ferreira, V.M., Fontenele, D.P., 2015. The Mara Rosa 2010 GT-5 earthquake and its possible relationship with the continental-scale transbrasiliano lineament. J. South Am. Earth Sci. 60, 1–9. https://doi.org/10.1016/j.jsames.2015.02.002

Benetatos, C., Málek, J., Verga, F., 2012. Moment tensor inversion for two micro-earthquakes occurring inside the Háje gas storage facilities, Czech Republic. J. Seismol. 17, 557–577. https://doi.org/10.1007/s10950-012-9337-0

Bouchon, M., 1981. A simple method to calculate Green's functions for elastic layered media. Bull. Seismol. Soc. Am. 71, 959–971.

Burridge, R., Knopoff, L., 1964. Body force equivalents for seismic dislocations. Bull. Seism. Soc. Am 54, 1875–1888.

Carvalho, J.M., Barros, L. V., Zahradník J., 2014. Seismic source parameters of local micro-earthquakes in Goiás State Brazil by waveform inversion (abstract),. Earth Sci. Res. J. 18, Spec. issue, 166–167.

Cesca, S., Heimann, S., Stammler, K., Dahm, T., 2010. Automated procedure for point and kinematic source inversion at regional distances. J. Geophys. Res. 115, B06304. https://doi.org/10.1029/2009JB006450

Chimpliganond, C., Assumpção, M., Von Huelsen, M., França, G.S., 2010. The intracratonic Caraíbas–Itacarambi earthquake of December 09, 2007 (4.9 mb), Minas Gerais State, Brazil. Tectonophysics 480, 48–56. https://doi.org/10.1016/j.tecto.2009.09.016

Delouis, B., Charlety, C., Vallée, M., 2008. Fast determination of earthquake source parameters from strong motion records: Mw, fo- cal mechanism, and slip distribution, in: EGU General Assembly, Geophysical Research Abstracts 10, Abstract 04939.

Dreger, D., 2003. International Handbook of Earthquake and Engineering Seismology, International Handbook of Earthquake and Engineering Seismology;, International Geophysics. Elsevier. https://doi.org/10.1016/S0074-6142(03)80290-5

Dreger, D.S., Helmberger, D. V., 1993. Determination of source parameters at regional distances with three-component sparse network data. J. Geophys. Res. https://doi.org/10.1029/93JB00023

Ferreira, J., 1997. Sismicidade e esforços no Nordeste do Brasil (Dissertação de mestrado). IAG-USP.

Fojtíková, L., Vavryčuk, V., Cipciar, A., Madarás, J., 2010. Focal mechanisms of micro-earthquakes in the Dobrá Voda seismoactive area in the Malé Karpaty Mts. (Little Carpathians), Slovakia. Tectonophysics 492, 213–229. https://doi.org/10.1016/j.tecto.2010.06.007

Fojtikova, L., Zahradnik, J., 2014. A New Strategy for Weak Events in Sparse Networks: The First-Motion Polarity Solutions Constrained by Single-Station Waveform Inversion. Seismol. Res. Lett. 85, 1265–1274. https://doi.org/10.1785/0220140072

Gephart, J.W., Forsyth, D.W., 1984. An improved method for determining the regional stress tensor using earthquake focal mechanism data: Application to the San Fernando Earthquake Sequence. J. Geophys. Res. 89, 9305. https://doi.org/10.1029/JB089iB11p09305

Hanks, T.C., Kanamori, H., 1979. A moment magnitude scale. J. Geophys. Res. 84, 2348. https://doi.org/10.1029/JB084iB05p02348

Havskov, J., Ottemöller, L., 2010. Routine Data Processing in Earthquake Seismology - With Sample Data, Exercises and Software.

Heidbach, O., Barth, A., Connolly, P., Fuchs, K., Müller, B., Tingay, M., Reinecker, J., Spencer, B., Wenzel, F., 2004. Stress maps in a minute: The 2004 world stress map release. Eos, Trans. Am. Geophys. Union 85, 521. https://doi.org/10.1029/2004EO490001

Herrmann, R.B., 1979. SH-wave generation by dislocation sources - a numerical study. Bull. Seism. Soc. Am., 69(1) 1–15.

Hirasawa, T., 1970. Focal mechanism determination from S wave observations of different quality,. J. Phys. Earth, 18 285–294.

Jiménez, E., Cara, M., Rouland, D., 1989. Focal mechanism of moderate-size earthquakes from the analysis of single-station three-component surface-wave records. Bull. Seism. Soc. Am., 79 955–972.

Kikuchi, B.Y.M., Kanamori, H., 1991. Inversion of complex body waves--iii. Phys. Earth Planet. Inter. 81, 205–222. https://doi.org/10.1016/0031-9201(86)90048-8

Kisslinger, C., 1980. Evaluation of S to P Amplitude ratios for determining focal mechanism from regional network observation. Bull. Seism. Soc. Am., 70, 999–1014.

Lay, T., Wallace T. C., 1995. Modern Global Seismology, Academic Press, California, EUA.

Maercklin, N., Zollo, A., Orefice, A., Festa, G., Emolo, A., De Matteis, R., Delouis, B., Bobbio, A., 2011. The Effectiveness of a Distant Accelerometer Array to Compute Seismic Source Parameters: The April 2009 L'Aquila Earthquake Case History. Bull. Seismol. Soc. Am. 101, 354–365. https://doi.org/10.1785/0120100124

Maruyama, T., 1963. On the force equivalents of dynamic elastic dislocations with reference to the earthquake mechanism. Bull. Earthq. Res. Inst. Univ. Tokyo 467– 486.

McCaffrey, R., Abers, G., Zwick, P., 1991. Inversion of teleseismic body waves. In: Lee, W.H.K. (Ed.), Digital Seismogram Analysis and Waveform Inversion. Int. Assoc. Seismol. Phys. Earth's Inter. El Cerrito, CA. 81–166.

Mendiguren, J.A., Richter, F.M., 1978. On the origin of compressional intraplate stresses in South America. Phys. Earth Planet. Inter. 16, 318–326. https://doi.org/10.1016/0031-9201(78)90070-5

Michael, A.J., 1984. Determination of stress from slip data: Faults and folds. J. Geophys. Res. Solid Earth 89, 11517–11526. https://doi.org/10.1029/JB089iB13p11517

Nakamura, M., 2002. Determination of focal mechanism solution using initial motion polarity of P and S waves,. Phys. Earth Planet. Inter. 130, 17–29.

Nakano, H., 1923. Notes on the nature of the forces which give rise to the earthquake motions. Seism. Bull. Centr. Met. Obs. Japan 1, 92–120.

Snoke, J.A., 2003. FOCMEC: FOCal MEChanism Determinations, Virginia, EUA.

Snoke, J.J.A.J., Munsey, J.J.W., Teague, A.A.C., Bollinger, G.G.A., 1984. A program for focal mechanism determination by combined use of polarity and SV-P amplitude ratio data,. Earthq. notes.

Soares, J., Berrocal, J., Fuck, R.A., Mooney, W., Ventura, D.B.R., 2006. Seismic characteristics of central Brazil crust and upper mantle: A deep seismic refraction study. J. Geophys. Res. 111, B12302. https://doi.org/10.1029/2005JB003769

Sokos, E.N., Zahradnik, J., 2008. ISOLA a Fortran code and a Matlab GUI to perform multiple-point source inversion of seismic data. Comput. Geosci. 34, 967–977. https://doi.org/10.1016/j.cageo.2007.07.005

Stauder, W.S.J., Bollinger, G.A., 1964. The S wave project for focal mechanism studies earthquakes of 1962. Bull. Seism. Soc. Am., 54 2.199-2.208.

Stein, W., Wysession, M., 2003. An Introduction to Seismology, Earthquakes, and Earth Structure.

Suarez, G., Assumpção, M., Suarez, G., 1988. Source mechanisms of moderate-size earthquakes and stress orientation in mid-plate South America. Geophys. J. Int. 92, 253–267. https://doi.org/10.1111/j.1365-246X.1988.tb01138.x

Vavryčuk, V., 2014. Iterative joint inversion for stress and fault orientations from focal mechanisms. Geophys. J. Int. 199, 69–77. https://doi.org/10.1093/gji/ggu224

Wang, C.Y., Herrmann, R.B., 1980. A numerical study of P-, SV-, and SH-wave generation in a plane layered medium,. Bull. Seism. Soc. Am., 70(4) 1015–1036.

Yagi Y. and Nishimura N., 2011. Moment tensor inversion of near source seismograms., Bull. Int. Indy. Sekem. Earthq. Engin.

Zahradník, J., Gallovič, F., 2010. Toward understanding slip inversion uncertainty and artifacts. J. Geophys. Res. 115, B09310. https://doi.org/10.1029/2010JB007414

Zoback, M. Lou, 1992a. Stress field constraints on intraplate seismicity in eastern North America. J. Geophys. Res. 97, 11761. https://doi.org/10.1029/92JB00221

Zoback, M. Lou, 1992b. First- and second-order patterns of stress in the lithosphere: The World Stress Map Project. J. Geophys. Res. 97, 11703. https://doi.org/10.1029/92JB00132

Zoback, M. Lou, Richardson, R.M., 1996. Stress perturbation associated with the Amazonas and other ancient continental rifts. J. Geophys. Res. Solid Earth 101, 5459–5475. https://doi.org/10.1029/95JB03256

CAPÍTULO 3 - ARTIGO 1

Compromising polarity and waveform constraints in focal-mechanism solutions; the Mara Rosa 2010 M_w 4 central Brazil earthquake revisited

J. Zahradník (a), L. Fojtíková (b, e), J. Carvalho (c), L.V. Barros (c), E. Sokos (d), J. Janský (a)

(a) Charles University in Prague, Faculty of Mathematics and Physics, Czech Republic
(b) Institute of Rock Structure and Mechanics, Academy of Sciences of the Czech Republic
(c) Seismologica Observatory of the University of Brasilia, Brazil
(d) University of Patras, Department of Geology, Seismological Laboratory, Greece
(e) Earth Science Institute, Slovak Academy of Sciences, Slovakia

Abstract

Focal-mechanism determination of weak events recorded in sparse networks is challenging. First-motion polarities are often available at relatively distant stations, and waveforms only at a few near stations can be modeled. A two-step approach of how to combine such data has been suggested recently (Cyclic Scanning of the Polarity Solutions, or CSPS method; Fojtíkova and Zahradník, 2014). It starts with creating a suite of first-motion polarity solutions, which is often highly non-unique. The next step consists of repeating full waveform inversion for all polarity solutions. Even few stations may efficiently reduce the non-uniqueness of the polarity solutions. Centroid depth, time, scalar moment and uncertainty estimate of the well-fitting double-couple solutions are obtained. The CSPS method has been extended in this paper by adding a new feature, i.e. repeated inversions using multiple first-motion polarity sets. The polarity sets are created by projecting the stations on focal sphere in several available velocity models, thus accounting for the takeoff angle uncertainty. The multiple polarity sets provide assessment of the CSPS solution stability. These ideas are demonstrated on a comprehensive analysis of a rare event in central Brazil. It is the M_w ~4 mainshock of the Mara Rosa 2010 earthquake sequence (Barros et al., 2015, Carvalho et al., 2015). We employ polarities at 11 stations (distances <730 km) and invert full waveforms at two stations (CAN3 and BDFB at distances ~120 and 240 km), for 0.1-0.2 and 0.05-0.125 Hz, respectively. Six polarity sets reflect the takeoff angle uncertainty. The obtained CSPS results

are very stable across all the polarity sets (in terms of depth, M_w, and strike/dip/rake angles). It is found that the Mara Rosa mainshock mechanism deviated from the composite solution of the whole sequence by 38°. The paper also includes a test simulating situations at which just a single waveform is used, and how it negatively affects the solution stability.

3.1 Introduction

Earthquakes in intraplate regions are rare, and many of them are relatively weak (below thresholds of global agencies). Therefore, their focal-mechanism determination is challenging. The mechanisms are necessary for studying stress field, as well as for calculating ground-motion scenarios for possible stronger events in the same region, whose occurrence is even less frequent. A typical example demonstrating these needs is the huge territory of Brazil. To focus our introductory discussion, let us consider an earthquake M_w ~4 for which P-wave unambiguous first-motion polarities at about ~10 stations with a relatively good azimuthal coverage can be acquired. Is this enough for obtaining a reliable focal mechanism? The answer is obviously 'not' (e.g. Hofstetter, 2014, giving also a good literature survey). We are facing at least two problems: (i) Even if the hypocenter is precisely located, projection of the polarities on focal sphere needs takeoff angles which are dependent on velocity model, and, for a given region, we may have several models. (ii) The polarity solution, inevitably allowing for some polarity error (-s), is non-uniqueness; many combinations of the strike/dip/rake angles agree with a given polarity distribution.

Therefore, waveform inversion is welcome. However, if an earthquake is relatively weak and stations are relatively distant, we face significant problems in fitting observed records by synthetics. As a rule, records cannot be fitted well at distances greater than a few (~10) wavelengths, which is equivalent to some high-frequency limit of the inversion. For example at distances ~20 or 200 km, only frequencies below 1 or 0.1 Hz, respectively, can be inverted. Availability of usable signals at low frequencies is another problem, because they might be either hidden by natural noise, or corrupted by instrument. As such, we may dispose with very few stations with waveforms enabling successful modeling, in

limiting case even just with a single three-component waveform. However, full waveform inversion for the centroid moment tensor with just few stations is an ill posed problem.

The first-motion polarities and waveforms should be jointly used. For example, Chiang and Dreger (2014) documented efficiency of the combined study of low-frequency full waveforms and high frequency P-wave polarities for the source-type discrimination in cases of sparse station coverage and very shallow sources, e.g. man-made explosions. Similarly, Boyd et al. (2013) identified a natural non-double-couple event. Polarities supported the interpretation of regional records of the 2013 North Korean nuclear explosion by Vavryčuk and Kim (2014). Along the same line, study of a historical Amorgos 1956 event, M~7, Aegean Sea, profited from combination of few analog waveforms with many first-motion polarities (Brüstle et al., 2014). Polarities are also needed for resolving the 180 ambiguity of rake in waveform inversions at narrow frequency bands (Zahradník et al., 2008). Obviously, polarities are even more important if inverting amplitude spectra instead waveforms (Cesca et al., 2006; Zahradník et al., 2001).

The mechanisms obtained from waveforms should be checked for consistency with polarities. However, a still open question is how to combine the two data types in the inversion. A two-step approach has been suggested recently as Cyclic Scanning of the Polarity Solutions (CSPS method); Fojtíkova and Zahradník (2014). In the first step a suite of first-motion polarity solutions is calculated. The second step consists of repeating full waveform inversion for all polarity solutions from the first step, seeking subset of the polarity solutions providing a good waveform match. Even few stations may efficiently reduce non-uniqueness of the polarity suite. Centroid depth and time, and scalar moment are also calculated. In this paper we extend the CSPS method by adding a new feature, i.e. repeated applications using multiple first-motion polarity sets. The polarity sets are created by projecting stations on focal sphere in several available velocity models (as in Hardebeck and Shearer, 2002, or Hofstetter, 2014), thus accounting for the takeoff angle uncertainty, and enabling assessment of the CSPS solution stability. In this sense we try to

determine focal mechanism by compromising the polarity and waveform constraints.

These ideas are developed in relation with an important event. The mainshock of the Mara Rosa earthquake sequence, which took place in Central Brazil from October 2010 to June 2011, has been chosen. The M_w ~4 mainshock occurred on October 8, 2010. The aftershock activity was analyzed with an 8-station local temporary network. Precise aftershock locations and the waveform correlation of the aftershocks and mainshock at regional stations enabled the mainshock to be located as a Ground Truth 5 event (GT5), i.e. with uncertainty less than 5 km.

3.2 Geotectonic setting

As detailed in Barros et al. (2015) and Carvalho et al. (2015), the Mara Rosa earthquake occurred in the Goias Tocantins seismic zone, see Fig. 3-1. Seismicity of this zone is weak with most low magnitude (<3.5) events distributed roughly parallel along the large-scale Transbrasiliano Lineament (TBL). The NE-SW (~225°) trending TBL is characterized by high gravity anomalies along the folding track Tocantins Araguaia (Assumpção et al.,1986; Fernandes et al., 1991). The lineament, denominated Brasilia belt, is characterized by folds and thrusts and is a result of the collision and convergence of three continental plates: the Amazon craton (West), São Francisco craton (East) and Paranapanema craton (SouthWest), presently covered by the Parana basin. The Transbrasiliano Lineament is composed of a set of geological features formed in the Neoproterozoic during the formation of the eastern part of the super continent Gondwana (Fuck, 1994 and Fuck et al., 1994).

The regional stress field in central Brazil is basically NW-SE maximum compression, as indicated by in situ measurements of Caproni & Armelin (1990) and theoretical studies (Coblentz & Richardson, 1996). The local stress field related to the Mara Rosa sequence has been calculated by Carvalho et al. (2015) based on 11 aftershocks. The principal stress axes σ_1, σ_2 (the maximum and intermediate compression) are nearly horizontal, while the σ_3 axis

(minimum compression) is nearly vertical, corresponding to the dominant reverse faulting regime; see table 4 of Carvalho et al. (2015). Two optimally oriented faults (OOFs) were also calculated in the mentioned paper. It appeared that Mara Rosa sequence corresponds just to one of the two OOFs, the low-angle fault dipping at 22° and striking at 254°. This OOF deviates by ~30° with respect to the main trend of the Transbrasiliano Lineament.
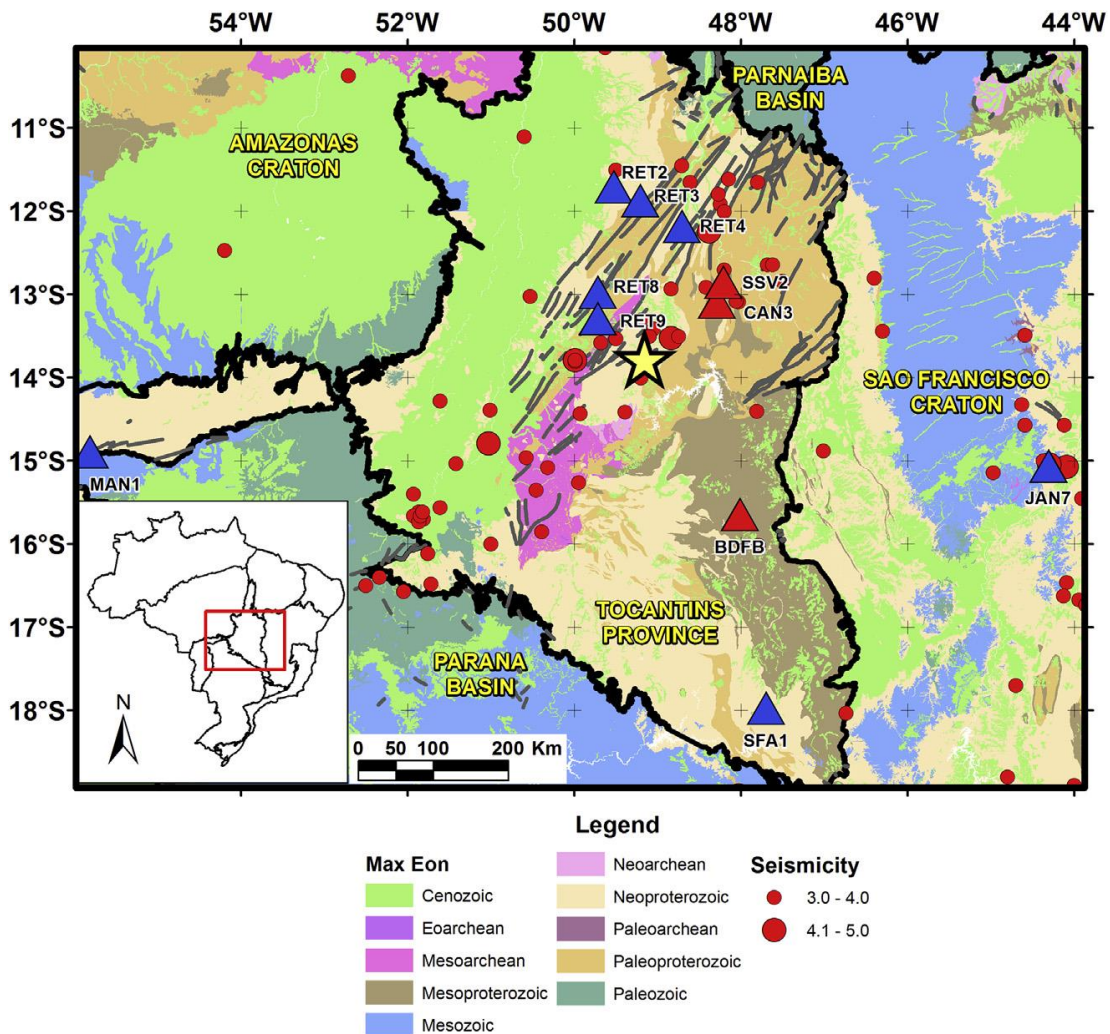
Figura 3-1. Regional geological setting and seismicity of the Tocantins Province and surrounding provinces (Phanerozoic sedimentary Parnaiba and Parana basins, Archean São Francisco and Amazonas cratons). Blue triangles denote stations at which only polarities were used. Red triangles denote stations used for waveform inversion and polarities. The yellow star denotes the Mara Rosa mainshock. Red circles denote earthquakes of magnitude greater than 3 for the period 1970-2011. Brown lines identify Transbrasiliano Lineament, a series of SW-NE trending faults. Geological data are from CPRM (Brazilian Geological Survey, 2004). Inset: geological provinces of Brazil. (For interpretation of the references to color in this figure legend, the reader is referred to the web version of this article.)

3.3 Methods

A brief description of the methods used in the paper is given here. They include the first-motion focal mechanism determination, waveform inversion for the centroid moment tensor calculation, and their combination.

First-motion solutions - Stations with very clear (unambiguous) P-wave first motion polarity and direction consistent with the station azimuth, checked by inspecting all three components, are used. To project the polarities on focal sphere, several velocity models have been employed in order to understand their effect upon the takeoff angles (for details, see Section 4). For each set of the takeoff angles all possible fault-plane solutions, allowing zero or one polarity misfit, have been calculated by FOCMEC code (Snoke, 2003). The solutions have been searched with P- and T-axis angular increments of 6°. Any other similar code can be used as well, e.g. FPFIT (Reasenberg and Oppenheimer, 1985), or HASH (Hardebeck and Shearer, 2002).

Let us comment that, besides polarities, the P- and S-wave amplitude ratios can be also used. The ratio taken from the corresponding wave groups, e.g. Pg and Sg, serves as an additional constraint, helping to reduce non-uniqueness of the polarity solution. Use of the amplitude ratio has not been tested in this paper. Our additional constraint is provided by full waveforms, discussed below.

Centroid-moment-tensor (CMT) solution - Green's functions are calculated by the discrete wavenumber and matrix methods (Kennett and Kerry, 1979; Bouchon, 1981; Coutant 1989) in 1D models with constant-velocity layers. Full waveforms are inverted for deviatoric moment tensor by the least-squares method under assumption of a point source. The inverted moment tensor is parametrized by strike/dip/rake angles, scalar moment Mo (or moment magnitude M_w) and the double-couple percentage (DC). Resolvability of the moment tensor is expressed in terms of condition number (CN). The centroid position and time is grid searched beneath epicenter and around origin time, respectively. The waveform fit is quantified with variance reduction (VR) or correlation (corr), which are related simply by VR = corr^2. The inversion is also made in a fixed-mechanism mode, which means that we prescribe the

strike/dip/rake angles of a given focal mechanism (DC 100%), and determine only the centroid position, time, and moment. We use code ISOLA (Sokos and Zahradník, 2008, 2013).

Methical details can be found elsewhere (Zahradník et al., 2008; Krízova et al., 2013; Zahradník and Sokos, 2014; Quintero et al., 2014). In particular, for choice of suitable frequency range and for previous application to Mara Rosa aftershocks, see Carvalho et al. (2015).

Combining polarities and waveform inversion (CSPS method) - To efficiently retrieve the focal mechanism when only few waveforms can be modeled, but many first-motion polarities can be used, we proceed as follows. The method starts with a suite of the first-motion polarity solutions (FOCMEC output). For each of them we run ISOLA in the fixed-mechanism mode and sort the solutions according the waveform fit. The acceptable solutions are defined, for example, as those with VR > 0.8 VRopt, where VRopt is the best fitting solution. The choice of the threshold (here taken as 0.8) is arbitrary, but must be same when comparing several results with each other. The CSPS method (Fojtíkova and Zahradník, 2014) is currently implemented in ISOLA GUI. Let us note that P-wave polarities and full waveforms represent complementary physical processes and, in general, different velocity models may be appropriate for these two data sets. This aspect will be discussed in the applications.

Kagan angle - To quantify deviation between arbitrary two double-couple focal mechanisms, the Kagan angle, or simply Kangle (Kagan, 1991) has been used. Physically similar mechanisms have K-angle less than ~10°-20° (e.g., Fig. 6 of Zahradník and Custódio, 2012, Fig. 3 of Sokos and Zahradník, 2013).

Code availability - All codes used in this paper are available as a part of ISOLA package at the following link: http://geo.mff.cuni.cz/~jz/isola_2015/. The link includes also Fortran codes to calculate takeoff angles in non-standard situations, e.g. in models with constant velocity gradients (anggrad), or codes providing takeoff angles and travel times of all phases arriving at a station (ang),

not only the first-arriving phase in the standard location-like codes. The latter might be useful when using polarities of several phases at a station.

3.4 Data

Location - Hypocenter position after Barros et al. (2015) is adopted: longitude (W) = 49.1602°, latitude (S) = 13.7713°, depth 1.3 km, origin time 20:16:54.79 UTC. Later, during waveform inversions, we allow the centroid depth to vary from 1.3 to 4.3 km, and centroid time ±3 s with respect to the origin time. A preliminary waveform inversion in the cited paper estimated the moment magnitude to be M_w 4.2.

Velocity models - Three crustal models with constant-velocity layers are used in this study (Fig. 3-2a). They include (i) the 'NewBR' model (Assumpção et al., 2010), (ii) model 'Barros' (Carvalho et al., 2015), and (iii) model 'Soares' (based on Fig. 6 of Soares et al., 2006). For polarity projection on focal sphere an ad-hoc model 'Soares_- grad' with constant velocity gradients is also used.

Polarities - The first-motion polarities at eleven stations of Fig. 3-1 were selected (Table 3-1), spanning the epicentral distance range from 81 to 729 km; the largest azimuthal gap is 98°. The polarities can be projected on focal sphere with several velocity models and, as such, the polarity constraint itself contains an uncertainty. We consider six polarity sets 1-6. The source depth of 1.3 km is assumed (except one case explicitly mentioned below).

Set 1 is based on velocity model NewBR. This set is an example of a 'discontinuous' behavior of the takeoff angles: angles 91° due to direct waves are present at the nearest 4 stations, a 'jump' at RET4 station with angle 64° is due to head wave from the 20-km discontinuity, and the 45° angle at the 6 most distant stations is due to Moho head wave.

Set 2 corresponds to model Barros. This is an example of a 'singularity' of angle 91° occurring only at the nearest station. The 65° angles appear due to the 12-km discontinuity.

Sets 3 and 4 were derived for model Soares which contains a 2 km discontinuity hence the effect of the source depth (1.3 and 2.3 km in Set 3 and 4, respectively) is quite important for the first three stations.

Set 5 is an analogy of model Soares in which the constant velocity layers were substituted by layers with a linear velocity increase (the constant-gradient layers, model Soares_grad), and the only velocity discontinuity is Moho. As such, due to missing internal discontinuities in the crust, the takeoff angles for the first four stations smoothly decrease with increasing epicentral distance.

Set 6 also makes use of model Soares_grad, but it considers only polarities at stations 5-11. The first four stations are discarded to reflect the fact, mentioned above, that their angles are strongly dependent on the assumed velocity model. The takeoff angles at remaining stations are much less uncertain. This set represents the weakest polarity constraint.

The considered polarity sets are displayed in Fig. 3-2b. The figure shows that the effect of the velocity model is most significant up to station 5 (RET4, epicentral distance of 183 km). At greater distances, where the first arrivals are due to Moho head waves, the takeoff angle variation across models is small. It is however to be mentioned that the considered variation of the takeoff angles is the simplest possible; for example, 3D heterogeneities may yield also variations of the station azimuths.

The reference focal-mechanism - For comparison of the individual solutions discussed in this paper, the composite first motion solution derived from the Mara Rosa aftershock sequence, including polarities from the mainshock, is adopted (Barros et al., 2015). It is characterized by the strike/dip/rake angles equal to 216°/49°/74°, see Fig. 3-2b. Note that the reference focal mechanism disagrees with some polarities of the mainshock, namely at stations RET3, RET4, JAN7, and SFA1, independently of the velocity model used to project polarities on focal sphere.
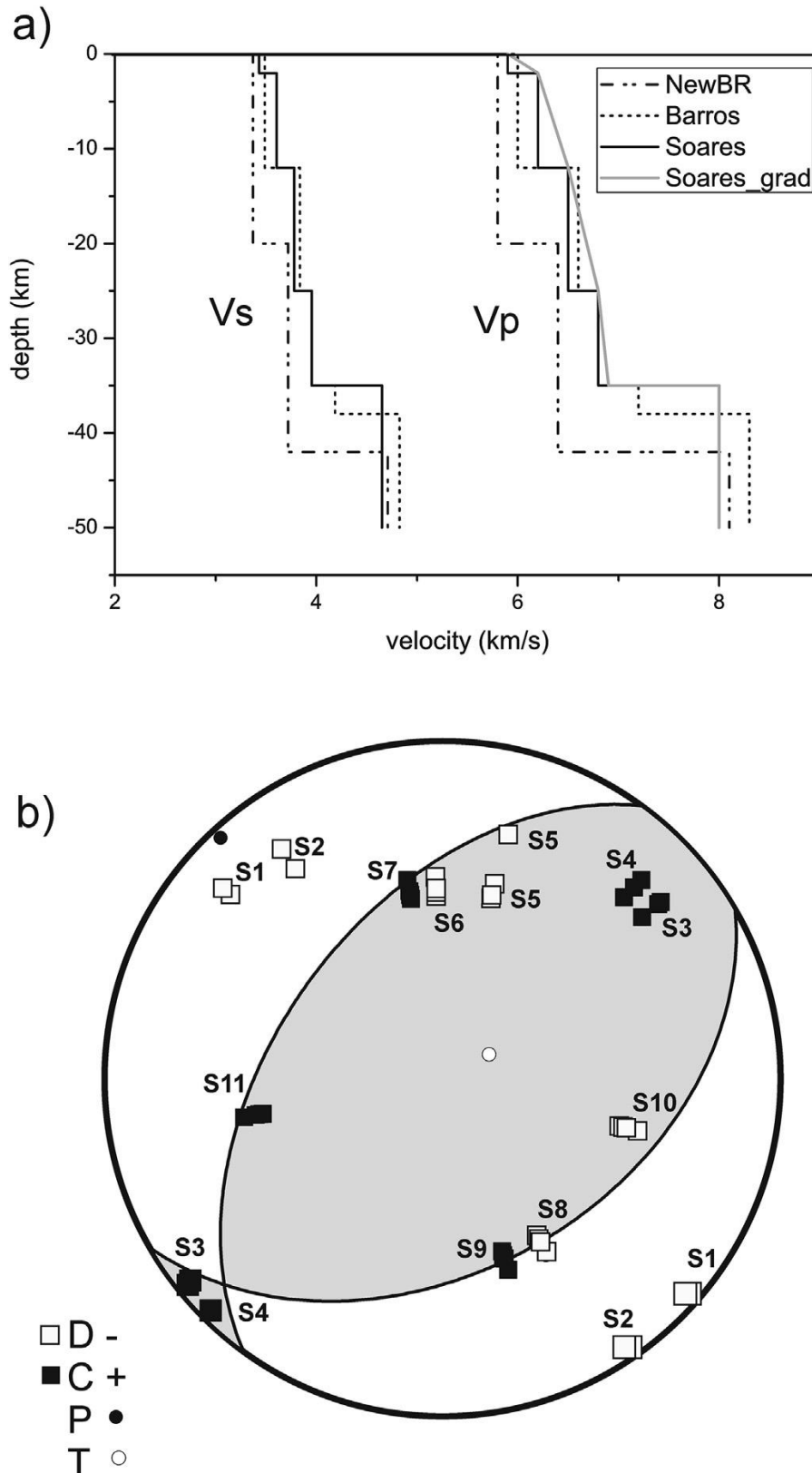
Figura 3-2. Velocity models and their effect upon the polarity projection on focal sphere. (a) The velocity models NewBR, Barros, Soares and Soares_grad. The latter model has been used just as a P-velocity model for the polarity projection. (b) Focal sphere with polarities at stations S1-S11 (for numbering, see Table 3-1). Each station is shown 6- times, according to sets 1-6 of Table 3-1; some sets coincide. Plotted for comparison is the reference focal mechanism (shaded).

Waveforms - The nearest stations that recorded the mainshock with enough quality for the waveform inversion (without saturation) are CAN3, SSV2 and BDFB; see in Fig. 3-1. The first two stations were equipped with 1-s short period sensor, while the latter was a 100-s broad-band instrument. Since CAN3 and SSV2 have almost same azimuths, the SSV2 waveform is not inverted, but the waveform fit at this station is checked. BDFB is a (100 m deep) borehole station. Based on particle motion and the known epicenter position, the recorded horizontal components (BH1 and BH2) were converted into NS-EW system by rotating 90° anticlockwise. The records are free of long-period disturbances (Zahradník and Plesinger, 2010; Vackar et al., 2015).

The frequency range for waveform inversion has been selected as (0.1, 0.2) Hz for CAN3 and (0.05, 0.125) Hz for BDFB, respectively. This choice reflects their different epicentral distances (121 and 241 km), and it satisfies the empirical rule that waveform modeling with common velocity models is typically possible only up to distances of a few (less than ~10) MSW, where MSW is the minimum shear wavelength (Fojtíkova and Zahradník, 2014). With Vs ~3 km/s, and the maximum frequencies of 0.2 and 0.125 Hz, the CAN3 and BDFB stations are situated at distances of 8 and 10 MSW, respectively. Waveforms at larger distances (or higher frequencies) can be sometimes modeled with ad-hoc models specifically derived for selected source-station paths, and we shall return to this possibility in the discussion Section 7. Frequencies lower than 0.1 and 0.05 Hz cannot be used due to noise. Naturally, the narrow usable range of CAN3 and SSV2, close to the natural noise spectral peak, and the fact that this range is below the instrument corner frequency, represent important data drawbacks, rather emphasizing the role of the BDFB station.

3.5   Waveform inversion without prior polarity constraint

Waveform inversion using ISOLA software without a priori constraining the moment tensor solutions by polarities has been applied (hereafter abbreviated as Standard ISOLA, or SI). Three velocity models are used to calculate Green's functions (NewBR, Barros, and Soares, see Section 4). We run two waveform inversions with each velocity model: (i) SI-1 using only BDFB station, (ii) SI-2

jointly inverting CAN3 and BDFB. The deviatoric centroid moment tensor is calculated, providing centroid depth and time, strike/dip/ rake angles, and scalar moment. The results, presented in Table 3-2, are as follows.

SI-1 Just a single station (BDFB) has been inverted in this test. Therefore, the variance reduction is obviously high, ranging in the individual velocity models from VR 0.89 to 0.94. Physical meaning of such a good waveform fit is however very limited (thus not graphically shown) because the inversion is ill posed. It is documented by large condition number (CN) values, ranging from 14 to 30, and also by a very large variation of the focal mechanism across the velocity models in Fig. 3-3.
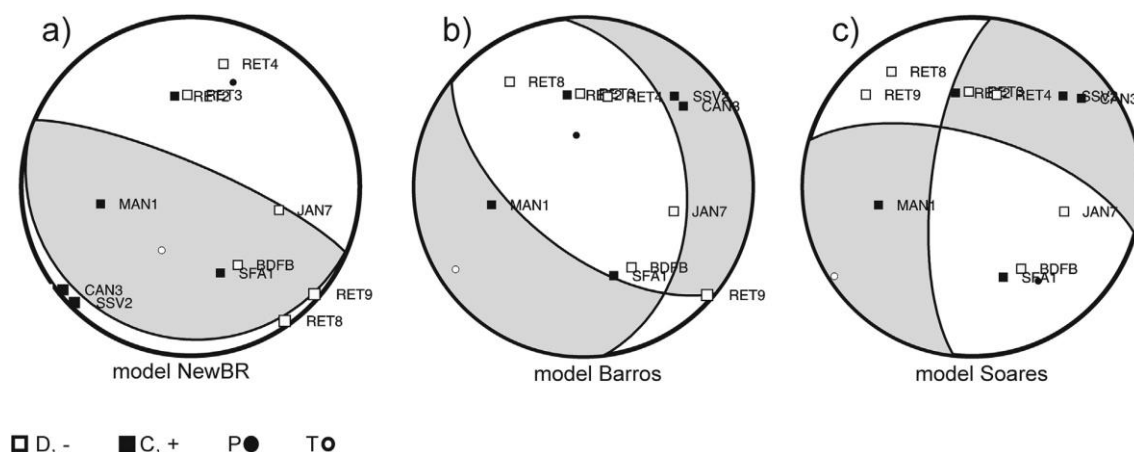
Figure 3-3. Focal mechanisms obtained by single-station (BDFB) waveform inversion, without pre-constraining the solution by polarities. Three velocity models are used: (a) model NewBR, (b) model Barros, (b) model Soares. The problem is ill posed, the results are physically meaningless.

Table 3-1 - First-motion polarities and six sets of takeoff angles for various velocity models.

Station no.	Station code	Polarity	Distance (km)	Azimuth (°)	Takeoff angle set (°)					
					1	2	3	4	5	6
S1	RET9	D	81	311	91	91	72 (2)	91	75	None
S2	RET8	D	107	325	91	65 (12)	72 (2)	91	72	None
S3	CAN3	U	121	51	91	65 (12)	72 (2)	91	71	None
S4	SSV2	U	144	45	91	65 (12)	65 (12)	72 (12)	69	None
S5	RET4	D	183	15	64 (20)[a]	46 (38)	47 (35)	50 (35)	47 (35)	47 (35)
S6	RET3	D	210	358	45 (42)	46 (38)	47 (35)	50 (35)	47 (35)	47 (35)
S7	RET2	U	233	350	45 (42)	46 (38)	47 (35)	50 (35)	47 (35)	47 (35)
S8	BDFB	D	241	149	45 (42)	46 (38)	47 (35)	50 (35)	47 (35)	47 (35)
S9	SFA1	U	490	161	45 (42)	46 (38)	47 (35)	50 (35)	47 (35)	47 (35)
S10	JAN7	D	542	105	45 (42)	46 (38)	47 (35)	50 (35)	47 (35)	47 (35)
S11	MAN1	U	729	259	45 (42)	46 (38)	47 (35)	50 (35)	47 (35)	47 (35)

a) The bracketed numbers after takeoff angles show the depth of discontinuity where the corresponding head wave is generated. The angles without any bracket are those of direct waves.

Table 3-2 Waveform inversions unconstrained by polarities for a single station BDFB (SI-1) and for two stations CAN3 and BDFB (SI-2).

Model	Centroid depth (km)	Centroid time[a] (s)	Mw	Strike (°)	Dip (°)	Rake (°)	DC (%)	VR	CN	K-angle[c] (°)	Stations with polarity misfit
SI-1 (station BDFB)											
NewBR	2.3	−3.0[b]	4.6	293	79	91	41	0.94	14	76	BDFB,JAN7, RET2,SSV2, CAN3
Barros	1.3	0.3	4.7	353	39	−53	9	0.89	30	102	RET2
Soares	1.3	0.3	4.6	286	65	−158	78	0.94	21	90	RET3,RET4, SFA1

Station and Model	Centroid depth (km)	Centroid time[a] (s)	Mw	Strike (°)	Dip (°)	Rake (°)	DC (%)	VR	CN	K-angle[c](°)	Stations with polarity misfit
SI-2 (stations CAN3 and BDFB)											
NewBR	1.3	−3.0[b]	4.6	225	83	87	98	0.78	5	36	BDFB,JAN7, RET2,MAN1
Barros	1.3	0.60	4.4	233	57	91	48	0.81	5	17	RET2,JAN7, BDFB
Soares	1.3	0.66	4.4	219	40	70	56	0.87	5	11	RET3,RET4, SFA1

a) Centroid time is expressed with respect to origin time.
b) At the limit of the temporal grid.
c) Angular deviation from the reference solution.

The posterior polarity check (using the corresponding sets 1-3) reveals severe polarity errors. Note also, that all the solutions are far from the reference solution (K-angle 76-102). The DC-percentage varies from 9 to 78%. The moment magnitude is too high 4.6-4.7. The results clearly show that with this single station the standard polarity-unconstrained CMT inversion is not possible.

SI-2 Two stations (CAN3 and BDFB) are inverted jointly in deviatoric mode for all CMT parameters in this test. As documented in the second part of Table 3-2 (SI-2) and in Fig. 3-4, the results are more reasonable than in the single-station test SI-1. The inversion stability is reflected by the relatively small CN (=5). At the same time, VR is quite high, 0.78-0.87. The preferred centroid depth in the considered models is 1.3 km. The fault plane solutions are self-similar, but far from being identical. Two models are close to the reference solution (K-angle 11 and 17), but their DC-percentage (48 and 56%) is low. At least three polarities are misfit by any of the solutions. Model NewBR produces the least appropriate results (the centroid time too far from origin time, four polarity disagreements).
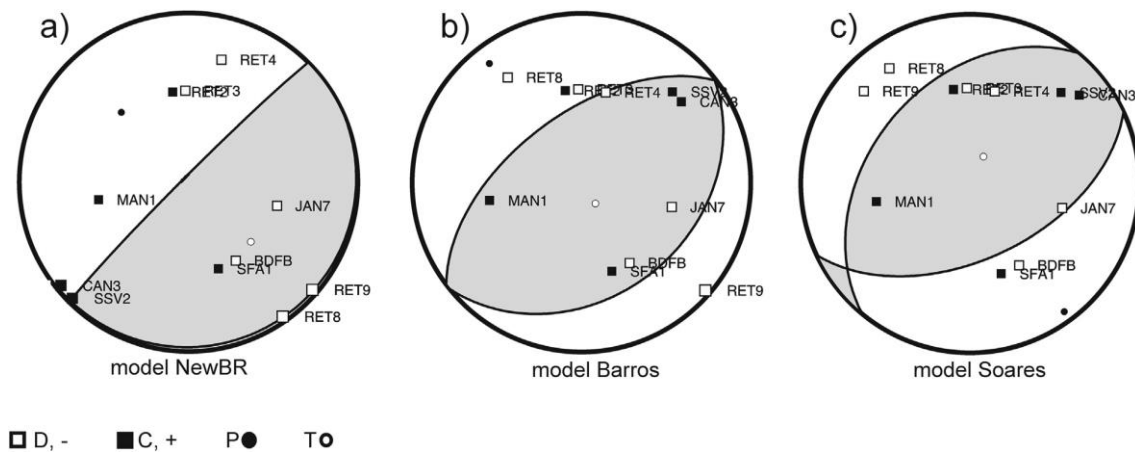
Figure 3-4. Focal mechanisms obtained by two-station (CAN3 and BDFB) waveform inversion, without pre-constraining the solution by polarities. Three velocity models are used: (a) model NewBR, (b) model Barros, (c) model Soares. The problem is well posed, the results are physically more reasonable than in Fig. 3-3.

A typical waveform fit, for model Barros, is shown in Fig. 3-5a. Very good match and a high signal-to-noise ratio at BDFB station can be seen. The CAN3 record is also fitted, but is evidently noisier. At the non-inverted station SSV2 the observed and synthetic data are of the same amplitude order.

As a whole, the results show that with these two stations the standard polarity-unconstrained CMT inversion is physically meaningful. Nevertheless, although the waveform fit is very good (VR is high), the solutions are not fully trustful because they contain several polarity misfits and their DC% is relatively low (Fig. 3-5c). These effects are due to limited accuracy of the velocity models and presence of noise. It implies that the focal-mechanism determination needs an additional constraint.

Finally, it is also useful to demonstrate the two-station (CAN3 and BDFB) modeling with the strike/dip/rake angles kept fixed at the reference focal-mechanism solution (DC = 100%). This kind of modeling includes just optimization of the waveform match as regards the centroid depth, time and moment. Compared to the free inversion, the focal mechanism produces a worse waveform match, see Fig. 3-5a,b; indeed, using velocity model Barros, variance reduction decreases from 0.81 to 0.66. As already mentioned in Section 4, the reference solution fails in satisfying four polarities. Therefore,

applying a polarity constraint in the next section, even lower VR can be expected.

Another notable (and rather general) feature is the considerably stronger variation of the waveform correlation with the trial source depth when the focal mechanism is kept fixed; Fig. 3-5d. The explanation is simple: fixing the mechanism removes its tradeoff with the source depth. This is useful for resolving the centroid depth when the used mechanism is estimated well. High correlations at the depth of 1.3 and 2.3 km represent a strong posterior validation of the hypocenter location.
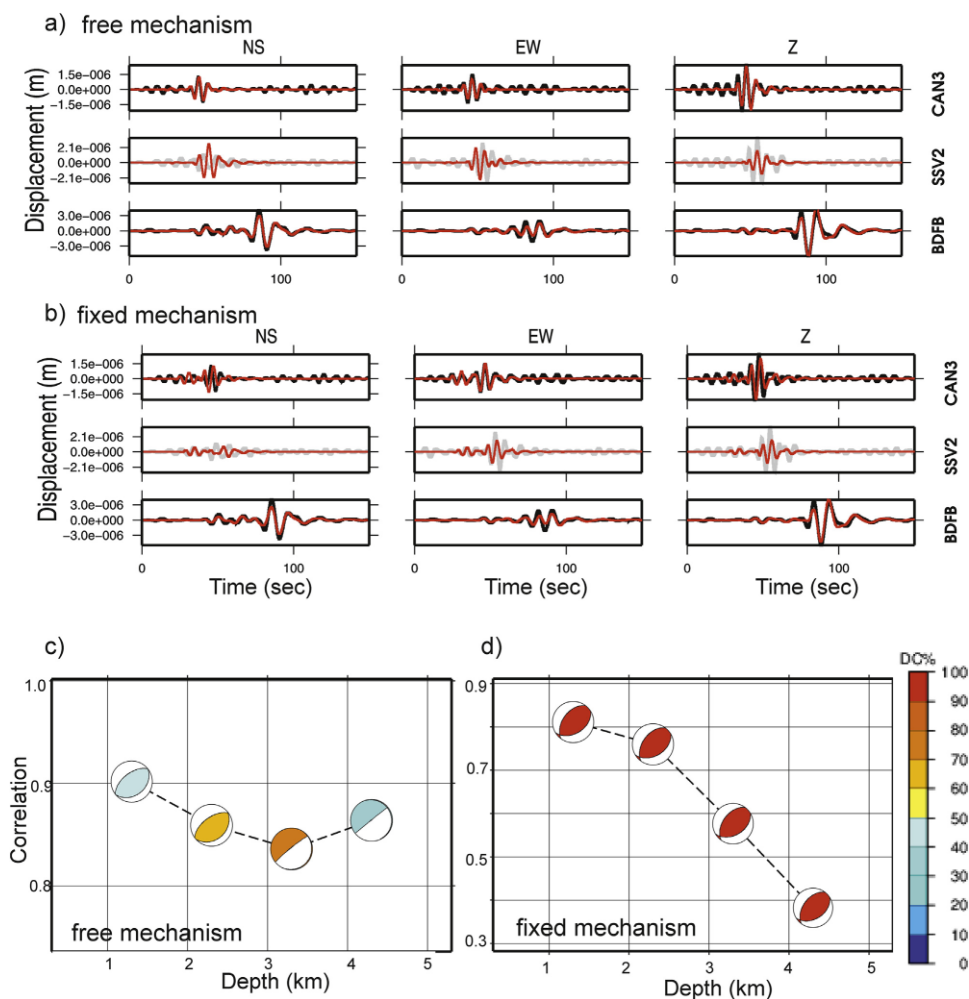
Figura 3-5. A typical waveform match for the two-station inversion (CAN3 and BDFB, model Barros). The observed and synthetic displacements are shown by black and red lines, respectively. Station SSV2 is not inverted, it is plotted just for checking purposes. (a) Free inversion (VR 0.81), (b) modeling with fixed strike/dip/rake angles corresponding to the reference solution (VR 0.66). Panels (c) and (d) demonstrate the waveform correlation as a function of trial source depth for the free and fixed mechanism, respectively. (For interpretation of the references to color in this figure legend, the reader is referred to the web version of this article.)

3.6 Waveform inversion with a prior polarity constraint

Six sets of takeoff angles (Table 3-1) have been employed to calculate first-motion focal mechanisms. The sets reflect the impact of the uncertain velocity model upon polarity projection on focal sphere. The FOCMEC code has been used allowing zero or maximum one polarity error. The following numbers of the solutions have been obtained in the six sets: 5/138, 0/62, 0/76, 0/105, 0/ 91, 28/636, while allowing for 0/1 error, respectively. The polarity solutions allowing for one error are shown in Fig. 3-6. We have found: (i) Although the polarities are relatively well azimuthally distributed, the focal-mechanism non-uniqueness in each set is large. (ii) Set 6 (with four polarities discarded) is an extreme example of an almost unconstrained solution. (iii) Effect of the velocity model, seen in the variation between sets 1-6, is significant.

Following the idea of CSPS method (Section 3), all polarity solutions of each set are repeatedly used, and their fixed strike/dip/rake angles are employed in waveform inversion. In this way we try to find out subsets of the polarity solutions with a good waveform fit. Seismograms at CAN3 and BDFB stations are modeled in the same frequency ranges as in the preceding section. Their joint inversion for velocity model Barros is presented (using model Soares the results are very similar). The inversion provides the optimum centroid depth, centroid time and scalar moment (or M_w). As before, station SSV2 is not inverted but its waveform fit is checked. The CSPS results for the six polarity sets e representing the main result of this paper e are shown in Fig. 3-7.

The figure shows all acceptable solutions defined by VR > 0.8 VRopt. Table 3-3 gives the best fitting solutions (VRopt), and these are identical for some of the sets. The results are quite interesting: In spite of significant differences between polarity solutions of sets 1-6 (in Fig. 3-6), the waveform inversion strongly prefers very similar focal mechanisms (strike 248°-259°, dip 47°-59°, and rake 115°-129°). Their deviation from the reference solution (K-angle 31°-45°) is larger than in Section 5. All best-fitting solutions prefer the shallowest source depth (1.3 km). The same source-depth preference holds for all acceptable solutions. Such a good depth resolution is due to fixing of the mechanisms, as

already mentioned in connection with Fig. 3-5d. The M_w of the best-fitting solutions is confined to a narrow range of 4.3-4.4, as well as VRopt 0.59-0.63. The waveform fit is very similar to that shown in Fig. 3-5b.

The amazing similarity between the CSPS solutions for all six polarity sets, including the almost unconstrained set 6, has a simple interpretation: the two-station waveform constraint is quite strong (being related to the relatively low CN~5, documented in Section 5). Fig. 3-7 as a whole can be considered as a final result of the Mara Rosa focal-mechanism determination, including the uncertainties.
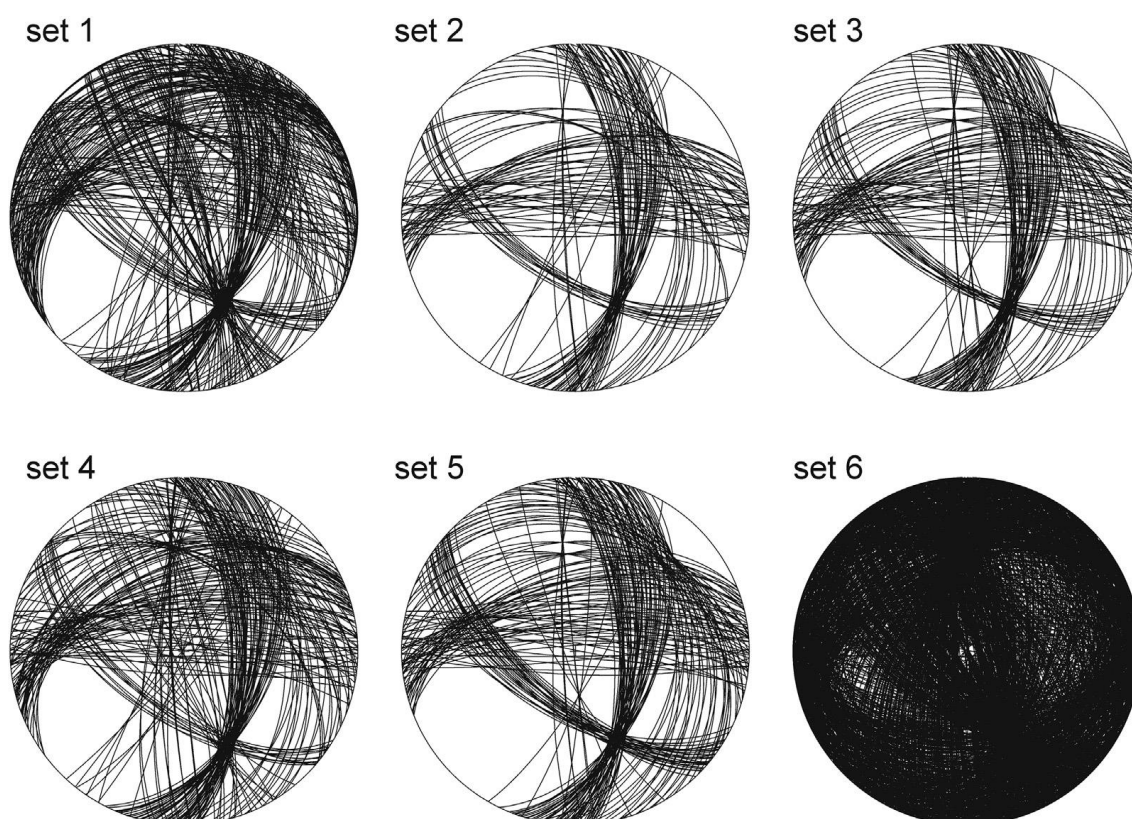
Figure 3-6. First-motion focal mechanism solutions for six polarity sets of Table 3-1, reflecting effects of the velocity model. One polarity error is allowed. The non-uniqueness of the focal mechanism is remarkable.

Table 3-3 Waveform inversion at two stations (CAN3 and BDFB) in model Barros, constrained by 11 polarities. Six sets of takeoff angles of Table 3-1 are used. The preferred solution is shown in bold.

Takeoff angle set	Centroid depth (km)	Centroid time[a](s)	Mw	Strike (°)	Dip (°)	Rake (°)	VRopt	K-angle[b] (°)	Stations with polarity misfit
1	1.3	0.84	4.3	**254**	**47**	**126**	0.59	38	RET2 (at nodal line)
2, 3, 5	1.3	0.96	4.3	256	54	129	0.60	43	RET2
4	1.3	1.02	4.3	259	59	127	0.62	45	RET2
6	1.3	0.84	4.4	248	50	115	0.63	31	RET2

a) Centroid time is expressed with respect to origin time.

b) Angular deviation from the reference solution.

All best-fitting solutions of sets 1-6 are characterized by polarity misfit at same station (RET2), but the station is close to nodal line. In particular, for set 1, station RET2 is just at the nodal line of the best fitting solution (strike/dip/rake = 254°/47°/126°). Therefore, if Fig. 3-7 has to be substituted by a concise representation, just this solution is useful. Indeed, it can be considered as the preferred mechanism, since it optimally balances the waveform and polarity constraints. Its deviation from the reference solution is characterized by K-angle 38°. Note that the obtained waveform fit is still acceptable (VR 0.59), although lower than in Section 5 where the waveforms were inverted without any polarity constraint. It is a price we pay for the improvement of the polarity fit and for strong decrease of the solution non-uniqueness compared to Fig. 3-6.
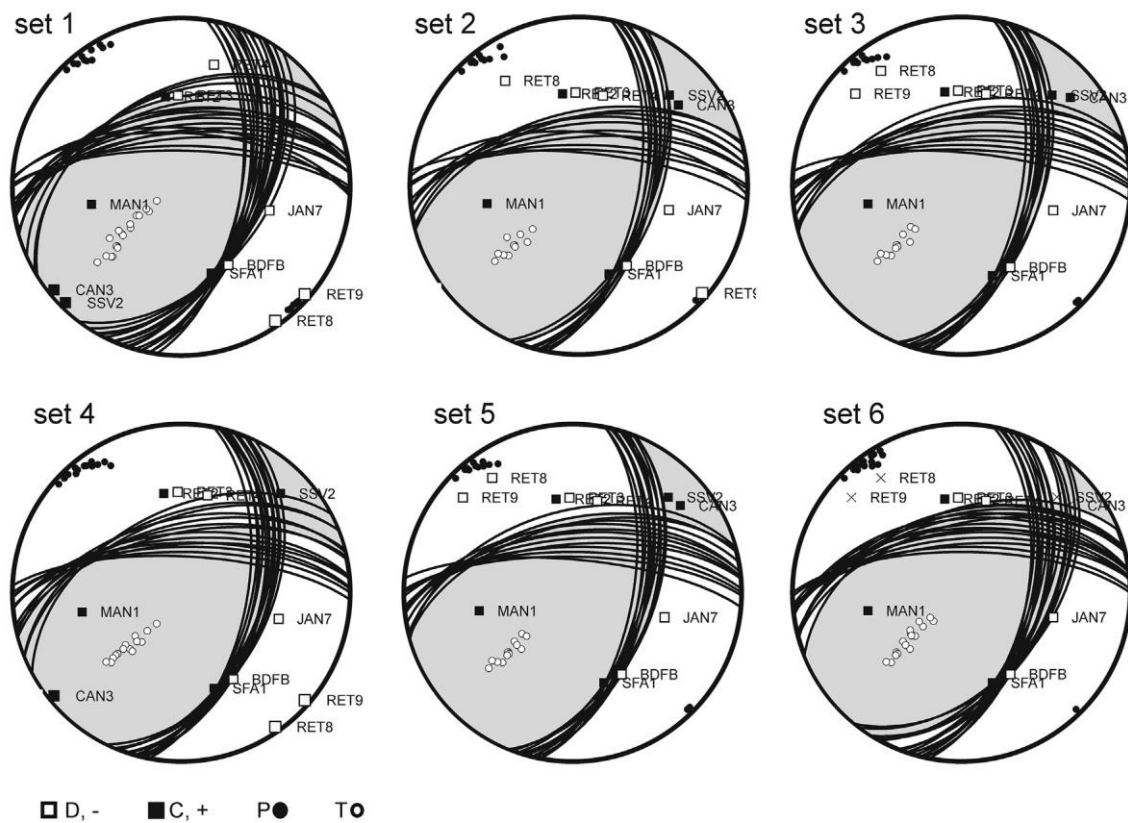
Figure 3-7. Focal mechanisms obtained by two-station (CAN3 and BDFB) waveform inversion, pre-constrained by the first-motion polarity sets 1 to 6, in which one polarity error is allowed. All CSPS solutions with VR > 0.8 VRopt are shown by nodal lines, while the VRopt solution is shaded. Note the similarity of the solutions across the polarity sets. Crosses (x) in set 6 denote the stations whose polarities were discarded.

3.7   Discussion

We have compared our calculations with the reference solution. It is necessary to better explain how to understand the 38° departure of the preferred mechanism (strike/dip/rake 254°/47°/126°) from the reference (216°/49°/74°). Recall that the reference solution was previously obtained as a composite solution of the Mara Rosa sequence, comprising the mainshock and aftershocks. The existence of a composite solution (i.e. the fact that some solution could be found) indicates that the events have had similar mechanisms, although not identical. The deviation of the individual aftershock mechanisms from the reference solution (K-angle 19°-61°) has already been demonstrated by Carvalho et al. (2015) in their Fig. 7b. Therefore, the mainshock may also deviate from the composite solution. Indeed, we found that 4 mainshock polarities disagree with the reference solution. On the other hand we cannot expect that the mainshock is completely different from the composite solution (e.g. being normal instead of reverse). In this light, the obtained 38° difference is reasonable, and represents a physically interesting result. It implies that the mainshock can be characterized as oblique faulting, rather than pure thrust. Note that the greater value of the rake angle compared to the reference value has been already detected also for aftershocks by Carvalho et al. (2015).

The preferred mechanism can be also compared to the mechanism obtained by Barros et al. (2015) from a preliminary waveform inversion: 228°/44°/70°. The solution did not combine waveforms with polarities. The K-angle deviation of this solution with respect to our preferred solution is 42°.

On several occasions we have mentioned that our knowledge of the velocity structure of the studied region is limited. As such, adhoc velocity models derived for specific source-station paths may facilitate the moment tensor inversion, as shown, for example, by Herrmann et al. (2011), or Dias and Assumpção (2015). We have tested a velocity model provided with permission by F. Dias (PhD thesis under preparation). It has been derived from Rayleigh and Love wave dispersion (period range 5-45 and 10-25 s, respectively) along the path between epicenter and BDFB station. The model is not much different

compared to the other tested models, e.g. model Barros, mainly except the topmost 3-km thick layer of a somewhat lower velocity (Vp = 5.61). This model is still under development and that is why we comment on it only in discussion. The model provided the following results: (i) the single-station BDFB inversion of the SI type, i.e. without priority constraint, was characterized by the largest VR value (0.96) among all tested models, but the double-couple percentage was as low as 20%. Nevertheless, that single-station mechanism (262°/55°/129°) was the closest to the preferred mechanism of this paper. (ii) When using this ad-hoc velocity model for both source-station paths, CAN3 and BDFB, and doing CSPS, the acceptable and best-fitting solutions were quite analogous to Fig. 3-7, which can be considered as an independent support of our solution. However, VRopt is lower with the ad-hoc model (0.53), because this model is not suitable for CAN3. It indicates that if ad-hoc models would be derived for all source-station paths, they could further improve the CMT resolvability (using the station-dependent velocity models supported in ISOLA code).

As a part of general comments we should recall advantage of broadband stations. Thanks to them we can make waveform inversion at relatively distant stations. In the Mara Rosa earthquake this was the favorable case of BDFB station (~240 km), modeled at (0.05-0.125) Hz. Much less favorable was the short-period CAN3 station (0.1-0.2 Hz), although situated closer to the source.

The reader interested in similar applications elsewhere might want to see how the CSPS approach would work if applied to single station (-s). It is a legitimate concern because users might dispose with many polarities, but just with a single station at the epicentral distance enabling waveform modeling. Therefore we simulate such a case by three times repeating tests like those of Fig. 3-7 (in velocity model Barros), this time using each station individually: CAN3, SSV2 and BDFB, see Figs. AC.S1-AC.S3 in the Electronic Supplement (Annex C), respectively. The first and important observation is that when keeping the former threshold VR > 0.8 VRopt, the number of acceptable solution is much greater than in the two-station CSPS approach, thus making plots quite unclear. Therefore, the present single-station tests are performed with VR > 0.95 VRopt,

and, for reader's comfort, the former two-station (CAN3 and BDFB) inversion of Fig. 3-7 is repeated in Fig. AC.S4 also with the 0.95 threshold.

The single-station CSPS tests yield the following results: (i) In contrast to Fig. 3-7, the best-fitting CSPS solutions (shaded) are no more same for all six polarity sets e see, e.g., CAN3 with set 6, or SSV2 with sets 1 and 2. (ii) The acceptable solutions are no more clustered around the best-fitting solutions; some nodal lines are quite far from the shaded sectors. It is most clearly seen in the weakly constrained set 6. (iii) We can even say that CSPS method for set 6 lost the resolution. (iv) Although inverting a single waveform, the waveform fit is good only at station BDFB. (VRopt ~0.8), while at CAN3 and SSV2 we get only ~0.5 and 0.6, respectively. (v) The BDFB inversion is the most stable one because it is a broadband station, and we were able to employ relatively low frequencies.

These examples are a good illustration of the situations possibly encountered when user (studying some other event) can use just a single station. The examples emphasize the role of multiple polarity sets, introduced and frequently used in this paper. Indeed, instability of the CSPS solution across the polarity sets (seen both for CAN3 and SSV2 in Figs. AC.S1 and AC.S2) can be used by user as an indicator that the single-station CSPS inversion may be inappropriate. Generally speaking, single-station waveform inversions are always dangerous (even when combined with polarities) and the cases when they provide good focal mechanisms are always to be understood as 'very favorable'.

A more advanced user of the method may be also interested in the internal performance of the CSPS method. How efficiently the waveforms eliminate non-uniqueness of the polarity solution? It is illustrated in Fig. AC.S5 related to the CSPS solution at CAN3 and BDFB stations, using the polarity set 1. Shown in this figure is the variance reduction for all nodal lines belonging to set 1 of Fig. 3-6. Most of the solutions produce a very poor waveform fit (low VR, blue color in Fig. S5). Only few solutions have large VR, and that is why the CSPS application to set 1 in Fig. 3-7 resulted in the very compact solution family. The

large-VR solutions clearly resolve M_w ~4.3, and strongly prefer the first trial source depth of 1.3 km.

3.8 Conclusion

A comprehensive analysis of the focal mechanism of the Mara Rosa mainshock has been made. Solutions based on first-motion polarities, waveform inversion, and combined polarity-waveform data were obtained. Now we summarize and compare these solutions with each other and also with the reference solution, previously calculated as composite solution of the mainshock and aftershocks.

Determining the mainshock mechanism by the single-station waveform inversion (standard ISOLA, SI-1, Table 3-2 and Fig. 3-3) yields an unstable solution. Two stations (SI-2, Fig. 3-4) provide a more reasonable solution if using velocity models Barros and Soares. The mechanisms are close to the reference solution (Kangle angle 17° and 11°, respectively), and the waveform fit is very good (VR~0.8). However, the DC percentage is low (<60%), and three (unambiguous) polarities are in error.

Determining the mainshock mechanism by first-motion polarities only (Fig. 3-6), leads to a highly non-unique solution. Moreover, the solution is uncertain thanks to possible variation of the takeoff angles due to limited knowledge of the velocity model used to project stations on the focal sphere (six polarity sets have been discussed, Table 3-1). We recall that effects of the velocity model upon takeoff angles are most significant at epicentral distances smaller than those where the Moho head wave is in the first arrival (in case of Mara Rosa at distances < 200 km).

Pre-constraining focal mechanisms by first-motion polarities and then doing two-station waveform inversion in model Barros (CSPS method, Table 3-3) we obtain very similar solutions for all six polarity sets (Fig. 3-7). In this sense, considering multiple polarity sets has proven to be useful innovation, serving as a stability indicator. Self-similarity of the solutions, all of which have presumably DC = 100%, includes their centroid depth (1.3 km), the strike/dip/ rake angles, M_w (4.3-4.4), and the same single polarity misfit (station RET2, close to nodal

line). Obviously, the joint polarity waveform inversion CSPS yields a worse waveform match (VR ~0.6) than in the SI method. If the mainshock needs to be characterized by a single solution we prefer the mechanism with strike/ dip/rake = 254°/47°/126°, having station RAT2 just at nodal line. This solution deviates from the reference (composite) solution (216°/49°/74°) in terms of K-angle by 38°. Such a deviation is not negligible, and represents an important improvement compared to the characterization of the mainshock by the composite solution. We believe that for the Mara Rosa mainshock, the CSPS approach based on inverting waveforms at two stations is the most appropriate one, because the result successfully compromises first motion polarities with limited number of waveforms.

Geologically, despite typical difficulties of associating very shallow earthquakes in stable continent interior with tectonic structures, it is to emphasize that the Mara Rosa mainshock has the same strike (254°) as one of the two OOFs, calculated from aftershocks in Carvalho et al. (2015). This strike indicates a global relation of the Mara Rosa mainshock to the Transbrasiliano Lineament, although, at closer look, there is a small deviation ~30° between the OOF and TBL trends.

To illustrate problems possibly encountered by users of the method elsewhere, when just a single station is available for the waveform inversion by CSPS approach, such a case has been imitated using the Mara Rosa data. To this goal the three stations CAN3, SSV2, and BDFB, were used individually (Figs. AC.S1-AC.S3 of Annex C). It has been shown that the inversion is considerably less well constrained, and the CSPS results vary with used polarity sets. Such a variation may serve as an important indicator that the single-station CSPS inversion is problematic. It again emphasized the role of considering several polarity sets, suggested in the present paper.

The present paper can be understood as an example of a critical analysis how to balance various constraints and assumptions (waveforms, polarities) when limited data are available. The main innovation has been the extension of the CSPS method by repeatedly using multiple first-motion polarity sets, reflecting

the takeoff angle uncertainty in the available velocity models. The idea goes back to Hardebeck and Shearer (2002), but in this paper it has been linked, for the first time, with the waveform inversion (through CSPS). Although focused on a single event, we tried to emphasize general methodical features to facilitate broad applications of the CSPS method in various focal-mechanism studies of sparsely recorded events.

Acknowledgments

Supplementary data (Annex C)

Supplementary data related to this article can be also found at http://dx.doi.org/10.1016/j.jsames.2015.08.011.

3.9   References (paper 1)

Assumpção, M., Lima, T.M., Tomas, L.A., 1986. O sismo de Araguapaz de 14.01.1986 e o Lineamento Transbrasiliano. In: 34o Congresso Brasileiro de Geologia, Goiânia (p. 5p).

Assumpção, M., Ardito, J.E., Barbosa, J.R., 2010. An improved velocity model for regional epicentre determination in Brazil. IV Simpósio Brasileiro de Geofísica. Brasília 13e16 de novembro de 2010.

Barros, L.V., Assumpção, M., Chimpliganond, C., Carvalho, J.M., Von Huelsen, M.G., Caixeta, D.F., França, G.S., Albuquerque, D.F., Martins, V.F., Fontenele, D.P., 2015.

The Mara Rosa 2010 GT-5 earthquake and its possible relationship with the continental-scale Transbrasiliano lineament. J. South Am. Earth Sci. 60, 1e9.

Bouchon, M., 1981. A simple method to calculate Green's functions for elastic layered media. Bull. Seism. Soc. Am. 71, 959e971.

Boyd, O.S., Dreger, D.S., Lai, V.H., Brutto, R., 2013. Full moment tensor analysis using first motion data at the Geysers geothermal field. In: Proceedings, Thirty-eighth Workshop on Geothermal Reservoir Engineering. Stanford University, Stanford, California. February 11-13, 2013. SGP-TR-198.

Brüstle, A., Friederich, W., Meier, T., Gross, C., 2014. Focal mechanism and depth of the 1956 Amorgos twin earthquakes from waveform matching of analogue seismograms. Solid Earth 5, 1027e1044. http://dx.doi.org/10.5194/se-5-1027- 2014.

Caproni, N., Armelin, J., 1990. Instrumentacão das escavações subterrâneas da UHE Serra da Mesa. In: Simpósio sobre Instrumentação Geotecnica de Campo - SINGEO'90 Associação Brasileira de Geologia de Engenharia, São Paulo, vol. 1, pp. 249e257.

Carvalho, J.M., Barros, L.V., Zahradník, J., 2015. Focal mechanisms and moment magnitudes of micro-earthquakes in central Brazil by waveform inversion with quality assessment and inference of the local stress field. J. South Am. Earth Sci. (in press).

Cesca, S., Buforn, E., Dam, T., 2006. Amplitude spectra moment tensor inversion of shallow earthquakes in Spain. Geophys. J. Int. 166, 839e854.

Coblentz, D.D., Richardson, R.M., 1996. Analysis of the South American intraplate stress field. J. Geophys. Res. 101 (B4), 8643. http://dx.doi.org/10.1029/96JB00090.

Chiang, A., Dreger, D.S., 2014. Moment tensor analysis of shallow sources. Section 27, pp. 67e68. In: Berkeley Seismological Laboratory Annual Report, July 2013eJune 2014.

Coutant, O., 1989. Program of Numerical Simulation AXITRA. Laboratoire de Geophysique Interne et Tectonophysique Report. University of Joseph Fourier, Grenoble.

CPRM e Serviço Geológico do Brasil, 2004. Brazilian Geological Survey. Geological Map of Brazil, scale 1:1,000,000, Geographic Information System, 2004. CD Rom.

Dias, F., Assumpção, M., 2015. Moment tensor solution of moderate events at large distances: using surface waves to build velocity models for the waveform inversion, examples from Brazil. J. South Am. Earth Sci. (submitted).

Fernandes, E., Blum, M., Ribeiro, R., 1991. The Goias seismic zone, a new approach. In: Extended Abstract. 35 Congress Braz. Geol. Soc., Salvador/BA, vol. 2, pp. 553e558.

Fojtíkova, L., Zahradník, J., 2014. A new strategy for weak events in sparse networks: the first-motion polarity solutions constrained by single-station waveform inversion. Seismol. Res. Lett. 85, 1265e1274. http://dx.doi.org/10.1785/0220140072.

Fuck, R.A., 1994. A Faixa Brasília e a Compartimentação Tectônica na Província Tocantins, IV Simpósio de Geologia do Centro-Oeste. SBG. Brasília 184e187.

Fuck, R.A., Pimentel, M., Silva, L., 1994. Compartimentação Tectônica na Porção Oriental da Província Tocantins, IV Simpósio de Geologia do Centro-Oeste., SBG. Brasília 215e216.

Hardebeck, J.L., Shearer, P.M., 2002. A new method for determining first-motion focal mechanisms. Bull. Seism. Soc. Am. 92, 2264e2276.

Herrmann, R.B., Malagnini, L., Munafo, I., 2011. Regional moment tensors of the 2009 L'Aquila earthquake sequence. Bull. Seismol. Soc. Am. 101, 975e993.

Hofstetter, A., 2014. On the reliability of focal plane solutions using first motion readings. J. Seismol. 18, 181e197. http://dx.doi.org/10.1007/s10950-013-9410-3.

Kagan, Y.Y., 1991. 3-D rotation of double-couple earthquake sources. Geophys. J. Int. 106, 709e716. http://dx.doi.org/10.1111/j.1365-246X.1991.tb06343.x.

Kennett, B.L.N., Kerry, N.J., 1979. Seismic waves in a stratified half space. Geophys. J. R. Astr. Soc. 57, 557e583.

Krízova, D., Zahradník, J., Kiratzi, A., 2013. Resolvability of isotropic component in regional seismic moment tensor inversion. Bull. Seism. Soc. Am. 103, 2460e2473. http://dx.doi.org/10.1785/0120120097.

Quintero, R., Zahradník, J., Sokos, E., 2014. Near-regional CMT and multiple-point source solution of the September 5, 2012, Nicoya, Costa Rica Mw 7.6 (GCMT) earthquake. J. South Am. Earth Sci. 55, 155e165.

Reasenberg, P., Oppenheimer, D., 1985. FPFIT, FPPLOT, and FPPAGE: FORTRAN Computer Programs for Calculating and Displaying Earthquake Fault-plane Solutions. U.S. Geol. Surv. Open-File Rept. 85-739, 109 pp.

Snoke, J.A., 2003. FOCMEC: Focal mechanism determinations. In: Lee, W.H.K.,

Kanamori, H., Jennings, P.C., Kisslinger, C. (Eds.), International Handbook of Earthquake and Engineering Seismology. Academic Press, San Diego (Chapter 85.12).

Soares, J.E., Berrocal, J., Fuck, R.A., Mooney, W.D., Ventura, D.B.R., 2006. Seismic characteristics of central Brazil crust and upper mantle: a deep seismic refraction study. J. Geophys. Res. 111, B12302. http://dx.doi.org/10.1029/ 2005JB003769.

Sokos, E., Zahradník, J., 2008. ISOLA a Fortran code and a Matlab GUI to perform multiple-point source inversion of seismic data. Comput. Geosci. 34, 967e977.

Sokos, E., Zahradník, J., 2013. Evaluating centroid-moment-tensor uncertainty in the new version of ISOLA software. Seism. Res. Lett. 84, 656e665.

Vackar, J., Burjanek, J., Zahradník, J., 2015. Automated detection of disturbances in seismic records; MouseTrap code. Seism. Res. Lett. 86, http://dx.doi.org/10.1785/0220140168 (in press).

Vavrycuk, V., Kim, S.G., 2014. Nonisotropic radiation of the 2013 North Korean nuclear explosion. Geophys. Res. Lett. 41, 7048e7056. http://dx.doi.org/10.1002/2014GL061265.

Zahradník, J., Plesinger, A., 2010. Toward understanding subtle instrumentation effects associated with weak seismic events in the near field. Bull. Seism. Soc. Am. 100, 59e73.

Zahradník, J., Custódio, S., 2012. Moment tensor resolvability: application to southwest Iberia. Bull. Seism. Soc. Am. 102, 1235e1254. http://dx.doi.org/10.1785/0120110216.

Zahradník, J., Sokos, E., 2014. The Mw 7.1 Van, Eastern Turkey, earthquake 2011: two-point source modelling by iterative deconvolution and non-negative least squares. Geophys. J. Int. 196, 522e538. http://dx.doi.org/10.1093/gji/ggt386.

Zahradník, J., Janský, J., Papatsimpa, K., 2001. Focal mechanisms of weak earthquakes from amplitude spectra and polarities. Pure Appl. Geophys. 158, 647e665.

Zahradník, J., Janský, J., Plicka, V., 2008. Detailed waveform inversion for moment tensors of M 4 events: examples from the Corinth Gulf, Greece. Bull. Seism. Soc. Am. 98, 2756e2771.

CAPÍTULO 4 - ARTIGO 2

INVERSION FOR FOCAL MECHANISMS USING WAVEFORM ENVELOPES AND INACCURATE VELOCITY MODELS, EXAMPLES FROM BRAZIL

Juraci Carvalho, Lucas Vieira Barros, Jirí Zahradník

4.1 Abstract

One of the major challenges for the moment tensor determination is associated with the relatively low-magnitude events (M_w ~4) recorded by few regional stations at relatively large distances (300–600 km) and analyzed with standard velocity models of the region. Difficulties arise from the fact that synthetics in standard models (e.g., those routinely used in the location) cannot properly match real waveforms and favor the appearance of un-modeled time shifts and amplitude discrepancies (e.g., if VMs are constructed to minimize location residuals, they are not sensitive to uppermost shallow layers, which are insufficiently sampled by rays if shallow sources are missing). The situation is even worse when real waveforms can be matched but the retrieved focal mechanism is incorrect. This article investigates an alternative methodology that is more robust with respect to inappropriate velocity models: the inversion of waveform envelopes. The method is built on an empirical basis. It studies the effects of velocity models on synthetic waveforms and finds that the information about focal mechanism is encoded in the variation of the envelope shapes and amplitudes among the seismogram components. Besides synthetic tests, the method has been tested on real data comprising two earthquakes in Brazil: the 2010 M_w 4.3 Mara Rosa (MR) and the 2017 M_w 4.3 Maranhão earthquakes. When compared with solutions from previous studies, based on many polarities and ad hoc path-specific velocity models, we obtained in both cases the same mechanism with a single 1D model and a single-station polarity constraint. The envelope inversion is a promising technique that might be useful in similar

sparse networks, such as the one in Brazil, where standard waveform inversion, in general, is not fully efficient.

Electronic Supplement Ⓔ (Annex D): Figures of waveform comparisons and tables of amplitude ratio due to velocity model (ARMOD) values and velocity models

4.2 Introduction

The initial determinations of focal mechanisms in Brazil were done by Mendiguren and Richter (1978), Assumpção and Suárez (1988), Assumpção (1998a,b, 1992), and Ferreira et al. (1998). New studies on focal mechanisms were done by Barros et al. (2009, 2015), Chimpliganond et al. (2010), Lima Neto et al. (2013), Agurto-Detzel et al. (2014), Oliveira et al. (2015), and Dias et al. (2016).Whereas the initial focal mechanism solution was constrained with the use of the first motion polarities (P phases) and/or the amplitude ratios of the body-wave phases, the more recent works also use waveform inversion. For example, Zahradník et al. (2015) revisited the previous solution of Barros et al. (2015) for the 2010 M_w 4.3 Mara Rosa (MR) earthquake, which occurred in the state of Goiás, Brazil, performing waveform inversion pre-constrained by first-motion polarities according to Fojtíková and Zahradník (2014). Carvalho et al. (2016) retrieved focal mechanisms of 11 aftershocks (M_w 0.8–1.4) of the MR earthquake by inverting full waveforms using temporary local stations and a local velocity model, the same as used in this work (VM2). The waveform inversion was feasible up to ~10 MSW, in which MSW is the minimum shear wavelength. For example, for V_s ~3:0 km=s, and the maximum inversion frequency ~2 Hz, the MSW is ~1:5 km; hence, 10 MSW is about 15 km. Dias et al. (2016) demonstrated the possibility of significantly extending the feasible epicentral distance range (65 MSW) using ad hoc velocity models, specifically derived for each source–station path by inverting Love- and Rayleigh-wave dispersion curves of the same event for which the moment tensor is calculated. Polarities were used in their consistency check of the inversion results.

In all these attempts, the authors struggle with the inaccuracy of the existing velocity models of the region. Although the models are usable in routine event location, their applicability to waveform inversion is limited because of the waveform match is deteriorating in direct relation to the epicentral distance. Synthetic seismograms differ from real ones in terms of amplitudes and time shifts. That is why in the previously cited articles, using waveform inversion, it was necessary to apply local velocity models (or path-specific models) and strong polarity constraints.

As for other attempts to deal with the limited accuracy of velocity models, it is worth highlighting the work of Hallo and Gallovič (2016) and the references therein. They proposed an efficient estimate of the covariance matrix reflecting the Green's function uncertainty. The authors assumed that the main effect of the inaccurate velocity model is a temporal shift. Including the covariance matrix in their Bayesian formulation, they were able to calculate moment tensors together with their uncertainties. Artificial (ad hoc empirically derived) temporal shifts represent another possible approach to account for differences between the real (unknown) velocity model and the velocity model used in the inversion. This is a central idea of the cut-and-paste method of Zhao and Helmberger (1994). Optimally, the surface-wave shifts can be derived from calibration events (Zhu et al., 2006).

Here, we investigate a different approach based on waveform envelopes. The envelopes were recently proposed by Zahradník and Sokos (2018a). The authors, having obtained focal mechanisms by waveform inversion from a relatively dense network in Greece, removed near stations and investigated the resolution power of remaining relatively distant stations. Waveform inversion from the distant stations failed, but envelopes retrieved the correct mechanisms. Several features make the present article different from that of Zahradník and Sokos (2018a): (a) We are much more concentrated on explaining that the key point of envelopes is fitting the relative strengths of three components at each station (Ⓔ study of amplitude ratio due to velocity model [ARMOD] parameter and the test with five elementary mechanisms, available in the electronic supplement to this article). (b) Here, we clearly show that standard waveform inversion in an inappropriate model can provide a wrong focal mechanism even

when fitting waveforms relatively well. (c) Zahradník and Sokos (2018a) studied only one case similar to our setup (their model A, with six stations at relatively narrow distance range of 381–609 km); we demonstrate two more difficult cases, with fewer stations and more non uniform epicentral distances. (4) Their work was focused on Greece, where many stations are available. Our article is the first attempt to implement the envelope methodology in more difficult conditions of Brazil, and we are planning to apply the method to future events.

In the present article, our aims are to understand (1) why the envelope inversion technique (ENV) could perform better than waveforms in poor velocity models and (2) how the method performs on real data in Brazil.

In a series of synthetic tests, we analyze the effects of three velocity models on synthetic seismograms (and on their waveform inversion). We arrive at an empirical finding that when substituting waveforms by their envelopes, at least in the relatively low-frequency range, the envelope shapes (normalized at each station) still carry information about focal mechanism via variation of the envelope shapes among the three recorded components. In other words, the envelope of the seismic record drops the phase information and retains mainly the information of the shapes and relative amplitudes of the different components. As such, envelopes are less sensitive to inaccurate velocity models than waveforms.

For the first time, the envelope method is applied to two M_w 4.3 earthquakes in Brazil, the MR and Maranhão earthquakes, both including inversion of distant stations (up to 637 km). According to the Brazilian Seismic Bulletin (BSB), events of this magnitude are rare in Brazil (about every 5 yrs), and because of the country's vast territory and the low seismic network density, each earthquake is well recorded only at a few stations. Nevertheless, their focal mechanisms are needed to calculate more precisely the present stress field. Using existing velocity models, complemented by just a single first-motion polarity for each event, we succeeded in retrieving the same focal mechanism as previously obtained with complex path-specific models and many polarities.

The envelope inversion method in this article is tested in comparison with two other techniques, the least-squares waveform inversion using the ISOLA

software (Sokos and Zahradník, 2013; Zahradník and Sokos, 2018b) and a grid search waveform inversion with free time shifts (WISH), specifically encoded for this article and explained in the Inversion of Envelopes: Synthetic Test section.

4.3   Synthetic tests and method

4.3.1   Velocity models

In this section, we analyze the effects of velocity models on waveforms and their inversion. We use velocity models VM1, VM2, and VM3, all coming from real-world data. The VM1 (BDFB-Disp) model was derived from dispersion analysis of surface waves observed during the MR mainshock at BDFB station (Dias, 2016). The VM2 (GT5) model was obtained from the MR aftershock study (Barros et al., 2015). The VM3 (NewBR) model is based on travel-time data from the BSB; it is a generic model for Brazil (Assumpção et al., 2010). The $V_P=V_S$ ratios in the VM1–VM3 models are 1.74, 1.70, and 1.72, respectively. Quite arbitrarily, we choose VM1 as a reference. The comparison of the models (Fig. 4-1; Ⓔ Table AD.S2) shows that above Moho, the difference in velocity of VM2 with respect to VM1, reaching ~10%, is considerably greater than the difference between VM3 and VM1. The used models adopt different depths for the Moho discontinuity, 42 km in VM1 and VM3 and 36 km in VM2.

4.3.2   Forward Simulation of Waveforms

An idealized example of forward simulation and inversion is provided in the Ⓔ electronic supplement. Synthetic waveforms and their envelopes are inverted in the same velocity model as used for their simulation. It is demonstrated that not only waveforms (Ⓔ Fig. AD.S1) but also envelopes (Ⓔ Fig. AD.S2) can retrieve the correct focal mechanism and depth.

In the present section, synthetic waveforms are forward simulated for the source– station configuration shown in Figure 4-2. It reflects the present configuration of the permanent seismic network in central Brazil and the source position of the 2010 MR mainshock. All stations are broadband. Few of these stations existed in 2010. Synthetics are calculated in displacement for a specific

focal mechanism identical to the MR mainshock (strike/dip/rake [hereafter, s/d/r] = 253°/36°/121°) at a depth of 5 km and seismic moment $M_0 = 2{:}0423 \times 10^{15}$ N.m.
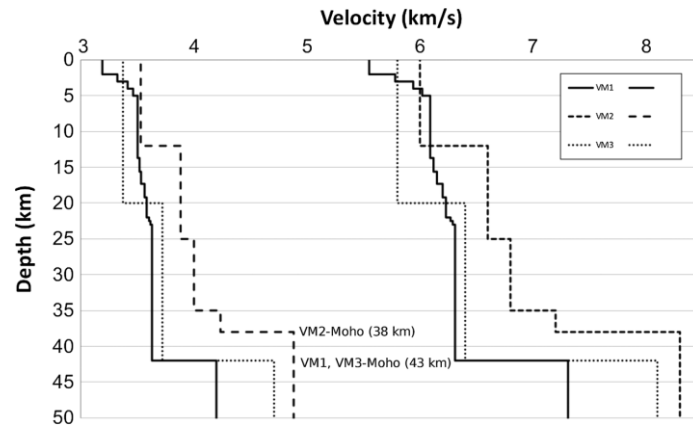
Figura 4-1 Three velocity models used in the study (VM1, VM2 and VM3).
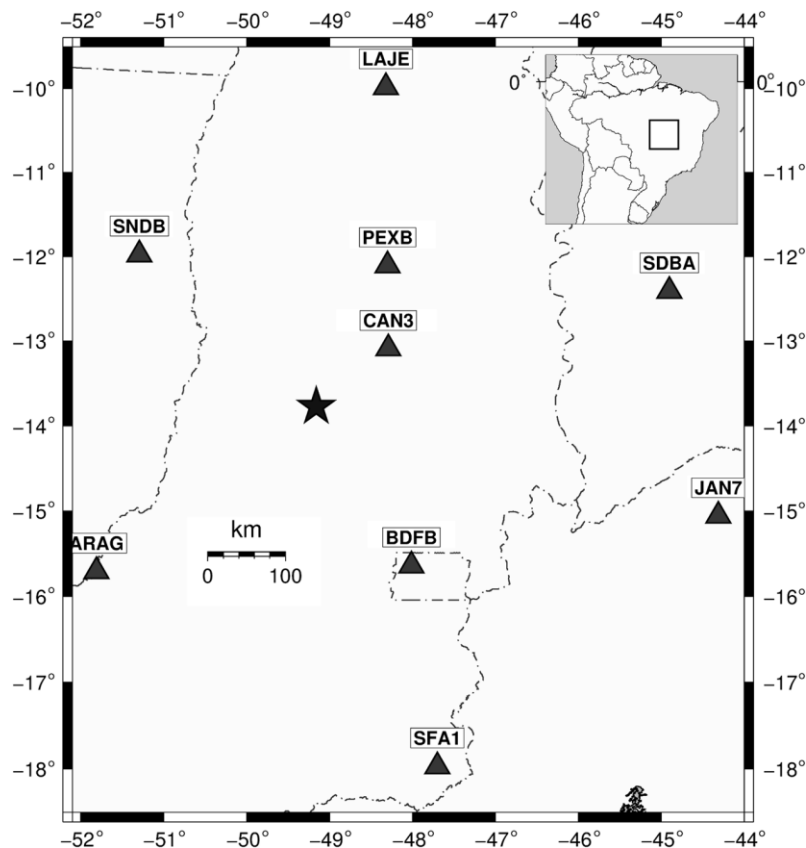
Figure 4-2 Seismic stations in central Brazil. The stations are shown by triangles. Star denotes the Mara Rosa epicenter. The dashed-dotted lines are the Brazilian states's borders. The operators of the stations and epicentral distances are as follows: The Brazilian Seismograph Network - PEXB (144 km), SNDB (305 km), ARAG (357 km), SDBA (486 km), JAN7 (542 km); the International Monitoring System (IMS-GT) - BDFB (241 km, borehole) and the Seismological Observatory of the University of Brasilia Network (SIS-OS) - LAJE (429 km) and CAN3 (121 km). The Mara Rosa event was recorded by CAN3, BDFB, SFA1 and JAN7.

For both models VM2 and VM3, we present comparisons of synthetic waveforms with VM1 in Figure 4-3. All tests are performed in the 0.05- to 0.1-Hz

low-frequency range. Real data of M$_w$ ~4 have a good signal-to-noise ratio in the dominant surface-wave group at the studied epicentral distances in this frequency range.

When comparing non-normalized waveforms, we found time shifts and amplitude differences due to different velocity models (see Ⓔ Fig. AD.S3). To balance the major amplitude effect, hereafter, just for plotting, we normalize synthetics in each model to the maximum value at each station.

When choosing VM1 as reference and comparing VM2 and VM3 with this reference (Fig. 4-3), we observe that the waveforms from VM2 and VM3 display time shifts compared with VM1. The shifts in VM2 are considerably greater, in agreement with the velocity differences in Figure 4-1 and Table AD.S2. The presence of these shifts clearly indicates that the standard waveform inversion may not be suitable to retrieve the correct focal mechanism. On the other hand, we also observe significant similarities between the VM2 and VM1 synthetics (and even more similarities between the VM3 and VM1 synthetics). The similarity in Figure 4-3 refers to the duration of the dominant surface-wave groups and to relative amplitudes of the individual components at each station. Additional tests, proving this similarity for five double-couple (DC) elementary mechanisms (Zahradník and Sokos, 2018b), fully describing an arbitrary deviatoric moment tensor, are given in Ⓔ Figure AD.S4. The goal of this test is to show that the similarities observed in Figure 4-3 are general, not related only to the specific focal mechanism of that figure.
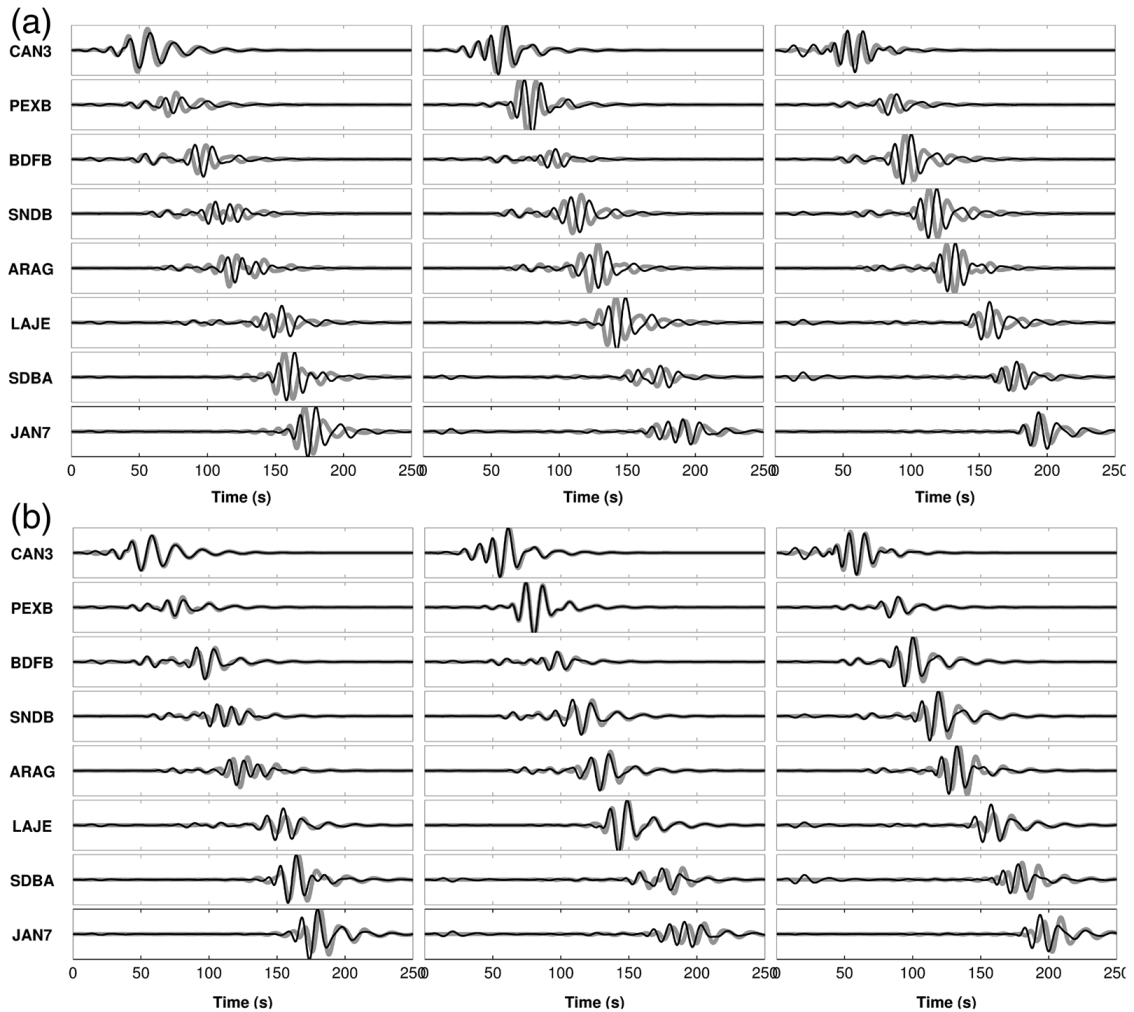
Figure 4-3 – Comparison of synthetic waveforms in the reference velocity model VM1 (black lines) and in two other models (grey lines): panel (a) is VM2 and (b) is VM3. Frequency band 0.05-0.1 Hz. The stations are sorted according to their epicentral distances, from 121 km (CAN3) up to 542 km (JAN7). For plotting purposes, synthetics in each model are normalized to the maximum component at each station. The zero in the axis time is the event origin time.

To quantify the relative amplitude variations among the components, we introduce an auxiliary parameter called ARMOD (see Table 1). ARMOD is defined as the ratio of maximum (absolute) values of the normalized components in two models (e.g., max Z[VM1]= max Z[VM2] = 1:15 for station CAN3). To better understand the meaning of ARMOD, consider the PEXB station as an example. We see in Figure 4-3a that at this station, the north-south component is weak, and the east–west component is strong in both velocity models VM2 and VM1; thus, the north–south and east–west components feature ARMOD values close to 1 (0.87 and 1.0). As shown in Table 4-1, the average ARMOD value over all stations is also close to 1. This

means that globally, for all stations, the relative amplitude variation among components is weakly affected by the model; see also Ⓔ Table AD.S1.

The similarity between relative amplitudes across components in different velocity models, together with the similarity between waveform durations (Fig. 4-3), suggests that normalized waveform shapes (i.e., envelopes) are less dependent on velocity model than waveforms. See also Ⓔ Figure AD.S3.

Table 4-1 Amplitude Ratio due to Velocity Model (ARMOD) Values for the Mara Rosa Focal Mechanism.

	VM1/VM2			VM1/VM3		
	N	E	Z	N	E	Z
CAN3	1.00	1.37	1.15	1.00	0.98	1.05
PEXB	0.87	1.00	1.22	1.30	1.00	1.28
BDFB	1.23	1.25	1.00	1.16	1.14	1.00
SNDB	1.19	1.00	1.00	1.16	1.19	1.00
ARAG	0.73	0.56	1.00	0.70	0.71	1.00
LAJE	1.79	1.00	1.38	1.72	1.00	1.49
SDBA	1.00	1.41	1.17	1.00	0.97	0.92
JAN7	1.00	1.16	1.13	1.00	1.16	1.08
Average ± standard deviation	1.11 ± 0.26			1.08 ± 0.23		

ARMOD values comparing the velocity models VM2 and VM3 with the reference model VM1 in the 0.05- to 0.1-Hz frequency range.

Thus, we assume that the envelope inversion of real data could be less affected by the inappropriate velocity model than the waveform inversion. To demonstrate this behavior, we further analyze synthetic data by performing inversion of the (normalized) envelopes. To be more realistic, white random Gaussian noise is added to the synthetics before bandpass filtering and calculating envelopes. The noise has a constant magnitude across the stations. Thus, as in real records, distant stations are more affected. We tested several noise levels, but here we present only the worst-case scenario.

4.3.3 Inversion of Envelopes - Method

The envelope method was recently proposed by Zahradník and Sokos (2018a). Its main features can be summarized as follows. Real, instrumentally corrected waveforms and synthetic waveforms are subjected to identical band-pass

fourth-order causal filtration. Point-source synthetics for an assumed moment rate function (e.g., delta function) and for unit moment are calculated with the use of the method of discrete wavenumbers from Bouchon (1981) and Coutant (1989). The point source is situated at an assumed hypocenter position. Envelopes of the bandpass-filtered displacement are calculated by Hilbert transform. The pure-shear (100% DC) focal mechanism is grid searched in terms of the s/d/r angles. Real envelopes and synthetic envelopes for every tested s/d/r are normalized to the maximum component at each station. For every s/d/r, the real and synthetic envelope shapes are compared in terms of their L2-norm difference (misfit), calculated with a time shift maximizing their cross correlation. The envelopes are plotted with the calculated time lags providing the best match, and the lag at each station component is recorded and reported. For the best-fitting solution (s/d/r), that is, the minimum misfit, the envelopes are returned to their non-normalized values, and scalar moment is calculated according to equation (9) of Zahradník and Gallovič (2010). The moment is converted to moment Magnitude.

Besides the best-fitting solution, the method also provides a group of s/d/r solutions fitting data within an adopted misfit threshold (e.g., 5% or 10% of to the best-fit solution). The misfit threshold depends on how deep is the misfit function minimum. A shallow minimum and a large threshold yield strongly non-unique solutions (see examples later). A suitable threshold is dependent on the data set, number of stations, network geometry, frequency band filter, event magnitude, and signal-to-noise ratio (Zahradník and Sokos, 2018a), in which typical values of 3%, 5%, and 10% are proposed.

The envelopes do not change if seismograms are multiplied by −1; therefore, any solution from the envelope inversion must be always checked a posteriori against at least one polarity to avoid flipping of the P and T axes. More than a single polarity match can be required if the s/d/r solutions need to be better constrained; the solutions not agreeing with all prescribed polarities are discarded. Another possibility is to apply a polarity pre-constraint; that is, the observed envelopes are inverted by grid searching in a limited group of s/d/r combinations, those that were previously derived from suitable software (e.g., FOCMEC; Snoke et al., 1984). The latter approach is similar to the polarity pre-

constrained waveform inversion in the cyclic scanning of the polarity solutions (CSPS) technique from Fojtíková and Zahradník (2014).

4.3.4 Inversion of envelopes – synthetic test

In this section, the synthetics in the reference model VM1 play a role of data, which we invert for the focal mechanism by means of inappropriate models VM2 and VM3 (two scenarios, VM1 × VM2 and VM1 × VM3). The low frequency range is 0.05–0.10 Hz. To avoid the flipping of P and T axes, we used one polarity, specifically at station BDFB (dilatation, D).

The result is shown in Figure 4-4. Despite differences of waveforms in VM1 and VM2 (shown previously in Fig. 4-3), the (normalized) envelope shapes can be well matched. Because the relative amplitudes of the components, controlled by focal mechanism, are well matched, the envelopes provide a good proxy of the focal mechanism. Indeed, in terms of K-angle (Kagan, 1991), its deviations from the reference focal mechanism are only 9° and 18° for VM2 and VM3, respectively. As expected and according to the differences of used velocity models, the group of solutions at the VM3 model, for which misfit is within a 3% threshold, is more compact compared with the VM2 model, as demonstrated by dispersion of nodal lines in the focal mechanism plots of Figure 4-4b,d. This means that variation of the envelope misfit with s/d/r angles possesses a relatively narrow global minimum in VM3. The retrieved moment magnitude is the same as that of the tested source.

It is useful to compare this result with an independent approach. In this test, we used the WISH algorithm, written to support the work in this article. WISH makes use of bandpass- filtered waveforms and inverts them into a pure DC constrained source model. The s/d/r angles are grid searched, as in ENV technique, and free time shifts, up to a prescribed time limit, are allowed to achieve the best fit between data and synthetics, hence minimum misfit. At each trial s/d/r combination, a single optimal shift is searched for each individual station component because we are interested in waveforms dominated by the surface-wave group. No envelopes are used in WISH. Figure 4-5 demonstrates the use of WISH at the same setup as ENV in Figure 4-4, that is, using the same velocity models VM2 and VM3 to invert data simulated in VM1, as well as

using the same frequencies and threshold. As a result, in this frequency band, the obtained WISH solutions are not better than ENV. In Figure 4-5, the WISH code provided similar results as ENV in Figure 4-4, just slightly more deviating from the true mechanism, with K-angles of 26° and 21° for VM2 and VM3, respectively.
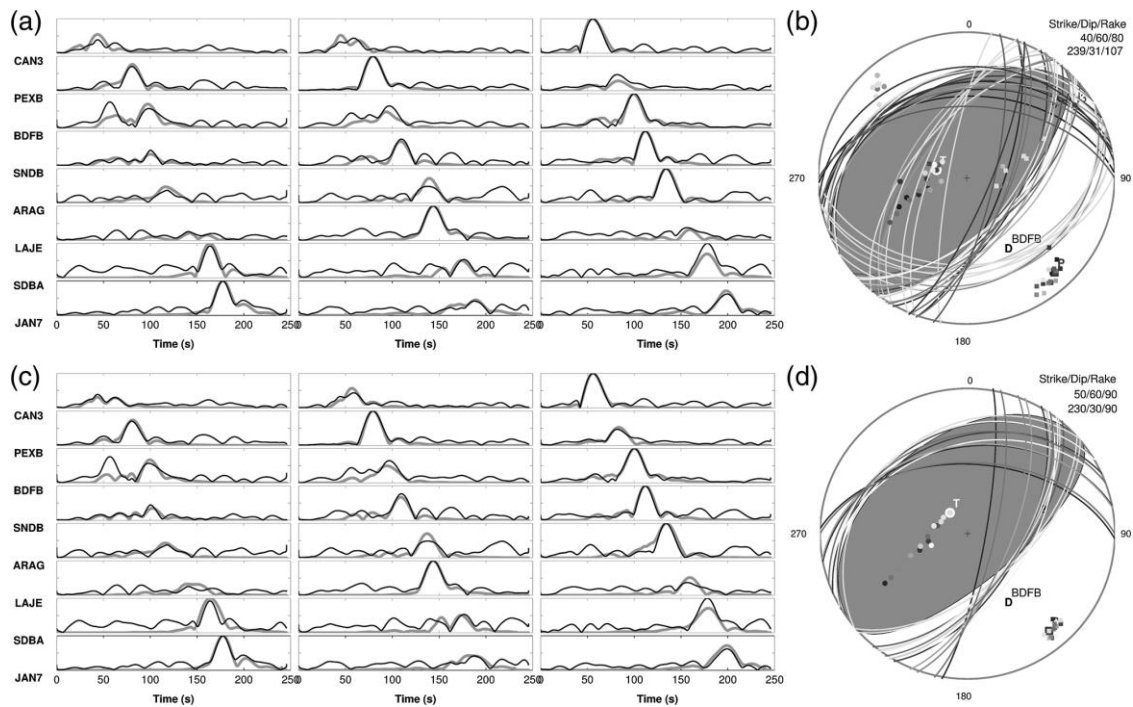
 Figure 4-4 The envelope (ENV) inversion of synthetic data in the low-frequency range. Synthetic waveforms in model VM1 played a role of 'data' and their envelopes (black) are inverted by means of synthetics calculated in different velocity models (grey). Panel (a): inversion in model VM2. Panel (c): inversion in VM3. Shown in the right panels, (b) and (d), are the results of the envelope inversions. The shaded areas show the best fitting solution VM2 and VM3, with K-angles of 9° and 18° respectively, relative to the reference mechanism. The polarity from BDFB (D) was used to avoid the flipping of P and T axes.

In summary, based on synthetic tests, we expect that if the real velocity model and the model used in the inversion differ in line with VM1 and VM2 or VM1 and VM3, the envelope inversion in the low-frequency range can provide a good approximation of the true focal mechanism and moment.

4.4 Real data applications

To validate the proposed waveform envelope inversion, we apply this new methodology to two real events for which reliable source parameters were independently obtained in previous studies. The study cases are (a) the 2010 MR mainshock and (b) the 2017 Maranhão earthquake (Table 4-2).

4.4.1 Mara Rosa earthquake

This event occurred on 8 October 2010 (Barros et al., 2015). At that time, the number of stations in central Brazil was lower than eight. We use the four nearest available stations (121–542 km) broadband stations BDFB and JAN7 and short-period stations CAN3 and SFA1. The inversion is performed in velocity models VM2 and VM3. The focal mechanism characterized by s/d/r = 253°/36°/121° (Dias, 2016) is adopted as a reference solution. That mechanism was obtained by a method of Dias et al. (2016) using an ad hoc set of source–station velocity models based on dispersion curves derived from the MR event. The waveform inversion of Dias et al. (2016) was constrained to fit as many of 11 polarities as possible; in that case, the 91% polarity match was achieved. Our intention is to show that we can obtain the correct mechanism without the path-specific models using envelopes. We use the lowest possible frequencies where the signal is above the noise (Table 2).

First, we demonstrate in Figure 4-6 that with the available simple 1D velocity models, the waveform inversion is not applicable. In the VM1 inversion, whereas the waveforms at stations CAN3 and BDFB are fitted relatively well, the waveforms are badly fitted at SFA1 and JAN7 (VR = 0:39), and the resulting focal mechanism is far from the reference (K-angle 35°). In the VM2 inversion, the waveforms at all stations are fitted generally well, except SFA1-EW (VR = 0:69), but the obtained focal mechanism is relatively far from the reference (K-angle 36°). In the VM3 inversion, we cannot trust the focal mechanism because real data and synthetics have significant amplitude differences and time shifts at distant stations SFA1 and JAN7 (VR = 0:22); indeed, the obtained solution is very far from the reference (K-angle 78°).
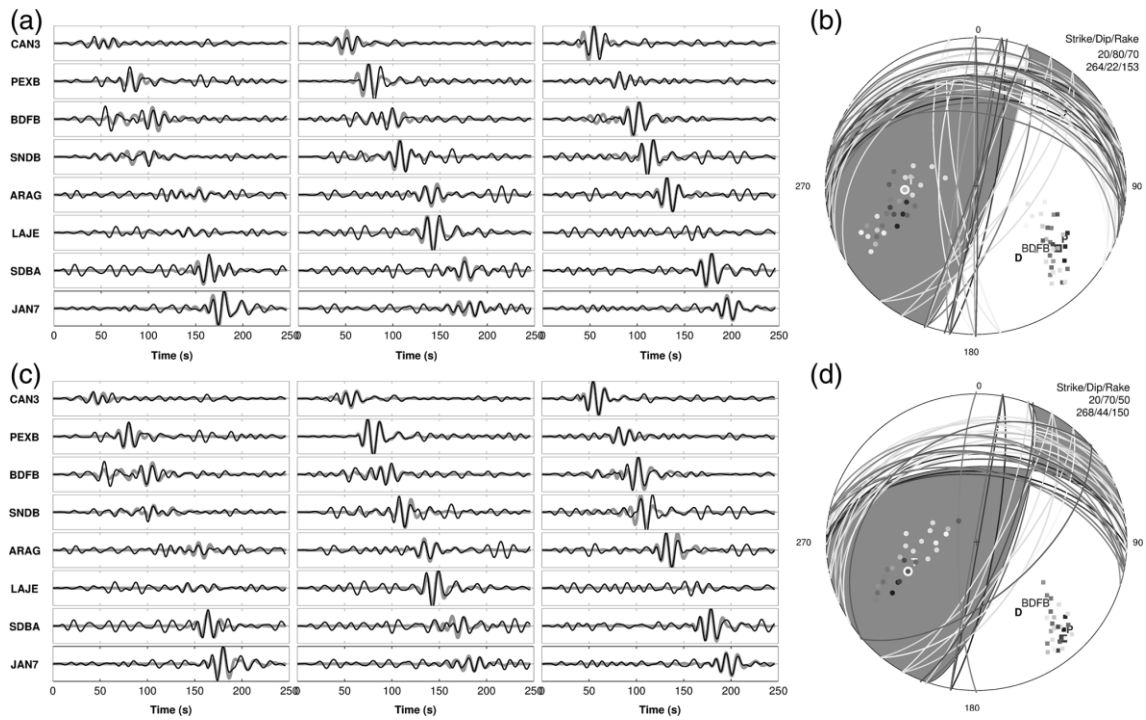
Figure 4-5 The waveform grid-search (WISH) inversion of synthetic data in two velocity models. Synthetic waveforms in model VM1 played a role of 'data' and their waveforms (black) are inverted by means of synthetics calculated in different velocity models (grey). Free shifts of waveforms are allowed. Left panels (a and b) are waveforms, right panels (c and d) are solutions for 0.05-0.1 Hz and with threshold of 5%. Top - inversion in model VM2, bottom in VM3.

Second, we perform the inversion of envelopes. The frequency range is the same as in the waveform inversion of Figure 4-6.We use grid searching of full parameter space (step 10° in s/d/r angles), and the solution is subjected to posterior polarity check at a single station, BDFB (dilatation D), just to avoid flipping of the P and T axes. The result is shown in Figure 4-7. In both velocity models, we observe a good match between the shape of the observed and synthetic envelopes. Because the envelopes are normalized per station (not per component), the match means that we fitted the relative amplitudes among the components related to the radiation pattern.

The best-fitting solution and the solutions within a 5% misfit threshold (i.e., matching data almost equally well) are presented in Figure 4-7. There are two families of P and Taxes, marked 1 and 2. Family 1 is closer to the reference solution. Indeed, the minimum Kagan angles of this family are 20° in the VM2 model and 6° in VM3. Family 2 is far from the reference solution, mainly as

regards the T axis; the minimum K-angles are 42° and 38° for the VM2 and VM3, respectively. The calculated magnitudes in both velocity models are the same, M_w 4.2; this value differs from the reference solution (M_w 4.6) but is consistent with the greatly scattered M_w estimates of 4.3–4.7 for this event (Zahradník et al., 2015).

4.4.2 Maranhão earthquake

The Maranhão earthquake occurred on 3 January 2017 at 12:43:47 (UTC), in the north of Brazil near the shore (Dias et al., 2017; Table 2). The event was felt in a wider area up to 250 km, with a maximum modified Mercalli intensity VI. The epicentral zone is basically aseismic. The event was detected by most stations of the Brazilian seismographic network at regional distances; the nearest station is situated at about 40 km (ROSB); the others that we use are above 470 km (TMAB, 478 km; PAL1, 562 km; TUC4, 641 km). All are broadband stations.

As for the MR event, the reference focal mechanism for the Maranhão event was obtained with a set of path-specific velocity models inferred from dispersion curves. The waveform inversion was constrained by 10 polarities, with the 79% polarity fit, and is characterized by s/d/r = 339°/83°/−2° (Dias et al., 2017). Here, we show that the same mechanism can be obtained by the envelope inversion constrained by just one polarity using a simple 1D model, the same for all source–station paths.

The inversion is performed with the lowest possible frequency range, 0.05–0.1 Hz. First (Fig. 4-8), we show that the waveform inversion in the VM1, VM2, and VM3 models could not match all stations simultaneously because of the unsuitability of the velocity model at distant stations. Only the nearest station (ROSB) was fitted very well (VR > 0:7), and the waveform inversion retrieved an incorrect focal mechanism, deviating from the reference by K-angle 81°, 89°, and 69°, for VM1, VM2, and VM3, respectively. In this case, it is possible to say that the inversion is prioritizing the fit at ROSB station because of its larger amplitudes.

Table 4-2 Summary of the Mara Rosa and Maranhão Earthquakes

	Mara Rosa				Maranhão			
Origin time (yyyy/mm/dd hh:mm:ss)	2010/10/08 20:16:55 (UTC)				2017/01/03 12:43:47 (UTC)			
Latitude (°N), Longitude (°E)	−13.771, −49.160				−03.193, −43.901			
Depth (km)	1.3				7–12			
Magnitude (m_R)	5.0				4.6			
Stations	**CAN3**	**BDFB**	**JAN7**	**SFA1**	**ROSB**	**TMAB**	**PAL1**	**TUC4**
Epicentral distance (km)	121	241	490	542	41	475	557	637
Frequency range (Hz)	0.1–0.2	0.05–0.1	0.05–0.1	0.08–0.13	0.05–0.1	0.05–0.1	0.05–0.1	0.05–0.1
Reference M_w, s/d/r (°)	4.6, 253/36/121				4.3, 339/83/−2			

The basic parameters of the events are taken from the Brazilian Seismic Bulletin. The reference strike/dip/rake (s/d/r) angles and M_w (at the bottom line) are from Dias (2016) and Dias et al. (2017), respectively. The magnitudes of the events are in the regional m_R scale, which is consistent with the teleseismic m_b scale (Assumpção, 1983).

Second (Fig. 4-9), the envelope inversion was applied using the same velocity models and frequency range. Following the reference, we fixed the depth to 7 km. Polarity was constrained just at a single station, TMAB (D). The best-fitting solutions for both VM2 and VM3 are identical (340°/80°/−10°), deviating from the reference by K-angle of 13° only. Except for one outlier, the nodal lines and P and T axes obtained in the 10% threshold with VM2 model have K-angle 13°–19°, but the solution with VM3 model is almost unique. The 10% threshold is used here because this event has a very narrow global minimum of the misfit function, so that in the 5% threshold (such as MR), we could observe just the best-fitting solution. Obtaining a small nodal-line scatter with a larger threshold is an indicator of a more reliable solution. The calculated magnitudes are 4.3 and 4.4 (M_w), in VM2 and VM3, respectively; these values are compatible with the reference magnitude (M_w 4.3).

.

4.5   Discussion and Conclusion

Inversion of waveforms into focal mechanisms is dependent on the quality of velocity models. Inaccurate models are responsible for temporal and amplitude discrepancies between real and synthetic data. According to our tests, we found that in most situations, the inaccurate model prevents good waveform matching. However, in some situations, the standard waveform inversion as in ISOLA, that is, without any artificial time shifts, can match real data with synthetics calculated using an inaccurate model, simply because the inversion distorts the

focal mechanism. This distortion or bias is clearly demonstrated in our example of Figure 4-6b, in which we obtained a good waveform match for a wrong source. Another possibility studied in this article (ENV) is to add freedom in the inversion by leaving waveforms and invert for an ensemble of the focal mechanisms, which fit only the normalized envelope shapes because they are simpler than waveforms.

The inherent inaccuracy of existing velocity models becomes critical if distant regional stations are used. Three velocity models are studied in this article, all based on geophysical measurements in Brazil. Synthetic waveforms calculated in these models show significant amplitude differences and time shifts. Contrary to waveforms, their overall shapes (formally described by envelopes) are less sensitive to velocity models. We investigated an empirical method in which envelopes are inverted for focal mechanism instead of waveforms. The method is based on systematically grid searching the parameter space (s/d/r angles), aiming to match the envelope form of normalized station records, mainly to reproduce relative amplitudes of the three recorded components at each station.

The method has been tested on synthetic data, which proved its ability to retrieve correct focal mechanisms. To avoid flipping between P and T axes, the envelope inversion must be complemented by at least one (well guaranteed) first motion polarity. If the available envelopes do not constrain the solution enough, additional polarities should be used.

The method has been applied to two M_w 4+ events, the MR and Maranhão events in Brazil, both with a previously known focal mechanism, taken here as a reference. It is important to highlight that these are the only shallow events above magnitude 4 that occurred in the previous 7 yrs in Brazil according to the BSB. The data set is on the limit of possibilities in terms of number of available stations and usable frequency range. For these earthquakes, recorded mostly at distant stations (~100–600 km), we demonstrated that in the available velocity models: (a) standard waveform inversion is not applicable, and (b) the newly proposed envelope inversion is more useful. By usefulness, we mean that a group of the solutions with similar misfit between the observed and

synthetic envelopes contains the focal mechanisms that are close to the reference solution, and that the moment magnitude M_w of the solutions is correct, too.
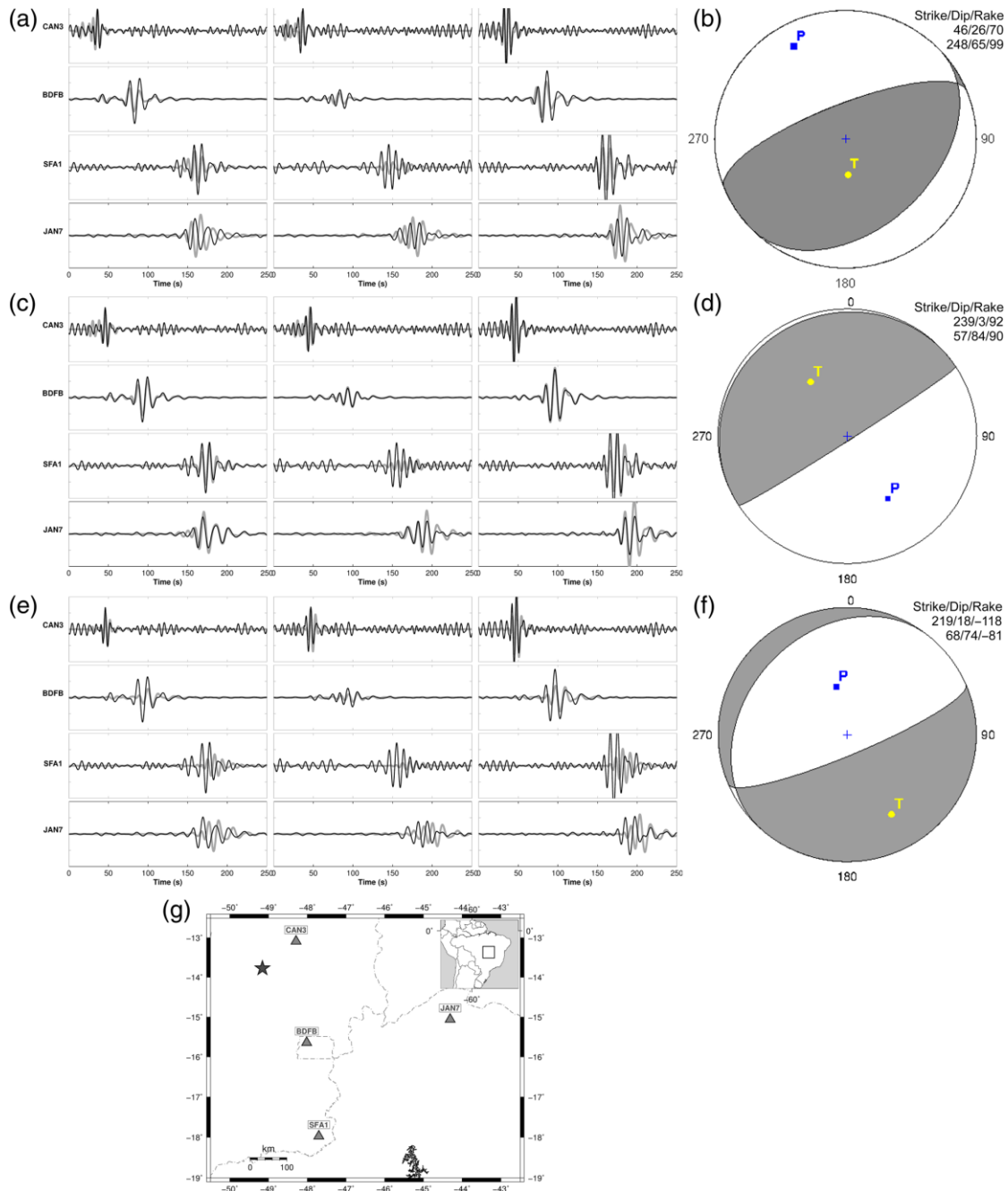
Figure 4-6 The unsuccessful waveform inversion of real data of Mara Rosa earthquake. Standard waveform inversion using ISOLA in velocity models VM1 panel (a, b), VM2 panel (c, d) and VM3 in panel (e, f), with station-dependent frequency ranges: CAN3 0.1-0.2 Hz, SFA1 0.08-0.13 Hz and BDFB/JAN7 0.05-0.1 Hz. Black and grey traces denote observed displacement data and synthetics, respectively. The panel (g) is the map with epicenter (star) and used stations (triangles).
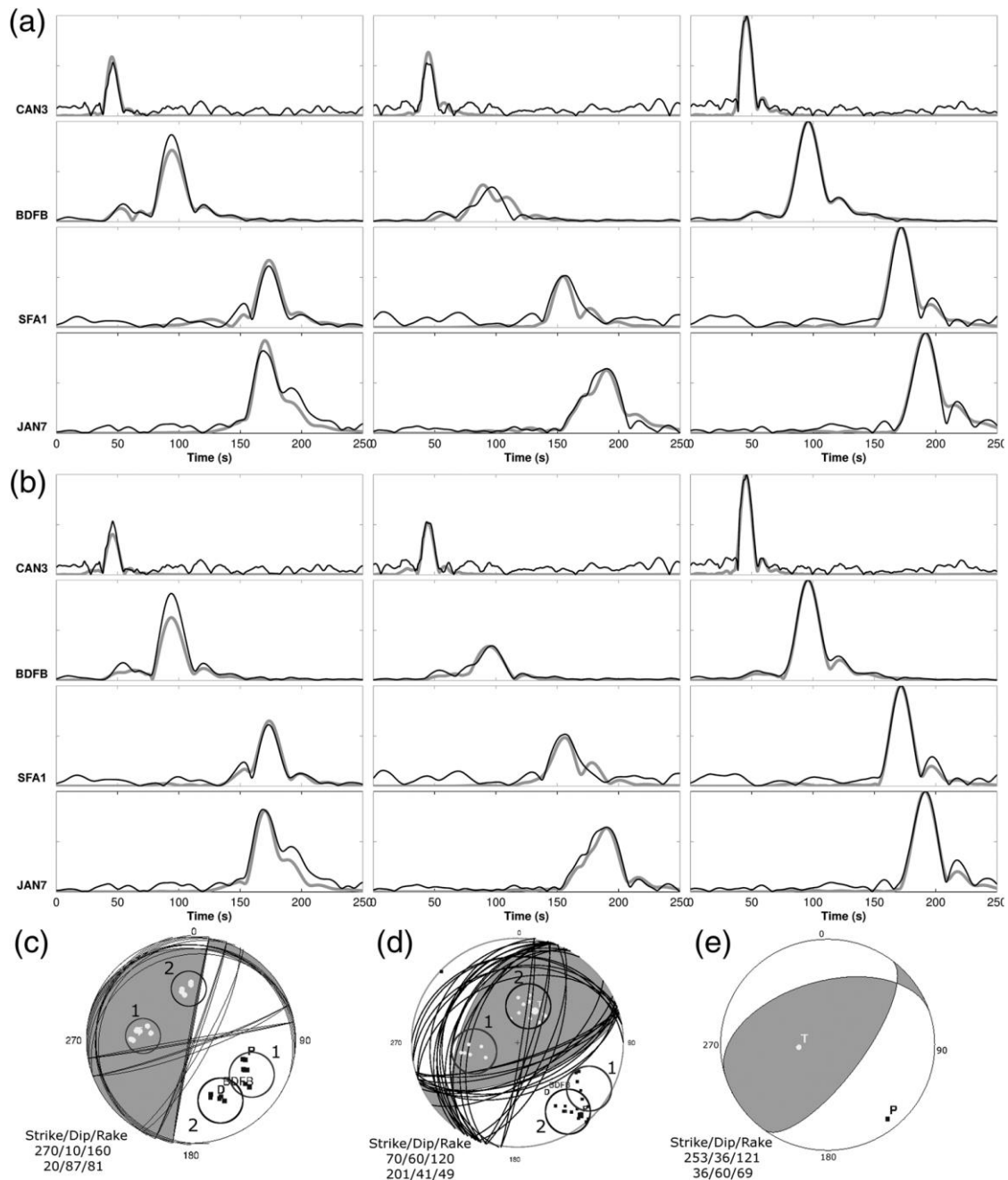
Figure 4-7 The successful envelope inversion of real data of Mara Rosa earthquake. Compared are the envelopes of observed data (black) and synthetic data (grey). The synthetic data correspond to the best-fitting solution found in model VM2 (a) and VM3 (b). The bottom panels show the obtained focal mechanisms in VM2 (c) and VM3 (d), and the reference solution (e); the legend and hatching refer to the best-fitting solution. Nodal lines correspond to the 5% misfit threshold. Numbers 1 and 2 indicate two distinct groups of P and T axes, discussed in the text. No.1 is close to the reference solution (s/d/r: 253/36/121).

Intentionally, we used only a very weak polarity constraint (single station) for each earthquake. Because the tested stations were far from the epicenter and small in number, the uncertainty, or non-uniqueness of the solution (as

represented by nodal lines within a given misfit threshold) was not small for the MR reverse-faulting event. On the contrary, despite the same limitations (few distant stations), the strike slip Maranhão earthquake revealed a very narrow global minimum of the misfit function, with perfect agreement with the reference solution derived by an independent method using independent data sets. The good performance of the method in the Maranhão case probably resulted from a combination of several factors: favorable position of the stations with respect to the radiation pattern of the surface waves (which dominate the records) and the use of only broadband stations, allowing implementation of lower frequencies than in the MR case.

Importantly, the envelope inversion results for MR and Maranhão earthquakes were very similar in both tested velocity models of the region—VM2 (GT5) and VM3 (NewBR), although waveforms in these models are significantly different. This is a clear indication of the robustness of envelopes.

More than 10 polarities are available for the MR and Maranhão events. We could easily use them as a posterior or prior constraint, thus obtaining an almost unique mechanism, very close to the reference solution. In this article, we tested the resolving power of the envelopes plus free time shift; thus, we intentionally reduced the polarity constraint to minimum (just a single polarity). Obviously, in practice, many polarities can be added as a constraint when processing real data. However, caution is needed to avoid a misleading over constraint, for example, by prescribing opposite polarities at stations close to each other on the focal sphere. Another danger comes from near-source stations for which polarities may have inaccurate take-off angles (e.g., 60° instead of 90°) if velocity models include formal shallow discontinuities (Zahradník et al., 2015).
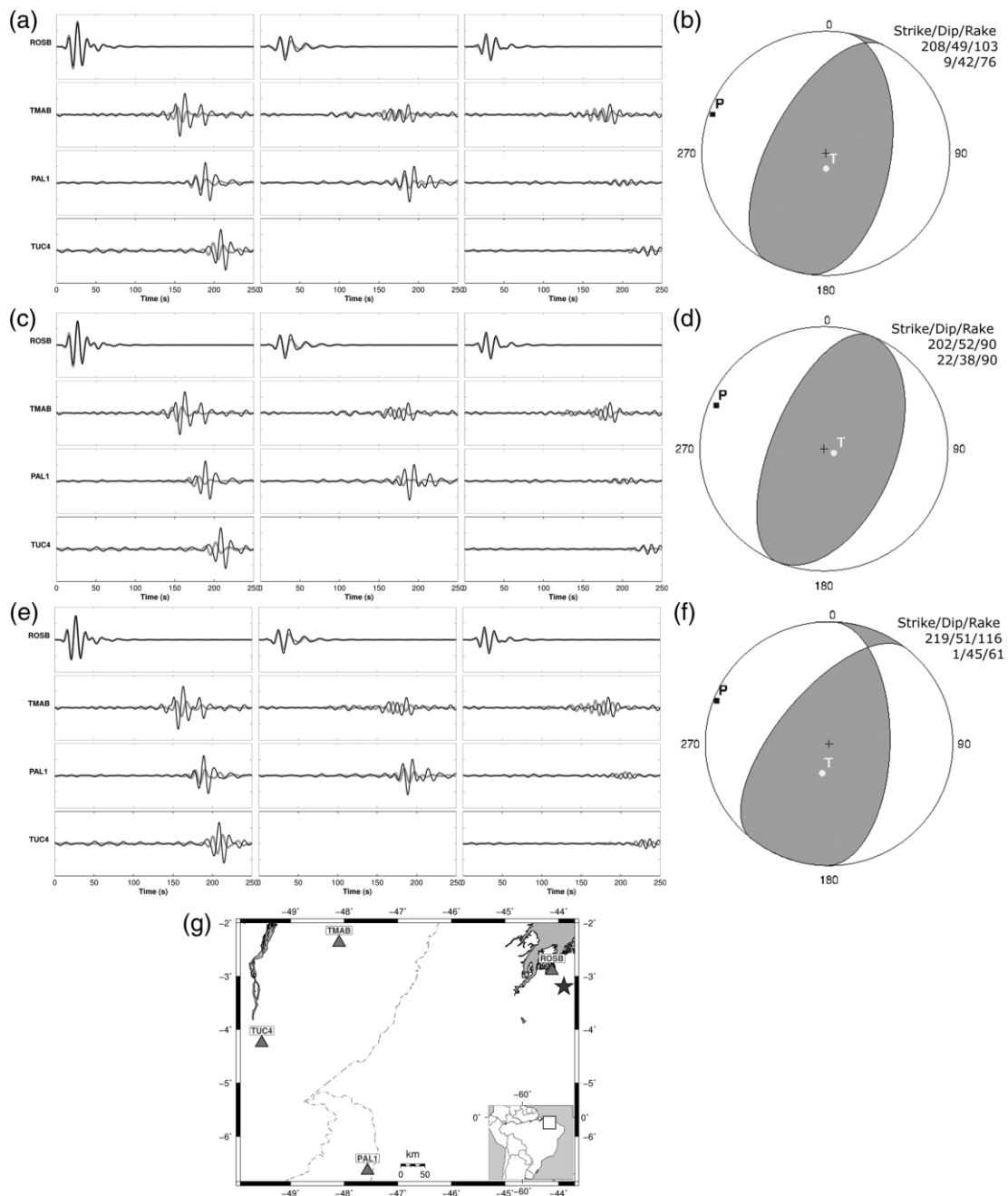
Figure 4-8 The unsuccessful waveform inversion of Maranhão earthquake. Inversion was done with velocity model VM1 panel (a, b); VM2, panel (c, d) and VM3, panel (e, f). The station TUC4-EW component was removed from the inversion due to the presence of a strong instrumental disturbance (Zahradnik et al. 2010). Black and grey traces are observed and synthetic waveforms; the traces are non-normalized. Panel (g) shows the map with epicenter (star) and used stations (triangles).
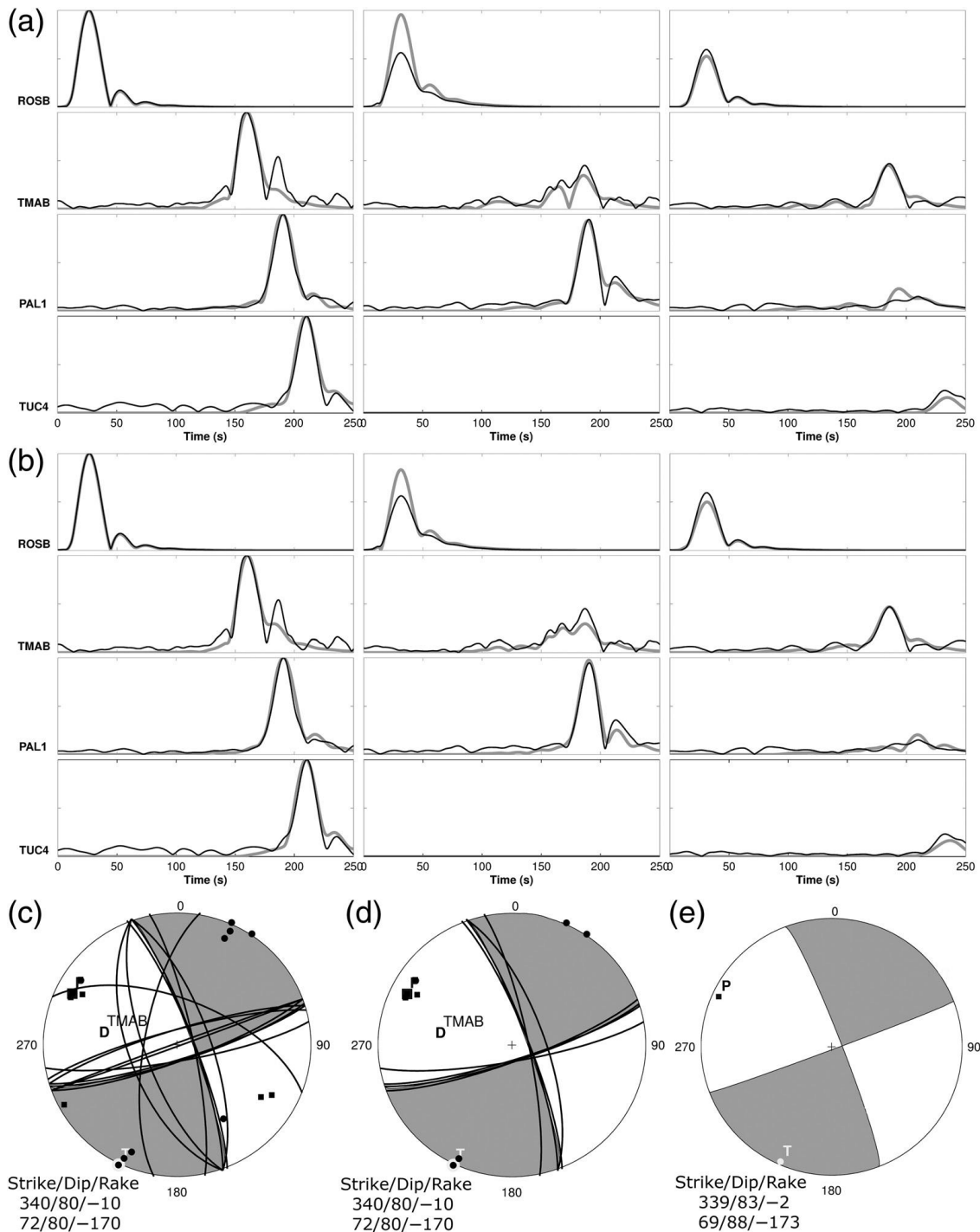
Figure 4-9 The successful envelope inversion of real data of Maranhão earthquake. Black and grey traces are observed data and synthetics. TUC4-EW was removed from the inversion due to a disturbance. The velocity models VM2 and VM3 were used (panels a and b for envelopes, panels c and d for beachballs; panel e is the reference solution).

Although the envelope method solves some problems not resolvable with waveforms, it also has limitations. Because the method is new, not all limitations are yet well known; however, a possibly poor performance in the absence of broadband stations is one of them. Using only short-period stations (and hence working at higher frequencies) could easily make it impossible to match real

envelopes by synthetics. Some of these problems are fortunately detectable—for example, when synthetics appear to have significantly shorter duration than real data, that is, indicating the presence of un-modeled high frequency waveform features. Other problems may be less easily recognizable such as in the case in which envelopes are seemingly well explained (because they are simpler than waveforms), but the solution is non-unique, and some of the focal mechanisms within the adopted ensemble are incorrect. It is possible that future applications will provide some simple criteria to discard unreliable solutions. Until that we can only recommend (1) to discard stations with instrumental disturbances, (2) to use as many stations with good signal-to-noise ratio as possible, (3) to use as low frequency as possible, (4) to include reasonable polarity constraints, (5) to repeatedly use several established velocity models of the studied region, and (6) to use a reliable location of the hypocenter.

As for (6), we also tested possible grid searches for the source depth, but in the context of distant stations and low frequencies, we did not find a sufficient depth resolution. For example, in synthetic test of Ⓔ Figure AD.S2 with a true source at 5 km, we ran the inversion from 1 to 10 km, in steps of 1 km, and we found a small preference to the correct depth, but the depth resolution was too small to encourage the depth search in real-data applications.

The studied source–station distance can be expressed in terms of MSW. Although standard waveform inversions almost always fail at distances > 10 MSW, in theMR example, we were able to invert envelopes into focal mechanism up to 18 MSW and in the Maranhão example up to 21MSW; similar results were obtained by Zahradník and Sokos (2018a). It seems to be a small improvement when comparing with the 65 MSW in path-specific models (Dias, 2016), but it should be noted that our inversion is based on simple standard 1D models, same for all stations. It is also worth to mention that the envelope inversion can be applied when missing one station component; this is the case in which it is generally not possible to obtain a path-specific model.

In this study, we proposed a new method, which may extend current possibilities of the focal mechanism and M_w retrieval, especially if only simple velocity models and few stations at relatively large regional distances are available. Robustness with respect to imperfect velocity models and the

simplicity of the method may be useful in real-time applications, where the derivation of path-specific velocity models is not trivial.

.

4.6 Data and Resources

The majority of waveform data used in this article belong to the Brazilian Seismograph Network (RSBR), and they are freely available at www.obsis.unb.br and www.sismo.iag.usp.br (last accessed April 2018). University of São Paulo (USP) provides federated (FDSNWS) web services for downloading event waveforms at http://seisrequest.iag.usp.br (last accessed September 2018). The plots were made with the use of the code Generic Mapping Tools v.4.2.1 (http://www.soest.hawaii.edu/gmt, last accessed April 2018). The waveform inversion was done with the software ISOLA and can be downloaded from http://geo.mff.cuni.cz/~jz/for_Costa_Rica (last accessed April 2018). The information on the Brazilian seismicity is from the Brazilian Seismic Bulletin (BSB) available at http://moho.iag.usp.br/eq/bulletin (last accessed June 2018). .

4.7 References (paper 2)

Agurto-Detzel, H., Assumpcao, M., Ciardelli, C., Albuquerque, D. F., Barros, L. V., & Franca, G. S. L. (2014). The 2012-2013 Montes Claros earthquake series in the Sao Francisco Craton, Brazil: new evidence for non-uniform intraplate stresses in mid-plate South America. Geophysical Journal International, 200(1), 216–226. doi:10.1093/gji/ggu333.

Assumpcao, M., 1992. The regional intraplate stress field in South America. Journal of Geophysical Research, 97(B8), p.11889.

Assumpção, M., 1983. A regional magnitude scale for Brazil. Bulletin of the Seismological Society of America, 73(1), pp.237–246.

Assumpção, M., 1998a. esfuerzos en Brasil. Física de la Tierra, pp.149–166.

Assumpção, M., 1998b. Seismicity and stresses in the Brazilian passive margin. Bulletin of the Seismological Society of America, 88(1), pp.160–169.

Assumpção, M., Ardito, J.E. & Barbosa, J.R., 2010. An improved velocity model for regional epicentre determination in Brazil. IV Simpósio Brasileiro de Geofísica. Brasília, p.13 e 16 de novembro de 2010.

Assumpcao, M. & Suarez, G., 1988. Source mechanisms of moderate-size earthquakes and stress orientation in mid-plate South America. Geophysical Journal International, 92(2), pp.253–267.

Barros, L. V., M. Assumpção, Chimpliganond, C. N., Carvalho, J. M., Huelsen, M. G. Von, Caixeta, D. F., Fontenele, D. P., 2015. The Mara Rosa 2010 GT-5 earthquake and its possible relationship with the continental-scale transbrasiliano lineament. Journal of South American Earth Sciences, 60, pp.1–9.

Barros, L. V., Assumpção, M., Quintero, R., & Caixeta, D., 2009. The intraplate Porto dos Gaúchos seismic zone in the Amazon craton — Brazil. Tectonophysics, 469(1–4), pp.37–47.

Bouchon, M., 1981. A simple method to calculate Green's functions for elastic layered media. Bulletin of the Seismological Society of America, 71(4), pp.959–971.

Carvalho, J., Barros, L.V. & Zahradník, J., 2016. Focal mechanisms and moment magnitudes of micro-earthquakes in central Brazil by waveform inversion with quality assessment and inference of the local stress field. Journal of South American Earth Sciences, 71, pp.333–343.

Chimpliganond, C., Assumpção, M., Von Huelsen, M., & França, G. S., 2010. The intracratonic Caraíbas–Itacarambi earthquake of December 09, 2007 (4.9 mb), Minas Gerais State, Brazil. Tectonophysics, 480(1–4), pp.48–56.

Coutant, O., 1989. Program of Numerical Simulation AXITRA, Research Report,

Dias, F., Zahradník, J. & Assumpção, M., 2016. Path-specific, dispersion-based velocity models and moment tensors of moderate events recorded at few distant stations: Examples from Brazil and Greece. Journal of South American Earth Sciences, 71, pp.344–358.

Dias, F.L., 2016. Mecanismos Focais e o Padrão de Tensões Intraplaca no Brasil. University of Sao Paulo. http://www.iag.usp.br/pos/sites/default/files/t_fabio_l_dias_corrigida.pdf (last accessed July 2018).

Dias, F.L., Assumpção, M., Bianchi, M., Barros, B., Carvalho, J. M., 2017. The intraplate Maranhão earthquake of 2017 Jan 03, northern Brazil: evidence for uniform regional stresses along the Brazilian equatorial margin. Geophysical Journal International, p.18.

Ferreira, J. M., Oliveira, T., Takeya, M. K., & Assumpção, M., 1998. Superposition of local and regional stresses in northeast Brazil: evidence from focal mechanisms around the Potiguar marginal basin. Geophysical Journal International, 134(2), pp.341–355.

Fojtikova, L. & Zahradnik, J., 2014. A New Strategy for Weak Events in Sparse Networks: The First-Motion Polarity Solutions Constrained by Single-Station Waveform Inversion. Seismological Research Letters, 85(6), pp.1265–1274.

Hallo, M. & Gallovič, F., 2016. Fast and cheap approximation of Green function uncertainty for waveform-based earthquake source inversions. Geophysical Journal International, 207(2), pp.1012–1029.

Kagan, Y.Y., 1991. 3-D rotation of double-couple earthquake sources. Geophysical Journal International, 106(3), pp.709–716.

Lima Neto, H. C., Ferreira, J.M., Bezerra, F.H.R., Assumpção, M. Do Nascimento, A.F., Sousa, M.O.L. and Menezes, E.A.S., 2013. Upper crustal earthquake swarms in São Caetano: Reactivation of the Pernambuco shear zone and trending branches in intraplate Brazil. Tectonophysics 608, 804–811.

Mendiguren, J.A. & Richter, F.M., 1978. On the origin of compressional intraplate stresses in South America. Physics of the Earth and Planetary Interiors, 16(4), pp.318–326.

Oliveira PHS, Ferreira JM, Bezerra FHR, Assumpção M, do Nascimento AF, Sousa MOL, Menezes EAS., 2015. Influence of the continental margin on the stress field and seismicity in the intraplate Acaraú Seismic Zone, NE Brazil. Geophys. J. Int. 202, 1453–1462.

Snoke, J.A., Munsey, J.W., Teague, A.G. & Bollinger, G.A., 1984. A program for focal mechanism determination by combined use of polarity and SV-P amplitude ratio data, Earthq. Notes, 55 (3), 15.

Sokos, E. & Zahradnik, J., 2013. Evaluating Centroid-Moment-Tensor Uncertainty in the New Version of ISOLA Software. Seismological Research Letters, 84(4), pp.656–665.

Zahradník, J., Fojtikova, L., Carvalho, J.M., Barros, L.V., Sokos, E., Jansky, J., 2015. Compromising polarity and waveform constraints in focal-mechanism solutions; the Mara Rosa 2010 Mw 4 central Brazil earthquake revisited. Journal of South American Earth Sciences, 63, pp.323–333.

Zahradník, J. & Gallovič, F., 2010. Toward understanding slip inversion uncertainty and artifacts. Journal of Geophysical Research, 115(B9), p.B09310.

Zahradník, J. & Plešinger, A., 2010. Toward understanding subtle instrumentation effects associated with weak seismic events in the nearfield,. Bulletin of the Seismological Society of America, 100(1), pp.59–73.

Zahradník, J. & Sokos, E., 2018a. Fitting Waveform Envelopes to Derive Focal Mechanisms of Moderate Earthquakes. Seismol. Res. Lett. doi:10.1785/0220170161

Zahradník, J. & Sokos, E., 2018b. ISOLA code for multiple-point source modeling –review. In S. D'Amico (ed.) Moment Tensor Solutions - A Useful Tool for Seismotectonics. Springer Natural Hazards, https://doi.org/10.1007/978-3-319-77359-9_1

Zhao, L.-S. & Helmberger, D. V, 1994. Source Estimation from Broadband Regional Seismograms. Bulletin of the Seismological Society of America, 84(1), pp.91–104.

Zhu, L., Tan, Y., Helmberger, D.V., Saikia, C.K., 2006. Calibration of the Tibetan Plateau Using Regional Seismic Waveforms. Pure and Applied Geophysics, 163(7), pp.1193–1213.

CAPÍTULO 5 - ARTIGO 3

Earthquake relocation, focal mechanism and stress field determination in central Brazil

Juraci M. Carvalho(1), Lucas V. Barros(1), Jiří Zahradník(2), Mônica G. Von Huelsen(1), Vinicius Martins Ferreira(1)

(1) Observatório Sismológico da Universidade de Brasília
(2) Charles University, Prague, Czech Republic

5.1   Abstract

In this work, we perform a seismological investigation in the central Brazil region. This large area (910.000 km^2) is surrounded by several geological provinces: Eastern Amazon craton; southwestern Parnaíba basin; western São Francisco craton; northern Paraná basin, and it includes almost the whole Tocantins province. The area is crossed integrally, in SW-NE direction, by the continental-scale discontinuity - Transbrasiliano lineament (LTB). In the Brazilian seismic catalog (1724-2019), it is possible to distinguish a seismic belt following the LTB lineament and some dispersed events in the northern, western and eastern areas. The study area is characterized mainly by low magnitude events (M < 4); only 11 events reported in the catalog with M > 4 occurred, and among them just one with magnitude 5. Based on a quality criteria, a set of 118 events from 337 present in the catalog, were selected for a thorough analysis on this paper. This work was divided in three parts: (i) Events relocation with the iLoc code and Regional Seismic Travel Time (RSTT) velocity model; (ii) Focal mechanisms determination of 10 events using waveform envelopes and polarities, and; (iii) Inversion of focal mechanisms for stress field. The study shows that the seismicity of the area is mainly concentrated in two relatively narrow belts and that the principal compressional stress axis of the whole zone is well resolved, featuring azimuth ~133 and plunge ~12°. To study events of small magnitudes in such a huge area, installation of additional seismic stations is needed, as well as more studies of aftershocks by local temporary networks.

5.2 Introduction

The earthquake activity in the stable Continental Interior of South America (SCI-SA) is heterogeneously distributed and it is very quiescent in terms of quantity and magnitudes compared to other similar intraplate regions. Models to explain intraplate earthquakes, in general, were proposed by (SBAR & SYKES 1973; Sykes 1978; Talwani 1989; Talwani & Rajendran 1991; Kenner & Segall 2000). Intraplate earthquakes appear to result from ruptures in weakness zones and stress concentration. The proposed models try to correlate intraplate earthquakes with geological features that could indicate zones of crustal weakness or with structural inhomogeneities, which could concentrate stresses in the upper crust. In the SCI-SA, few studies brought light to the causes of intraplate earthquakes. The work of Assumpção et al. (2014, 2004) correlates the Brazilian seismicity with weakness zones and stress concentration in areas of thin lithosphere and craton edges. This seismicity is explained by the deformation resulting from the stress concentration in upper crust (Assumpção, Bianchi, et al. 2013; Assumpção, Feng, et al. 2013), which is explained by the lateral density variation causing flexural deformation (Assumpção & Sacek 2013; Zoback & Richardson 1996). At some zones, local stress is as important as regional stress (Rocha et al. 2016; Tingay et al. 2006; Heidbach et al. 2010; Heidbach et al. 2007). According to Agurto-Detzel et al. (2017) the Brazilian seismicity, in average, is concentrated in the Neoproterozoic fold belts, thinner crust, higher heat flow regions and in areas marked by relevant high gravity anomalies.

The instrumental monitoring of earthquakes in Brazil started in 1906 with the installation of Rio de Janeiro seismograph station (RDJ) in the National Observatory and after that the installation of SAAS (South American Array System) in 1968, BDF from the World-Wide Standard Seismographic Network (WWSSN) in 1972. In 70´s the deployment of additional stations was motivated by the installation of the nuclear power plant (Angra dos Reis) and hydroelectric power-plant dams for induced seismicity monitoring (Berrocal et al. 1984). But, only after the complete installation of the Brazilian Seismographic Network (RSBR) in 2014, the monitoring became uniform in the whole country and

lowered the detection magnitude threshold to ~3.5 everywhere (Bianchi et al. 2018).

The Brazilian earthquake catalog comprises of historical and instrumental events reported initially by Berrocal et al. (1984) and continuously upgraded by the seismological centers of the University of Brasilia (UnB), University of São Paulo (USP), University of Rio Grande do Norte (UFRN), Technological Research Institute of São Paulo state (IPT), National Observatory (ON) and Brazilian Geological Survey (CPRM). Due to the sparseness of the seismic stations and the territory extension, the seismic monitoring in Brazil, represented by the catalog, is very heterogeneous in terms of completeness and location quality. Nevertheless, the monitoring quality was improved substantially after the implementation of the RSBR, completed in 2014 (Bianchi et al. 2018).

The catalog event location uses the 1D velocity model NewBR developed by Assumpção et al. (2010) with a limited number of stations, mainly analog and the location process does not consider any station correction. In this work, the events were relocated with iLoc code (Bondár and Storchak, 2011) and the velocity model RSTT (Myers et al., 2010), version RSTT2014um including the Moho depths for South America (Assumpção et al., 2013a). Additionally the code addresses the phase's assignment uncertainties (Pg and Lg) and depending on the station geometry, the relocation is done with an epicentral error of about 10 km.

The region of low magnitude events combined with the sparseness of the network makes difficult to obtain focal mechanism (FM). Except the Nazca subduction region in the northwest, the Brazilian catalog contains only few dozen of FM solutions, most of them in the northeast and southeast regions, as expected due to the presence of more stations. In the central and north region of the country only few solutions were obtained so far and this is explained by the lack of monitoring stations.

Initially in the 80´s, the focal mechanisms were obtained using the P phase polarities (Mendiguren & Richter 1978) and more recently it was possible to employ the waveform inversion technique for small events recorded by local

network (Agurto-Detzel et al. 2014; Carvalho et al. 2016; Chimpliganond et al. 2010; Barros et al. 2018) and events M > 5 recorded at regional distances (Barros et al. 2015). Dias et al. (2016) succeeded to invert some medium magnitude events using specific velocity models for each source-station pair. The used models, obtained from dispersion of surface waves, compensate the small number of available stations and the lack of signals at low frequency range (typical for small earthquakes). However, this technique is only applicable to few events of magnitude 4 and above, which is not the case for the majority of the events observed within the area of study.

To overcome this limitation, we used the inversion of waveform envelopes (ENV) (Carvalho et al. 2017; Zahradník & Sokos 2018a; Carvalho et al. 2019). In this method, the information about focal mechanism is in fact deciphered from the mutual relation between the three recorded components at each station. This technique assumes a 100% Double Couple (DC) source and does a grid search for the possible focal mechanism solutions based on correlation between the observed and synthetic envelopes, which are more robust relative to velocity models than waveforms.

For one case reported in this work it was also possible to use the waveform inversion pre-constrained by a few available polarities, Cyclic Scanning of the Polarity Solutions - CSPS (Fojtikova and Zahradnik, 2014). The CSPS technique uses a limited number of possible focal-mechanism solutions originated from the polarity inversion and inspects the solutions for agreement with waveforms from a few available stations. It also assumes 100% DC sources. Both techniques are included in the ISOLA package (Sokos & Zahradnik 2013; Zahradník & Sokos 2018b), written in Fortran and running with the help of a Matlab Graphic User Interface (GUI).

The goal of this work is to study the seismicity of central Brazil, delimitating the seismic zones according to events relocation and stress distribution, which is important for future seismic hazard assessment. To achieve this, we filter the catalog for quality events and proceed with their relocation using the iLoc code and velocity model RSTT, proceed with the determination of focal mechanisms of some events, and invert them for stress field. The results of the events relocation showed that the seismicity of the central Brazil is concentrated mainly

in two relatively narrow belts. To assess the stress field acting in the study area, we inverted 12 focal mechanisms, 10 from this work and 2 from previous studies: Mara Rosa Oct 10, 2010 (Barros et al. 2015) and the Brasília event of November 20, 2000 (Assumpção et al. 2016). The results showed that the stress axis σ_1 of the largest compressional stress is well resolved, featuring azimuth ~133° and plunge ~12°.

5.3   Brazilian catalog and monitoring stations

The Brazilian seismic catalog hereafter, "*the catalog*", Figure 5-1 (grey circle) is very heterogeneous, assembled by different institutions with different location methodologies/techniques and various analysts as well as a mixture of historical and instrumental events. All events of the catalog, with few exceptions, have the depth fixed to the surface (zero depth).

The catalog has no error control and for some old events unreported errors of the order of 100 km are expected. Recently, with the deployment of RSBR stations and the standardization of the location procedure, the hypocenter errors started being reported, but the location process still needs an improvement in the velocity model.

The RSBR installation with 91 stations was completed in 2014 with the installation of the Amazon stations. The stations infrastructures are physically standardized and equipped with broadband sensors (120s to 50 Hz) coupled to a 24-bit digitizer and recording at 100 sps. Most of them sending data in real time to the network nodes located at UnB, USP, UFRN, ON and CPRM. It is worth to mention that the RSBR database is freely available without any restriction.

The study area is monitored by 8 real time acquisition RSBR stations (Figure 5-1, blue triangle) and 23 stations from other projects, composed by a mixture of short period and broad band sensors (Figure 5-2, orange triangle).
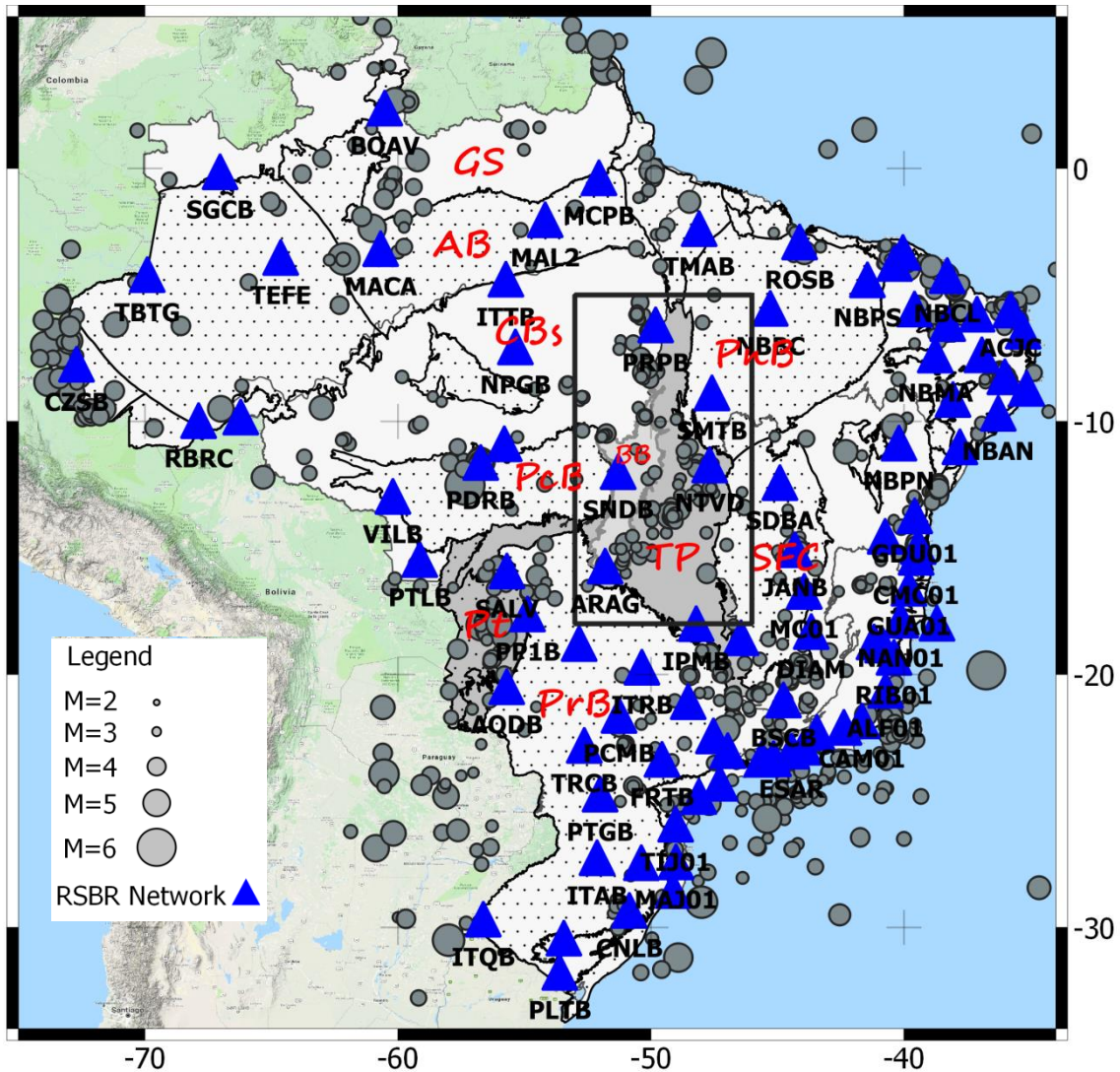
Figure 5-1 Brazilian seismicity catalog from 1724 to 2019 (grey circles) and geological provinces. The study area is represented by the black rectangle. Major geological provinces are indicated : São Francisco craton (SFC), Central Brazil shield (CBs), Guiana Shield (Gs), Parnaiba Basin (PnB), Parecis Basin (PcB), Paraná Basin (PrB), Pantanal Basin (Pt) and Tocantins foldbelt province (TP).

5.3.1 Regional seismicity and data

The study area located in the central Brazil region is a large area (910.000 km^2) bordered by several geological provinces (Figure 5-2). The Catalog reported 337 events in the study area, 11 of them with magnitude equal or above 4 and one with magnitude 5.0 (Mara Rosa Oct 10, 2010). So, the area is characterized by low magnitude events with 98% below magnitude 4. The catalog reports only some parameters: origin time; magnitude; intensity (Imax); epicentral location and a short comment. There are no details on the data picking, phase amplitudes, etc., therefore we could not reprocess the events for relocation. Only recently, after 2010, the location input data are available as well

as the increase in the network stations density, making possible the reprocessing of the data for relocation.

It is well known that quality of the locations depend on the number and the quality parameters, i.e., identified phases (P and S), azimuthal gap (stations coverage), epicentral distances and the velocity model. Taking into account two quality parameters, events recorded by 4 or more stations and azimuthal gap lower than 180°, from the 337 events we managed to sort 118 events (data set).
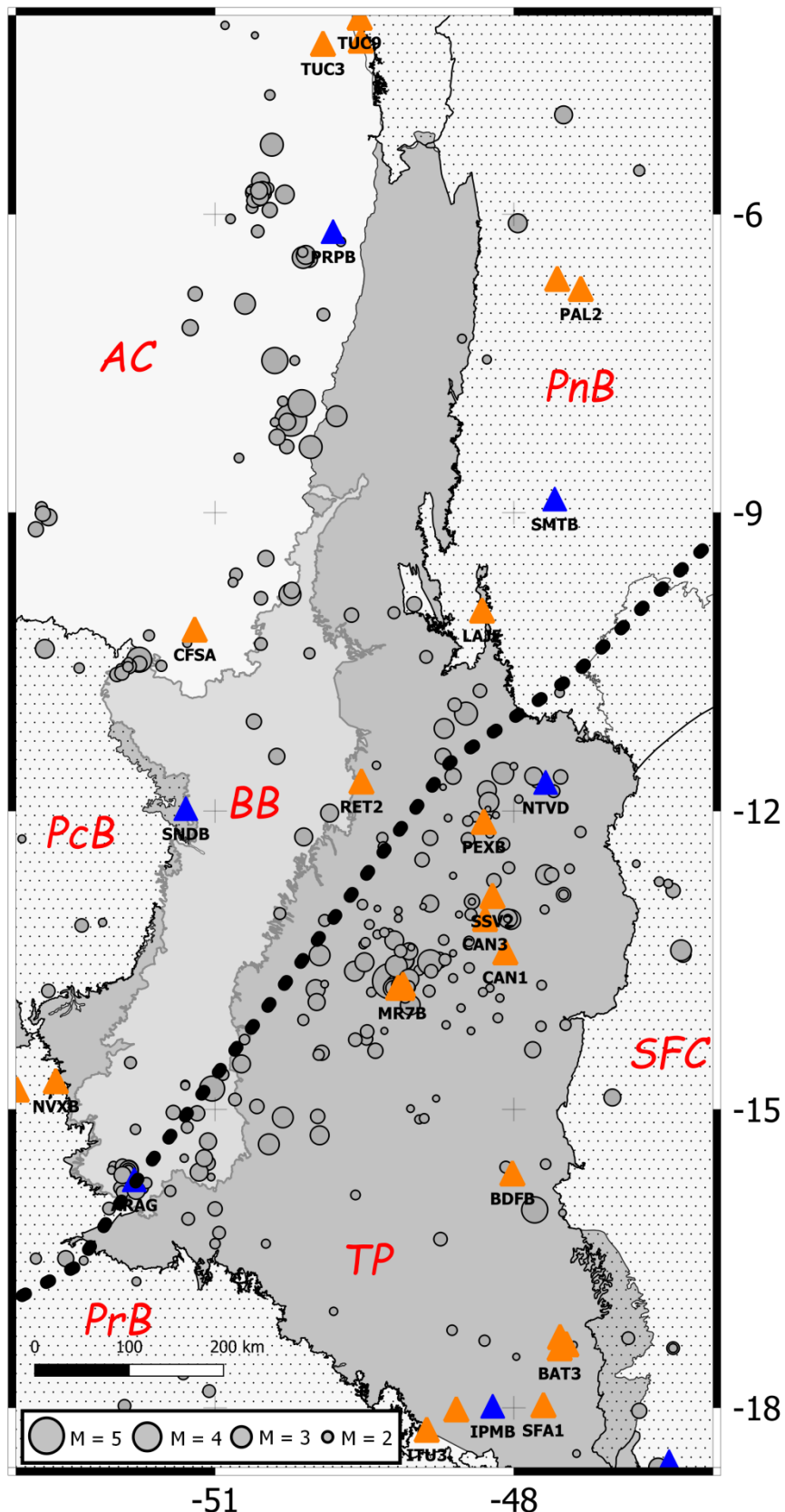
Figure 5-2 The study area with the geological provinces, the LTB and seismicity. The grey circles indicate the epicenters of the Brazilian Seismic Catalog, the blue triangles are the seismic station of the RSBR and the orange triangles are the seismic station from other projects. The geological provinces are described in Figure 5-1.

5.4   Geological setting

The central Brazil region (Figure 5-2) is mostly covered by the Tocantins province, which resulted from the convergence and collision of three continental blocks: the Paranapanema block in the south, currently covered by rocks of the Paraná basin; the Amazonian craton in the west and the São Francisco craton in the east portion (Cordani et al. 1984; Fuck et al. 2008). This province is basically constituted by neoproterozic fold belts terrains i.e., the Araguaia and Paraguay fold belt along the eastern and southeastern margins of Amazonas craton and the Brasília belt along the western edge of São Francisco craton. The area margins include the eastern boarder of the Amazon craton; southwestern border of the Parnaiba basin; the western border of the São Francisco craton and northern border of the Paraná basin.

The Tocantins province is divided in three major tectonic domains, shown in Figure 5-3, the northern, with NNE-SSW trend, the Araguaia belt, is separated from the NNW-SSE striking Brasilia Belt by the NE-SW Goiás Magmatic Arc. The Neoproterozoic Magmatic rocks along a dextral strike-slip shear zone, is part of the Transbrasiliano lineament (TBL), a continental scale discontinuity extending from north-east Brazil, to Argentina (Curto et al. 2014; Schobbenhaus et al. 1975).

An important gravimetric anomaly (Soares et al. 2006), associated with the juvenile Goiás Magmatic Arc (930–600 Ma), are coincident with the final structural differentiation of the Brasília Belt, resulted from the closure of a wide ocean basin during the Neoproterozoic Brasiliano Orogeny (Pimentel et al. 1997; Soares et al. 2006; Fuck et al. 1994).

At Mara Rosa region, the Goiás massif, made of Archean granite-greenstone terrains, is in contact with juvenile arc rocks of the Neoproterozoic Goiás Magmatic Arc through a dextral strike-slip shear zone, which appears to merge southwards with the Rio dos Bois thrust fault (Fuck et al. 2014).
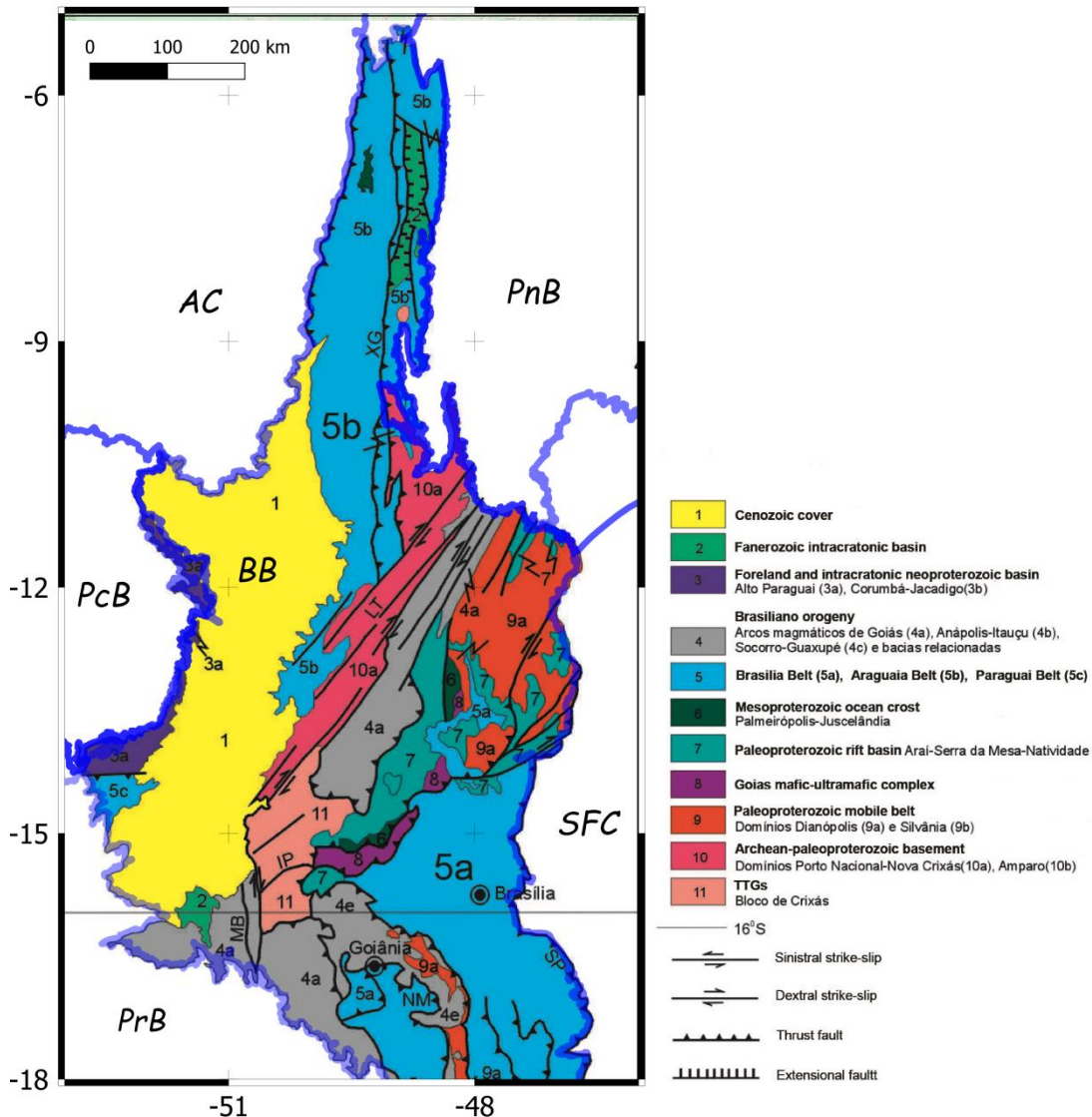
Figure 5-3 Geological map of Tocantins province sub divided in tree major tectonic domains, to the northern the Araguaia belt, trending NNE-SSW, at the center the Goiás Magmatic Arc striking NNW-SSE and at southern, the Brasilia Belt trending NE-SW. (Map from CPRM Geological Map)

5.5 Events relocation

The data set (118 events) were relocated with the iLoc code currently used in the International Seismological Centre (ISC) (Bondár & Storchak 2011) using the RSTT velocity model. The RSTT is a 3D model where the earth is divided in tessellation nodes representing the structures in tri-dimension spaced by 111 km each (Myers et al. 2010). The source of information for the RSTT model compilation is the global model corrected with time delays computed from the ground truth events (GTx), i.e., the events located with a precision better than 5

km, and information on the crustal thickness. The Brazilian GT database was established just recently (Assumpção, 2014; Agurto-Detzel et al., 2014; Barros et al., 2015; Chimpliganond et al., 2010).

5.5.1 Code iLoc and relocation test

The code iLoc processes local and regional events and run by default with the RSTT velocity model. Additionally, the code also supports a local 1D velocity model to improve the hypocenter determination with local network. In the last issued version of the code, release 2018, used here, it includes the Pg/Pn and Sn/Lg phase's assignment uncertainty. The latest version also integrates the crust and Moho depths for South America (Assumpção et al., 2013a).

The iLoc code either calculates the event depth or fixes it to a standard value; this decision is based on the depth resolution comprising four configurable parameters: i) Local network: Time-defining phases from minimum of (1) station at maximum epicentral distance of 0.2°; ii) Depth phase: at least (3) time-defining depth phase pairs reported by more than (1) agency; iii) Core reflection: at least (3) time-defining first arriving P and core reflection pairs, PcP, ScS, reported by at least (1) agency; iv) Local/near regional S: at least (3) S-P pairs reported by stations at maximum 2°. If these parameters indicate that the depth cannot be reliable calculated, then it is fixed to a configurable standard value. Within the data set there are 22 events that satisfied the depth resolution parameters allowing for the depth calculation. More detailed info are available in the iLoc manual (http://www.seismology.hu/index.php/en/home/iloc)

The iLoc code was used in Brazil by Neves et al. (2018) for the relocation of 10 offshore seismic events. With the help of data from a seismic line, which had recorded the event of July 1, 2010 occurred in the Campos basin, he succeeded to show that the catalog location was wrong by 18 km and the relocation repositioned the event to its correct location.

Prior to the data set relocation, we tested the iLoc code and RSTT model with the Mara Rosa (MR) main event (Oct, 2010) and 15 of its aftershocks, Figure 5-4, Table 1. The test comprised by a comparison of the relocated events and their respective location from the catalog. It is worth to mention that at both location procedures, i.e., iLoc and catalog, only stations at regional distances

were used. The iLoc code is an improved absolute location technique of individual events. The reference event (Figure 5-4, yellow star), MR-GT5 was relocated with cross-correlation technique using as reference two aftershocks located by local and regional stations (Barros et al. 2015). As a result, we notice that the events from Table 1 relocated and plotted in Figure 5-4 (blue circles) are less scattered than their respective location from the catalog (red circles). The average iLoc error is about 9 km (Figure 5-4, error ellipses, Table S1). Comparing to the MR GT5 reference position, the relocation has an average error of about 10 km.
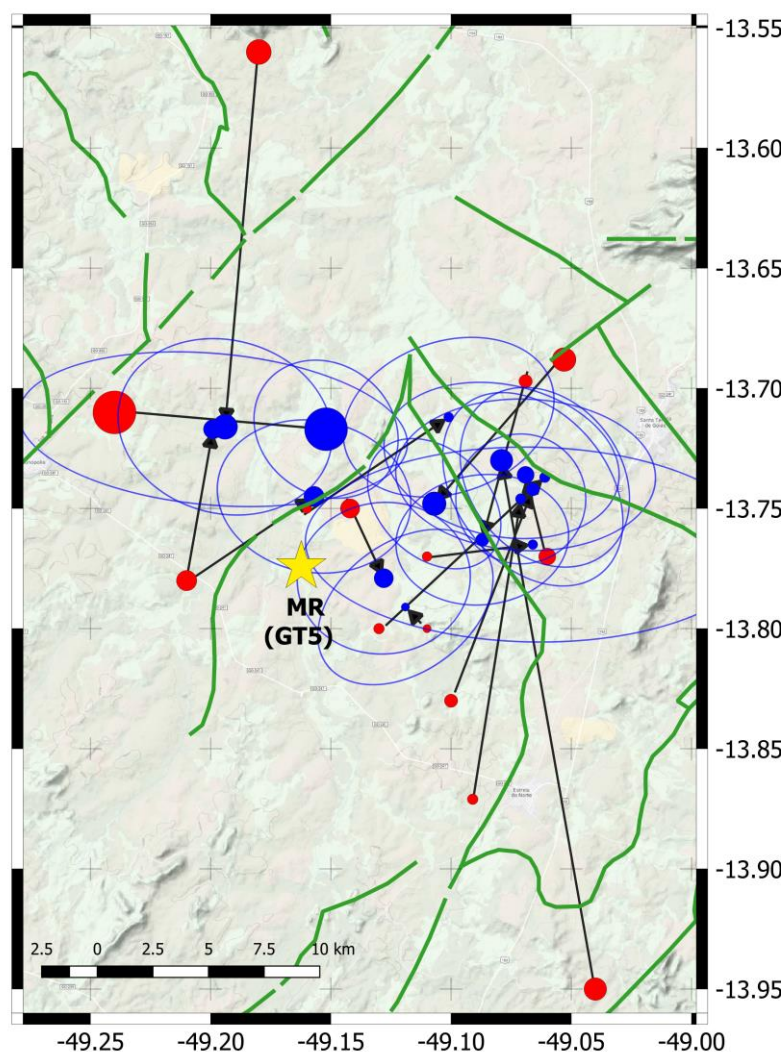
Figure 5-4 Aftershocks of Mara Rosa main event position from the catalog located with the Hypocenter code (Lienert 1994; Havskov & Ottemöller 2008) + NewBR model (Assumpção et al. 2010) (red circles) and relocated with the iLoc code + RSTT model (blue circles). The iLoc epicenter errors are represented by the blue ellipses (Table S1). The green lines are the geological structures. The star represents the Mara Rosa main event (GT5), i.e., the plotted mainshock position has a 5-km uncertainty. The "center of gravity" of the relocated aftershocks is situated in this 5-km uncertainty range, which proves good performance of the adopted location method.

Table 5-1 Cluster of events occurred in Mara Rosa region and classified as Aftershock of the main event (events 2-15) with magnitudes ranging from 2.0 to 3.7. The event 1 is the main event (M 5.0) relocated with cross correlation and classified as a GT5 (Figure 5-4 yellow star), (Barros et al. 2015). The magnitudes of the events are in the regional magnitude scale (m_R), which is consistent with the teleseismic m_b scale (Assumpção, 1983).

Nu./	iLoc Origin Time (UT)		Brazilian catalog		iLoc location (RSTT)		Mag	Shift
S1	Date	Hour	Lat (°)	Lon (°)	Lat (°)	Lon (°)	m_R	(km)
1/1	08/10/2010	20:16:52	-13.710	-49.240	-13.717	-49.152	5.0	10
2/3	26/02/2011	22:51:31	-13.780	-49.210	-13.717	-49.199	3.2	7
3/5	04/03/2011	06:59:41	-13.780	-49.210	-13.745	-49.157	3.3	7
4/7	24/04/2012	01:34:13	-13.770	-49.110	-13.765	-49.066	2.2	5
5/11	08/12/2012	18:52:34	-13.560	-49.180	-13.716	-49.194	3.7	17
6/13	22/06/2013	06:04:50	-13.950	-49.040	-13.73	-49.079	3.5	25
7/14	30/07/2013	04:22:02	-13.770	-49.060	-13.736	-49.069	3.0	4
8/45	19/05/2015	20:24:18	-13.800	-49.130	-13.737	-49.061	2.3	10
9/69	30/01/2016	07:40:30	-13.871	-49.091	-13.746	-49.071	2.3	14
10/72	29/03/2016	03:35:21	-13.697	-49.069	-13.763	-49.087	2.6	8
11/82	07/10/2016	19:59:57	-13.688	-49.053	-13.748	-49.107	3.6	9
12/97	21/09/2017	08:33:58	-13.750	-49.142	-13.779	-49.128	3.2	4
13/101	09/11/2017	06:18:24	-13.750	-49.160	-13.712	-49.101	2.2	8
14/113	26/05/2018	13:45:40	-13.830	-49.100	-13.742	-49.066	2.6	10
15/116	21/08/2018	00:19:27	-13.800	-49.110	-13.791	-49.119	2.0	1

5.5.2 Application of ILOC to 118 events

To achieve the goal of this work we performed two main actions: first, we screened the events from the catalog that matches the two pre-established quality parameters and, second we proceed with the screened events relocation using iLoc code and RSTT model. Hence, the comparison of the full catalog (Figure 5-2) and the screened and relocated events (Figure 5-5), are not to be compared event per event, but rather to bring the attention that the full catalog should be used with care. The relocated events compared with the catalog, Figure 5-5, changed (hopefully improved) the epicentral location between 1 and 95 km, with median of 9 km (not clearly seeing in the Figure 5-5 due to the map scale). The iLoc average epicenter error (Table AE.S1, smajax and sminax) is about 8 km. For details (comparison of the old and new locations), see Supplement Table AE.S1. The data set, screened by the quality criteria and its relocation, better defines two seismic zones: i) Goiás Tocantins seismic zone of (GTSZ) along the LTB. This zone looks to be entirely confined to the Goiás Magmatic Arc; ii) Amazon craton east seismic zone (ACESZ) following the eastern edge of the Amazon craton towards north. Additionally to that, a

disperse cluster of events is present in the south of the Tocantins province. The two zones have a well-defined band shapes.
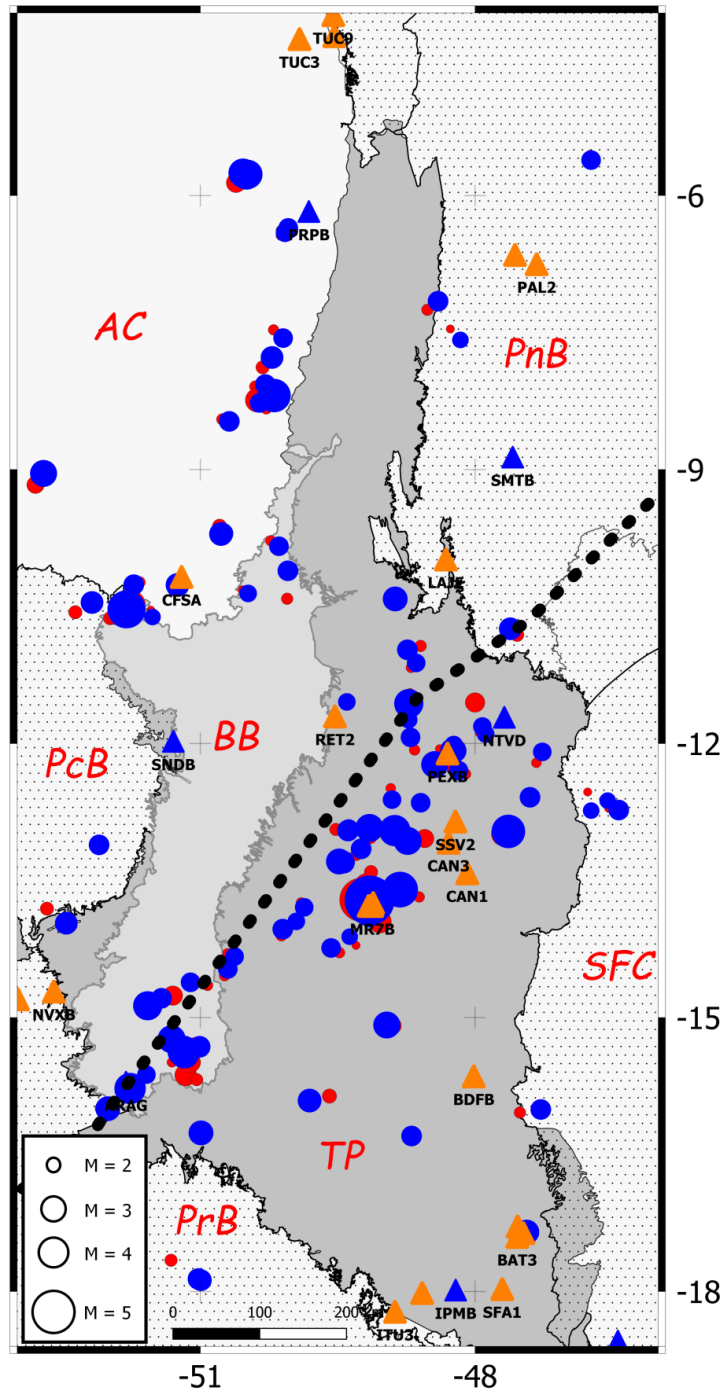
Figure 5-5 Events sorted from the catalog (red circles) and relocated with the iLoc code and RSTT model (blue circles). Stations from the RSBR (blue triangle) and stations from other project (orange triangle). The geological provinces are alike in Figure 5-1.

5.6 Moment tensor determination

The events of the study area are mostly weak, being a challenge to obtain focal mechanisms with polarities or waveform inversion. To succeed in obtaining the focal mechanisms for such weak events, we used the technique of waveform envelope inversion (Carvalho et al. 2017; Carvalho et al. 2019; Zahradník & Sokos 2018a). We selected 9 events for inversion, Table 2, events 1-9, magnitudes ranging from 2.1 to 4.1 m_R. The selection criteria was: events recorded by at least 4 stations at distances below 300 km and SNR > 5 in the frequency band of 0.8-1.2 Hz. By good signal we mean that the envelope maxima are >~ 5x stronger than the noise and that the duration of the main wave groups in real data is comparable to synthetics, i.e. the data do not contain long unmodeled codas. Additionally, we succeeded to invert one event (event 10 of Table 2) with the CSPS technique (Fojtikova & Zahradnik 2014). This was possible due to the available polarities (6) being sufficient for a reasonable run of FOCMEC (Snoke et al. 1984), providing input for the waveform inversion.

As per the velocity model, to which the envelopes are less sensitive than waveforms, we employ the same simple model (VM3) used originally in Carvalho et al. (2019), i.e., 2 crustal layers of the depth range 0-20 km, 20-42 km and a homogeneous half-space below Moho at 42 km, with Vp of 5.8, 6.4, 8.1 km/s respectively, and Vp/Vs=1.72. Due to limited depth resolution of ENV method (see Figure S2 appendix of Carvalho et al., 2019) we fixed the events at a shallow depth. For the consistency we used the same constraint parameters at all inversions. In the ENV technique we used at least one polarity to avoid the flip of the P-T axes, but avoiding polarities near the nodal planes. For the quality control we used the following parameters: Variance Reduction (VR), polarity match and stability of the set of solutions within the prescribed threshold (5%). The threshold parameter includes grid-search solutions from VRmax to VRmax-5%. Within this threshold, all the 9 events have stable (condensed) nodal planes (Figure 5-6a). The formally best-fitting results, characterized by the strike, dip, rake angles (S/D/R) are in Table 2. The envelopes variance reductions (VR) had a good adjustment at all inversions with an average of VR=0.64, (Figure 5-6b). The example of envelopes in Figure 5-6b is from the

Retiro Tocantins state (Table 2, event 1) with VR=0.54 when measuring in the whole time window of 130 s (of about 0.8 when considering only the major wavelets).

Table 5-2 Events 1-9 inverted for focal mechanisms with ENV code, event 10 inverted with the CSPS technique and events 11-12 are from previous studies. The magnitudes of the events are in the regional magnitude scale (m_R), which is consistent with the teleseismic m_b scale (Assumpção, 1983). The numbering of events used here differs from Table S1.

Nu.	Data	Time	Lat. (°)	Lon. (°)	Mag (m_R/M_w).	Location and State	Stations (Figure 5-7)	VR	Metod.	S/D/R 1 S/D/R 2	P&T 1 P&T 2	**Ref.
1	15/11/2015	10:55:08	-12.223	-48.465	2.9 1.6	Retiro, TO	PEXB, SSV2, CAN3, CAN1	0.5	ENV	330/80/-30 66/61/-168	284/28 21/13	1
2	12/04/2018	03:56:33	-17.349	-47.435	2.1 2.5	Paracatu, MG	BAT3, SFA1, IPMB, BDFB	0.6	ENV	180/70/80 27/22/116	278/24 74/64	1
3	07/07/2015	21:17:31	-12.057	-48.192	2.4 1.4	Peixe, TO	PEXB, SSV2, CAN3, CAN1	0.6	ENV	160/90/-30 250/60/-180	11/21 209/21	1
4	02/03/2011	19:16:55	-11.813	-47.920	2.5 3.0	Natividade, TO	PEXB, SSV2, CAN3, CAN1	0.6	ENV	50/70/100 203/22/64	132/24 336/64	1
5	09/04/2015	16:09:26	-16.297	-48.693	2.7 2.9	Anapolis, GO	BDFB, BAT2, IPMB, SFA1	0.6	ENV	270/20/140 38/77/74	141/31 289/55	1
6	04/10/2017	16:46:56	-5.767	-50.480	3.4 2.9	Carajas, PA	PRPB, TUC3, TUC4, PAL2	0.8	ENV	290/30/170 29/85/60	143/33 270/42	1
7	30/01/2016	07:40:29	-13.746	-49.071	2.4 2.6	Mara Rosa2, GO	CAN3, CAN1, SSV2, PEXB	0.7	ENV	190/40/20 84/77/128	146/23 32/44	1
8	25/12/2017	13:59:35	-6.420	-50.090	3.8 1.6	Canaã, PA	SNDB, ITTB, NPGB, PRPB	0.6	ENV	70/70/160 167/71/21	298/1 29/28	1
9	11/02/2015	09:46:31	-10.530	-51.806	4.1 3.4	Confresa, MT	SNDB, SMTB, PRPB, NPGB	0.6	ENV	320/60/170 55/81/30	184/14 282/27	1
10	08/01/2011	11:49:23	-13.580	-48.890	4.1 3.3	Formoso, GO	MR08, MR07, CAN3		CSPS	234/63/125 357/43/42	300/11 192/57	1
11	08/10/2010	20:16:55	-13.717	-49.152	5.0 4.3	Mara Rosa, GO	Other work		ISOLA (WFI)	216/49/74 60/43/108	317/3 60/78	2
12	20/11/2000	09:36:32	-16.054	-47.779	3.7	Brasilia, DF	Other work		ISOLA (WFI)	188/81/-34 284/56/-169	141/30 240/16	3

** References: 1-This work; 2-Barros et al., 2015; 3-Assumpção et al., 2016.
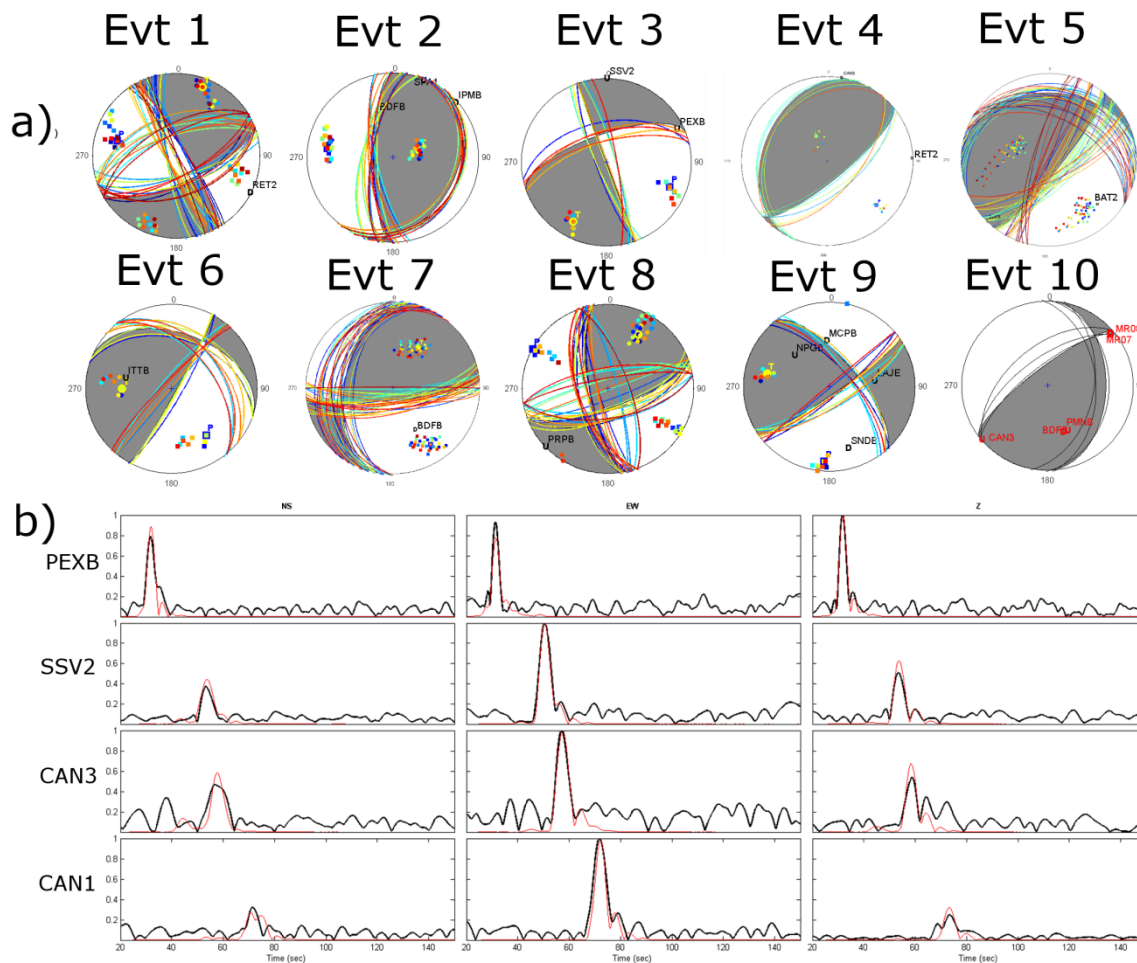
Figure 5-6 a) Beachballs of the focal mechanisms from ENV inversions (1-9) and from CSPS inversion (10), following the order of Table 2. The nodal planes plotted in the beachballs are limited to the threshold of 5%. Shaded sectors correspond to the formally best-fit solution. b) Plotted envelopes for the stations PEXB (0.5-0.8Hz), and SSV2, CAN3, CAN1 (0.8-1.0Hz) for event 1 (Table 2).

The selection criteria for inversion did not include epicenter position, but luckily the selected events fell evenly distributed in the study area: 3 to the south; 6 in the center and 3 to the north (Figure 5-7). The resulted focal mechanisms are reverse faults, strike slip, and or a mixture of both (Figure 5-8).
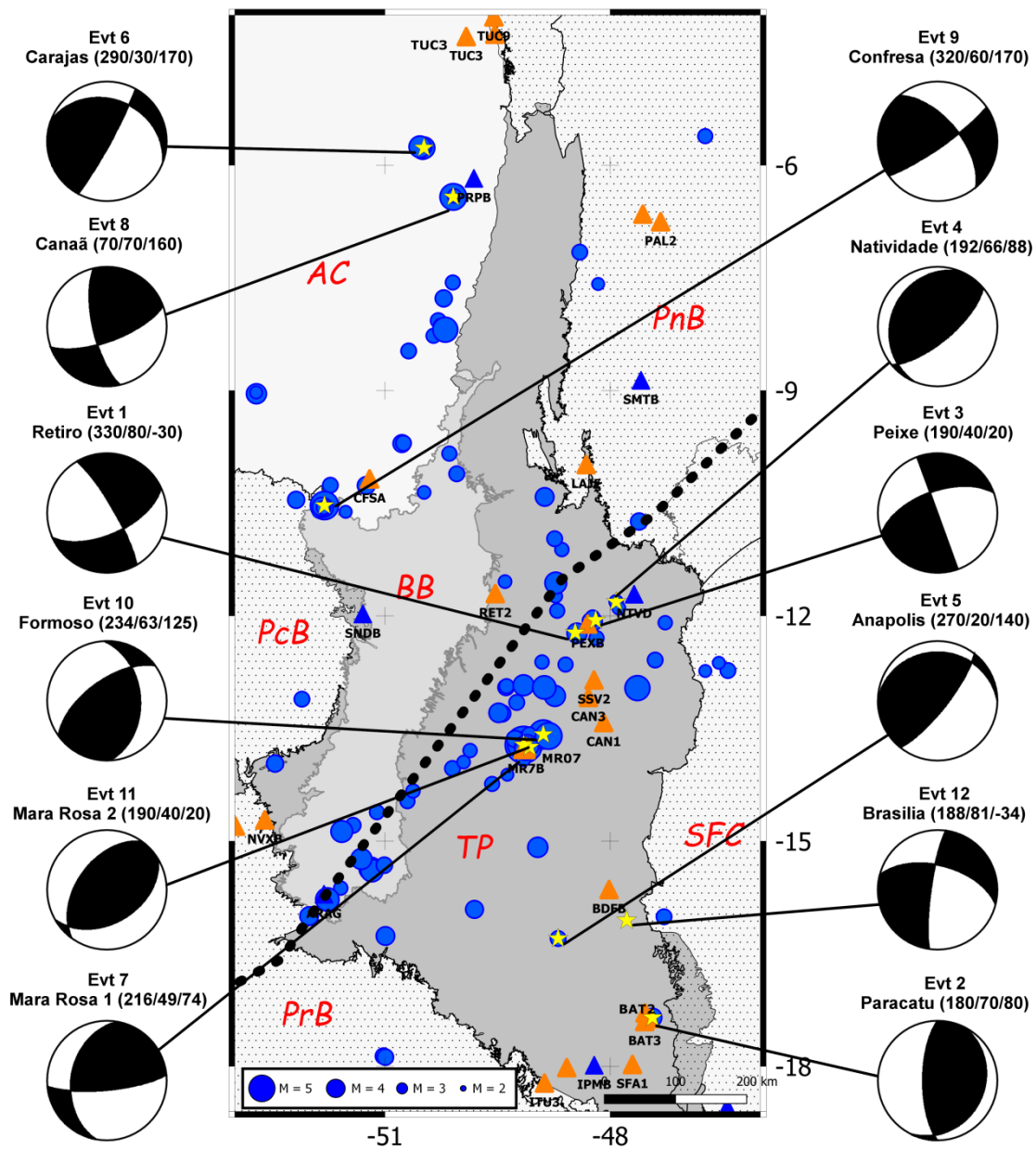
Figure 5-7 Beachballs for focal mechanism solutions of 12 events (Strike/Dip/Rake). Relocated epicenters (blue circles) and the focal mechanism solutions (yellow star), Table 2. The circle size represents the magnitude. For stations used in the envelope inversion, see Table 2. Geological provinces are as in Figure 5-1.

5.7 Stress field in central Brazil

The knowledge of stress field in the intraplate environment plays a very important role in the seismicity understanding. In Brazil the focal mechanism data base, from which the stress field is obtained, has only few dozen solutions not allowing high resolution studies.

Recently, Assumpção et al. (2016) presented a stress map of South America and for the central region of Brazil he used 7 focal mechanisms for stress inversion and, among them only two fall in the study area of this work. Here, we focus on a much smaller area and we are using 12 focal mechanisms for the stress inversion, 9 from ENV inversion, 1 from CSPS and 2 events from other works: Mara Rosa, 2010 main event (Barros et al. 2015) and Brasilia, 2000 (Assumpção et al. 2016).

Several methods are currently available for stress inversion (Angelier, 2002; Gephart and Forsyth, 1984; Hardebeck and Michael, 2006; Michael, 1984a; Vavryčuk, 2014; Michael (1987). For this work we employed the STRESSINVERSE code of Vavryčuk (2014), last updated in 2018. This code is a modification of the Michael (1984a) method, adding the calculation of instability to identify the fault plane of each focal mechanism solution, thus possibly increasing robustness of the shape ratio parameter. The method is linear and run iteratively.

The obtained twelve focal mechanisms were classified as following: five reverse faulting (2, 4, 5, 11 and 10); two strike slip (3 and 8) and five undefined (1, 6, 7, 9 and 12), (Figure 5-8a). The trade-off (Figure 5-8b) between the two axes, σ_2 and σ_3, fully corresponds to the above mentioned mixture of strike-slip and reverse mechanisms, which both are supported by the stress existing in the study region. As such, principal stresses σ_2 and σ_3 are close to each other, and, consequently, the directions of the stress axes σ_2 and σ_3 are poorly resolved. Similar result was obtained in the work of Hallo et al. (2019). The axis of the largest principal compressional stress axis σ_1 of the area is well resolved, featuring azimuth ~133° and plunge ~12°. The shape ratio (Figure 5-8c) defined as R = (σ_1- σ_2) / (σ_1- σ_3), is R = ~0.9. Mohr´s circles (Figure 5-8d) illustrate the closeness of the σ_2 and σ_3 values. The jackknifing test, i.e., repeated stress inversion each time removing one of the focal mechanisms, provides the σ_1 range as follows: azimuth 129°-139°, plunge 9°-18°.
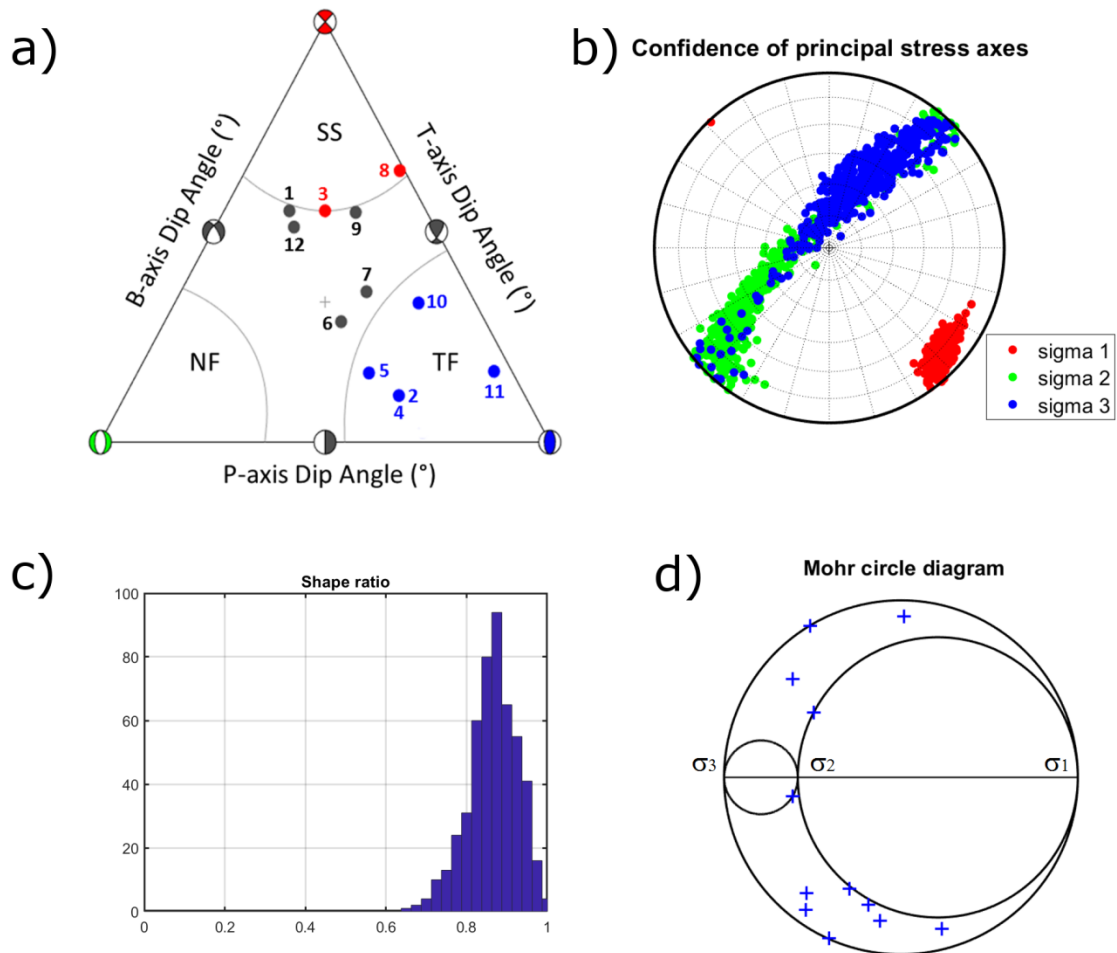
Figure 5-8 Stress inversion calculated from 12 events. a) Ternary diagram with the classification of the focal mechanisms (Frohlich 1992). Blue dots are reverse mechanisms, red dots are strike slip and black dots have no classification. Note in the panel a) that the events 2 and 4 have the same type (the same P&T plunges). b) Uncertainty of the stress axes from random perturbation of the input data. c) The shape ratio. d) Mohr´s circles with identified faults (blue crosses).

5.8 Discussion and conclusions

In this work we study the seismic-tectonic features of the central Brazil region, comprising of seismic events relocation, moment tensor and stress field determination. A data set of 118 events was selected from 337 events of the catalog (Figure 5-2). This set was relocated with the iLoc code and RSTT model; the epicenter uncertainty (estimated by the Mara Rosa GT5 benchmark) is less than 10 km. From the data set, only 22 events fulfil depth calculation requirement: 18 from 0-10 km depth; 4 from 10-20 km depth. We did not find any pattern or justification for these 4 deeper events and further investigation is required.

The events relocation allowed a better definition of two seismic zones: the Goiás Tocantins seismic zone (GTSZ) and the Amazon Craton east seismic zone (ACESZ). The seismicity of the GTSZ is in a form of a narrow band and indicates a close relationship with the LTB, highlighting its preferential direction and geographically position. The ACESZ is also in a shape of a narrow band following the eastern edge of the Amazon Craton and could be correlated to a transition zone between the craton and the Tocantins Province.

The seismicity of the GTSZ is correlated with a high positive Bouguer anomalies (244-290 mGal), (Figure 5-9a) corresponding to the Neoproterozoic Magmatic Arc. The high gravimetric can be explained by the thinning of the crust or in some areas by addition of the oceanic crust during the collision and subduction process of the paleo continent São Francisco and the Parnaíba and Paranapanema blocks. The Transbrasiliano lineament is a transcontinental structure, and in this area the LTB can be observed on the map of the Anomaly Bouguer and on the map of the Total Magnetic Intensity (TMI), Figure 5-9b, seismic events (epicenters) with shallow depth (<10 km), mostly follow the direction of the lineament. The events north of the area in the ACESZ seismic zone are in a high gravimetric area, in an area of magnetic anomaly of large wavelengths and high amplitudes, with direction of magnetic lineaments preferably E-W. According to (Assumpção et al. 2004; Assumpção & Sacek 2013; Rocha et al. 2016) the seismicity of the GTSZ results from a combination of regional stress concentration in the upper crust and a local flexural stress effects. About the Moho depth and seismology (Figure AE.S1) we did not find any clear correlation. In addition to the two zones, a disperse cluster of events is present to the south of the Tocantins Province.
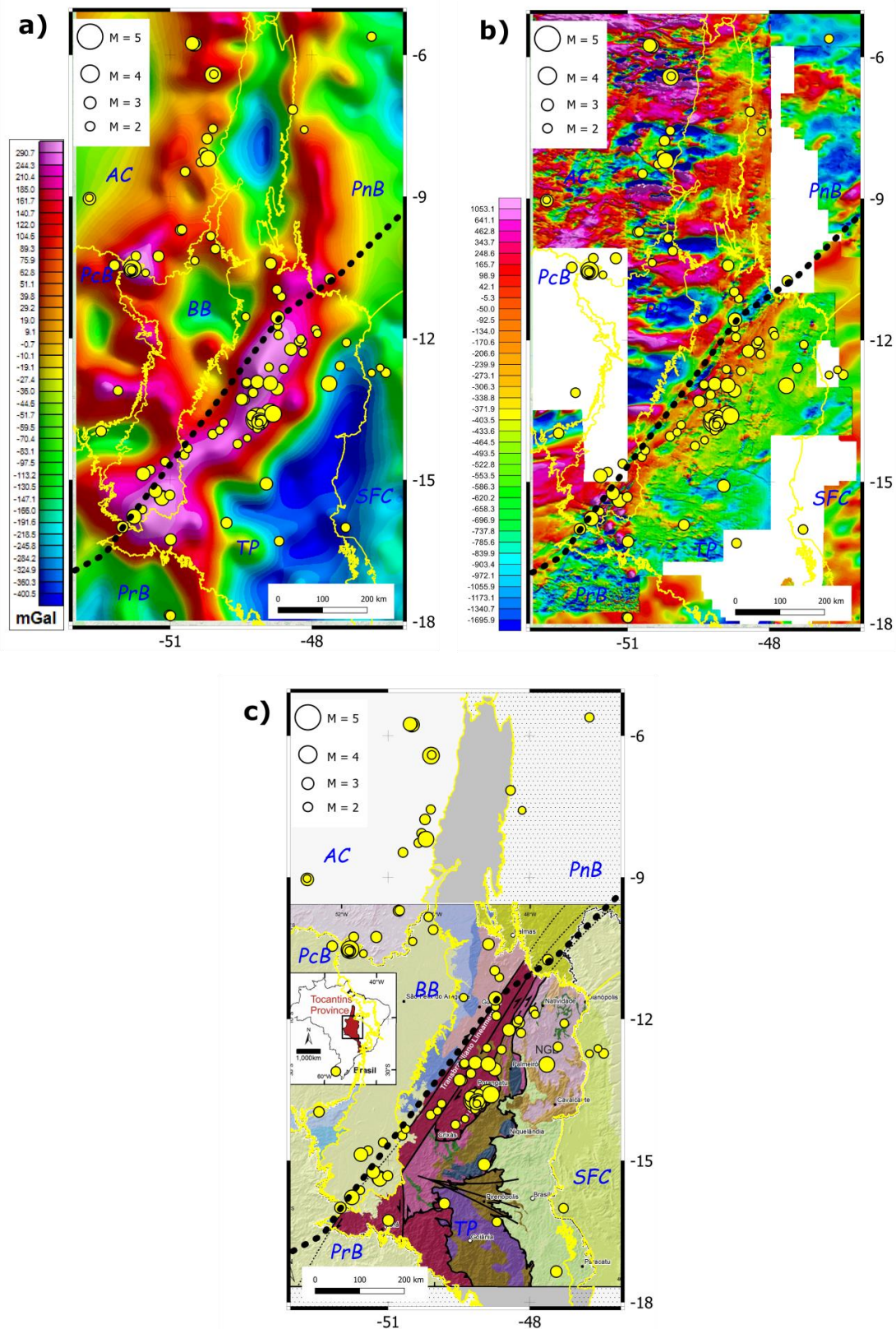
Figure 5-9 Geology and geophysics of the study area and its relation with the seismicity. a) Gravimetric map and, b) Total magnetic intensity field. Yellow circles, proportional to the magnitudes, denote the seismicity. c) Simplified Geological setting of the Tocantins Province (Corrêa et al. 2015). The yellow lines are the geological provinces boundaries. The magnetic map white space denotes lack of data lack. The geological provinces are described in Figure 5-1.

The focal mechanism studies in this area are very rare and it is a challenge due to the low magnitude events. The area is monitored by a sparse network and poor velocity model. As a consequence, up to this work, only two reliable focal mechanisms solutions were obtained: the Brasilia earthquake of 2000 (Assumpção et al., 2016) and to Mara Rosa event of 2010 (Barros et al., 2015). To obtain additional focal mechanisms, we used the inversion of waveform envelopes which is less sensitive to inaccurate velocity models. We used data recorded by at least four stations, distances below to 300 km, presence of signal at the frequency band of 0.8-1.2 Hz and constrained by at least one polarity to avoid the rake swap. We succeed with the inversion of 9 events with ENV code and one with the CSPS code (Fojtikova and Zahradnik, 2014), the last one constrained by a set of polarity forming a grid set of solutions from FOCMEC code (Snoke 2003). The focal mechanism of events in this region is concordant to the strike-slip faults associated with the LTB lineament, as indicated by events 1 and 3 (Figure 5-7). It's also noted that the stress responsible by the closure of a wide ocean basin during the Neoproterozoic Brasiliano Orogeny (Pimentel & Fuck 1992; Pimentel et al. 2004) could still be active as noted by reverse focal mechanism of events 7, 10 and 11 indicating an NW-SE compression. The compressive regime of these events is in agreement with the Rio dos Bois thrust zone (Figure 5-9c).

A total of twelve focal mechanisms were inverted resulting in a well resolved maximum compressional stress axis (σ_1) featuring azimuth 129°-139°, and plunge 9°-18°, which is consistent with other studies (Assumpção, Dias, et al. 2014 and Carvalho et al. 2016) inverting 11 aftershocks of the Mara Rosa event computed the σ1 azimuth of 155°. The stress axis (σ_1) is also compatible with the *in situ* measurement of Caproni & Armelin (1990).

5.9   Data and Resources

The majority of waveform data used in this article belong to the Brazilian Seismograph Network (RSBR), and they are freely available at www.obsis.unb.br and www.sismo.iag.usp.br (last accessed April 2019). University of São Paulo (USP) provides federated (FDSNWS) webservices for downloading event waveforms at http://seisrequest.iag.usp.br (last accessed

April 2019). The plots were made with the QGIS Geographic Information System http://qgis.osgeo.org" (last accessed April 2019). The waveform inversion was done with the software ISOLA and can be downloaded from http://geo.mff.cuni.cz/~jz/for_Costa_Rica (last accessed April 2019). The information on the Brazilian seismicity is from the Brazilian Seismic Bulletin (BSB) available at http://moho.iag.usp.br/eq/bulletin (last accessed May 2019) and at http://http:obsis.unb.br/portalsis/ (last accessed May 2019).

5.10 Acknowledgments

5.11 References (paper 3)

Agurto-Detzel, H., Assumpção, M., Bianchi, M., Pirchiner, M., 2017. Intraplate seismicity in mid-plate South America: correlations with geophysical lithospheric parameters. Geol. Soc. London, Spec. Publ. 432, 73–90. https://doi.org/10.1144/SP432.5

Agurto-Detzel, H., Assumpcao, M., Ciardelli, C., Albuquerque, D.F., Barros, L. V., Franca, G.S.L., 2014. The 2012-2013 Montes Claros earthquake series in the Sao Francisco Craton, Brazil: new evidence for non-uniform intraplate stresses in mid-plate South America. Geophys. J. Int. 200, 216–226. https://doi.org/10.1093/gji/ggu333

Albuquerque, D.F., França, G.S., Moreira, L.P., Assumpção, M., Bianchi, M., Barros, L.V., Quispe, C.C., Oliveira, M.E., 2017. Crustal structure of the Amazonian Craton and adjacent provinces in Brazil. J. South Am. Earth Sci. 79, 431–442. https://doi.org/10.1016/j.jsames.2017.08.019

Angelier, J., 2002. Inversion of earthquake focal mechanisms to obtain the seismotectonic stress IV-a new method free of choice among nodal planes. Geophys. J. Int. 150, 588–609. https://doi.org/10.1046/j.1365-246X.2002.01713.x

Assumpção, M., Ardito, J.E., Barbosa, J.R., 2010. An improved velocity model for regional epicentre determination in Brazi. IV Simpóosio Bras. Geofísica. Brasília 13 e 16 de novembro de 2010.

Assumpção, M., Bianchi, M., Julià, J., Dias, F.L., Sand França, G., Nascimento, R., Drouet, S., Pavão, C.G., Albuquerque, D.F., Lopes, A.E.V., 2013a. Crustal thickness map of Brazil: Data compilation and main features. J. South Am. Earth Sci. 43, 74–85. https://doi.org/10.1016/j.jsames.2012.12.009

Assumpção, M., Dias, F.L., Zevallos, I., 2014. Intraplate Stress Field in South America from Earthquake Focal Mechanisms. South Am. Earth Sci.

Assumpção, M., Dias, F.L., Zevallos, I., Naliboff, J.B., 2016. Intraplate stress field in South America from earthquake focal mechanisms. J. South Am. Earth Sci. 71, 278–295. https://doi.org/10.1016/j.jsames.2016.07.005

Assumpção, M., Feng, M., Tassara, A., Julià, J., 2013b. Models of crustal thickness for South America from seismic refraction, receiver functions and surface wave tomography. Tectonophysics 609, 82–96. https://doi.org/10.1016/j.tecto.2012.11.014

Assumpção, M., Sacek, V., 2013. Intra-plate seismicity and flexural stresses in central Brazil. Geophys. Res. Lett. 40, 487–491. https://doi.org/10.1002/grl.50142

Assumpção, M., Schimmel, M., Escalante, C., Roberto Barbosa, J., Rocha, M., Barros, L. V., 2004. Intraplate seismicity in SE Brazil: stress concentration in lithospheric thin spots. Geophys. J. Int. 159, 390–399. https://doi.org/10.1111/j.1365-246X.2004.02357.x

Assumpção, M.S., 2014. A Test of the RSTT Model for South America with Brazilian GT Events, in: IASPEI 2014. IASPEI Regional Assembly, Bogota, Colombia, Bogota, Colombia, pp. 23–25.

Barros, L.V., Assumpção, M., Ribotta, L.C., Ferreira, V.M., de Carvalho, J.M., Bowen, B.M.D., Albuquerque, D.F., 2018. Reservoir-Triggered Seismicity in Brazil: Statistical Characteristics in a Midplate Environment. Bull. Seismol. Soc. Am. 108, 3046–3061. https://doi.org/10.1785/0120170364

Barros, L. V., Assumpção, M., Chimpliganond, C., Carvalho, J.M., Von Huelsen, M.G., Caixeta, D., França, G.S., de Albuquerque, D.F., Ferreira, V.M., Fontenele, D.P., 2015. The Mara Rosa 2010 GT-5 earthquake and its possible relationship with the continental-scale transbrasiliano lineament. J. South Am. Earth Sci. 60, 1–9. https://doi.org/10.1016/j.jsames.2015.02.002

Berrocal, J., Assumpção, M., ARTEZANA, R.DIAS NETO, C.M., Ortega, R., FRANÇA, H., VELOSO, J.A.V., Antezana, R., Neto, C.M.D., Franca, H., 1984. Sismicidade do Brasil. Instituto Astronômico e Geofísico, Sao Paulo.

Bianchi, M.B., Assumpção, M., Rocha, M.P., Carvalho, J.M., Azevedo, P.A., Fontes, S.L., Dias, F.L., Ferreira, J.M., Nascimento, A.F., Ferreira, M. V., Costa, I.S.L., 2018. The Brazilian Seismographic Network (RSBR): Improving Seismic Monitoring in Brazil. Seismol. Res. Lett. 89, 452–457. https://doi.org/10.1785/0220170227

Bondár, I., Storchak, D., 2011. Improved location procedures at the International Seismological Centre. Geophys. J. Int. 186, 1220–1244. https://doi.org/10.1111/j.1365-246X.2011.05107.x

Caproni, N., Armelin, J., 1990. Instrumentacão das escavações subterrâneas da UHE Serra da Mesa. In: Simpósio sobre Instrumentação Geotecnica de Campo - SINGEO'90 Associação Brasileira de Geologia de Engenharia, São Paulo, vol. 1, pp. 249e257.

Carvalho, J., Barros, L.V., Zahradník, J., 2019. Inversion for Focal Mechanisms Using Waveform Envelopes and Inaccurate Velocity Models: Examples from Brazil. Bull. Seismol. Soc. Am. 109, 138–151. https://doi.org/10.1785/0120180119

Carvalho, J., Barros, L.V., Zahradník, J., 2016. Focal mechanisms and moment magnitudes of micro-earthquakes in central Brazil by waveform inversion with quality assessment and inference of the local stress field. J. South Am. Earth Sci. 71, 333–343. https://doi.org/10.1016/j.jsames.2015.07.020

Carvalho, J.M., Lucas, L. V., Zahradník, J., 2017. Towards Focal Mechanisms in Poorly Known Velocity Models: Inverting Waveform Envelopes, in: Science and Technology - Conference CTBT. pp. 11–11.

Chimpliganond, C., Assumpção, M., Von Huelsen, M., França, G.S., 2010. The intracratonic Caraíbas–Itacarambi earthquake of December 09, 2007 (4.9 mb), Minas Gerais State, Brazil. Tectonophysics 480, 48–56. https://doi.org/10.1016/j.tecto.2009.09.016

Cordani, U.G., Fuck, R.A., Brito Neves, B.B., Filho, A.T., Cunha, F.M.B., 1984. Estudo preliminar de integração do Pré-Cambriano com os eventos tectônicos das Bacias Sedimentares Brasileiras, Ciência Técnica Petróleo.

Corrêa, R. de S., Oliveira, C.G. de, Vidotti, R.M., Souza, V. da S., 2015. Regional-scale pressure shadow-controlled mineralization in the Príncipe Orogenic Gold Deposit, Central Brazil. Ore Geol. Rev. 71, 273–304. https://doi.org/10.1016/j.oregeorev.\ 2015.06.008

Curto, J.B., Vidotti, R.M., Fuck, R.A., Blakely, R.J., Alvarenga, C.J.S., Dantas, E.L., 2014. The tectonic evolution of the Transbrasiliano Lineament in northern Paraná Basin, Brazil, as inferred from aeromagnetic data. J. Geophys. Res. Solid Earth 119, 1544–1562. https://doi.org/10.1002/2013JB010593

Dias, F., Zahradník, J., Assumpção, M., 2016. Path-specific, dispersion-based velocity models and moment tensors of moderate events recorded at few distant stations: Examples from Brazil and Greece. J. South Am. Earth Sci. 71, 344–358. https://doi.org/10.1016/j.jsames.2016.07.004

Fojtikova, L., Zahradnik, J., 2014. A New Strategy for Weak Events in Sparse Networks: The First-Motion Polarity Solutions Constrained by Single-Station Waveform Inversion. Seismol. Res. Lett. 85, 1265–1274. https://doi.org/10.1785/0220140072

Frohlich, C., 1992. Triangle diagrams: ternary graphs to display similarity and diversity of earthquake focal mechanisms. Phys. Earth Planet. Inter. 75, 193–198. https://doi.org/10.1016/0031-9201(92)90130-N

Fuck, R. a., Dantas, E.L., Pimentel, M.M., Botelho, N.F., Armstrong, R., Laux, J.H., Junges, S.L., Soares, J.E., Praxedes, I.F., 2014. Paleoproterozoic crust-formation and reworking events in the Tocantins Province, central Brazil: A contribution for Atlantica supercontinent reconstruction. Precambrian Res. 244, 53–74. https://doi.org/10.1016/j.precamres.2013.12.003

Fuck, R.A., Brito Neves, B.B., Schobbenhaus, C., 2008. Rodinia descendants in South America. Precambrian Res. 160, 108–126. https://doi.org/10.1016/j.precamres.2007.04.018

Fuck, R.A., Pimentel, M., Silva, L., 1994. Compartimentação Tectônica na Porção Oriental da Província Tocantins, IV Simpósio de Geologia do Centro-Oeste,. SBG , Brasília, 215–216.

Gephart, J.W., Forsyth, D.W., 1984. An improved method for determining the regional stress tensor using earthquake focal mechanism data: Application to the San Fernando Earthquake Sequence. J. Geophys. Res. 89, 9305. https://doi.org/10.1029/JB089iB11p09305

Hallo, M., Opršal, I., Asano, K., Gallovič, F., 2019. Seismotectonics of the 2018 northern Osaka M6.1 earthquake and its aftershocks: joint movements on strike-slip and reverse faults in inland Japan. Earth, Planets Sp. 71, 34. https://doi.org/10.1186/s40623-019-1016-8

Hardebeck, J.L., Michael, A.J., 2006. Damped regional-scale stress inversions: Methodology and examples for southern California and the Coalinga aftershock sequence. J. Geophys. Res. Solid Earth 111, n/a-n/a. https://doi.org/10.1029/2005JB004144

Havskov, J., Ottemöller, L., 2008. SEISAN: The Earthquake Analysis Software, Version 8.2.

Heidbach, O., Reinecker, J., Tingay, M., Müller, B., Sperner, B., Fuchs, K., Wenzel, F., 2007. Plate boundary forces are not enough: Second- and third-order stress patterns highlighted in the World Stress Map database. Tectonics 26, n/a-n/a. https://doi.org/10.1029/2007TC002133

Heidbach, O., Tingay, M., Barth, A., Reinecker, J., Kurfeß, D., Müller, B., 2010. Global crustal stress pattern based on the World Stress Map database release 2008. Tectonophysics 482, 3–15. https://doi.org/10.1016/j.tecto.2009.07.023

Kenner, S.J., Segall, and P., 2000. A mechanical model for intraplate earthquakes: application to the new madrid seismic zone. Science 289, 2329–32. https://doi.org/10.1126/SCIENCE.289.5488.2329

Lienert, B.R., 1994. Hypocenter 3.2: A computer program for locating earthquakes locally, regionally and globally 102.

Mendiguren, J.A., Richter, F.M., 1978. On the origin of compressional intraplate stresses in South America. Phys. Earth Planet. Inter. 16, 318–326. https://doi.org/10.1016/0031-9201(78)90070-5

Michael, A.J., 1987. Use of focal mechanisms to determine stress: A control study. J. Geophys. Res. 92, 357. https://doi.org/10.1029/JB092iB01p00357

Michael, A.J., 1984. Determination of stress from slip data: Faults and folds. J. Geophys. Res. Solid Earth 89, 11517–11526. https://doi.org/10.1029/JB089iB13p11517

Myers, S.C., Begnaud, M.L., Ballard, S., Pasyanos, M.E., Phillips, W.S., Ramirez, A.L., Antolik, M.S., Hutchenson, K.D., Dwyer, J.J., Rowe, C.A., Wagner, G.S., 2010. A Crust and Upper-Mantle Model of Eurasia and North Africa for Pn Travel-Time Calculation. Bull. Seismol. Soc. Am. 100, 640–656. https://doi.org/10.1785/0120090198

Neves, F. dos A., Assumpção, M., Dourado, J.C., Le Diagon, F., Ortolan, A., 2018. Improved epicentral relocation in the offshore Campos basin, SE Brazil, with the RSTT 3D model. J. South Am. Earth Sci. 85, 121–125. https://doi.org/10.1016/j.jsames.2018.05.002

Pimentel, M.M., Filho, C.F.F., Armstrong, R.A., 2004. SHRIMP U–Pb and Sm–Nd ages of the Niquelândia layered complex: Meso- (1.25 Ga) and Neoproterozoic (0.79 Ga) extensional events in central Brazil. Precambrian Res. 132, 133–153. https://doi.org/10.1016/j.precamres.2004.02.009

Pimentel, M.M., Fuck, R.A., 1992. Neoproterozoic crustal accretion in central Brazil. Geology 20, 375. https://doi.org/10.1130/0091-7613(1992)020<0375:NCAICB>2.3.CO;2

Pimentel, M.M., Whitehouse, M.J., Viana, M. das G., Fuck, R.A., Nuno, M., 1997. The Mara Rosa Arch in the Tocantins Province: further evidence for Neoproterozoic crustal accretion in Central Brazil. Precambrian Res. 81, 299–310. https://doi.org/10.1016/S0301-9268(96)00039-3

Rocha, M.P., Araújo De Azevedo, P., Sant', G., Marotta, A., Schimmel, M., Fuck, R., 2016. Causes of intraplate seismicity in central Brazil from travel time seismic tomography. https://doi.org/10.1016/j.tecto.2016.05.005

Rocha, M.P., Schimmel, M., Assumpção, M., 2011. Upper-mantle seismic structure beneath SE and Central Brazil from P- and S-wave regional traveltime tomography. Geophys. J. Int. 184, 268–286. https://doi.org/10.1111/j.1365-246X.2010.04831.x

SBAR, M.L., SYKES, L.R., 1973. Contemporary Compressive Stress and Seismicity in Eastern North America: An Example of Intra-Plate Tectonics. Geol. Soc. Am. Bull. 84, 1861. https://doi.org/10.1130/0016-7606(1973)84<1861:CCSASI>2.0.CO;2

Schobbenhaus, C., Ribeiro, C.L., Oliva, L.A., Takanohashi, J.T., Lindenmayer, A.G., Vas- concelos, J.C., Orlandi, V., 1975. Carta Geológica do Brasil ao Milionésimo. DNPM, Brasília Folha Goiá.

Snoke, J.A., 2003. FOCMEC: FOCal MEChanism Determinations, Virginia, EUA.

Snoke, J.J.A.J., Munsey, J.J.W., Teague, A.A.C., Bollinger, G.G.A., 1984. A program for focal mechanism determination by combined use of polarity and SV-P amplitude ratio data,. Earthq. notes.

Soares, J.E., Berrocal, J., Fuck, R.A.R.A., Mooney, W.D., Ventura, D.B.R., 2006. Seismic characteristics of central Brazil crust and upper mantle: A deep seismic refraction study. J. Geophys. Res. 111, B12302. https://doi.org/10.1029/2005JB003769

Sokos, E., Zahradnik, J., 2013. Evaluating Centroid-Moment-Tensor Uncertainty in the New Version of ISOLA Software. Seismol. Res. Lett. 84, 656–665. https://doi.org/10.1785/0220130002

Sykes, L.R., 1978. Intraplate seismicity, reactivation of preexisting zones of weakness, alkaline magmatism, and other tectonism postdating continental fragmentation. Rev. Geophys. 16, 621–688. https://doi.org/10.1029/RG016i004p00621

Talwani, P., 1989. Characteristic Features of Intraplate Earthquakes and the Models Proposed to Explain Them, in: Earthquakes at North-Atlantic Passive Margins: Neotectonics and Postglacial Rebound. Springer Netherlands, Dordrecht, pp. 563–579. https://doi.org/10.1007/978-94-009-2311-9_33

Talwani, P., Rajendran, K., 1991. Some seismological and geometric features of intraplate earthquakes. Tectonophysics 186, 19–41. https://doi.org/10.1016/0040-1951(91)90383-4

Tingay, M., Muller, B., Reinecker, J., Heidbach, O., 2006. State and Origin of the Present-Day Stress Field in Sedimentary Basins: New Results from the World Stress Map Project.

Vavryčuk, V., 2014. Iterative joint inversion for stress and fault orientations from focal mechanisms. Geophys. J. Int. 199, 69–77. https://doi.org/10.1093/gji/ggu224

Zahradník, J., Cízková, H., Bina, C.R., Sokos, E., Janský, J., Tavera, H., Carvalho, J., 2017. A recent deep earthquake doublet in light of long-term evolution of Nazca subduction. Sci. Rep. 7. https://doi.org/10.1038/srep45153

Zahradník, J., Sokos, E., 2018a. Fitting Waveform Envelopes to Derive Focal Mechanisms of Moderate Earthquakes. Seismol. Res. Lett. 89, 1137–1145. https://doi.org/10.1785/0220170161

Zahradník, J., Sokos, E., 2018b. ISOLA Code for Multiple-Point Source Modeling—Review. pp. 1–28. https://doi.org/10.1007/978-3-319-77359-9_1

Zoback, M. Lou, Richardson, R.M., 1996. Stress perturbation associated with the Amazonas and other ancient continental rifts. J. Geophys. Res. Solid Earth 101, 5459–5475. https://doi.org/10.1029/95JB03256

CAPÍTULO 6 - DISCUSSÃO E CONCLUSÔES

Nesta tese de doutorado foi estudada a sismicidade do Brasil central, considerando suas características de baixa magnitude, monitorada por poucas estações a distâncias regionais.

6.1 Incertezas em mecanismos focais por polaridades

A determinação de mecanismos focais de eventos de baixas magnitudes registrados em redes esparsas é um desafio. Como forma de superar esse problema foram usadas duas técnicas: inversão de envelope de formas de ondas e; CSPS (Cyclic Scanning of the Polarity Solutions). A última tem como característica principal a utilização conjunta de duas outras técnicas: polaridades e inversão de formas de ondas. Como eventos de baixas magnitudes registrados a distâncias regionais normalmente tem um número baixo de polaridades, não é possível obter uma solução única e sim um conjunto de soluções. Neste caso, é feita então a inversão somente desse conjunto de soluções buscando o melhor ajuste entre os sismogramas sintéticos e observados. O problema é que as polaridades disponíveis de estações locais/regionais quando combinadas com modelos de baixa resolução, causam incertezas no ângulo de saída (takeoff angle) que é projetado na esfera focal, propagando essas incertezas para o resultado de mecanismo focal por polaridade.

O evento de Mara Rosa de 2010 (M_w 4.3) foi usado como referencia para testar a influência dessas incertezas na solução dos planos nodais. Para calcular os ângulos takeoff e projetar as posições das polaridades na esfera focal foram utilizados quatro modelos de velocidades NewBR (Assumpção et al. 2010), Barros (Barros et al. 2015), Soares (Soares et al. 2006) e Soares_gradiente. A partir desses modelos foram gerados seis possíveis cenários (Sets 1-6, Figura 3-6) de ângulos de saída, NewBR, Barros, Soares1 (profundidade fixada em 1.3 km), Soares2 (profundidade fixada em 2.3 km), Soares_gradient (todas estações) e Soares_gradient (estações 5-11, Tabela 3-1).

Para o evento de referência com onze polaridades foi possível obter apenas um grupo disperso soluções (Fig. 3-6). Além da dispersão existem ainda as incertezas devido às variações nos ângulos de saída causados pela baixa

resolução dos modelos (Fig. 3.2). Seis modelos e respectivos conjuntos de polaridades projetadas na esfera focal (Sets) foram testados (Tabela 3.1). Essas incertezas são mais significativas a distâncias epicentrais menores (<200 km). O objetivo desse estudo é mostrar a necessidade de avaliar as restrições e inversões (polaridades e formas de ondas) quando poucos dados estão disponíveis. A principal inovação tem sido a extensão do método CSPS usando vários conjuntos de polaridade de primeiro movimento (Sets) que refletem as incertezas, nos ângulos de saída, inerentes aos modelos. Nesse sentido, consideramos que as polaridades projetadas na esfera focal influenciadas pelas variações nos modelos é uma inovação útil e um indicador de estabilidade.

6.2 Inversão de envelope de formas de ondas (ENV)

A inversão de formas de ondas com modelos imprecisos é responsável por discrepâncias temporais e de amplitudes entre dados reais e sintéticos. Um modelo impreciso dificulta um bom ajuste, mostrando claramente que a inversão não obteve sucesso. A imprecisão inerente aos modelos de velocidades torna crítico à utilização de estações regionais distantes.

Ao contrário das formas de ondas, seus envelopes são menos sensíveis às imprecisões nos modelos. O ENV é um método empírico no qual os envelopes de formas de ondas são invertidos para o mecanismo focal. O método é baseado em busca sistemática em uma grade no espaço dos parâmetros strike, dip e rake, com objetivo de encontrar o melhor ajuste nos sismogramas normalizado por estação, principalmente para reproduzir as amplitudes relativas nas três componentes (ZNE).

O método ENV foi testado com dados sintéticos comprovando a sua capacidade de recuperar mecanismo focal da fonte original. Para evitar a inversão entre os eixos P e T, a inversão do envelope deve ser complementada por ao menos uma polaridade de primeiro movimento (bem determinada). Se os envelopes disponíveis não restringirem a solução o suficiente, polaridades adicionais devem ser usadas.

O método foi testado com dois eventos reais com magnitudes M_w 4+, eventos Mara Rosa 2010 e Maranhão 2017, ambos com mecanismo focal conhecido e

adotados aqui como referência. É importante destacar que estes são os únicos eventos rasos com magnitude acima de 4 (M_w) nos últimos dez anos no Brasil. O conjunto de dados desse dois eventos está no limite de possibilidades em termos de número de estações e faixa de frequência utilizável para inversão de formas de ondas. Para esses terremotos, registrados principalmente em estações distantes (~100-600 km), demonstramos que com os modelos de velocidade disponíveis: a) a inversão de forma de onda padrão não é aplicável, e b) a inversão de envelope recentemente proposta é mais eficiente. Por "eficiência" queremos dizer que um grupo de soluções com desajuste similar entre os envelopes observados e sintéticos contém os mecanismos focais que estão próximos da solução de referência, e que a magnitude de momento (M_w) das soluções também é compatível com as referências.

Intencionalmente para testar o método usamos apenas uma polaridade (estação única) para cada terremoto. Como as estações testadas estavam longe do epicentro e em pequeno número, a incerteza da solução, representada por linhas nodais dentro de um dado limiar de desajuste, não é pequena para o evento de falha reversa de Mara Rosa. Ao contrário, apesar das mesmas limitações, poucas estações e distantes, na inversão do terremoto de Maranhão obtivemos um grupo de soluções bem compacto e concordante com a referência. O bom desempenho do método no caso do evento do Maranhão resultou provavelmente de uma combinação de vários fatores: posição favorável das estações em relação ao padrão de radiação das ondas de superfície (que dominam os registros) e uso de apenas estações de banda larga, permitindo a utilização de frequências mais baixas que no caso de Mara Rosa.

É importante ressaltar que os resultados de inversão de envelope para os terremotos de Mara Rosa e Maranhão foram muito semelhantes para ambos os modelos de velocidade testados VM2 (Barros) e VM3 (NewBR), embora as formas de onda sintéticas para esses modelos sejam significativamente diferentes. Esta é uma indicação clara da robustez do método de inversão por envelopes.

Para os dois eventos de existem mais de 10 polaridades e poderíamos facilmente utilizá-las como restrição prévia obtendo assim um mecanismo muito

próximo da solução de referência. No entanto, é necessário ter cuidado para evitar restrição falsa. Outro perigo provém de polaridades de estações próximas que podem ter ângulos de saída imprecisos (por exemplo, 60° em vez de 90°) se os modelos de velocidade incluir descontinuidades rasas (tema do primeiro artigo).

Embora o método ENV resolva problemas que não podem ser resolvidos com inversão de formas de onda, ele também possui limitações. Como o método é novo, nem todas as limitações são conhecidas. É possível que estudos futuros forneçam alguns critérios bem definidos para descartar soluções não confiáveis. Até aqui o que podemos recomendar é: (i) descartar as estações com distúrbios instrumentais; (ii) usar tantas estações com boa relação sinal-ruído quanto possível; (iii) usar baixas frequências; (iv) incluir restrições razoáveis de polaridade; (v) usar repetidamente vários modelos de velocidade estabelecidos na região estudada; (vi) usar localização confiável do evento.

Quanto ao item (vi), também testamos possíveis variações na profundidade da fonte e com estações distantes e baixas frequências não encontramos boa resolução de profundidade. Por exemplo, no teste sintético da Figura AC.S2 com uma fonte verdadeira a 5 km de profundidade, invertemos de 1 a 10 km, em passos de 1 km, e encontramos uma pequena preferência pela profundidade correta, mas a resolução de profundidade foi muito pequena para incentivar a busca em profundidade para aplicações com dados reais.

A distância entre a estação e a fonte em relação a frequência invertida pode ser expressa em termos de MSW (Minimum Shear Wavelenght). Embora as inversões de formas de onda padrão quase sempre falham para distâncias acima de 10 MSW, no exemplo de Mara Rosa, conseguimos inverter envelopes em mecanismos focais com até 18 MSW e, no exemplo do Maranhão, até 21 MSW; Resultados semelhantes foram obtidos por Zahradnik e Sokos (2018). Parece ser uma pequena melhoria quando comparado aos 65 MSW com modelo ponto-a-ponto cobrindo o trajeto fonte estação (Dias et al., 2016), mas deve-se notar que nossa inversão aqui é baseada em modelos 1D padrão.

Neste estudo, propusemos um novo método que pode estender as possibilidades atuais de obtenção de mecanismo focal e cálculo de magnitude

de momento (M_w), especialmente com modelos de velocidade 1D simples e poucas estações em distâncias regionais. A robustez em relação a modelos de velocidade imprecisos e a simplicidade do método podem ser úteis em aplicações em tempo real, onde a derivação de modelos de velocidade especializados não é trivial.

6.3 Earthquake relocation, focal mechanism and stress field determination

O primeiro artigo abordou incertezas inerentes às técnicas que utilizam polaridades como medidas restritivas para obtenção de mecanismos focais e, o segundo, formulou e testou uma nova metodologia de inversão para obtenção da fonte sísmica, menos sensível às imprecisões nos modelos. Essas duas facilidades foram empregadas no estudo sísmico-tectônico na região central do Brasil, compreendendo a relocalização de eventos sísmicos e a determinação de mecanismos focais, bem como sua inversão para o campo de esforços.

As incertezas dos epicentros relocalizados com o código iLoc e o modelo RSTT foram avaliadas com a utilização do evento principal de Mara Rosa (GT5) e réplicas (Figura 5-4, Tabela 5-1). A média dos erros de localização foi inferior a 10 km. Do conjunto de 118 eventos relocalizados, apenas 22 preencheram os requisitos mínimos requeridos para o cálculo de profundidades, distribuídos da seguinte forma: 18 eventos de abaixo de 10 km e quatro entre 10 km e 20 km de profundidade. Não encontramos nenhuma justificativa para esses quatro eventos serem mais profundos e futuros estudos são necessários.

A relocalização permitiu uma melhor definição de duas zonas sísmicas: a zona sísmica Goiás Tocantins (GTSZ) e a zona sísmica leste do Cráton Amazônico (ACESZ). A sismicidade do GTSZ é na forma de uma faixa estreita indicando relação direta com o LTB (Figura 5-9a), destacando sua direção preferencial e posição geográfica. A ACESZ, com forma semelhante, seguindo a borda leste do Cráton Amazônico, pode ser correlacionada com a uma zona de transição entre o cráton e a Província Tocantins.

A sismicidade do GTSZ está correlacionada com altas anomalias positivas de Bouguer (244-290 mGal), (Figura 5-9a) correspondentes ao Arco Magmático neoproterozóico do Goiás correlacionada com o afinamento da litosfera.

A sismicidade do GTSZ resulta de uma combinação de concentração de esforço regional na crosta superior (Assumpção et al., 2004) e um efeito de esforço local do tipo flexura (Assumpção e Sacek, 2013; Rocha et al., 2016). Em relação à profundidade da descontinuidade da Moho (Figura AD.S1), não foi encontrada correlação clara. Além das duas zonas, um conjunto disperso de eventos está presente ao sul da Província Tocantins.

Estudos de mecanismos focais nessa área são raros e representa um desafio devido às baixas magnitudes, escassez de estações e modelos de velocidade de baixa resolução. Como consequência até o momento, apenas duas soluções de mecanismos focais foram obtidas: o terremoto de Brasília em 2000 (Assumpção et al., 2016) e Mara Rosa em 2010 (Barros et al., 2015).

Para obter mecanismos focais adicionais, usamos a técnica de inversão de envelopes de forma de onda, que é menos sensível a imprecisão no modelo de velocidade. As inversões foram realizadas apenas para eventos registrados por no mínimo quatro estações localizadas a distâncias <300 km, com boa relação sinal-ruído na faixa de frequência de 0.8-1.2 Hz e com uma ou mais polaridades (evitar rotação dos eixos P & T). Nove eventos foram selecionados para inversão com código ENV e um evento com o código CSPS. Dessa forma foi possível aumentar o banco de dados de MFs de dois para doze soluções (Tabela 5.2).

Os mecanismos focais transcorrentes 1 e 3 (Figura 5.7) são concordantes com as falhas associadas ao LTB.

As falhas reversas dos eventos 7, 10 e 11 de compressão NW-SE mostram que o esforço responsável pelo fechamento da Bacia oceânica durante a Orogenia Neoproterozóica Brasiliano pode ainda estar ativo, conforme Pimentel et al.(2004); Pimentel e Fuck (1992). O regime de compressão desses eventos está de acordo com as falhas de empurrão do Rio dos Bois (Figura 5.9c).

Doze mecanismos focais foram invertidos (Tabela 5.2, Figura 5.7), resultando em um eixo de esforço máximo de compressão bem resolvido (σ_1) com azimute variando entre 129° e 139° e mergulho variando entre 9° e 18° (Figura 5.8), consistente com os resultados de Assumpção et al. (2014) e com o estudo do campo de esforços na região de Mara Rosa-Goiás (Carvalho et al., 2016).

6.4 Conclusões:

1. A seleção e relocalização dos eventos possibilitou uma melhor definição das áreas sísmicas mostrando que a SZGT está confinada no Arco Magmático de Goiás;

2. O emprego da técnica ENV possibilitou a obtenção de MFs de eventos de baixas magnitudes em uma área com poucas estações sismográficas;

3. A inversão do conjunto de MFs possibilitou melhorar o conhecimento do campo de esforços na região.

6.5 Sugestões para estudos futuros na área:

4. Aumentar o banco de dados de MFs na área com estudo de replicas com redes locais. O que será possível com as redes *aftershocks* recém-adquiridas;

5. Melhorar os estudos de eventos com profundidades superiores a 10 km;

6. Estudar a área da Bacia do Bananal e sua assismicidade;

7. Estudar a sismicidade do leste do Cráton Amazônico com vistas a uma melhor definição de suas características espaciais.

ANEXOS

Anexo A – Artigos no período dentro do tema da tese

Relação de artigos publicados no período de realização do doutorado.

Artigo 1 - publicado

Compromising polarity and waveform constraints in focal-mechanism solutions; the Mara Rosa 2010 Mw 4 central Brazil earthquake revisited

J. Zahradník [a], L. Fojtíková [b, e, *], J. Carvalho [c], L.V. Barros [c], E. Sokos [d], J. Janský [a]

[a] Charles University in Prague, Faculty of Mathematics and Physics, Czech Republic
[b] Institute of Rock Structure and Mechanics, Academy of Sciences of the Czech Republic, Czech Republic
[c] Observatório Sismológico, Universidade de Brasília, Brazil
[d] University of Patras, Department of Geology, Seismological Laboratory, Greece
[e] Earth Science Institute, Slovak Academy of Sciences, Slovakia

ARTICLE INFO

ABSTRACT

Focal-mechanism determination of weak events recorded in sparse networks is challenging. First-motion polarities are often available at relatively distant stations, and waveforms only at a few near stations can be modeled. A two-step approach of how to combine such data has been suggested recently (Cyclic Scanning of the Polarity Solutions, or CSPS method; Fojtíková and Zahradník, 2014). It starts with creating a suite of first-motion polarity solutions, which is often highly non-unique. The next step consists of repeating full waveform inversion for all polarity solutions. Even few stations may efficiently reduce the non-uniqueness of the polarity solutions. Centroid depth, time, scalar moment and uncertainty estimate of the well-fitting double-couple solutions are obtained. The CSPS method has been extended in this paper by adding a new feature, i.e. repeated inversions using multiple first-motion polarity sets. The polarity sets are created by projecting the stations on focal sphere in several available velocity models, thus accounting for the takeoff angle uncertainty. The multiple polarity sets provide assessment of the CSPS solution stability. These ideas are demonstrated on a comprehensive analysis of a rare event in central Brazil. It is the Mw ~4 mainshock of the Mara Rosa 2010 earthquake sequence (Barros et al., 2015, Carvalho et al., 2015). We employ polarities at 11 stations (distances < 730 km) and invert full waveforms at two stations (CAN3 and BDFB at distances ~120 and 240 km), for 0.1–0.2 and 0.05–0.125 Hz, respectively. Six polarity sets reflect the takeoff angle uncertainty. The obtained CSPS results are very stable across all the polarity sets (in terms of depth, Mw, and strike/dip/rake angles). It is found that the Mara Rosa mainshock mechanism deviated from the composite solution of the whole sequence by 38°. The paper also includes a test simulating situations at which just a single waveform is used, and how it negatively affects the solution stability.

Artigo 2 - publicado

Inversion for Focal Mechanisms Using Waveform Envelopes Inaccurate Velocity Models: Examples from Brazil

by Juraci Carvalho, Lucas Vieira Barros, and Jiří Zahradník

Abstract One of the major challenges for the moment tensor determination is associated with the relatively low-magnitude events ($M_w \sim 4$) recorded by few regional stations at relatively large distances (300–600 km) and analyzed with standard velocity models of the region. Difficulties arise from the fact that synthetics in standard models (e.g., those routinely used in the location) cannot properly match real waveforms and favor the appearance of unmodeled time shifts and amplitude discrepancies (e.g., if VMs are constructed to minimize location residuals, they are not sensitive to uppermost shallow layers, which are insufficiently sampled by rays if shallow sources are missing). The situation is even worse when real waveforms can be matched but the retrieved focal mechanism is incorrect. This article investigates an alternative methodology that is more robust with respect to inappropriate velocity models: the inversion of waveform envelopes. The method is built on an empirical basis. It studies the effects of velocity models on synthetic waveforms and finds that the information about focal mechanism is encoded in the variation of the envelope shapes and amplitudes among the seismogram components. Besides synthetic tests, the method has been tested on real data comprising two earthquakes in Brazil: the 2010 M_w 4.3 Mara Rosa (MR) and the 2017 M_w 4.3 Maranhão earthquakes. When compared with solutions from previous studies, based on many polarities and *ad hoc* path-specific velocity models, we obtained in both cases the same mechanism with a single 1D model and a single-station polarity constraint. The envelope inversion is a promising technique that might be useful in similar sparse networks, such as the one in Brazil, where standard waveform inversion, in general, is not fully efficient.

Artigo 3 - submetido

Earthquake relocation, focal mechanism and stress field determination in central Brazil

Juraci M. Carvalho(1), Lucas V. Barros(1), Jiří Zahradník(2), Mônica G. Von Huelsen(1), Vinicius Martins Ferreira(1)

(1) Observatório Sismológico da Universidade de Brasília
(2) Charles University, Prague, Czech Republic

ABSTRACT

In this work, we perform a seismological investigation in the central Brazil region. This large area (910.000 km^2) is surrounded by several geological provinces: Eastern Amazon craton; southwestern Parnaíba basin; western São Francisco craton; northern Paraná basin, and it includes almost the whole Tocantins province. The area is crossed integrally, in SW-NE direction, by the continental-scale discontinuity - Transbrasiliano lineament (LTB). In the Brazilian seismic catalog (1724-2019), it is possible to distinguish a seismic belt following the LTB lineament and some dispersed events in the northern, western and eastern areas. The study area is characterized mainly by low magnitude events (M < 4); only 11 events reported in the catalog with M > 4 occurred, and among them just one with magnitude 5. Based on a quality criteria, a set of 118 events from 337 present in the catalog, were selected for a thorough analysis on this paper. This work was divided in three parts: (i) Events relocation with the iLoc code and Regional Seismic Travel Time (RSTT) velocity model; (ii) Focal mechanisms determination of 10 events using waveform envelopes and polarities, and; (iii) Inversion of focal mechanisms for stress field. The study shows that the seismicity of the area is mainly concentrated in two relatively narrow belts and that the principal compressional stress axis of the whole zone is well resolved, featuring azimuth ~133 and plunge ~12°. To study events of small magnitudes in such a huge area, installation of additional seismic stations is needed, as well as more studies of aftershocks by local temporary networks.

Anexo B – Artigos no período fora do tema da tese

Relação de artigos publicados no período de realização do doutorado.

Artigo 4 - publicado

SCIENTIFIC REP✺RTS

OPEN

A recent deep earthquake doublet in light of long-term evolution of Nazca subduction

J. Zahradník[1], H. Čížková[1], C. R. Bina[2], E. Sokos[3], J. Janský[1], H. Tavera[4] & J. Carvalho[5]

Earthquake faulting at ~600 km depth remains puzzling. Here we present a new kinematic interpretation of two Mw7.6 earthquakes of November 24, 2015. In contrast to teleseismic analysis of this doublet, we use regional seismic data providing robust two-point source models, further validated by regional back-projection and rupture-stop analysis. The doublet represents segmented rupture of a ~30-year gap in a narrow, deep fault zone, fully consistent with the stress field derived from neighbouring 1976–2015 earthquakes. Seismic observations are interpreted using a geodynamic model of regional subduction, incorporating realistic rheology and major phase transitions, yielding a model slab that is nearly vertical in the deep-earthquake zone but stagnant below 660 km, consistent with tomographic imaging. Geodynamically modelled stresses match the seismically inferred stress field, where the steeply down-dip orientation of compressive stress axes at ~600 km arises from combined viscous and buoyant forces resisting slab penetration into the lower mantle and deformation associated with slab buckling and stagnation. Observed fault-rupture geometry, demonstrated likelihood of seismic triggering, and high model temperatures in young subducted lithosphere, together favour nanometric crystallisation (and associated grain-boundary sliding) attending high-pressure dehydration as a likely seismogenic mechanism, unless a segment of much older lithosphere is present at depth.

Ongoing debate over seismogenic mechanisms of deep-focus earthquakes[1] revolves around transformational faulting[2,3], thermal shear instabilities[4,5], and dehydration embrittlement[6]. Here we report new seismic source analyses and associated geodynamic modelling to better constrain the most plausible mechanism behind a recent South American deep-focus doublet. An enigmatic earthquake 'nest' exists close the Peru-Brazil border at latitudes 6°–12° S. Approximately 20 deep-focus events of Mw > 6 (GCMT[7,8] catalogue 1976–2015) form a narrow belt delineating a deep fault zone, ~400 km long and striking ~160° (Fig. 1a), with depths confined (in 70% of cases) to a 30-km narrow range (590–620 km). Why such well-expressed, spatially limited seismicity, and how does it relate to ongoing Nazca plate subduction beneath South America at 7–8 cm/year[9-13]? The so-called thermal parameter[14] of ~1300–2000 km ranks this subduction as 'warm', but the slab geometry[15] is only weakly constrained by seismicity, because the depths 200–600 km are aseismic. Below 650 km, an almost horizontal stagnant slab has been imaged by seismic tomography[16]. To better understand the physics of Peru-Brazil subduction, we investigate fault processes of the most recent strong earthquakes, in the context of neighbouring seismicity. We derive a stress field that is successfully explained by a dynamical model of ~100-My slab evolution consistent with tomography. Finally, we combine seismic source properties (rupture geometry and velocities, seismic triggering) and geodynamic temperature estimates to compare competing hypotheses of seismogenic mechanism.

Artigo 5 - publicado

Geophysical Journal International

The intraplate Maranhão earthquake of 2017 January 3, northern Brazil: evidence for uniform regional stresses along the Brazilian equatorial margin

Fábio L. Dias,[1] M. Assumpção,[2] Marcelo B. Bianchi,[2] Lucas V. Barros[3] and Juraci M. Carvalho[3]

[1] *Department of Geophysics, Observatório Nacional, Rua General Cristino 77, Rio de Janeiro, RJ 20921-400, Brazil*
[2] *Institute of Astronomy, Geophysics and Atmospheric Sciences, University of São Paulo, Rua do Matão 1226, São Paulo, SP 05508-090, Brazil. E-mail: marcelo@iag.usp.br*
[3] *Observatório Sismológico, University of Brasília, Brasília, DF 70910, Brazil*

SUMMARY
Lithospheric stresses in intraplate regions can be characterized by many different wavelengths. In some areas, stresses vary over short distances of less than $\sim$100 km, but in other regions uniform stresses can be recognized for more than $\sim$1000 km or so. However, not all intraplate regions are well sampled with stress measurements to allow a good characterization of the lithospheric stresses. On 2017 January 3, a magnitude m_b 4 earthquake occurred near the equatorial coast of the Maranhão State, an aseismic area of northern Brazil. Despite the few permanent stations in northern Brazil, a well-constrained strike-slip mechanism was obtained from regional moment-tensor inversion. A detailed analysis of the backazimuths of aftershocks recorded by the closest station ($\sim$40 km away) allowed the identification of the fault plane to be the NNW–SSE trending nodal plane. An estimate of the rupture length, about 2 km, was also possible. The strike-slip mechanism has coast-parallel P axis and coast-perpendicular T axis, in agreement with most of the focal mechanisms found further to the east. The coast parallel P axis is also similar to the SHmax orientations from breakouts measurements further along the coast. The Maranhão earthquake fills an important gap of stress indicators in northern Brazil and suggests that the intraplate stress field is uniform along the 2000 km long northern coast.

Key words: South America; Waveform inversion; Earthquake source observations; Dynamics: seismotectonics.

Artigo 6 - publicado

Seismological Research Letters

Archive   Content ⌄   About The Journal ⌄   About the Society ⌄   SSA Member Sign In

The Brazilian Seismographic Network (RSBR): Improving Seismic Monitoring in Brazil ⊘

Marcelo B. Bianchi; Marcelo Assumpção; Marcelo P. Rocha; Juraci M. Carvalho; Paulo A. Azevedo; Sérgio L. Fontes; Fábio L. Dias; Joaquim M. Ferreira; Aderson F. Nascimento; Marcos V. Ferreira; Iago S. L. Costa

⊞ Standard View   🗐 PDF   66 Cite ⌄   ⸙ Share ⌄   🔧 Tools ⌄

ABSTRACT

The Brazilian Seismographic Network (RSBR) began operating in 2011 with the joint effort of four different institutions: Universities of São Paulo (USP), Brasília (UnB), Rio Grande do Norte (UFRN), and the National Observatory (ON). Initially funded by Petrobras (Brazilian State Oil Company) in a large-scale infrastructure project that started in 2009, RSBR is now sponsored by Brazilian Geological Survey (CPRM). Station installation began in 2011 in southeast (SE) Brazil and finished in 2014 in the Amazon. The network is composed of 84 stations (as of December 2017) operated by those four institutions. CPRM now coordinates the general maintenance and compilation of the Brazilian Seismic Bulletin. RSBR has lowered the detection threshold down to m_b 3.5 for earthquakes in Brazil as a whole, and in some areas, such as northeast (NE) and SE Brazil, detection thresholds are about m_b 3.0. Besides monitoring Brazilian and South American seismicity, RSBR serves as a backbone for temporary deployments to study crustal and upper-mantle structure.

GeoRef Subject

Artigo 7 - publicado

Reservoir-Triggered Seismicity in Brazil: Statistical Characteristics in a Midplate Environment

by Lucas Vieira Barros, Marcelo Assumpção, Luis Carlos Ribotta, Vinicius M. Ferreira, Juraci M. de Carvalho, Brigida M. D. Bowen, and Diogo F. Albuquerque

Abstract Reservoir-triggered seismicity (RTS) was first reported in Brazil in the early 1970s. Here, we update the compilation of Assumpção *et al.* (2002), increasing the number of RTS from 16 to 26 cases. We briefly describe eight new cases that had been published in congress proceedings. We compare this updated RTS database with all Brazilian dams taller than 20 m. The reservoirs that triggered earthquakes were analyzed in relation to dam height, reservoir volume, geology, seismicity level, and stress provinces. The chance of a reservoir-triggering seismicity clearly increases with dam height, as is well known: the chance is only 2% for heights between 20 and 50 m in Brazil, increases to 8% between 50 and 100 m, and reaches 65% for dams taller than 100 m. The reservoir volume also has a clear influence: 26% of the reservoirs with volumes between 1.0 and 10 km^3 triggered earthquakes, and the chance increases to 47% for volumes larger than 10 km^3. No clear correlation with the geology was found. Dams built on igneous rocks tend to be slightly more prone to RTS, compared with those built on sedimentary rocks, but the difference is not statistically significant. No difference was found among the three main types of geological provinces (cratonic basement, Neoproterozoic fold belts, and intracratonic Phanerozoic basins). A tentative comparison with the yet poorly defined stress provinces in Brazil did not show any difference between regions of compressional stresses and regions with shear stresses. On the other hand, comparison of the fraction of reservoirs producing RTS in natural seismic and aseismic areas showed that regions with natural seismicity have twice as much potential for RTS than aseismic regions. Although dam height is the most influential characteristics, the maximum magnitude does not show any clear correlation with dam height or reservoir size, similar to other cases worldwide.

Electronic Supplement: Figures of focal mechanisms, waveform fits, epicenter locations, reservoir locations, frequency–magnitude distributions, tentative definition of compressional and shear-stress provinces, and distributions of dams.

Anexo C - Suplemento eletrônico (Artigo 1)

Compromising polarity and waveform constraints in focal-mechanism solutions; the Mara Rosa 2010 M_w 4 central Brazil earthquake revisited
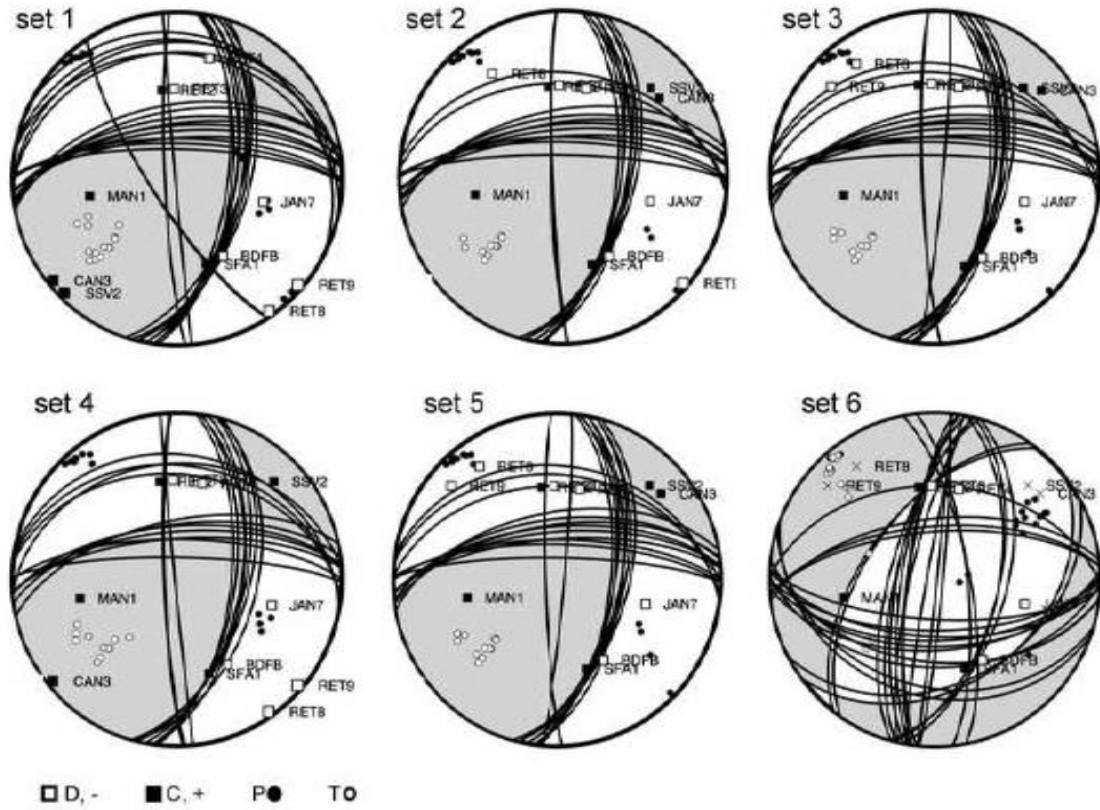
Fig. AC.S1. Focal mechanisms obtained by a single-station waveform inversion (*station CAN3*), pre-constrained by the first-motion polarity sets 1 to 6. All CSPS solutions with VR > 0.95 VRopt are shown by nodal lines, while the VRopt solution is shaded.
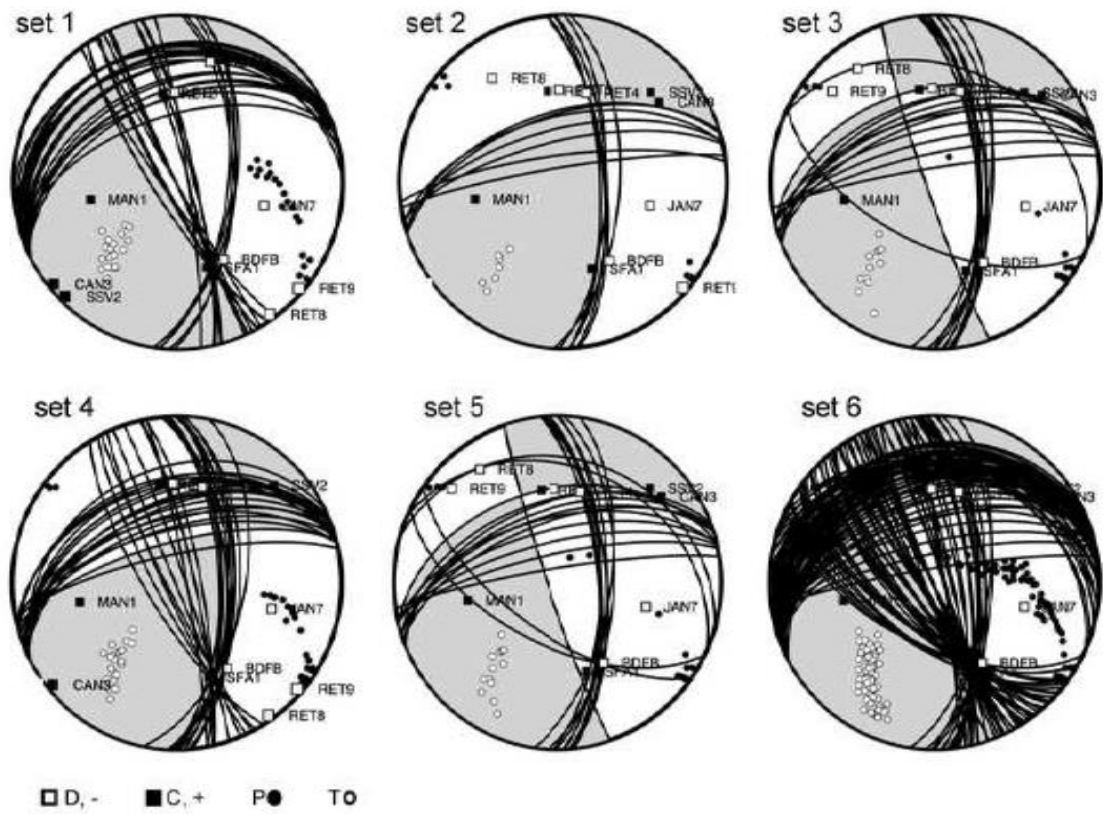
Fig. AC.S2. Focal mechanisms obtained by a single-station waveform inversion (*station SSV2*), pre-constrained by the first-motion polarity sets 1 to 6. All CSPS solutions with VR > 0.95 VRopt are shown by nodal lines, while the VRopt solution is shaded.
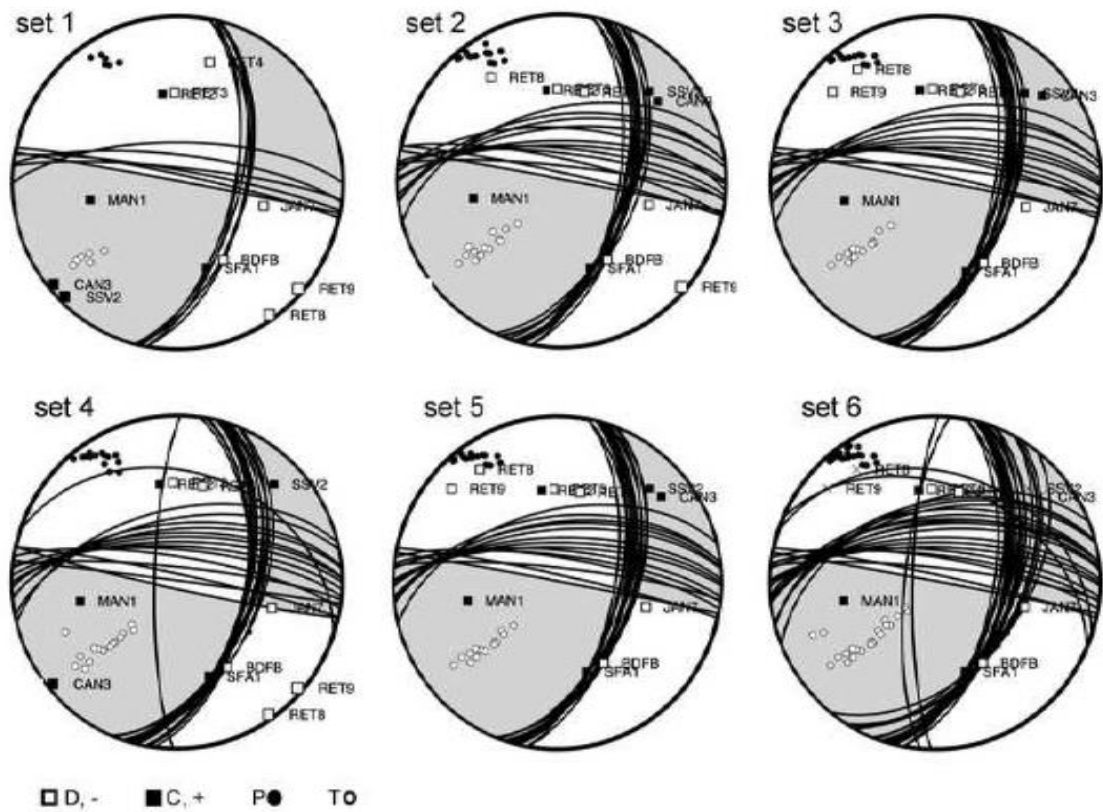
Fig. AC.S3. Focal mechanisms obtained by a single-station waveform inversion (*station BDFB*), pre-constrained by the first-motion polarity sets 1 to 6. All CSPS solutions with VR > 0.95 VRopt are shown by nodal lines, while the VRopt solution is shaded.
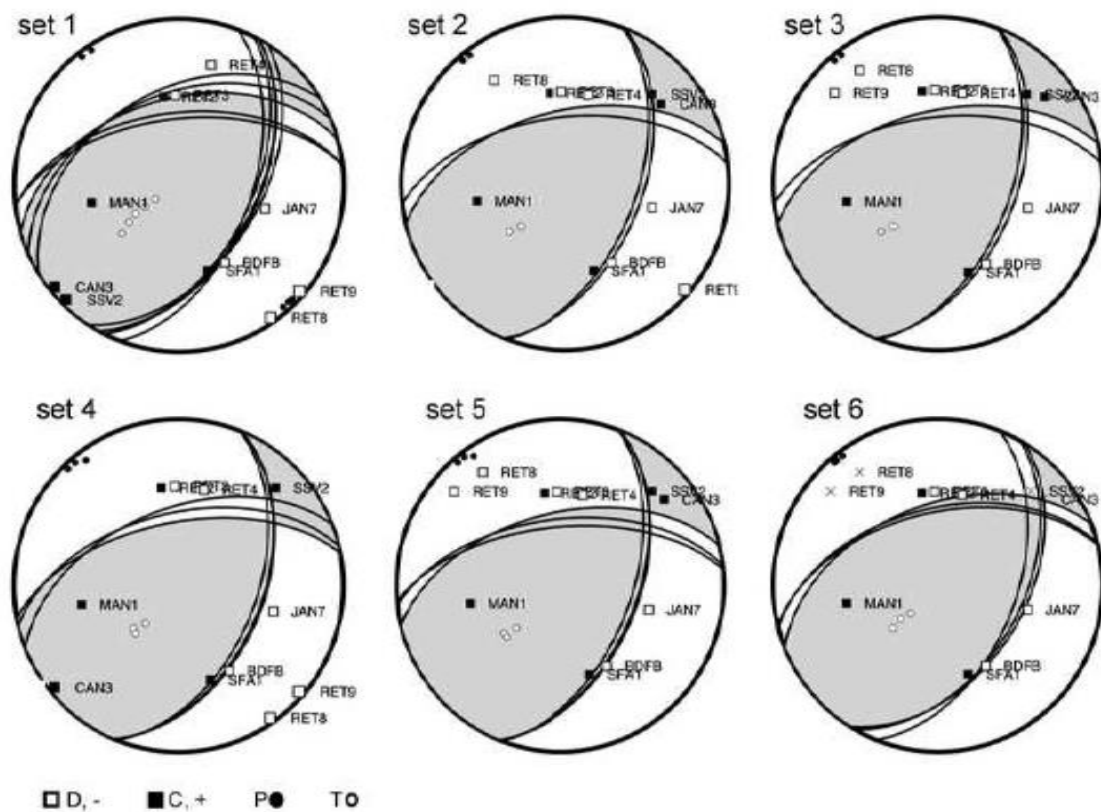
Fig. AC.S4. Focal mechanisms obtained by two-station waveform inversion (*stations CAN3 and BDFB*), pre-constrained by the first-motion polarity sets 1 to 6. This is analogy of Figure 7, but using the same VR threshold as in Figures S1-S3.
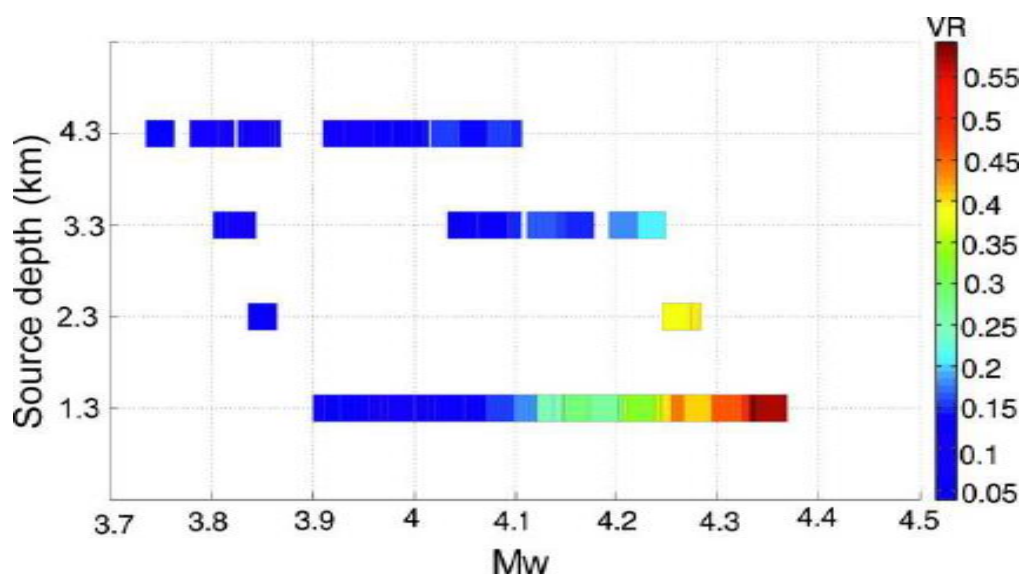
Fig. AC.S5. Internal performance of the CSPS method for the waveform inversion at stations CAN3 and BDFB, pre-constrained by the first-motion polarity set 1. Variance reduction (VR) is shown by color for all polarity solutions (panel 'set 1' in Figure 6). Only a few polarity solutions have a good waveform fit (large VR, corresponding to panel 'set 1' in Figure 7), and these clearly prefer $M_w \sim 4.3$ and the first trial source depth of 1.3 km.

Table - AC.S1

SI-1 (station BDFB)

Model	Centroid depth (km)	Centroid time * (s)	Mw	Strike (°)	Dip (°)	Rake (°)	DC (%)	VR	CN	K-angle $ (°)	stations with polarity misfit
NewBR	2.3	-3.0 #	4.6	293	79	91	41	0.94	14	76	BDFB,JAN7, RET2,SSV2, CAN3
Barros	1.3	0.3	4.7	353	39	-53	9	0.89	30	102	RET2
Soares	1.3	0.3	4.6	286	65	-158	78	0.94	21	90	RET3,RET4, SFA1

* Centroid time is expressed with respect to origin time.
\# At the limit of the temporal grid.
$ Angular deviation from the reference solution.

Table - AC.S2

SI-2 (stations CAN3 and BDFB)

Station and Model	Centroid depth (km)	Centroid time * (s)	Mw	Strike (°)	Dip (°)	Rake (°)	DC (%)	VR	CN	K-angle $ (°)	stations with polarity misfit
NewBR	1.3	-3.0 #	4.6	225	83	87	98	0.78	5	36	BDFB,JAN7, RET2,MAN1
Barros	1.3	0.60	4.4	233	57	91	48	0.81	5	17	RET2,JAN7, BDFB
Soares	1.3	0.66	4.4	219	40	70	56	0.87	5	11	RET3,RET4, SFA1

* Centroid time is expressed with respect to origin time.
\# At the limit of the temporal grid.
$ Angular deviation from the reference solution.

Anexo D - Suplemento eletrônico (Artigo 2)

Electronic Supplement to Inversion for Focal Mechanisms Using Waveform Envelopes and Inaccurate Velocity Models: Examples from Brazil

by Juraci Carvalho, Lucas Vieira Barros, and Jiří Zahradník

This electronic supplement contains figures of waveform comparisons and tables of amplitude ratio due to velocity model (ARMOD) values and velocity models.

For the initial validation, to certify that the waveform envelope preserves the source information (focal mechanism and depth), we used synthetics for the envelope inversion in comparison with the standard waveform inversion. The synthetics were obtained from the ISOLA Forward Simulation tool (Zahradník and Sokos, 2018), free of noise, a local velocity model (1D), focal mechanism reference (strike/dip/rake = 260°/40°/60°, 100% double couple [DC]) and the source depth of 5.0 km (Fig. AD.S1a). We used the station geometry of the Brazilian Seismographic Network (RSBR) with a low azimuthal gap and distances ranging from 120 to 550 km. For both inversions, we used the same velocity model as the one used in the calculation of synthetics. Later, the synthetics are called pseudo-observed data.

In the waveform inversion, as expected, the best-fit synthetic waveforms (red) matches perfectly the pseudo-observed data (black) with variance reduction (VR) = 1 at all stations components (Fig. AD.S1b); the inversion at a frequency

band of 0.05–0.1 Hz exactly recovered the source focal mechanism (260°/40°/60°) and depth (5.0 km; Fig. AD.S1c,d).

The envelope inversion was done with the same setup as the waveform inversion (Fig. AD.S2a), and envelopes were normalized per station. As in the waveform inversion, the results showed a perfect match (VR = 1) of the envelopes at all station components. The traces are envelope synthetics (red) and pseudo-observed data (black; Fig. AD.S2b). The inversion succeeded to resolve the source focal mechanism and depth (Fig. AD.S2c,d). As explained in the Synthetic Tests and Method section of the main article, to avoid the flipping of P and T axes, we used one polarity in this test, specifically at station JAN7 (compression, U).

The test clearly showed that the envelopes carry information about the source, that is, about the focal mechanism and its variation with the trial source depth, although the optimum depth resolution is worse than in the waveform inversion.

Velocity models produce variations of waveforms. In Figure 4-3 of the main article, we discussed time shifts; the waveforms at each station were normalized to maximum value, independently in VM1, VM2, and VM3. In Figure AD.S3, we again compare synthetic seismograms in the reference model VM1 and two other models, VM2 and VM3, but seismograms in VM2 and VM3 share the same normalization constants as in VM1. It enables us to observe not only the time shifts but also significant amplitude differences, mainly between VM1 and VM2, see, for example, the Z component at ARAG, SDBA, JAN7, the north–south component at LAJE, and so on in Figure AD.S3a.

It was shown in Figure 4-3 of the main article that despite significant differences between synthetic waveforms in models VM1 and VM2, the duration and shape of major wave groups in the normalized synthetics remains stable with respect to the velocity model change. Although in the main article we demonstrated this stability for a single specific focal mechanism, here (Fig. AD.S4) we show that the same is true for five elementary focal mechanisms from which arbitrary mechanisms can be composed. The amplitude similarity in the two models is documented also by ARMOD values close to 1 (Table AD.S1). Because the waveform shapes can be mathematically represented by envelopes, the

observed model independency of waveform shapes suggested envelopes as suitable substitute for waveforms in the inversion for focal mechanism.

Tables:

Tabela -AD.S1. Average Amplitude Ratio due to Velocity Model (ARMOD) Values.

		0°/45°/90°			0°/90°/0°			0°/90°/90°			90°/45°/90°			270°/90°/−90°		
		N	E	Z	N	E	Z	N	E	Z	N	E	Z	N	E	Z
VM1/VM2	CAN3	1.21	0.88	1.16	0.80	1.34	1.00	0.92	1.15	1.00	1.00	1.55	1.40	1.31	0.92	1.00
	PEXB	1.44	0.98	1.36	1.11	0.70	1.03	0.95	1.05	1.00	1.00	0.99	1.01	1.11	0.95	1.00
	BDFB	1.20	0.97	1.09	1.04	0.88	0.90	0.86	1.43	1.00	0.93	1.00	0.89	1.12	0.86	1.00
	SNDB	1.00	1.39	1.17	1.27	1.00	1.00	1.30	0.93	1.00	1.18	0.90	1.07	0.87	1.30	1.00
	ARAG	0.73	1.13	1.06	1.18	0.92	1.00	1.20	1.04	1.00	1.00	0.74	1.12	1.01	1.20	1.00
	LAJE	1.17	1.00	1.41	1.04	1.00	1.28	1.21	0.76	1.00	1.10	0.72	1.00	1.02	1.21	1.00
	SDBA	0.82	1.03	1.00	1.00	0.99	1.15	1.10	1.06	1.00	1.00	1.01	1.19	1.58	1.10	1.00
	JAN7	0.94	1.08	1.00	1.00	1.11	1.11	1.12	1.15	1.00	1.00	1.04	1.15	1.35	1.12	1.00
ARMOD norm		1.093 ± 0.179			1.036 ± 0.143			1.051 ± 0.139			1.042 ± 0.172			1.084 ± 0.165		
VM1/VM3	CAN3	1.01	0.88	1.06	0.89	1.08	1.00	0.98	1.19	1.00	1.00	1.22	1.24	1.35	0.98	1.00
	PEXB	1.25	0.98	1.33	1.00	0.71	1.06	0.99	1.19	1.00	1.26	0.99	1.12	1.18	0.99	1.00
	BDFB	1.32	0.97	1.16	1.07	0.75	0.90	0.85	1.90	1.00	0.79	1.00	0.87	1.24	0.85	1.00
	SNDB	1.14	1.13	0.92	1.20	1.14	1.00	1.18	0.98	1.00	1.00	0.97	0.80	0.95	1.18	1.00
	ARAG	0.78	0.87	1.00	0.97	1.03	1.00	1.11	1.05	1.00	1.00	0.92	1.20	1.10	1.11	1.00
	LAJE	1.34	1.00	1.43	0.93	1.00	1.37	1.24	0.76	1.00	1.09	0.63	1.00	1.11	1.24	1.00
	SDBA	0.95	1.12	1.00	1.00	0.88	0.94	1.14	1.10	1.00	1.00	1.00	1.03	2.48	1.14	1.00
	JAN7	0.95	1.05	1.00	1.00	1.06	1.06	1.07	1.08	1.00	1.00	1.06	1.11	2.04	1.07	1.00
ARMOD norm		1.068 ± 0.162			1.001 ± 0.132			1.076 ± 0.201			1.013 ± 0.143			1.167 ± 0.353		

Average ARMOD values (±σ) for five elementary moment tensors (strike/dip/rake); comparing the velocity models VM2 and VM3 with the reference model VM1. The frequency band used in the calculations is 0.05–0.1 Hz. N, north; E, east; Z, vertical.

Tabela - AD.S2. Comparison of Three Tested Velocity Models, VM1–VM3.

	VM1		VM2		VM3		(VM2-VM1)/VM1×100		(VM3-VM1)/VM1×100	
Depth	V_P	V_S	V_P	V_S	V_P	V_S	V_P diff%	V_S diff%	V_P diff%	V_S diff%
0.0	5.6	3.2	6.0	3.5	5.8	3.4	7.1	9.4	3.6	6.2
2.0	5.8	3.3	6.0	3.5	5.8	3.4	3.4	6.1	0.0	3.0
3.0	5.9	3.4	6.0	3.5	5.8	3.4	1.7	2.9	−1.7	0.0
4.0	6.0	3.5	6.0	3.5	5.8	3.4	0.0	0.0	−3.3	−2.9
5.0	6.1	3.5	6.0	3.5	5.8	3.4	−1.6	0.0	−4.9	−2.9
12.0	6.1	3.5	6.6	3.9	5.8	3.4	8.2	11.4	−4.9	−2.9
13.7	6.1	3.5	6.6	3.9	5.8	3.4	8.2	11.4	−4.9	−2.9
15.6	6.2	3.5	6.6	3.9	5.8	3.4	6.5	11.4	−6.5	−2.9
17.3	6.2	3.6	6.6	3.9	5.8	3.4	6.5	8.3	−6.5	−5.6
19.2	6.2	3.6	6.6	3.9	5.8	3.4	6.5	8.3	−6.5	−5.6
22.0	6.3	3.6	6.6	3.9	6.4	3.7	4.8	8.3	1.6	2.8
22.5	6.3	3.6	6.6	3.9	6.4	3.7	4.8	8.3	1.6	2.8
23.0	6.3	3.6	6.6	3.9	6.4	3.7	4.8	8.3	1.6	2.8
25.0	6.3	3.6	6.8	4.0	6.4	3.7	7.9	11.1	1.6	2.8
35.0	6.3	3.6	7.2	4.2	6.4	3.7	14.3	16.7	1.6	2.8
38.0	6.3	3.6	8.3	4.9	6.4	3.7	31.7	36.1	1.6	2.8
42.0	7.3	4.2	8.3	4.9	8.1	4.7	13.7	16.7	11.0	11.9
54.3	7.4	4.2	8.3	4.9	8.1	4.7	12.2	16.7	9.5	11.9
Average velocity differences							7.8	10.6	−0.3	1.4

The P- and S-wave velocity difference of VM2 and VM3 with respect to VM1 is shown. VP, P-wave velocity; VS, S-wave velocity.

Figures
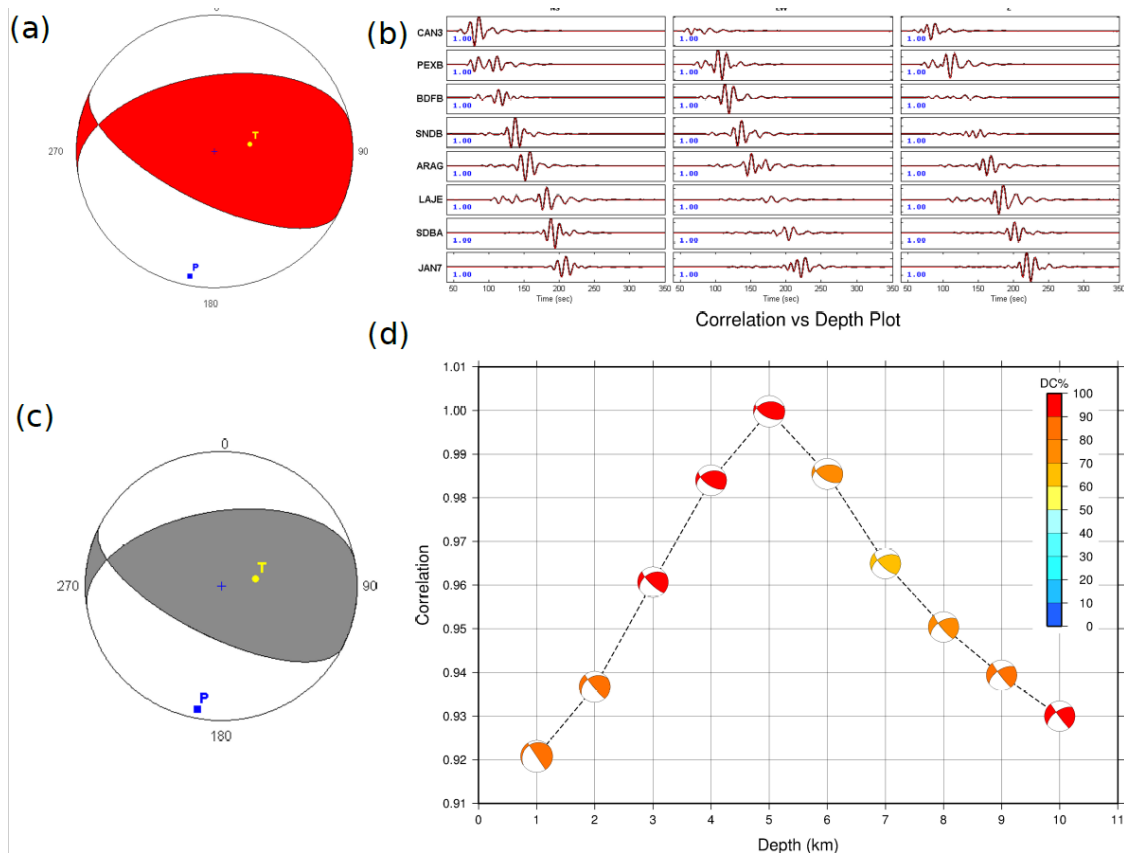
Figura - AD.S1. Synthetic waveform inversion of an ideal scenario, that is, no noise and the same velocity model used in forward simulation and inversion. (a) Reference focal mechanism used in the forward simulation (260°/40°/60°); (b) waveforms of synthetics (red) and pseudo-observed data (black). Blue numbers are VR per station component; (c) focal mechanism obtained with the waveform inversion for the optimum depth (260°/40°/60°); (d) plot of correlation versus depth with focal mechanism plot color representing the DC percentage.
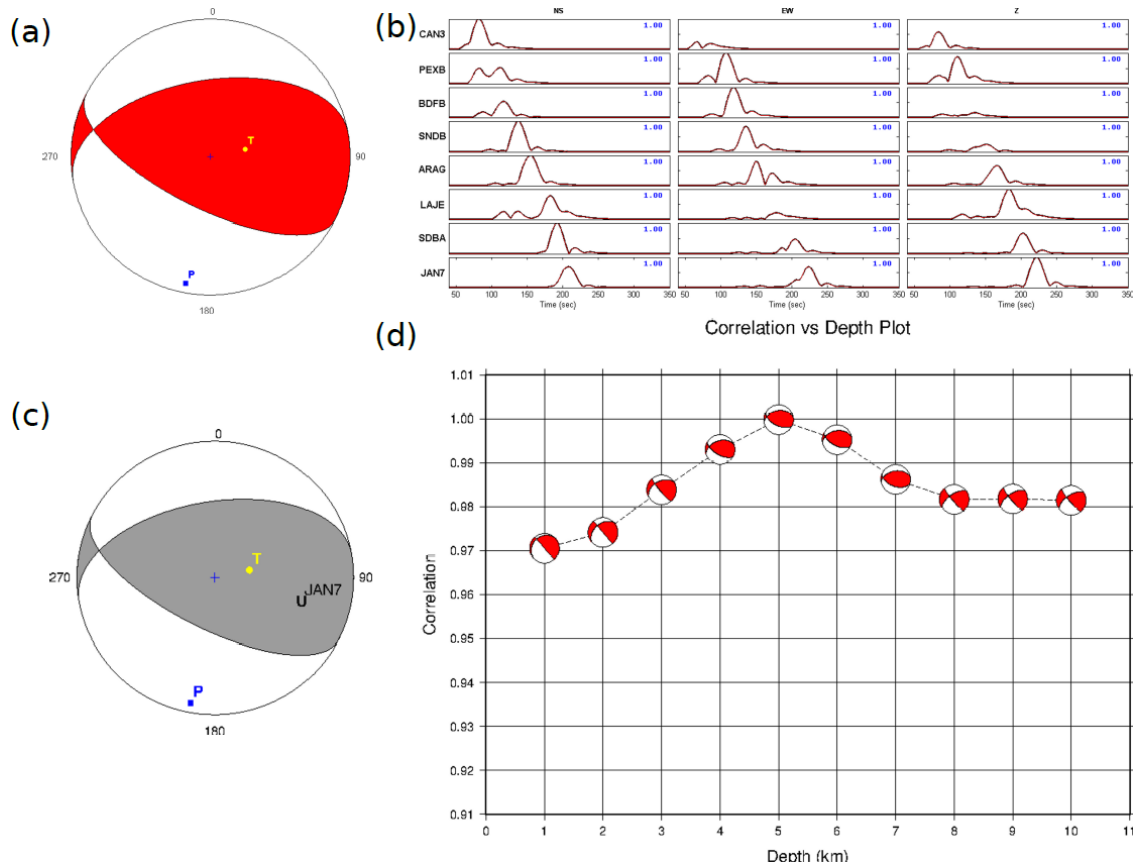
Figura - AD.S2. Synthetic envelope inversion of the same setup as in the waveform inversion (Fig. S1). Reference focal mechanism used for forward simulation (260°/40°/60°); (b) envelopes of synthetics (red) and pseudo-observed data (black). Blue numbers are VR per station component; (c) the envelope inversion optimum result at the depth of 5.0 km retrieved the source (260°/40°/60°); (d) correlation versus depth (color red = constrained to 100% DC).
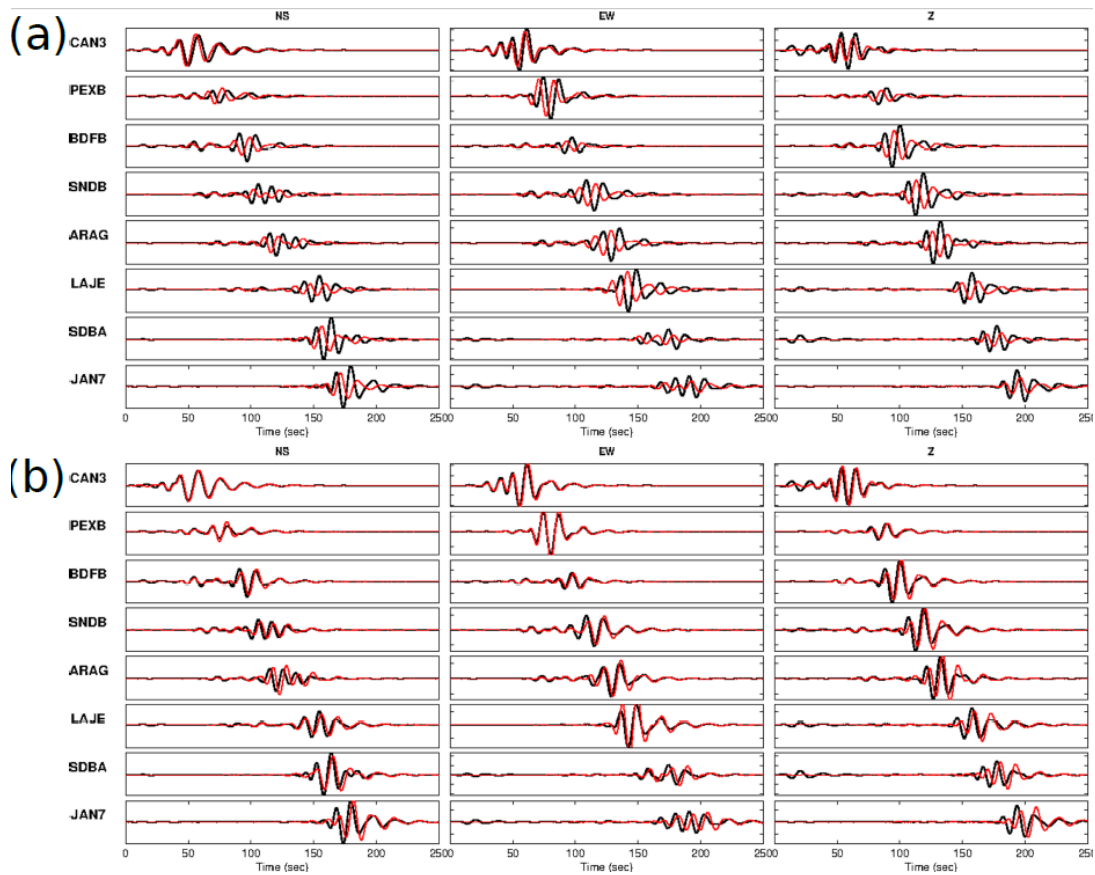
Figura - AD.S3. Comparison of synthetic waveforms in the reference velocity model VM1 (black lines) and in two other models (red lines): (a) the VM2 model and (b) the VM3 model. The frequency band is of 0.05–0.1 Hz. The stations are sorted according to their epicentral distances, from 121 km (CAN3) up to 542 km (JAN7). The synthetics preserve their true relative amplitude with respect to VM1.
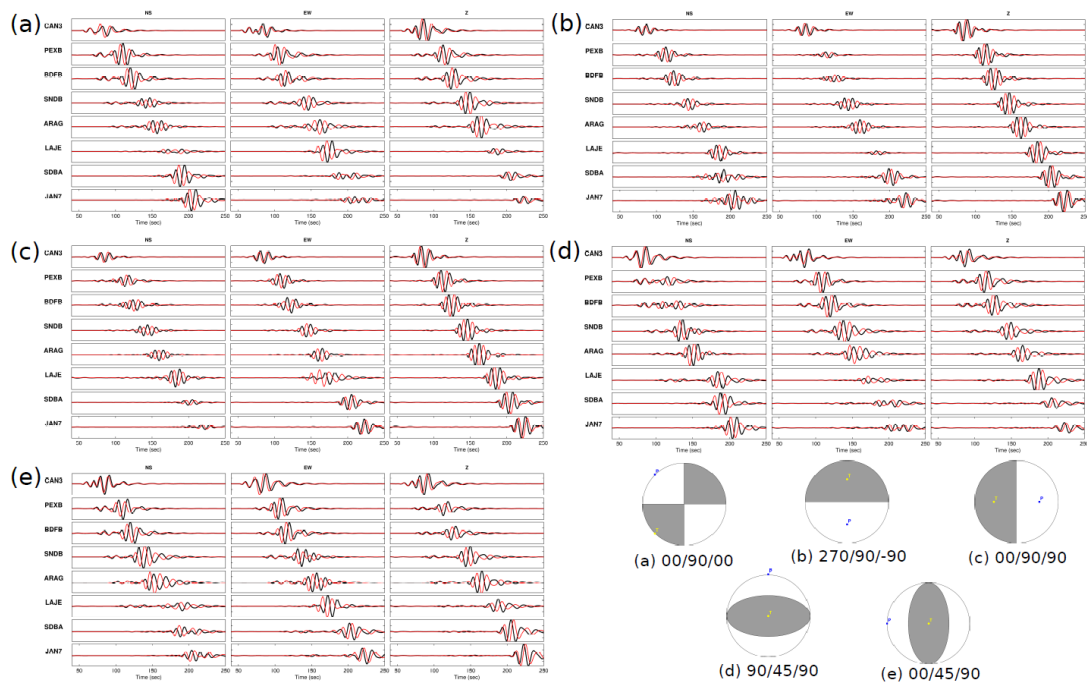
Figura - AD.S4. Synthetic waveforms forward simulated for the five elementary moment tensors. Waveforms in the reference velocity model VM1 (black lines) are compared with those in model VM2 (red lines). The frequency band is of 0.05–0.1 Hz. The stations are sorted according to their epicentral distances, from 121 km (CAN3) up to 542 km (JAN7). Synthetics in each model are normalized to maximum component at each station. The elementary moment tensors (inset) are shown by focal mechanism plots and strike, dip, and rake values have the same graphic layout as in the waveform panels.

Data and Resources

The waveform inversion was done with the software ISOLA and can be downloaded from http://geo.mff.cuni.cz/~jz/for_Costa_Rica (last accessed April 2018).

References

Zahradník, J., and E. Sokos (2018). ISOLA code for multiple-point source modeling—Review, in Moment Tensor Solutions—A Useful Tool for Seismotectonics, S. D'Amico (Editor), Springer Natural Hazards, Cham, Switzerland, doi: 10.1007/978-3-319-77359-9_1.

Anexo E - Suplemento eletrônico (Artigo 3)
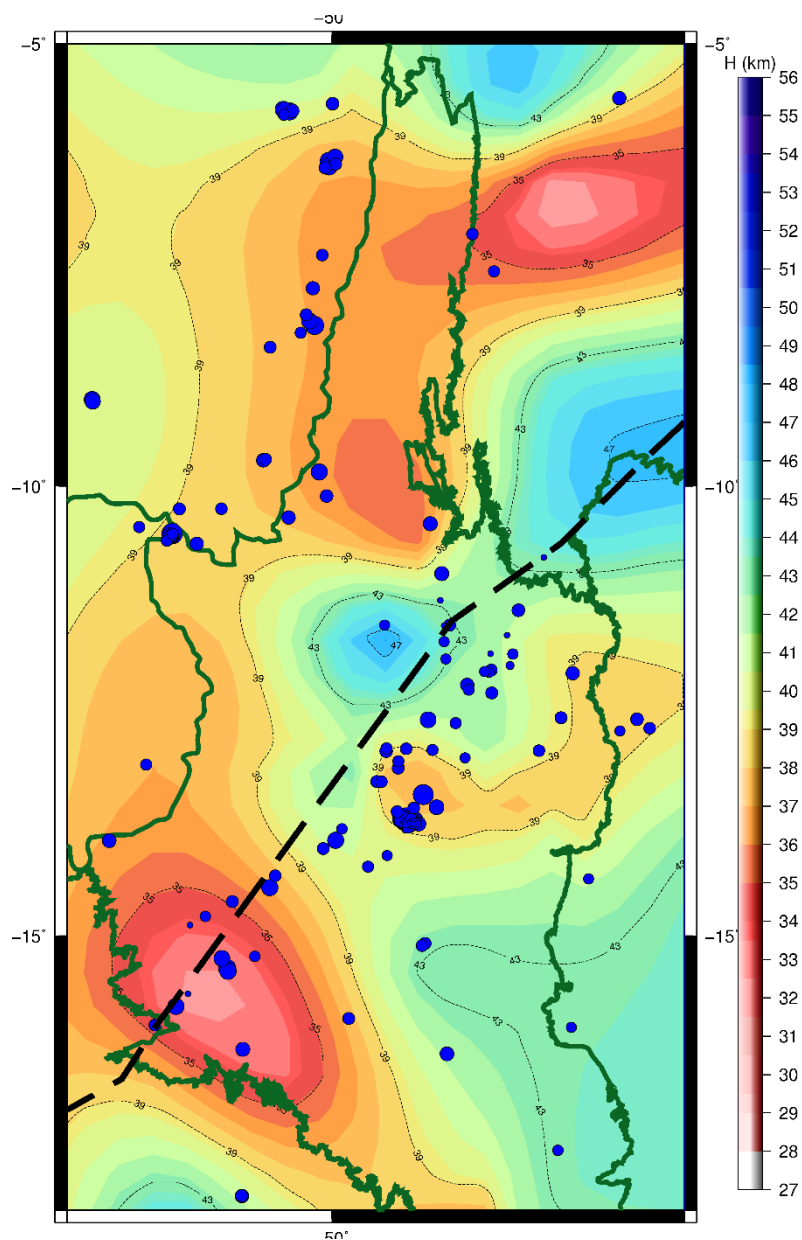
Figura 6-S1 – Seismicity, Moho depth, LTB and geological provinces (modified from Albuquerque et al. (2017).

Tabela 6-S1 – Screened events from the catalog and relocated with iLoc+RSTT. The magnitude m_R is equivalent to the teleseismic body wave magnitude m_b.

Nu.	Date (RSTT)	OTime (RSTT)	Lat (°) (Cat)	Lon (°) (Cat)	Lat (°) (RSTT)	Lon (°) (RSTT)	Cat x RSTT (km)	Mag (mR*)	Smajax (km)	Sminax (Km)	Strike (°)
1	08/10/2010	20:16:52	-13.71	-49.24	**-13.717**	**-49.152**	10	5	7	6	127
2	08/10/2010	20:25:20	-13.77	-49.16	**-13.911**	**-49.156**	16	2.2	19	22	19
3	26/02/2011	22:51:31	-13.78	-49.21	**-13.717**	**-49.199**	7	3.2	18	7	95
4	02/03/2011	19:16:56	-11.45	-48.71	**-11.813**	**-47.92**	95	2.2	20	11	175
5	04/03/2011	06:59:41	-13.78	-49.21	**-13.745**	**-49.157**	7	3.3	9	7	101
6	30/04/2011	08:16:21	-11.17	-48.7	**-11.117**	**-48.643**	9	2.2	24	10	38
7	24/04/2012	01:34:13	-13.77	-49.11	**-13.765**	**-49.066**	5	2.2	21	9	91
8	19/07/2012	14:59:06	-15.63	-51.16	**-15.369**	**-51.188**	29	3.4	13	8	179
9	25/12/2017	13:59:35	-6.4	-50.1	**-6.42**	**-50.09**	2	3.8	7	5	18
10	28/07/2012	12:49:26	-15.49	-51.11	**-15.392**	**-51.174**	13	3.3	11	9	150
11	08/01/2011	11:49:23	-13.5	-48.8	**-13.58**	**-48.89**	13	4.1	9	5	30
12	08/12/2012	18:52:34	-13.56	-49.18	**-13.716**	**-49.194**	17	3.7	10	8	105
13	22/06/2013	06:04:50	-13.95	-49.04	**-13.73**	**-49.079**	25	3.5	11	7	102
14	30/07/2013	04:22:02	-13.77	-49.06	**-13.736**	**-49.069**	4	3	12	7	92
15	15/05/2014	15:03:30	-10.45	-48.88	**-10.416**	**-48.872**	4	2.8	11	9	115
16	19/06/2014	04:39:30	-16.24	-50.96	**-16.263**	**-50.993**	4	2.8	11	7	28
17	19/07/2014	12:37:06	-13.68	-48.61	**-13.578**	**-49.077**	52	2.3	11	6	114
18	07/08/2014	20:13:41	-14.29	-49.48	**-14.238**	**-49.572**	11	2.3	11	8	133
19	06/09/2014	23:11:17	-12.94	-49.52	**-12.952**	**-49.387**	14	2.5	9	8	98
20	09/09/2014	16:02:19	-14.21	-49.3	**-14.115**	**-49.369**	13	2	13	7	144
21	30/09/2014	05:02:26	-11.88	-47.95	**-11.897**	**-47.884**	7	2.1	11	8	16
22	28/10/2014	01:40:29	-12.98	-49.37	**-12.936**	**-49.38**	5	2.3	14	7	145
23	23/11/2014	00:46:09	-15.321	-51.071	**-15.237**	**-51.314**	28	3.1	8	6	153
24	25/12/2014	16:41:50	-10.234	-51.664	**-10.26**	**-51.727**	7	2.4	8	7	49

25	31/12/2014	03:09:34	-7.88	-50.32	**-7.772**	**-50.217**	17	2.6	9	8	120
26	18/01/2015	00:33:13	-8.09	-50.4	**-8.068**	**-50.29**	12	2.4	8	7	35
27	19/01/2015	03:54:16	-7.47	-50.2	**-7.56**	**-50.096**	15	2.3	8	6	40
28	23/01/2015	05:06:29	-13.22	-49.3	**-13.153**	**-49.244**	10	2.4	8	6	172
29	29/01/2015	05:22:04	-15.49	-51.31	**-15.625**	**-51.589**	33	2.2	33	9	67
30	11/02/2015	09:46:33	-10.478	-51.762	**-10.53**	**-51.806**	8	4	7	7	46
31	12/02/2015	04:44:39	-12.53	-46.77	**-12.734**	**-46.732**	23	2	14	8	179
32	12/02/2015	13:07:35	-10.518	-51.761	**-10.553**	**-51.82**	8	2.7	8	8	36
33	15/02/2015	12:25:25	-10.543	-51.867	**-10.559**	**-51.817**	6	2.9	8	6	48
34	19/02/2015	01:25:07	-12.65	-48.61	**-12.648**	**-48.594**	2	2.3	11	6	77
35	05/03/2015	20:05:42	-15.1	-48.95	**-15.107**	**-48.974**	3	2.3	8	6	102
36	11/03/2015	03:57:51	-10.564	-51.95	**-10.602**	**-51.872**	10	2.3	10	6	22
37	11/03/2015	11:24:01	-14.1	-50.114	**-14.032**	**-50.1**	8	2.4	8	7	128
38	16/03/2015	19:44:54	-9.62	-50.79	**-9.705**	**-50.774**	10	2.7	10	8	70
39	30/03/2015	03:32:37	-10.627	-51.986	**-10.569**	**-51.839**	17	2.6	9	7	9
40	01/04/2015	08:09:08	-10.612	-51.936	**-10.546**	**-51.845**	12	2.8	9	6	18
41	07/04/2015	11:50:18	-9.167	-52.8	**-9.042**	**-52.712**	17	3	8	7	17
42	08/04/2015	20:25:21	-15.09	-48.9	**-15.082**	**-48.964**	7	3	9	7	81
43	09/04/2015	16:09:26	-16.304	-48.736	**-16.297**	**-48.693**	5	2.4	10	5	74
44	18/04/2015	13:19:29	-10.31	-51.28	**-10.263**	**-51.249**	6	2.7	12	9	76
45	19/05/2015	20:24:18	-13.8	-49.13	**-13.737**	**-49.061**	10	2.3	9	7	142
46	16/06/2015	08:20:19	-9.7	-50.82	**-9.699**	**-50.753**	7	2.4	9	8	74
47	19/06/2015	01:13:01	-14.75	-51.3	**-14.789**	**-51.424**	14	2.4	13	7	113
48	19/06/2015	03:01:40	-11.76	-48.71	**-11.739**	**-48.725**	3	2.1	9	7	70
49	22/06/2015	14:00:27	-9.01	-52.73	**-9.024**	**-52.716**	2	2	8	7	9
50	24/06/2015	13:00:45	-13.04	-48.55	**-13.066**	**-48.736**	20	3.1	10	5	19
51	07/07/2015	21:17:32	-12.057	-48.388	**-12.057**	**-48.192**	21	2	7	6	46

52	29/07/2015	06:55:04	-8.45	-50.76	**-8.472**	**-50.684**	9	2.4	8	6	1
53	16/08/2015	19:47:10	-13.12	-52.13	**-13.109**	**-52.106**	3	2.4	9	7	122
54	15/09/2015	21:27:05	-14.542	-50.735	**-14.468**	**-50.7**	9	2.3	8	7	50
55	17/09/2015	10:24:47	-14.76	-51.3	**-14.871**	**-51.575**	32	3.2	11	9	59
56	21/09/2015	22:13:54	-10.5	-51.87	**-10.557**	**-51.819**	8	2.2	10	8	175
57	27/09/2015	07:15:10	-5.56	-46.74	**-5.611**	**-46.733**	6	2.3	10	6	133
58	27/09/2015	17:41:58	-13.808	-52.675	**-13.967**	**-52.464**	29	2.6	7	5	142
59	08/10/2015	18:25:41	-15.86	-49.59	**-15.909**	**-49.807**	24	2.7	10	7	39
60	12/10/2015	03:21:25	-12.73	-46.45	**-12.728**	**-46.431**	2	2.4	12	6	38
61	24/10/2015	20:02:28	-12.07	-48.66	**-11.932**	**-48.705**	16	2.3	8	5	41
62	15/11/2015	10:55:11	-12.284	-48.46	**-12.223**	**-48.465**	7	2	8	7	55
63	25/11/2015	20:19:07	-13.34	-49.51	**-13.299**	**-49.437**	9	2.6	7	6	2
64	13/12/2015	17:46:21	-8.085	-50.275	**-8.135**	**-50.255**	6	2.3	7	7	109
65	16/12/2015	03:12:42	-13	-49.16	**-12.924**	**-49.153**	8	3.1	9	6	161
66	16/12/2015	18:59:33	-14.648	-50.921	**-14.614**	**-51.107**	20	2.3	12	7	92
67	25/12/2015	18:10:14	-12.58	-47.44	**-12.588**	**-47.4**	4	2.4	7	5	32
68	18/01/2016	18:29:12	-14.297	-50.704	**-14.332**	**-50.626**	9	2.2	6	6	120
69	30/01/2016	07:40:30	-13.871	-49.091	**-13.746**	**-49.071**	14	2.3	6	6	137
70	13/02/2016	09:02:48	-10.414	-50.052	**-10.108**	**-50.044**	34	2.4	9	6	8
71	28/03/2016	02:41:42	-17.832	-51.06	**-17.863**	**-51.02**	5	2.5	9	7	140
72	29/03/2016	03:35:21	-13.697	-49.069	**-13.763**	**-49.087**	8	2.6	8	6	83
73	06/04/2016	07:40:49	-7.46	-48.27	**-7.58**	**-48.16**	18	2	7	5	94
74	01/05/2016	02:33:30	-9.78	-50.23	**-9.839**	**-50.142**	12	2.3	7	6	111
75	08/06/2016	12:28:43	-11.55	-48	**-11.562**	**-48.724**	79	3.2	21	6	87
76	11/06/2016	21:51:17	-12.21	-47.33	**-12.091**	**-47.266**	15	2.2	6	5	23
77	08/07/2016	23:07:11	-12.04	-48.18	**-12.08**	**-48.218**	6	2.6	11	7	59
78	03/08/2016	21:41:29	-10.54	-51.54	**-10.614**	**-51.523**	8	2	13	6	24

79	08/08/2016	02:02:18	-13.407	-49.136	**-13.639**	**-49.268**	29	2.6	7	6	80
80	12/08/2016	17:14:47	-7.25	-48.52	**-7.156**	**-48.404**	17	2.4	11	6	7
81	04/10/2016	01:18:01	-8.335	-50.28	**-8.27**	**-50.353**	11	2.3	7	7	179
82	07/10/2016	19:59:57	-13.688	-49.053	**-13.748**	**-49.107**	9	3.6	7	5	133
83	29/10/2016	03:47:32	-8.24	-50.377	**-8.189**	**-50.196**	21	3.6	7	7	55
84	07/12/2016	03:30:18	-12.99	-47.69	**-12.962**	**-47.636**	7	3.6	6	5	39
85	25/12/2016	13:59:35	-6.434	-50.116	**-6.353**	**-50.04**	12	2.3	7	6	165
86	11/01/2017	10:05:12	-13.61	-48.83	**-13.599**	**-48.819**	2	3.8	7	6	124
87	28/01/2017	00:36:39	-13.32	-49.49	**-13.291**	**-49.486**	3	2.9	7	6	48
88	12/03/2017	02:27:41	-13.769	-49.057	**-13.796**	**-49.029**	4	2.4	9	7	129
89	14/04/2017	16:01:02	-15.996	-52.065	**-15.998**	**-52.01**	6	2.8	8	6	165
90	18/05/2017	16:55:57	-12.333	-48.104	**-12.296**	**-48.181**	9	2.3	8	6	87
91	26/05/2017	17:58:20	-12.13	-48.29	**-12.065**	**-48.267**	8	2.4	8	5	89
92	07/06/2017	08:41:15	-12.71	-46.54	**-12.625**	**-46.552**	10	2	7	5	2
93	12/06/2017	01:23:43	-17.658	-51.32	**-17.876**	**-50.994**	42	2.5	6	5	155
94	22/06/2017	02:25:29	-16.04	-47.51	**-16.007**	**-47.282**	25	2.4	6	5	94
95	31/08/2017	06:41:00	-6.408	-50.089	**-6.376**	**-50.022**	8	2	6	6	121
96	09/09/2017	04:13:42	-15.814	-51.793	**-15.777**	**-51.767**	5	3.4	9	7	7
97	21/09/2017	08:33:58	-13.75	-49.142	**-13.779**	**-49.128**	4	3.2	8	7	85
98	01/10/2017	01:46:22	-5.832	-50.563	**-5.775**	**-50.497**	10	3.2	9	6	17
99	04/10/2017	16:46:57	-5.779	-50.547	**-5.767**	**-50.48**	8	3.2	7	6	38
100	12/10/2017	22:40:22	-12.96	-48.91	**-12.953**	**-48.877**	4	3.4	10	6	179
101	09/11/2017	06:18:24	-13.75	-49.16	**-13.712**	**-49.101**	8	2.2	10	7	71
102	23/11/2017	02:52:25	-5.75	-50.57	**-5.757**	**-50.467**	11	2.2	10	7	29
103	03/12/2017	07:03:28	-10.81	-47.54	**-10.743**	**-47.615**	11	2.6	12	6	86
104	03/01/2018	05:55:23	-12.06	-48.25	**-12.016**	**-48.233**	5	2.2	11	6	85
105	18/01/2018	11:39:51	-13.74	-49.9	**-13.793**	**-49.866**	7	2.2	11	9	50

106	20/01/2018	12:09:24	-13.92	-49.98	**-13.947**	**-49.952**	4	2.1	12	7	42
107	24/01/2018	22:53:23	-5.86	-50.61	**-5.753**	**-50.534**	15	3.2	10	7	34
108	13/02/2018	04:51:05	-12.23	-48.24	**-12.23**	**-48.441**	22	3	9	5	76
109	02/03/2018	04:17:51	-6.38	-50.12	**-6.407**	**-50.075**	6	2.2	11	7	37
110	15/03/2018	20:48:58	-10.931	-48.594	**-10.973**	**-48.739**	17	2.4	9	6	110
111	12/04/2018	03:56:34	-17.37	-47.400	**-17.349**	**-47.435**	4	2.8	7	6	7
112	12/05/2018	02:36:22	-10.32	-50.540	**-10.356**	**-50.478**	8	2.1	8	6	135
113	26/05/2018	13:45:40	-13.83	-49.100	**-13.742**	**-49.066**	10	2.6	10	7	141
114	03/07/2018	01:25:12	-15.68	-51.040	**-15.32**	**-51.008**	40	2.5	9	6	133
115	04/08/2018	13:42:32	-11.54	-49.380	**-11.544**	**-49.4**	2	2.1	10	7	19
116	21/08/2018	00:19:27	-13.800	-49.110	**-13.791**	**-49.119**	1	2	9	6	54
117	11/09/2018	05:57:19	-10.562	-52.365	**-10.455**	**-52.183**	23	2.6	10	7	44
118	14/09/2018	06:08:26	-12.49	-48.921	**-12.614**	**-48.907**	14	2.2	7	7	149

iLoc/RSTT epicenter errors: *Sminax: semi-minor axis (km); Smajax: semi-major axis (km) and strike azimuth: semi-major axis(°).*